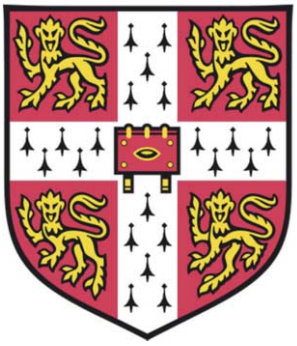
UNIVERSITY OF CAMBRIDGE
DEPARTMENT OF ENGINEERING



RESPONSE OF PILED BUILDINGS TO THE CONSTRUCTION OF DEEP EXCAVATIONS

MANDY KORFF

Jesus College

A dissertation submitted for the degree of Doctor of Philosophy at the University of Cambridge

December 2012

IOS Press

This thesis was supervised by prof. Robert Mair (Cambridge University) and approved by prof. Malcolm Bolton (Cambridge University) and Dr. Michael Long (University College Dublin).

© 2013 Mandy Korff and IOS Press

All rights reserved. No part of this book may be reproduced, stored in a retrieval system, or transmitted, in any form or by any means, without prior written permission from the publisher.

Reuse of the knowledge and information in this publication is welcomed on the understanding that due credit is given to the source. However, neither the publisher nor the author can be held responsible for any consequences resulting from such use.

ISBN 978-1-61499-273-8 (print)
ISBN 978-1-61499-274-5 (online)
DOI 10.3233/978-1-61499-274-5-i

Publisher
IOS Press BV
Nieuwe Hemweg 6B
1013 BG Amsterdam
Netherlands
fax: +31 20 687 0019
e-mail: order@iospress.nl

Distributor in the USA and Canada
IOS Press, Inc.
4502 Rachael Manor Drive
Fairfax, VA 22032
USA
fax: +1 703 323 3668
e-mail: iosbooks@iospress.com

PRINTED IN THE NETHERLANDS

Acknowledgements

This thesis is the result of a complex cooking recipe, starting with a hunger for deeper understanding of the processes related to the projects encountered in my work at Deltares. The nicely pictured result in the cookbook was first painted together with my supervisor professor Robert Mair, who guided the process ever since with subtle hints on scientific quality and practical experience from projects all over the world. Professor Malcolm Bolton as my advisor encouraged me with his wisdom and always positive approach. During the five years in which I came to the Scofield Centre regularly, I met many PhD students, staff and technicians. Although I could not work with you on a daily basis, I always felt most welcome and supported. You introduced me to the Cambridge way of doing things, the Cambridge alumni network and typical British topics. Surely, especially Anama and Martin, who provided me with a 'home away from home', made me feel truly part of Cambridge life.

The basic ingredients came from the North South Line project in Amsterdam. My special thanks goes to Frank Kaalberg and his team, who dared to share with me their most valuable treasure, the monitoring data. The experience of the senior staff at the Amsterdam building control departments (DMB, Oud-Zuid and Centrum) helped me put together the historic context of the Amsterdam pile foundations. The people at DIVV who are responsible for the project I wish to thank for their permission to use their challenging project as a study object.

The kitchen was provided by Deltares, who made it possible for me to pursue this PhD while remaining in touch with on-going research, consulting work and management issues along the way, even when this meant I could not be around all the time. Some of the cooking tools were provided by colleagues, from which I am most indebt to Hans Sellmeijer for his rigorous way of dealing with the data. Without him, I would have lost or mixed up most of the ingredients along the way. Also Mart Borsboom, Jaap Bijnagte, Thomas Bles, John Kimenai, Thomas van der Linden, Vasco Veenbergen and especially Frits van Tol each helped by discussing the topic with me on several occasions.

The icing on the cake is provided by my family and friends. You coloured this thesis by being proud of me long before it was ready for consumption. I know it took a long time as my now 95 year old Grandma once mentioned: 'If you just have to learn about foundation piles, why does it take so long before I get to go to Cambridge?' To her and my parents I dedicate this work.

Abstract

Trends in the construction of deep excavations include deeper excavations situated closer to buildings. This research provides insight into mechanisms of soil-structure interaction for piled buildings adjacent to deep excavations to be used in the design and monitoring of deep excavations in urban areas. Most methods to assess building response have originally been developed for tunnelling projects or buildings with shallow foundations. Monitoring data of the construction of three deep excavations for the North South metro Line in Amsterdam, The Netherlands have been used to validate these methods specifically for piled buildings.

In all three of the Amsterdam deep excavations studied, the largest impact on the ground surface and buildings is attributed to preliminary activities instead of the commonly expected excavation stage. The in situ preliminary activities caused 55-75% of the surface settlement and 55-65% of the building settlements. Surface settlements measured behind the wall were much larger than the wall deflections and reached over a distance of 2-3 times the excavated depth away from the wall. The shape of the surface settlements found resembles the hogging shape as defined by Peck (1969). For the excavation stage only, the shape of the displacement fits the profile proposed by Hsieh and Ou (1998). Most prediction methods overestimate the soil displacement at depth.

An analytical method has been established and tested for the behaviour of piled buildings near excavations. This method includes the reduction of pile capacity due to lower stress levels, settlement due to soil deformations below the base of the pile and development of negative (or positive) skin friction due to relative movements of the soil and the pile shaft. The response of piles in the case of soil displacements depends on the working load of the pile, the percentages of end bearing and shaft friction of the pile, the size and shape of the soil settlements with depth and the distribution of the maximum shaft friction with depth. A method is derived to determine the level for each pile at which the pile and soil settlement are equal. Buildings in Amsterdam built before 1900 and without basement are most sensitive to soil displacements. For all other buildings, the pile settlement depends mainly on the working load.

The actual damage experienced in buildings depends also on the relative stiffness of the building compared to the soil. Cross sections in Amsterdam have been evaluated and it is concluded that the Goh and Mair (2011) method provides a realistic, although rather large range of possible modification factors for the deflection of buildings next to excavations, deforming in hogging shape. For the incidents that happened at Vijzelgracht some well known damage indicators have been evaluated.

Nomenclature

Latin Symbol	*Meaning*
A	Surface area influencing the pile considered
b or B	Width of the building
B	Width of the excavation in Bolton et al. (2008) and Caspe (1966)
C	Length of the wall in MSD method
cu	Undrained Shear Strength
d	Height of the foundation slab
D	Pile diameter
D_{cpt}	CPT diameter
D_{eq}	Equivalent pile diameter
D_0	Influence distance behind retaining wall at surface level
D_{0i}	Influence distance for horizontal displacements
Dy	Influence distance behind retaining wall at depth y
Dz	Relative displacement to reach full slip along the shaft
E or E_b	Young's modulus building
E_p	Young's modulus pile
E_s	Young's modulus soil, representative soil stiffness e.g. at 0.01% axial strain at half the tunnel depth or weighted over the excavation depth
F_{nk}	Load due to negative skin friction
G	Shear modulus building
G_{ave}	Shear modulus soil, average
h	Average prop spacing in MSD method
H	Excavation depth
H	Height of the building (usually distance from foundation to the roof)
Hd	Influence depth below the excavation
He	Excavation depth
Hg	Excavation depth
Hw	Length of the wall or depth at zero diaphragm wall deflection
Hwi	Length of the wall minus depth Zi
i	Half the height of the excavation
I	Moment of inertia of the building ($H^3/12$ for sagging and $H^3/3$ in hogging)
I_p	Moment of inertia of the pile
ks	Soil stiffness in spring model
$K_{o;j}$	Neutral soil pressure factor in layer j, assuming a horizontal green field level and no overconsolidation
l	Distance between two footings or points on a building
L	Specific length L of the building in sagging / hogging
L	Depth of Neutral Plane from Broms and Badholms (1976)
Lp	Length of the pile
Ls	Width of the influence zone according to Hsieh & Ou (1998)
Lw	Length of the wall

M	Ratio between deformation of the building and the green field displacement (denoted with g).
O_s	Pile circumference
p	pile settlement
p_{sur}	Overburden load on the surface
q	Increase of Vertical Effective Stress in Subsoil
$q_{c;av}$	Cone resistance average of measured values
$q_{b;max}$	Average cone resistance by Van Mierlo and Koppejan (1952)
q_b	Cone resistance average (IC-method)
Q_b	Base capacity
Rb;cal, i	Mobilized pile base resistance, calculated from ground test results
Rb;cal, maxi	Maximum pile base resistance, calculated from ground test results
Rs;cal, i	Mobilized shaft friction, calculated from ground test results
Rs;cal, maxi	Maximum pile base resistance, calculated from ground test results
Rc	Shaft resistance in compression
Rt	Shaft resistance in tension
s	Settlement of the top of the pile
s_b or $s_{b;i}$	Settlement of the pile base
s_{el}	Settlement due to compression of the soil under the pile tip
s_2	Settlement of the top of the pile due to elastic compression of the pile
S or S_v	Settlement behind retaining wall
S	Pile Spacing
Shwi	Horizontal displacement at the wall in Aye et al. (2006)
Shi	Horizontal displacement in the soil in Aye et al. (2006)
Si_0	Settlement behind retaining wall at surface level at distance x
Si_y	Settlement behind retaining wall at depth Y at distance x
S_{max} or Svm	Maximum settlement at the wall
Sw_0	Maximum settlement behind retaining wall at surface level
Sw_y	Maximum settlement behind retaining wall at depth y
S_0	Soil settlement at z=0
S_{Lp}	Soil settlement at z=Lp
S_z	Soil settlement at depth z
t	Distance of the neutral axis to the edge of the beam
V_0	Deflected volume of wall
Vt_0	Volume of settlement trough behind retaining wall at surface level
Vty	Volume of settlement trough behind retaining wall at depth y
Vy	Deflected volume of wall below depth Y
W	Settlement trough width, given by Caspe (1966)
W	Width of the influence zone according to Caspe (1966)
W	Working load
Wmax	Maximum capacity of the pile in failure
x	Horizontal distance from the wall
X1	Distance to the nearest facades along the side street
Y	Depth below surface, defined as distance from toe of the wall

z	Depth from the surface
z_0	Depth of the tunnel
z_i	Interaction depth
Zi	Depth of the level of horizontal displacements considered Aye et al. (2006)

Greek Symbol	*Meaning*
α	Pile shaft friction factor (for c_u)
α_p	Pile base factor (CPT method)
α_s	Pile shaft friction factor (CPT method)
α^*_{mod}	Relative axial stiffness parameter according to Franzius (2006)
α^*_{exc}	Relative axial stiffness parameter according to Goh (2010)
β	Relative rotation or angular distortion, the rotation of the line joining two reference points, relative to the tilt
γ'_j	volumetric weight of the layer
δ_j	Friction angle between soil layer j and pile shaft
δS	Relative settlement or differential settlement
δv	Deflection of the wall
δvm	Maximum deflection of the wall
Δ/L	Deflection ratio or relative deflection; the maximum vertical displacement relative to the straight line connecting two reference points
$\varepsilon_{b,\,max}$	Maximum bending strain
ε_c	Maximum horizontal compressive strain
$\varepsilon_{d,\,max}$	Maximum diagonal strain
ε_h	Horizontal strain
$\varepsilon_{p\,(=d,tot)}$	Principal tensile strain
ε_t	Tensile strain
θ	Rotation between two points on a building or slope of a settlement curve
θ	Direction of the crack, measured from a vertical plane
λ	Length of the influence zone in MSD method
ν	Poisson's ratio
ρ^*_{mod}	Relative building stiffness parameter according to Franzius (2006)
ρ^*_{exc}	Relative building stiffness parameter according to Goh (2010)
$\sigma'_{v;j}$	Vertical effective stress at the bottom of layer j
$\sigma'_{v;sur;j}$	Effective vertical stress in layer j caused by the weight of the soil above and the overburden load psur without the influence of the other piles
$\sigma'_{v;m;j}$	Reduction of the effective vertical stress in layer j, caused by the negative skin friction transferred to the pile group
τ	Shaft friction
τ_{max}	Maximum shaft friction at the depth considered
φ'	Internal friction angle of the soil
ω	Tilt, rigid body rotation of the entire superstructure

Contents

CHAPTER 1 INTRODUCTION 1

1.1 UNDERGROUND CONSTRUCTION IN DENSELY POPULATED AREAS 1
1.2 FAILURE COSTS IN UNDERGROUND CONSTRUCTION 1
1.3 DEEP EXCAVATIONS IN SOFT SOIL CONDITIONS 2
1.4 SCOPE AND OBJECTIVE OF THIS RESEARCH 2
1.5 RESEARCH QUESTIONS 3
1.6 PROJECT COOPERATION 3
1.7 OUTLINE THESIS 3

CHAPTER 2 LITERATURE REVIEW 5

2.1 INTRODUCTION 5
2.2 DEEP EXCAVATIONS 6
2.2.1 Empirical methods, all construction activities combined 6
2.2.2 Empirical methods, effect of excavation and installation 8
2.2.3 Semi-empirical methods, shape of settlement trough due to excavation 12
2.2.4 Predicting displacements due to installation of diaphragm walls 17
2.3 BUILDING BEHAVIOUR 20
2.3.1 Causes of damage in buildings 20
2.3.2 Classification of damage 22
2.3.3 Criteria for damage to buildings 24
2.3.4 Limiting tensile strain method 27
2.4 INTERACTION SOIL – BUILDING FOR SHALLOW FOUNDATIONS 31
2.4.1 Introduction 31
2.4.2 The effect of building stiffness 31
2.4.3 The effect of building weight 33
2.4.4 The effect of the interface between building and soil 33
2.5 THE RESPONSE OF PILE FOUNDATIONS NEAR DEEP EXCAVATIONS 36
2.5.1 Pile behaviour 36
2.5.2 Response of piles to tunnelling 40
2.5.3 Response of piles to deep excavations 44
2.6 SUMMARY OF LITERATURE 45
2.6.1 Green field displacements 46
2.6.2 Building deformations and damage 46
2.6.3 Soil-structure interaction 47

CHAPTER 3 PREVIOUS CASE HISTORIES 49

3.1 INTRODUCTION 49
3.2 CHATER STATION, HONG KONG (DAVIES AND HENKEL, 1982) 49
3.2.1 Situation 49
3.2.2 Effects of the construction 50
3.2.3 Final deformations and damage 52
3.2.4 Conclusion from Chater station case history 53
3.3 KPE SINGAPORE (LEE ET AL., 2007) 53
3.3.1 Introduction 53
3.3.2 Damage prediction and results 54
3.3.3 Conclusion from Lee et al. (2007) case history 56
3.4 EXCAVATION NEXT TO XAVIER WARDE SCHOOL, CHICAGO (FINNO ET AL., 2002) 56
3.4.1 Situation and construction works 56
3.4.2 Deformations and building damage 57
3.4.3 Conclusion from Xavier Warde School case history 59
3.5 WILLEMSPOORTUNNEL – WHITE HOUSE ROTTERDAM 59
3.5.1 Introduction and soil conditions 59
3.5.2 Details of the White House building 60
3.5.3 Construction characteristics for Willemspoortunnel 62

3.5.4 Response of the 'White House' ... *63*
3.5.5 Conclusions ... *67*
3.6 CONCLUSIONS FROM PREVIOUS CASE HISTORIES ... 68

CHAPTER 4 FIELD DATA NORTH SOUTH LINE ... 71

4.1 INTRODUCTION ... 71
4.2 SOILS CHARACTERISTICS ... 72
4.2.1 Geology and geohydrology ... *72*
4.2.2 Soil profile ... *73*
4.2.3 Soil parameters ... *75*
4.2.4 Subsidence in Amsterdam ... *76*
4.3 BUILDING CHARACTERISTICS ... 78
4.3.1 Buildings in Amsterdam ... *78*
4.3.2 Typical timber foundations ... *79*
4.3.3 Foundation quality assessment method Amsterdam ... *80*
4.3.4 Pile capacity and load-settlement behaviour ... *82*
4.4 ROKIN STATION ... 83
4.4.1 History ... *83*
4.4.2 Station overview ... *84*
4.4.3 Cross sections ... *86*
4.4.4 Diaphragm wall and excavation supports ... *87*
4.4.5 Buildings around Rokin Station ... *88*
4.4.6 Construction activities and timelines ... *89*
4.5 VIJZELGRACHT STATION ... 92
4.5.1 Station overview ... *92*
4.5.2 Cross section 12197 ... *92*
4.5.3 Cross section 12270 ... *94*
4.5.4 Diaphragm wall and excavation supports ... *95*
4.5.5 Buildings around Vijzelgracht Station ... *96*
4.5.6 Construction activities and timelines ... *96*
4.5.7 Incidents ... *100*
4.6 CEINTUURBAAN STATION ... 101
4.6.1 Station overview ... *101*
4.6.2 Cross section 13044 ... *101*
4.6.3 Cross section 13110 ... *102*
4.6.4 Diaphragm wall and excavation supports ... *103*
4.6.5 Building characteristics around Ceintuurbaan Station ... *104*
4.6.6 Construction activities and timelines ... *104*
4.7 MONITORING SYSTEM ... 108
4.7.1 Introduction monitoring system ... *108*
4.7.2 Deformation measurements for buildings ... *109*
4.7.3 Surface measurements ... *110*
4.7.4 Extensometers ... *111*
4.7.5 Inclinometers ... *112*
4.7.6 Other equipment ... *115*
4.7.7 Corrections for background settlement ... *116*
4.7.8 Reference of inclinometers in the wall ... *117*

CHAPTER 5 GROUND DISPLACEMENTS ... 119

5.1 GROUND SETTLEMENT RESPONSE ... 119
5.2 GREEN FIELD PREDICTION MODELS FOR SURFACE DISPLACEMENT ... 119
5.3 GROUND DISPLACEMENTS AT DEPTH ... 133
5.4 PRESENCE OF THE BUILDINGS ... 140
5.5 CONCLUSIONS ON GROUND DISPLACEMENTS DUE TO DEEP EXCAVATIONS ... 142

CHAPTER 6 PILE LOAD TESTS DAPPERBUURT ... 145

6.1 INTRODUCTION TESTS DAPPERBUURT AMSTERDAM ... 145

6.2 SOIL CONDITIONS 146
6.3 TEST RESULTS 147
6.4 ANALYSIS OF SPECIAL PILES WITH/WITHOUT CASING 150
6.4.1 Shaft friction in Holocene layer 150
6.4.2 Shaft friction in foundation layer 150
6.4.3 Base capacity in foundation layer 153
6.4.4 Mobilization of negative skin friction / shaft capacity 154
6.4.5 Mobilization of base capacity 156
6.4.6 Neutral level for new piles 158
6.5 OLD TIMBER PILES 160
6.5.1 Mobilization of negative skin friction / shaft capacity 161
6.5.2 Mobilization of base capacity 162
6.5.3 Neutral level for old piles 165
6.6 CONCLUSIONS BASED ON TEST RESULTS DAPPERBUURT 167
6.7 COMBINATION OF TWO PILES (AMSTERDAM FOUNDATION) 168
6.8 TIMBER CHARACTERISTICS 168
6.9 RESULTS DAPPERBUURT COMPARED TO OTHER PILE LOAD TESTS 169
6.10 INITIAL CONDITION PILES IN AMSTERDAM 172

CHAPTER 7 SOIL-PILE INTERACTION MODEL 177

7.1 PILES IN INFLUENCE ZONE OF EXCAVATION 177
7.2 AXIAL INTERACTION FOR SINGLE PILE 180
7.2.1 Introduction 180
7.2.2 Soil displacement profile 183
7.2.3 Analytical solution if shaft friction is constant with depth 184
7.2.4 Analytical solution if shaft friction increases with depth 186
7.2.5 Effect of pile base capacity 190
7.2.6 Effect of pile flexibility 193
7.2.7 Resulting shaft friction with depth 195
7.2.8 Amsterdam timber pile 198
7.2.9 Summary interaction levels 199
7.3 EFFECTS ON PILES NOT RELATED TO CONSTRUCTION 201
7.4 SUMMARY 202

CHAPTER 8 SOIL- PILE INTERACTION BASED ON MEASUREMENTS IN AMSTERDAM 205

8.1 INTRODUCTION 205
8.2 CEINTUURBAAN 205
8.3 ROKIN 217
8.4 VIJZELGRACHT 222
8.5 INFLUENCE OF BUILDING CHARACTERISTICS ON SOIL- PILE INTERACTION 226
8.6 HORIZONTAL INTERACTION OF SOIL AND PILED BUILDINGS 231
8.7 SUMMARY AND CONCLUSIONS OF SOIL- PILE INTERACTION BASED ON MEASUREMENTS IN AMSTERDAM 234

CHAPTER 9 BUILDING DISPLACEMENTS 237

9.1 INTRODUCTION 237
9.2 VERTICAL DEFORMATIONS OF PILED BUILDINGS 237
9.2.1 Construction stages 237
9.2.2 Prism versus manual levelling 242
9.2.3 Effect of building stiffness 245
9.3 HORIZONTAL DEFORMATIONS OF PILED BUILDINGS 250
9.4 SUMMARY OF BUILDING DISPLACEMENTS 252

CHAPTER 10 BUILDING DAMAGE AT VIJZELGRACHT 255

10.1 INTRODUCTION AND EVENTS LEADING TO BUILDING DAMAGE 255
10.2 TECHNICAL ANALYSES CAUSE OF THE LEAKAGE 256
10.3 EFFECT ON THE SOIL AROUND THE EXCAVATION 257
10.4 DAMAGE TO THE BUILDINGS 259
10.5 DEFORMATIONS AND DAMAGE ARISING FROM FIRST INCIDENT 261
10.6 DEFORMATIONS AND DAMAGE ARISING FROM THE SECOND INCIDENT 264
10.7 REPAIR OF THE BUILDINGS 268
10.7.1 Corrective grouting of the buildings affected by the first incident 268
10.7.2 Lifting the buildings affected by the second incident 268
10.8 CONTINUATION OF THE EXCAVATION 270
10.9 CONCLUSIONS AND LESSONS LEARNED 271

CHAPTER 11 CONCLUSIONS AND RECOMMENDATIONS FOR FUTURE RESEARCH 273

11.1 INTRODUCTION 273
11.2 GROUND DISPLACEMENTS 273
11.3 SOIL – PILE INTERACTION 275
11.3.1 Pile behaviour 275
11.3.2 Response to deep excavations 275
11.3.3 Interaction level 276
11.3.4 Specific for the Amsterdam Cases 277
11.4 BUILDING RESPONSE 278
11.5 RECOMMENDATIONS FOR FUTURE RESEARCH 279
11.5.1 General recommendations 279
11.5.2 Recommendations for typical Dutch conditions with timber piles 280

REFERENCES

ANNEX A TYPICAL CPT PER STATION
ANNEX B SOIL PARAMETERS
ANNEX C GROUND DISPLACEMENTS
ANNEX D DAPPERBUURT TEST
ANNEX E BUILDING AND SOIL DEFORMATION

CHAPTER 1 INTRODUCTION

1.1 Underground construction in densely populated areas

In many cities in densely populated areas around the world, the application of deep excavations for the realisation of underground spaces (such as car parks, shops or cellars) or for other infrastructure is becoming common practice. Underground construction supports the quality of life in cities due to the availability and quality of the space that remains above ground. Due to increasing demands for space for many functions such as transportation, housing, power lines and sewers, the conditions in which these projects have to be built have increased in complexity in recent years. Although a lot of effort is put into design and construction of these facilities, this does not mean that their construction is without problems. On the contrary, during many underground construction activities problems such as damage, delays and cost overrun will be encountered. To limit damage to buildings and nuisance for neighbouring residents all kinds of measures can be taken. That the desired result is not always achieved becomes clear from several examples such as described by Van Tol (2007), Simpson et al. (2008) and many others.

1.2 Failure costs in underground construction

This research aims to contribute to the reduction of failure costs in the building industry and more specifically in underground construction. Problems and failure costs related to underground construction (e.g. for underground parking facilities, basements, infrastructure) are increasingly acknowledged, since it has become clear that they have a large influence on the image of the construction sector and the results in terms of money (5-10% loss of effectiveness due to failure costs compared to 2-3% net profit, as stated by Van Staveren (2006). Risk management is a key element to achieve reduction of these costs. To improve quantitative risk analyses, which form part of good risk management, improvements are needed to methods that can be used to indicate whether or not and to what extent buildings will be influenced by adjacent construction activities. Based on these analyses, relevant measures can be taken in a cost-effective way.

Underground construction is likely to be more sensitive to failure costs due to the following aspects or especially in the following circumstances:

- the inability to check the quality of many construction parts simply because they are made and remain under ground
- heterogeneity of the ground and the limitations in soil investigation techniques and procedures
- when soft soils are present causing potentially larger deformations
- when high ground water tables are present, due to potential for leakages etc.
- presence of (often unexpected) obstacles such as former foundations, pipes, piles, cables and large stones or rock, causing potential deviations in quality and performance.

1.3 Deep excavations in soft soil conditions

In underground construction, both tunnelling and (deep) excavations are commonly used. Both types of construction affect the structures directly adjacent to them. To identify which buildings will be influenced and to what extent, an assessment of the building damage is usually performed. This assessment might be either very simple or complex, but ideally should consist of the following steps: 1) determine green field displacements, 2) impose displacements onto building, 3) assess potential damage, 4) design protective measures if necessary. Most methods to assess the impact on the buildings are originally developed for tunnelling projects and buildings with shallow foundation and could be improved by specifically looking at piled buildings near deep excavations. Since trends in construction include deeper excavations situated closer to buildings, this research aims to improve the methods to assess building damage related to deep excavations.

This research deals with deep excavations in soft soil conditions only. Soft soils typically cause large displacements due to their low strength and high compressibility and are usually combined with high groundwater tables. In Western Europe, these soils are found in large parts of the Netherlands, Ireland, Norway, Denmark, Sweden and some parts of the UK. Other parts of the world such as Singapore and Hong Kong also have significant amounts of soft soils. Soft soils are often found in deltaic areas, where rivers and oceans supplied fine grained sediments such as clay, peat and fine sands. These Deltaic areas also happen to be the most densely populated areas in the world. The results of this research may best be used in these areas.

1.4 Scope and objective of this research

Following the setting of the problem as described above, the scope of this research is narrowed down to typical Dutch conditions of underground construction. Experience, field data, models and experiments developed elsewhere in the world will be used to obtain a model that suits typical Dutch conditions. This means that the assumed ground conditions include soft clays and sands, high ground water table, deep excavations from about 10 to 30

m deep, usually made with vertical cut off walls and close to neighbouring buildings. Buildings might have a shallow foundation, but more commonly a pile foundation.

The objective of this study is to gain insight into mechanisms of soil-structure interaction for piled buildings adjacent to deep excavations and to find a reliable method to design and monitor deep excavations in urban areas with soft soil conditions. The research focuses on typical Dutch conditions.

1.5 Research questions

Taking the end result, a general method to assess excavation induced building damage for soft soil conditions, there is a need to answer several research questions. The main questions are: how can we predict the behaviour of one or more (piled) buildings when a deep excavation will be constructed? What kind of modelling and/or measurements can be used to predict this effect?

The research questions for the behaviour during excavation are:

- How do the strains and displacements in the soil behind the deep excavation change with increasing excavation depth?
- What is the difference between the predicted and measured influence on soil surface, deeper soil levels and (piled) buildings and why does it occur? This must be related to the construction phases.
- Which assessment method fits best with the measured displacements of the surface and the (piled) buildings?

These questions on soil-structure interaction for deep excavations will be reconsidered in Chapter 11 based on the results presented in this report.

1.6 Project cooperation

This PhD study is part of a research project in cooperation with the Netherlands Centre of Underground Construction and Deltares, the Dutch Institute for Water, Subsurface and Infrastructure. The Netherlands Centre for Underground Construction (COB) performs studies at all shield-tunnelling projects in the Netherlands. These studies include the behaviour of deep excavations and tunnelling constructions. The most recent project, the North South Line project in Amsterdam, where several deep excavations for deep stations are constructed, forms the main source of field data and focus of this PhD study.

1.7 Outline thesis

This thesis describes the literature reviewed for this topic in Chapter 2 and several case histories related specifically to piled buildings in Chapter 3. In Chapter 4, the project of the Amsterdam Subway North-South Line is introduced with a summary of the necessary information on the soil conditions, the buildings and the construction works. In Chapter 5 the Amsterdam data on ground displacements are related to the construction of the deep

excavations, which are used for the input of the analysis of the pile-soil interaction in later chapters. Before studying this topic, it was first necessary to understand the pile behaviour of historic timber piles better, for which an old test series has been reanalysed in Chapter 6. Chapter 7 then describes the analytical soil-pile interaction model that has been derived. The results of Chapter 5-7 are jointly used to analyse the Amsterdam data on soil-pile interaction in Chapter 8 and building deformations in Chapter 9. The last step of the damage assessment procedure, the damage category of the building, is determined for the buildings influenced by the leakage incidents of Vijzelgracht in Chapter 10. Conclusions and recommendations for further research are given in Chapter 11.

CHAPTER 2 LITERATURE REVIEW

2.1 Introduction

Assessing the response of (piled) buildings to excavation-induced displacements involves both geotechnical and structural aspects. First, the excavation imposes displacements and stress changes on its surroundings in so-called green field conditions. The second important aspect is the response of the building. On both topics, an extensive amount of literature is available, of which the most relevant articles are reported in this chapter. The key question in predicting the response of the (piled) building to the changing ground conditions is however the interaction between the two aspects.

- The soil displacements cause an effect in the building such as deformations, strain and sometimes cracks or other types of damage.
- The presence of the building modifies the soil displacements immediately beneath it.

For piled buildings, additionally, the soil – pile and pile- building interaction become part of the system. The main focus of this study is summarized in
Figure 2.1.

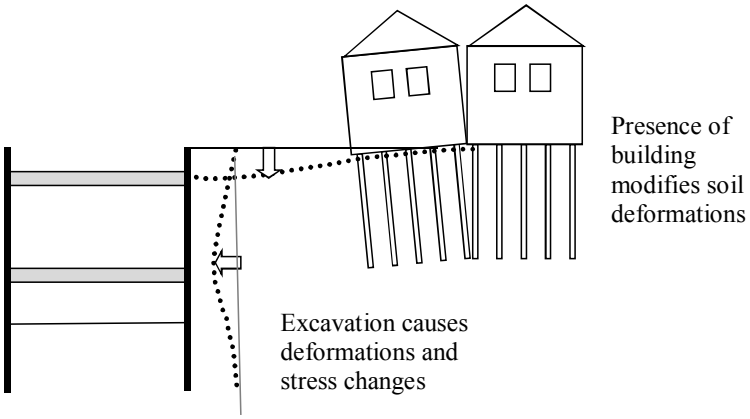


Figure 2.1 Interaction between excavation and adjacent buildings

2.2 Deep excavations

The first step in the prediction of building response to excavations is to predict the green field displacements. Ground movements related to the construction of deep excavations may originate from multiple sources, such as:

- Installation of walls and other construction elements, including densification caused by vibrations
- Excavation and associated deformation of the construction parts (walls and struts)
- Possible lowering of groundwater levels
- Consolidation effects due to all activities mentioned above.

Several methods exist to determine these ground movements. Some of these methods include all construction activities, whereas others only describe a specific aspect, so that the different contributions have to be added together. Section 2.2.1 presents empirical results for displacements due to the combined effect of all activities, whereas section 2.2.2 presents data on the displacements caused by the excavation itself. Prediction of effects of installation of walls are shortly presented in section 0.

2.2.1 Empirical methods, all construction activities combined

Methods that include all construction activities are mostly empirical, due to the complex nature of the construction, for example the early work by Peck (1969) and Goldberg et al. (1976).

Peck (1969) published graphs to conservatively estimate settlements caused by excavations, mainly based on projects from Chicago around that time. The projects usually involved temporary construction with several wall types, such as Berliner walls and sheet pile walls. His empirical method distinguishes between sands, stiff clays and soft clays. Peck's method includes all building activities, the stability of the excavation and even consolidation during construction. Peck's settlement envelopes are designed to be conservative. Peck relates the settlement of the ground level, normalized by the depth of the excavation (H), to the distance from the excavation, also normalized to its depth. For sand and hard clays, the maximum settlement directly beside the wall is 0-1% H and reaches to a distance of about 2H, depending on the thickness of the clay, the stability of the excavation and the workmanship of the crew. For soft clays, the maximum settlement directly beside the wall is 1-2%H and reaches to a distance of 3 to 4H, see Figure 2.2. The use of Peck's model is restricted to excavations in which the supports have been installed at an early depth, because late installation is noted as an important cause of subsequent displacement. The work by Peck was extended by Goldberg et al. (1976) to include more wall types. Goldberg et al. found a factor of 0.5-2.0 between the vertical soil movements behind the wall and the horizontal wall deflection. Soil settlements behind the wall are generally less than 0.5% of the excavation depth in sands and stiff clays, and over 1% for soft clays (except for pre-stressed diaphragm walls which stay within 0.25%H). The observed smaller displacements compared to Figure 2.2 are explained by improvements of excavation and support techniques over time.

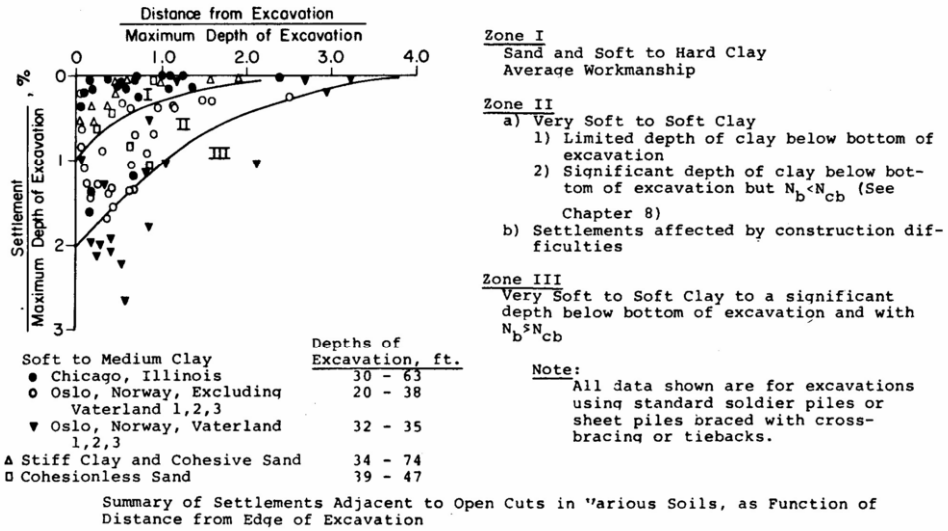


Figure 2.2 Settlements caused by all activities relating to deep excavations in various soils by Peck (1969)

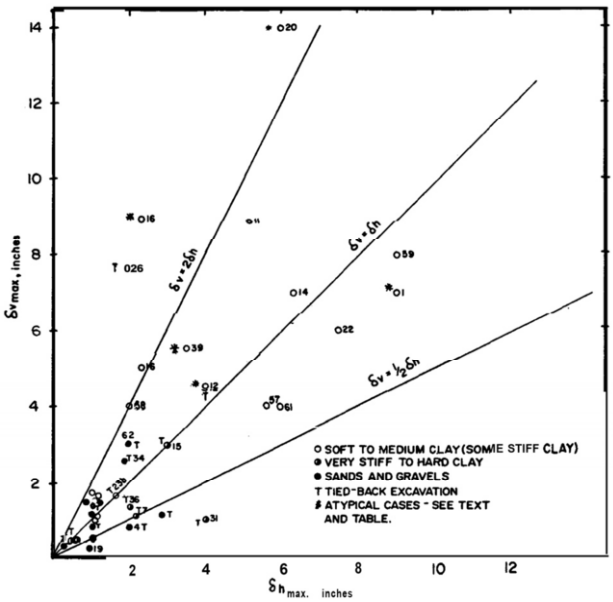


Figure 2.3 Wall deflection compared to ground settlements for soft soils by (Goldberg et al., 1976)

In soft clays, the settlements are generally well in excess of the horizontal wall deformation, as shown in Figure 2.3. This is attributed to consolidation settlements due to lowering of pore pressures outside the excavation.

In more recent literature, see section 2.2.2, the main sources of ground displacements are usually considered separately, with a clear focus on the effect of the excavation, with or without the effect of consolidation.

2.2.2 Empirical methods, effect of excavation and installation

Clough and O'Rourke (1990) extended the work by Goldberg et al. and Peck, but excluded the cases with unusual construction effects or with late strut installation and focussed on sheet piles and soldier piles with struts. All displacements they presented are caused by excavation works and normal installation of walls and struts. Depending on the presence and number of struts, the deflected shape of the wall is attributed to cantilever or deep movement deformation, as can be seen in Figure 2.4. In stiff clays, residual soils and sands the maximum horizontal wall deflection tends to average about 0.2% of the excavation depth with a maximum soil settlement behind the wall of about 0.15% - 0.3% of the excavation depth. The zone of influence reaches to a distance of 3 times the excavation depth. The design graph, as shown in Figure 2.5, includes the type of wall, although this proved to be not very important in these cases.

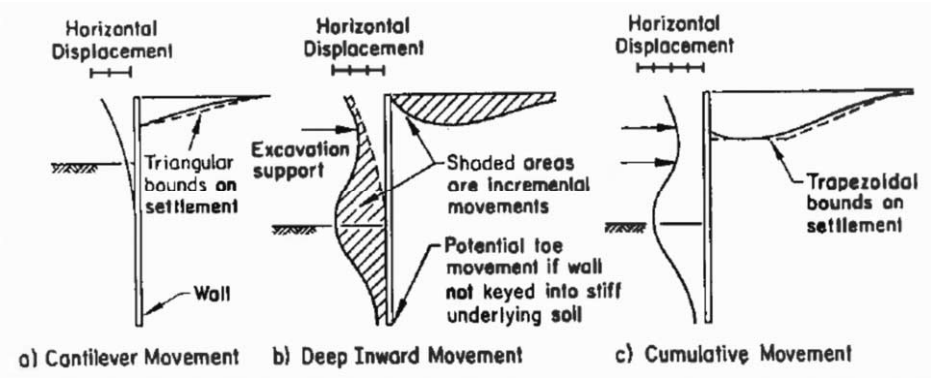


Figure 2.4 Typical profiles of movement for braced and tied-back walls (Clough and O'Rourke, 1990)

In soft clay the data from Clough and O'Rourke (1990) show a significant influence of the wall stiffness and support spacing on the wall deflection. Generally the same maximum settlements as observed by Peck (1969) are found, see Figure 2.6. The surface settlement profile from the edge of the excavation shows that the maximum settlement occurs in a zone up to 0.75 times the excavation depth from the wall. The settlement decreases linearly to zero at a distance of twice the excavation depth.

For design purpose Clough and O'Rourke (1990) recommended dimensionless settlement envelopes for estimating the distribution of ground settlement adjacent to excavations in different soil conditions, see Figure 2.7.

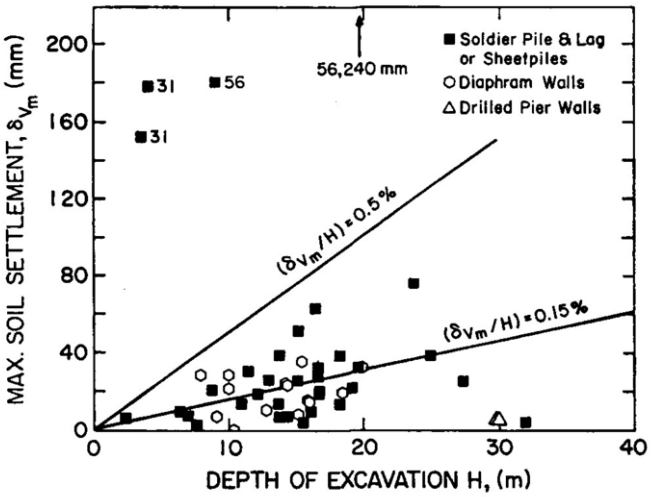


Figure 2.5 Observed maximum wall deflection and settlements for stiff clays, residual soils and sands (Clough and O'Rourke, 1990)

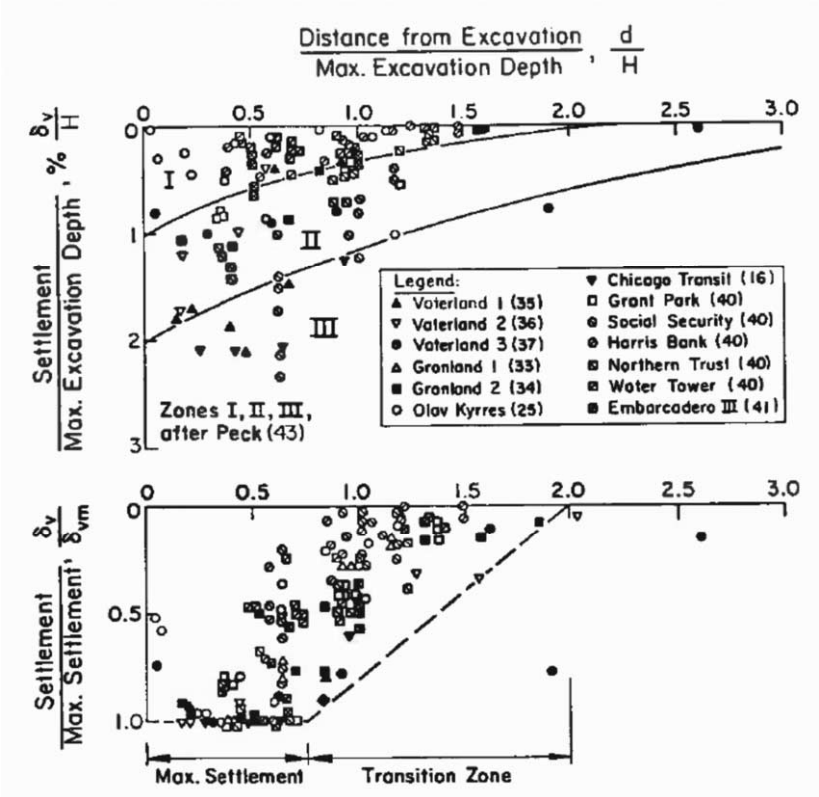


Figure 2.6 Measured settlements adjacent to excavations in soft to medium clay (Clough and O'Rourke, 1990)

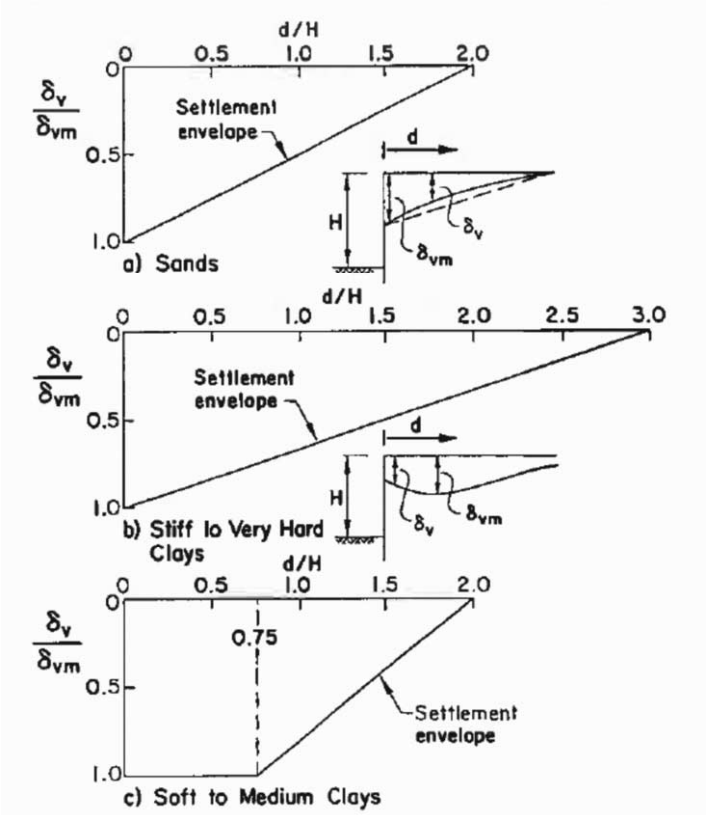


Figure 2.7 Dimensionless envelopes of settlement profiles for estimating settlement adjacent to excavations in different soil types (Clough and O'Rourke, 1990)

In the early 21st century the amount of data available to present in design charts grew steadily, especially as a result of an extensive survey presented by Long (2001) and later extended by Moormann and Moormann (2002) to over 500 cases. For excavations in stiff clay, the average maximum wall deflection is 0.16-0.19% H (where H is the excavation depth) and the average maximum vertical soil settlement is 0.12-0.20% H (Long, 2001). For excavations with struts in soft clay, the average maximum wall deflection is 0.39% H with an average maximum vertical settlement of 0.50% H when there is a high factor of safety against basal heave, or about double that amount for lower factors of safety. For top-down construction similar values have been found as for propped and anchored walls.

The extended database by Moormann and Moormann (2002) concentrates on excavations in soft soils (c_u<75 kPa) and consists merely of cases collected between 1991 and 2001. The new data is plotted on the chart by Peck (1969), see Figure 2.9, to show that displacements are generally much smaller than Peck's cases, but with some large displacements in cases with soft soils and low factor of safety against basal heave. It is concluded from these data that technological developments and increase in stiffness of retaining systems did not reduce the wall deflection. The maximum wall deflection averages 0.87% H for soft clays, with a

rather large variation, see Figure 2.8. Maximum vertical soil displacements tend to be 50%-200% of the horizontal deflection, with an average for soft clays of 1.1%H and occur within a distance smaller than 0.5H. Soil displacements tend to become zero at 2H, which is similar to results presented by Peck (1969).

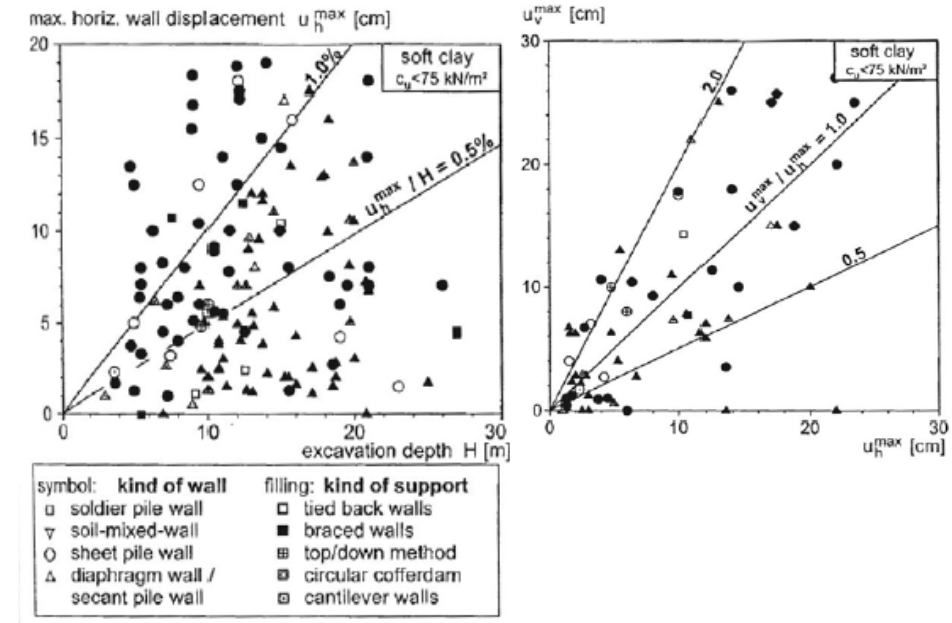


Figure 2.8 Horizontal displacement as a function of excavation depth (left) and versus vertical displacement (right) (Moormann and Moormann, 2002).

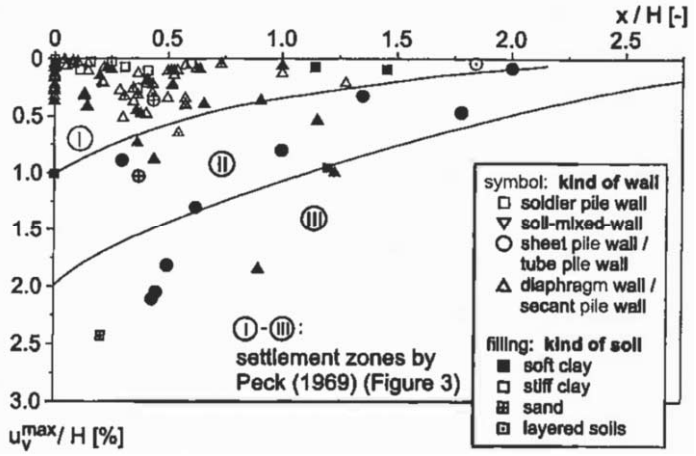


Figure 2.9 Database results plotted against settlement zones by Peck (1969) (Moormann and Moormann, 2002).

According to Moormann and Moormann (2002) there does not seem to be a relationship between the maximum horizontal deflection and the support spacing, although theoretically there should be one. The influence of the retaining wall stiffness could not be found as well, although in contrast to the data reported by Long (2001) top-down construction seems to induce smaller movements. Konstantakos (2008) introduced a database of 39 deep excavation projects from the United States of America. Most cases involve diaphragm walls and excavation depths ranging from 6 to 31 m in rather soft soils with high ground water tables. Settlements behind the wall were given for half of the number of cases and averaged about 0.2 – 0.4%H for braced and top-down constructions, which is generally similar to or a little less than the maximum horizontal deflection of the wall. A relationship is found with the basal stability factor (BS), giving a sharp distinction between BS < 1.8 and BS > 1.8. At BS<1.8 the deflection of the wall was much higher than 0.2%H.

Lam (2011) collected over 150 cases from 9 countries in a database of deep excavations in soft clays. Lam (2011) suggests to estimate the maximum soil displacement as equal to the maximum wall deflection (see MSD method in section 2.2.3). The maximum wall deflection is estimated based on the depth of the soft clay, the excavation depth and the distance between the supports, in combination with the characteristic reference shear strain in the soil (which could be typically between 1% and 5% in soft clay conditions).

2.2.3 Semi-empirical methods, shape of settlement trough due to excavation

Most literature presented in the first part of this chapter focuses on the maximum wall deflection and settlement behind the wall. However, the shape of the settlement trough especially determines the deformation of the building and thus the strains within it. Some of the literature presented in sections 2.2.1 and 2.2.2 describe the shape of the trough behind the wall based on empirical data. Other researchers have found, usually based on analytical or Finite Element models, specific shapes for certain support situations.

Bowles (1988) proposed an easy-to-use parabolic shape of the settlement curve, given a certain maximum value at the location of the wall:

$$S(x) = S_{\max}\left(\frac{W-x}{W}\right)^2 \tag{2.1}$$

Where
x is the horizontal distance from the wall
S is the settlement at location x
S_{max} is the maximum settlement at the wall
W is the settlement trough width, given by Caspe (1966):

$$W_{caspe} = \left(H + H_d\right)\tan(45 - \varphi'/2) \tag{2.2}$$

With

$$H_d = 0.5 \cdot B \cdot \tan\left(45 - \frac{\varphi'}{2}\right) \text{ for soils with } \varphi' > 0$$

$$H_d = B \qquad \text{for cohesive soil}$$

Where H is the excavation depth and H_d is the influence depth below the excavation; φ' is the internal friction angle of the soil and B is the width of the excavation.

Peck's Gaussian curve for tunnelling (Peck 1969) can also be used for deep excavations, assuming the wall is located at the point of inflection and only displacements in hogging occur. Lee et al. (2007) describe this formula for excavations as:

$$S(x) = S_{\max} \cdot e^{\left(0.5 - 0.5\left(\frac{1+2x}{W}\right)^2\right)} \qquad (2.3)$$

The Gaussian shape with assumed trough width equal to 2i, with i = half the height of the excavation from Lee et al. (2007) compares well with the estimation of the trough width from Bowles (1988). The trough is constructed from the depth of zero moment in the wall at an angle of $(45 - \varphi'/2)$ to the vertical line to the ground surface. Lee et al. (2007) took φ' = 0 for soft clay to construct this line.

Rather than the fully hogging shapes, usually related to cantilever walls, some researchers have suggested a more complex shape with sagging just behind the wall and hogging a little further away for excavations with more than one level of supports.

Hsieh and Ou (1998) suggested, just like Clough and O'Rourke (1990), that the soil settlement profile behind the wall depends on the shape of the wall deflection. A concave type of soil displacement, in which maximum settlement occurs at a distance away from the wall, is expected if the wall shows deep inward movement. Hsieh and Ou (1998) presented settlement profiles versus the distance from the wall normalized by the excavation depth based on 10 case histories from Taipei, Taiwan. For the concaved settlement profile Hsieh and Ou (1998) concluded that the distance from the wall to the point where the maximum ground surface settlement occurred was approximately equal to half the excavated depth (rather than 75% as presented by Clough and O'Rourke (1990). See Figure 2.10 for the corresponding wall deflection and surface settlement profile.

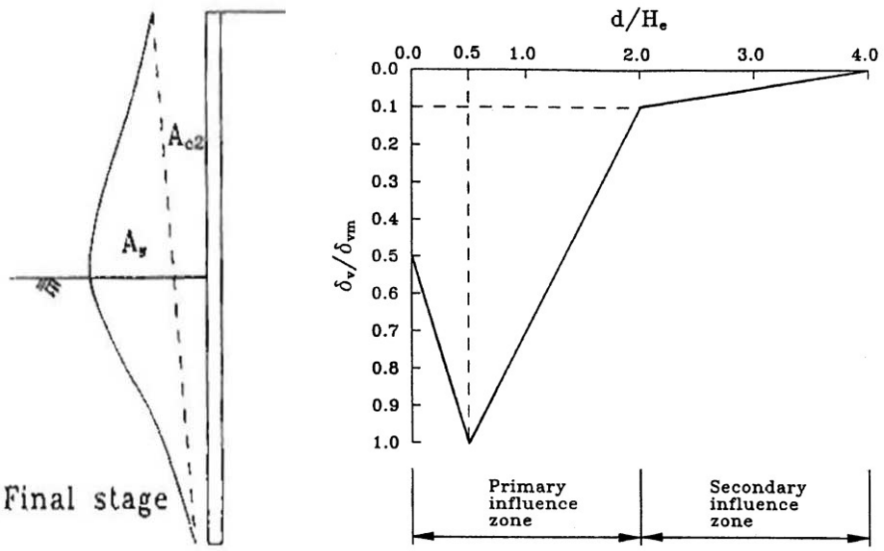


Figure 2.10 Shape of settlement trough by Hsieh and Ou (1998) for deep inward wall deflection

A more analytical approach is taken by Bolton et al. (2008). They describe a unified design method developed based on the use of plastic deformation mechanisms. The method, called Mobilizable Strength Method (MSD) combines equilibrium of the wall with the deformation of the wall and the soil. This approach has been developed over the last 10 years and is successfully validated for undrained analysis of deep excavations in clays (both in the field and in centrifuge modelling) and checked against numerical modelling for example in Bolton et al. (2008) and Osman and Bolton (2007).

The deformations of the retaining wall and the soil behind it are described in each phase from the level of the lowest strut downward and these increments are than added for an overall deformation pattern. Bolton et al. (2008) use a cosine function for the wall deflection. Each excavation phase will increase the maximum deformation of the wall and based on this maximum and the cosines function, the mobilized shear strain and the energy needed to obtain this are calculated. The total amount of energy needed to deform the wall and the soil are balanced. The new shear strain for each soil layer is deduced using a real stress-strain curve (thus including non linearity).

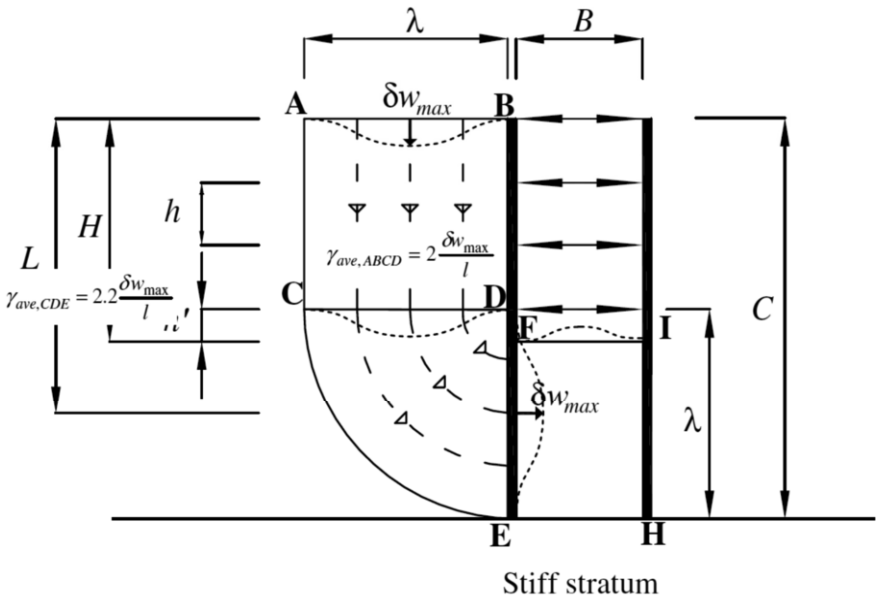
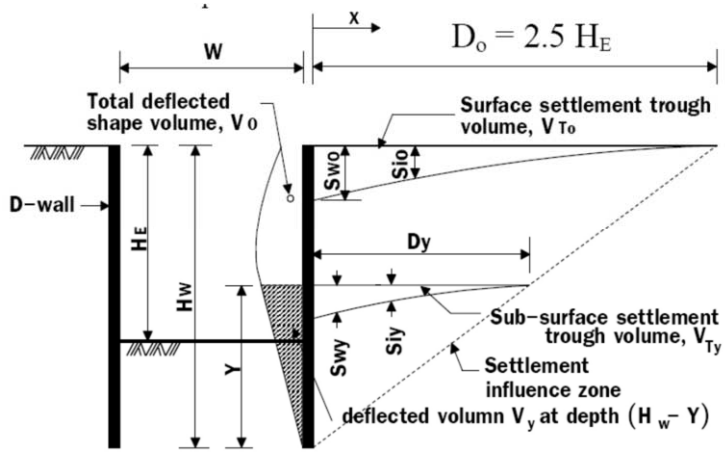


Figure 2.11 Incremental displacement field for narrow excavations (Bolton et al., 2008)

The MSD method combines an analytical approach based on equilibrium with an empirical approach for the shape and maximum deformation of the wall (see Figure 2.11). It explains why and how there is a relationship between the shape of the wall deflection and the soil displacements and soil strain pattern, as described earlier in this section based on empirical data. The method is extended and validated by Lam (2011) for soft clay conditions and includes narrow excavations and floating or embedded walls. The method is considered conservative in the sense that the maximum displacement behind the wall is equal to the wall deflection and that stiffness of any sand layers present is usually assumed equal to the clays. The method is not designed for deep excavations in sands, but layered soils can be taken into account.

Another simplified prediction of subsurface settlement can be carried out according to Aye et al. (2006). The settlement influence zone is assumed to decrease with depth from "D_0" at the surface to zero at the wall toe. With the assumption of a linear relationship between the volume of deflected wall shape and the volume of settlement trough at any depth within settlement influence zone, subsurface settlement at different depths can be calculated.



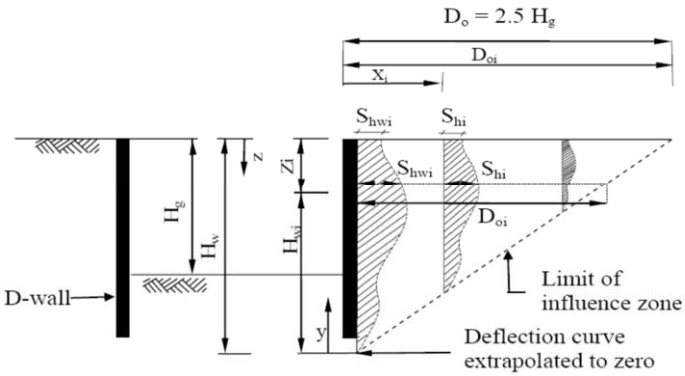
$$S_{WO} = \frac{4V_O}{D_O}$$

$$S_{io} = S_{WO} * \left(\frac{x}{D_O}\right)^2$$

$$D_Y = Y * \frac{D_O}{H_W}$$

$$V_{TY} = V_Y * \frac{V_{TO}}{V_O}$$

(a)



$$D_{Oi} = \frac{D_O}{H_W} * H_{Wi}$$

$$H_{Wi} - H_W - Z_i$$

$$S_{hi} = S_{hwi} * \frac{D_{Oi} - X_i}{D_{Oi}}$$

(b)

Figure 2.12 Subsurface soil displacements by Aye et al. (2006) with vertical ground displacements (a) and horizontal ground displacements (b)

The influence distance of horizontal displacement behind the diaphragm wall is assumed to be 2.5 H_g at ground level. The influence depth of the horizontal displacement is a depth at zero diaphragm wall deflection, Hw, which can be obtained by extrapolating the diaphragm wall deflection profile. The horizontal ground movement influence zone was constructed by connecting the end points of D_o and H_w as shown in Figure 2.12(b). The horizontal displacement is assumed to decrease linearly with distance from the wall, with the maximum found at wall face and zero at the end of the influence zone. By using the method proposed by Aye et al. (2006) in Figure 2.12 assuming a linear relationship for horizontal and vertical sub-surface displacements with depth, the absolute displacement of the soil at depth can be larger than at the surface, leading to larger differential settlements at depth.

2.2.4 Predicting displacements due to installation of diaphragm walls

Stresses in the soil around retaining walls not only change during excavation, but also during installation of the wall. These changes may be due to dynamic effects during sheet pile driving or change of horizontal effective stress in case of bored or auger piles and diaphragm walls. These stress changes lead to soil displacements. This section gives a short overview of some of the methods available for predicting wall installation effects for diaphragm walls.

Clough and O'Rourke (1990) show the amount of settlement found behind a diaphragm wall after installation as a function of the depth of the wall for several types of soil.

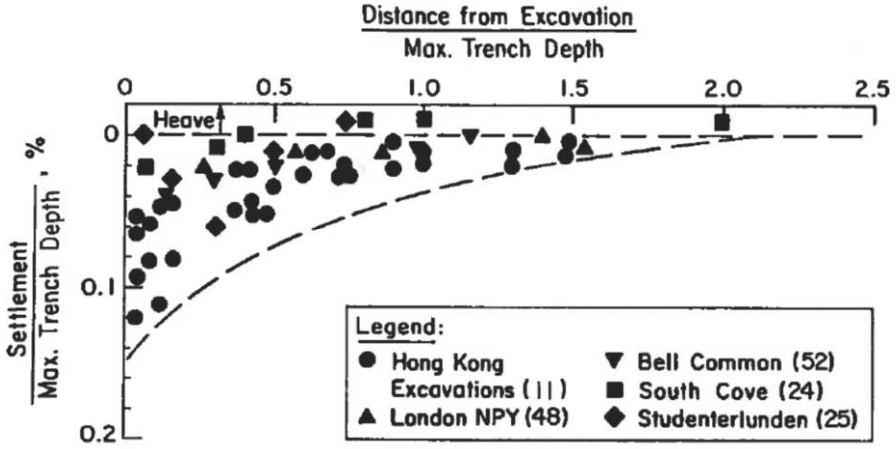


Figure 2.13 Settlement due to installation of a diaphragm wall (Clough and O'Rourke, 1990)

Soil types include granular soil (Hong Kong, but extremely deep panels, large settlements), soft to medium clay (Studenterlunden, Norway), stiff to very hard clay (London, Bell Common, South Cove). The upper bound of the settlement data in Figure 2.13 is largely influenced by the Hong Kong data, which were not fully representative due to problems with ground-water lowering, see Chapter 3. Clough and O'Rourke (1990) overestimate the ground movements in cases of stiff clays and good workmanship (which would include small panel lengths and high slurry levels).

Other authors, such as Leung and Ng (2007) and Ter Linde (1999), have found that not only the depth of the wall but also the length of the panels, the margin of safety against trench instability (depending on the slurry level) and the amount of time needed for the construction of a panel influence the amount of settlement around the diaphragm wall. At the Tramtunnel in The Hague, installation effects of diaphragm walls were measured for a 30m deep wall with 1.5m wall thickness and panel widths of 4-5m. Ter Linde (1999) confirms, as presented in Figure 2.14, the general trend that with a high factor of safety (1.3-1.5, according to DIN 4126) the settlement (of the building or the soil) can be limited to 5-6 mm at 2-3 m distance.

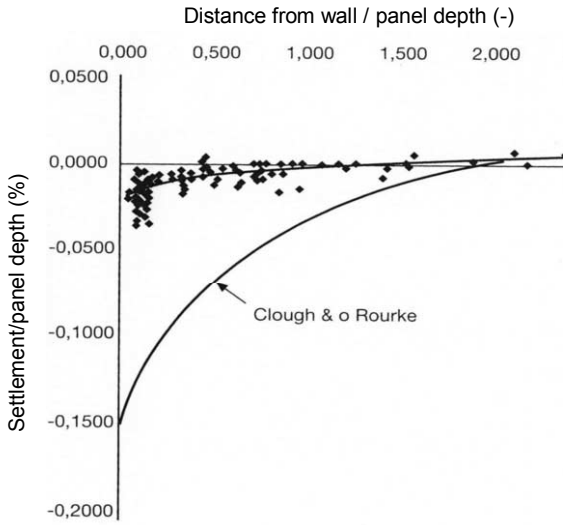


Figure 2.14 Settlement due to installation of a diaphragm wall (Ter Linde, 1999)

CIRIA report 580 (Gaba et al., 2003) summarizes horizontal and vertical wall movements due to installation of diaphragm walls and bored pile walls in stiff clays (see Figure 2.15 and Table 2.1). The results fall between the upper bound by Clough and O'Rourke (1990) and the values by Ter Linde (1999).

Table 2.1 Movements due to wall installation (Gaba et al., 2003)

Wall type	**Horizontal movements**		**Vertical movements**	
	Max % depth wall	Extent influence (*Hw)	Max % depth wall	Extent influence (*Hw)
Contiguous bored pile	0.04	1.5	0.04	2
Secant bored pile	0.08	1.5	0.05	2
Diaphragm walls	0.05	1.5	0.05	1.5

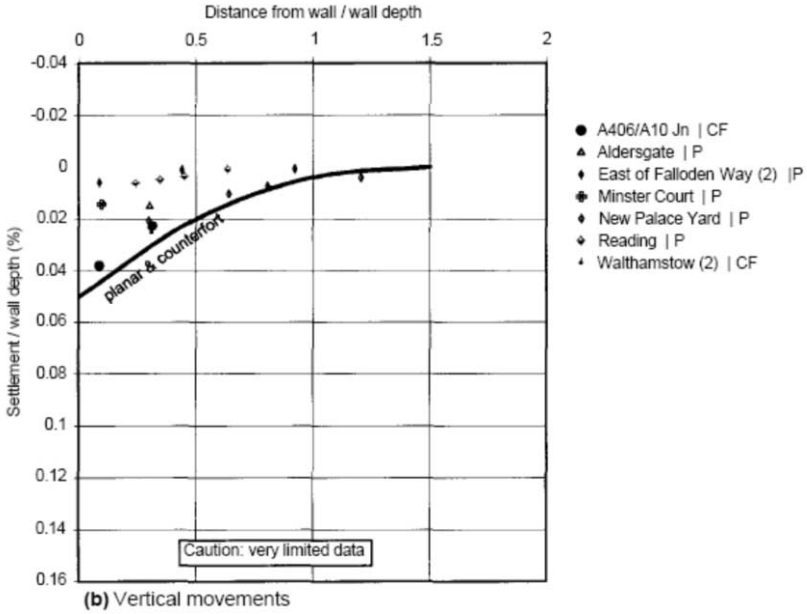


Figure 2.15 Vertical displacements due to diaphragm wall installation (Gaba et al. 2003)

Performance of geotechnical models for soil displacements

A lot of experience exists in the use of models (whether finite element or analytical) for deep excavations. Most experiences are either described on a case by case basis or never published at all. Some relevant literature is available in which for several cases measurements and models have been compared.

A database established by Konstantakos (2008) was used to perform back analysis on several case studies. Although in some cases not all information necessary was available, one of the main findings is that wall deformations initially are cantilever shaped, even if multiple struts or anchors have been installed. Only by significantly reducing the stiffness of the top levels of struts would the predicted deformation match the measurements. This effect has also been shown in several other cases, such as at Pannerdensch Kanaal (COB, 2009). This phenomenon is expected to be caused by the installation process of the struts and or initial deformations of the anchors before they reach their working load. In top down construction, the top slab stiffness is usually only about 10-15% lower in the field than the theoretical value, probably due to concrete shrinkage. The French MOMIS database (Mestat et al., 2004) compares model results with measurements in order to estimate the performance of the models and generate recommendations for future applications. Its applications include embankments, underground structures and shallow foundations. For sheet pile walls a total number of 77 projects with wall deflections were available and 38 for settlements behind the wall at the time of publication. Projects were located in Europe (over 50%), followed by Asia, North America, Africa and then South America. Wall lengths range from 15-30 m and

excavation depths from 5-20 m. Overall wall deflections measured fall within a margin of 25% from the calculated ones (for 54% of the total) or within 50% (for 75% of the total). Due to the large variety of cases and numerical methods used, it is difficult to generalize conclusions, but Mestat et al. clearly find that settlements behind the wall are usually under predicted. Cases with diaphragm wall deflections (98) give similar results, although the absolute values are smaller. Displacements behind the wall are generally more consistent with calculated ones than for sheet piles. The settlement behind the wall in general is smaller than the maximum wall deflection, but can also be much larger (up to a factor of 2 for sheet piles and 2.5 for diaphragm walls).

2.3 Building behaviour

2.3.1 Causes of damage in buildings

When evaluating a damaged building, it is important to distinguish between different deformation modes related to damage. This section describes the identification of cracks related to deformation of the foundation (such as caused by excavations or tunnelling). Cracks are the main indicator of damage to a building. Cracks can be caused by external effects, such as temperature/moisture/chemical reactions or by deformations of the building. Already during construction, the building deforms under its self-weight. Bonshor and Bonshor (1996) distinguish between several types of cracks as shown in Figure 2.17. Cracks that are of uniform width throughout their length are usually temperature or moisture related and unlikely to progress in time (once cracked the stresses have gone and unless bigger temperature changes or moisture changes than before occur, no widening of the cracks is expected). Temperature cracks are usually much less than 5 mm. Cracks due to changes in moisture content of the soil (e.g. when a tree is removed) will be caused by reversion of the soil to its original volume, leading to a relatively rapid change. Fast changes are usually more damaging than slower changes.
Cracks due to deformations of the building have a number of specific characteristics:

- Cracks are usually tapered (small at one end and wider at the other).
- Significant cracks are often seen on the inside and the outside of the building.
- Cracks continue below and above ground level.

The location and the direction of the crack are directly related to the deformation mode (hogging, sagging). Other damage might include broken windows and jamming doors because windows and door openings are distorted, sloping floors and tilting walls (see Figure 2.16 for tilting walls).

BRE (1995) shows how to identify cracks by their nature and divides between tensile cracks, compressive cracks and shear cracks. Compressive cracks often show small flakes of brick squeezed from the surface or localised crushing. Shear cracks (Figure 2.16) show relative movement of points on opposite side of the crack. When the cracks originate from foundation movement, they tend to concentrate in areas where maximum distortion occurs, or at weak points in the structure.



Figure 2.16 Crack due to shear deformation (left) and relative rotation of one building to the other (right)



Figure 2.17 Crack patterns due to different deformation modes (Bonshor and Bonshor, 1996)

2.3.2 Classification of damage

The nature of the crack does not say anything about the amount of damage it causes. Classification of damage is usually based on the size and number of visible cracks, but more important also is the effect these cracks have on the appearance or use of the building. This is related to the necessary amount and ease of repair. BRE (1995) summarizes the amount of damage into three broad categories:

- Aesthetic damage comprises damage that affects only the appearance of the property.
- Serviceability damage includes cracking and distortion that impair the weather tightness or other function of the wall (eg sound insulation), fracturing of service pipes and jamming of doors and windows.
- Stability damage is present where there is an unacceptable risk that some part of the structure will collapse unless preventive action is taken.

Burland et al. (1977) refine these broad categories into six categories of damage, numbered 0 to 5 with increasing severity, see Table 2.2. The classification is based on the ease of repair of visible damage to the building fabric and structure. For most cases, Categories 0, 1 and 2 can be taken to represent ‘aesthetic’ damage, Categories 3 and 4 ‘serviceability’ damage and Category 5 ‘stability’ damage. This classification is widely used for building damage assessment due to tunnelling, deep excavations and other causes. It must be emphasized that Table 2.2 relates to visible damage and more stringent criteria may be necessary where damage may lead to corrosion, penetration or leakage of harmful liquids and gases or structural failure. Localized effects, such as the instability of an arch over a doorway, may influence the categorization. Judgment is always required in ascribing an appropriate category to a given situation.

Table 2.2 Classification of visible damage by Burland et al. (1977), slightly modified by BRE (1995)

Category of damage	**Normal degree of severity**	**Description of typical damage** **Ease of repair in italic type**
0	Negligible	Hairline cracks of less than about 0.1 mm
1	Very slight	Fine cracks which can be treated easily using normal decoration. Damage generally restricted to internal wall finishes; Close inspection may reveal some cracks in external brickwork or masonry. Typical crack widths up to 1 mm.
2	Slight	Cracks easily filled. Redecoration probably required. Recurrent cracks can be masked by suitable linings. Cracks may be visible externally and some repoin-ting may be required to ensure weather-tightness. Doors and windows may stick slightly. Typical crack widths up to 5 mm.
3	Moderate	Cracks which require some opening up and can be patched by a mason. Repointing of external brickwork and possibly a small amount of brickwork to be replaced. Doors and windows sticking. Service pipes may fracture. Weather-tightness often impaired. Typical crack widths 5 -15 mm, or several > 3 mm.
4	Severe	Extensive repair work involving breaking-out and replacing sections of walls, especially over doors and windows. Windows and door frames distorted, floor sloping noticeably*. Walls leaning or bulging noticeably*, some loss of bearing in beams. Service pipes disrupted. Typical crack widths 15 - 25 mm, but also depending on the number of cracks.
5	Very severe	Structural damage which requires a major repair job, involving partial or complete rebuilding. Beams lose bearing, walls lean badly and require shoring. Windows broken with distortion. Danger of instability. Typical crack widths are greater than 25 mm, but depends on number of cracks.

* Local deviation of slope, from the horizontal or vertical, of more than 1/100 will normally be clearly visible. Overall deviations in excess of 1/150 are undesirable.

The following points should be noted about this table, according to BRE (1995):

- The classification applies only to brick or block work and is not intended to be applied to reinforced concrete elements.
- The classification relates only to visible damage at a given time and not its cause or possible progression, which should be considered separately.
- Great care must be taken to ensure that the classification of damage is not based solely on crack width since this factor alone can produce a misleading concept of the true scale of the damage. It is the ease of repair of the damage that is the key factor in determining the overall category of damage for the whole building.

2.3.3 Criteria for damage to buildings

Damage often originates from curvature of the building, which can be determined as the second derivative of the settlement. More curvature means higher strains and more damage. The most likely deformation modes in case of excavations are the 'hogging' mode and the 'sagging' mode, such as described by Burland and Wroth (1974). Hogging is the mode where the sides of the building settle more than the average, whereas in sagging the centrepiece of the building settles most (Figure 2.17). Curvature can be calculated as derivative of the deformation and uses symbol κ. Similar to curvature the radius R (R=1/ κ) is an indicator for possible damage. More curvature means higher strains and more damage. This means that buildings that rotate rather than bend usually experience less damage. Curvature of the building can be specified in more detail into several modes of deformation, such as shear deformation and bending as well as extension or compression. Generally, a combination of deformation modes occurs simultaneously.

This report will follow the definitions of ground and foundation movements as proposed by Elshafie (2008), which follows up on the work by Burland and Wroth (1974), Boscardin and Cording (1989), Burland et al. (2004) and Mair et al. (1996). See also Figure 2.18.

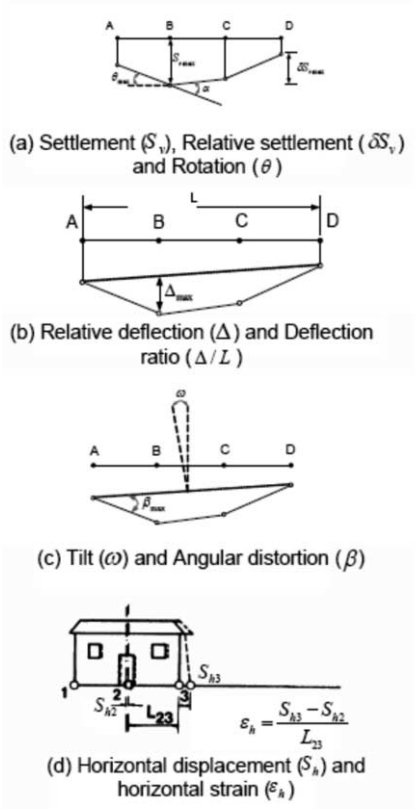


Figure 2.18 Definitions used in this research as given by Elshafie (2008)

Limits for damage to buildings are available in various forms and can be derived either theoretically or from field observations. The simplest limits are given in the form of maximum deformation of the structure or differential displacement; others describe the maximum rotation of the building, the deflection ratio or relative rotation. Calculating strains from the deformation (by using deflection ratio, relative rotation or any other method such as fully coupled FEM) is currently the state of the art for predicting building damage from expected deformations. The first criteria for assessing building damage were mainly derived for damage due to the self-weight of the building. Later, from Rankin (1988) and onwards, specific attention has been given to the damage caused by construction activities. For damage due to self-weight of the building in unreinforced load bearing walls, such as the masonry walls in Amsterdam, the deflection ratio Δ/L is used and the ratio L/H plays an important role. Sagging is in that case the main deformation mode and limiting values are given in Table 2.3.

Table 2.3 Empirical values limiting building deformations for unreinforced load bearing walls

Damage description	**Limiting Δ/L**	**Source**
Sagging $L/H \leq 3$	1/3300-1/2500	(Polshin and Tokar 1957)
Sagging $L/H \geq 5$	1/2000-1/1400	
Sagging	1/2500	(Meyerhof 1953)

For damage related to external sources, Rankin (1988) states that damage in any building experiencing not more than 10 mm of settlement and a maximum slope of any part of the building of 1/500 is unlikely, even for superficial damage. Rankin also gives values for moderate and severe damage, but those are not supported by data. Rankin does not include horizontal deformations in the criteria, but does mention them as being important. Buildings are more vulnerable in hogging deformation than in sagging. For construction related damage, Table 2.4 and Table 2.5 summarize the limiting values of relative rotation and deflection ratio for frame structures and unreinforced load bearing walls respectively.

Table 2.4 Limiting relative rotation for frame structures

Damage description	**Limiting relative rotation**	**Source**
superficial damage unlikely	1/500	(Rankin, 1988)

Table 2.5 Limiting deflection ratio for unreinforced load bearing walls

Damage description	**Limiting Δ/L**	**Source**
hogging L/H = 1	1/5000	(Burland and Wroth, 1974)
hogging L/H = 5	1/2500	

Deflection ratio and relative rotation are used as measure for damage, whereas the cracks themselves will be caused more directly by the amount of strain in the building. Boscardin and Cording (1989) related the degree of damage to tensile strains from Bjerrum (1963) and Skempton and MacDonald (1956). This work was later updated by Son and Cording (2005). An overview of these values is given in Table 2.6.

Table 2.6 Summary of limiting tensile strains for different damage categories

Category of damage	Normal degree of severity	Approximate crack widths (mm)	Limiting tensile strain (%)	
		(Burland and Wroth 1974)	(Son + Cording 2005)	(Boscardin+Cording 1989), (Burland 1995)
0	negligible	<0.1	5.00E-04	5.00E-04
1	very slight	0.1 - 1	7.50E-04	7.50E-04
2	slight	1-5	1.67E-03	1.50E-03
3	moderate to severe	5-15 or several cracks ≥3	3.33E-03	3.00E-03
4	severe	15-25, depends on number of cracks	> 3.33E-03	>3.00E-03
5	very severe	> 25, or large number		

These values are also used by Boone et al. (1999), who show that a better agreement between the damage and crack width (calculated values according to section 2.3.4, not observed values) was found by increasing the threshold values in the fourth column of Table 2.6 by a factor of 1.5. Boone (2001) compiled an overview of physical tests, which show critical strains at the onset of cracks for poor mortar and brick construction. Brick buildings tend to crack at 0.04-0.06% strain, or even from 0.02% based on full-scale tests.

Zhang and Ng (2005, 2007) obtained limiting tensile strains by statistically comparing field data of damage with tensile strains based on over 200 cases from the databases of Skempton and MacDonald (1956), Grant et al. (1974) and over 180 cases from South-east Asia. The cases mainly consist of buildings loaded by self-weight. They distinguish between tolerable and non-tolerable cases, with non-tolerable including architectural and functional issues, cracks in panels and even structural damage (in 20 buildings). In terms of damage category, it seems that this study determines the threshold between category 2 and category 3 as the boundary between tolerable and intolerable, although this is not stated in any of the papers. Most of the buildings are situated on clay. Based on a statistical analysis they find for tolerable cases that the limiting relative rotation is in the range of 0.002-0.006 (1/500-1/167) and limiting deformations in the order of 100-220 mm for deep and shallow foundations respectively, but with large standard deviations (about as much as the average values). Some buildings experienced functional and architectural problems even when relative rotations were smaller than 1/1000.

Zhang and Ng (2007) also compared the characteristics of the buildings and the following conclusions are supported by their data:

- Buildings with deep foundations as opposed to shallow foundations are found to experience damage (being intolerable) at lower values of building deformations (maximum) and relative rotations. This effect might be related to the way the decision between tolerable and intolerable is made. Buildings with shallow foundations are more likely to spread the deformation or relative rotation more smoothly than buildings on individual piles, which may lead to lower experienced damage.
- Buildings on clay have larger limiting tolerable vertical deformations compared to those on sand and fill, mainly supported by the slower occurrence of soil settlements with time. Tolerable soil settlements for sand tend to be half those for clay, but tolerable relative rotations do not show large differences for clay or sand.
- Given the same vertical settlement, frame structures can accommodate differential displacements by deformation of the beams, whereas load-bearing walls need to deform, which leads to cracking more easily. This leads to a 20-25% lower tolerable relative rotation and deformation for load bearing walls.

The method used in these papers is interesting because rather than being derived from a simplified theoretical understanding of the building it relates to visual inspections of buildings, just like the earlier empirical methods for self-weight induced deformations. The results obtained are within reasonable boundaries using the framework of the limiting tensile strains, but might possibly be improved when linked to damage categories as specified by Burland et al. (1977).

2.3.4 Limiting tensile strain method

Burland and Wroth (1974) first introduced the concept of limiting tensile strain to translate the effect of ground displacement into strain in the building. The building is seen as a simple beam model. When soil displacements affect the building (or the beam) direct tensile strains occur due to bending deformation and diagonal strains due to shear deformation, generally both at the same time. Burland and Wroth introduced a relationship between the deflection and the maximum extreme fibre strain as well as the maximum diagonal strain. The load can be modelled by a central point load or a uniform load. In hogging, the neutral axis for bending is assumed at the bottom of the beam or wall and in sagging it remains at mid-height.

Table 2.7 gives the solutions for these four cases, based on Burland and Wroth (1974), but altered slightly according to nomenclature by Mair et al. (1996). These equations have formed the basis of work by many researchers assessing strains in buildings.

Table 2.7 Bending and shear strains from beam model

	Maximum strain (bending)	Diagonal strain (shear)
Central point load	$\frac{\Delta}{L}=\left[\frac{L}{12t}+\frac{3I}{2tLH}\frac{E}{G}\right]\varepsilon_{b\max}$	$\frac{\Delta}{L}=\left[1+\frac{HL^2}{18I}\frac{G}{E}\right]\varepsilon_{d\max}$
Uniform load	$\frac{\Delta}{L}=\left[\frac{5L}{48H}+\frac{3I}{2tLH}\frac{E}{G}\right]\varepsilon_{b\max}$	$\frac{\Delta}{L}=\left[\frac{1}{2}+\frac{5HL^2}{144I}\frac{G}{E}\right]\varepsilon_{d\max}$

In which:

Δ	mid span deflection
t	distance of the neutral axis to the edge of the beam (which is in a sagging case 0,5H if we assume the neutral axis in the middle, and H for the hogging case if we assume the neutral axis to be at the bottom)
H	height of the building from foundation to roof
L	length in sagging / hogging
G	shear modulus building
E	young's modulus building
I	moment of inertia of the building ($H^3/12$ for sagging and $H^3/3$ in hogging)
t	Distance to neutral axis = H/2 (sagging), H (hogging)
E/G	2.6 for masonry (elastic), 12.5 for frames
ε_h	horizontal strain
$\varepsilon_{b,\max}$	Maximum bending strain
$\varepsilon_{d,\max}$	Maximum diagonal strain

In contrast to the deformation of a building under its own weight as considered by Burland and Wroth, deformations caused by excavation or tunnelling cause horizontal strains as well. To account for excavation induced ground movements, an important adaption to this method was made by Boscardin and Cording (1989), by adding horizontal strains to the bending and shear deformations. In later work Burland, Mair and co-workers extended their framework to include horizontal strain as well. The total bending strain (which is the bending strain due to deflection and lateral extension) is obtained by directly adding the horizontal strain to the strain obtained in Table 2.7 by Mair et al. (1996):

$$\varepsilon_{b,tot}=\varepsilon_{b\max}+\varepsilon_h \tag{2.4}$$

The diagonal strain is more difficult to obtain, because it depends on the angle at which the strains appear. At the maximum angle (θ_{max}) with the horizontal the combined strain will be:

$$\varepsilon_{d,tot}=2\varepsilon_{d\max}\cos\theta_{\max}\sin\theta_{\max}+\varepsilon_h\cos^2\theta_{\max} \tag{2.5}$$

Burland et al. (2004) described this combined diagonal strain using Mohr's circle of strain

$$\varepsilon_{d,tot}=\sqrt{\left[\varepsilon^2{}_h\left[\frac{1-\nu}{2}\right]^2+\varepsilon^2{}_{d,\max}\right]}+\varepsilon_h\left[\frac{1-\nu}{2}\right] \tag{2.6}$$

Where ν is the Poisson's ratio.

Mair et al. (1996) used the same equation but assumed a Poisson's ratio of 0.3.

$$\varepsilon_{d,tot} = 0.35 \cdot \varepsilon_h + \left[\left(0.65 \cdot \varepsilon_h \right)^2 + \varepsilon^2_{d,\max} \right]^{0.5} \tag{2.7}$$

These authors compare the limiting tensile strains with the maximum combination of bending or shear strains and horizontal strain. As stated above, Boscardin and Cording (1989), who were the first who used this combination of horizontal and vertical deformations, based their relationships on angular distortion rather than deflection ratio. Their work was later updated by Cording et al. (2001) and Son and Cording (2005) to get a lateral strain independent of L/H, E/G and the position of the neutral axis, see Figure 2.19.

$$\varepsilon_{p(=d,tot)} = \varepsilon_{l(=h)} \cos^2 \theta_{\max} + \beta \sin \theta_{\max} \cos \theta_{\max} \tag{2.8}$$

with

$$\tan(2\theta_{\max}) = \frac{\beta}{\varepsilon_{l(=h)}}$$

Where:

θ is the direction of the crack, measured from a vertical plane

$\varepsilon_{p\,(=d,tot)}$ = principal tensile strain

$\varepsilon_{l\,(=h)}$ = lateral or horizontal strain

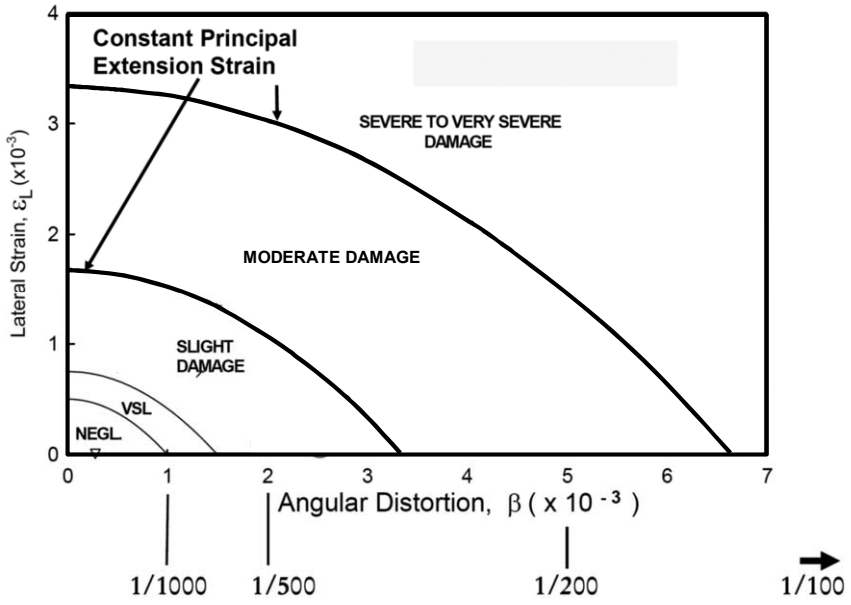


Figure 2.19 Relationship between angular distortion and horizontal strain (Cording et al. 2010)

Even as early as 1974 discussions started on the use of β versus Δ/L (Grant et al., 1974) and later this was returned to several times (e.g. Burland et al., 2004 and Netzel, 2009). Netzel (2009) shows that the translation of "real" situations to elastic beam models may give significant differences in using β or Δ/L. Even when it would be possible to find the theoretical strain in a building, it is still hard to assess what kind of damage will follow from it. The exact material parameters are usually not known and the history of the building and any previous loading are just as important as the additional strain levels. The relationship between damage and strain level in Figure 2.19 might be known for homogenous, individual parts of the building, but has to be tested more extensively for real buildings.

Rigid body tilt of a building can be included or excluded from the damage assessment. Usually rigid body tilt is considered not to contribute to the stresses and strains in the building and thus not to the damage. However, looking in a more detailed way, tilt causes indirect damage due to gravity forces on structural elements like walls. Leonards (1975) states that for framed structures on isolated footings, tilting contributes to stress and strain in the frame, unless each footing tilts or rotates through the same angle as the overall structure, which is unlikely. Burland et al. (1977) also suggested that accounting for tilt in frame buildings on separate footings might be quite inappropriate. Tilt is also difficult to ascertain unless several aspects of the distortion of the building are known. Measurements of deformation at the top of the building combined with the base provide an indication of tilt, which can also be obtained from direct tilt measurements.

Skempton and McDonald (1956) give an example of how to include tilt in Figure 2.20. A three-dimensional deformation contour of a building is projected, the tilt is considered as the rigid body rotation, in this case diagonally over the building. In any cross section (perpendicular to the excavation), this overall tilt is subtracted before calculating the deflection ratio. This procedure is repeated for the vertical translation. Both tilt and overall translation values are based on the deformations at the edges of the building. Any cross section of the building assessed can be corrected for the overall tilt and translation. This approach leads in plane strain deformations to the fact that tilt and translation are the same for each cross section. Tilt is rather easily calculated in plane strain as the connecting line between the outermost points of the building.

Almost all literature examples exclude the effect of tilt or use the approach as stated by Skempton and McDonald (1956), based on the deformation of the bottom of building. Only Son and Cording (2003) assess tilt from measurements at the top of the building.

In a row of attached buildings a separation between two tilting bodies would not result in high deflection ratios and thus not considered as severe damage, although it might be clearly visible damage that has to be repaired. This all makes tilt an important parameter when discussing excavation induced damage and it should always be made clear exactly in what way tilt is considered.

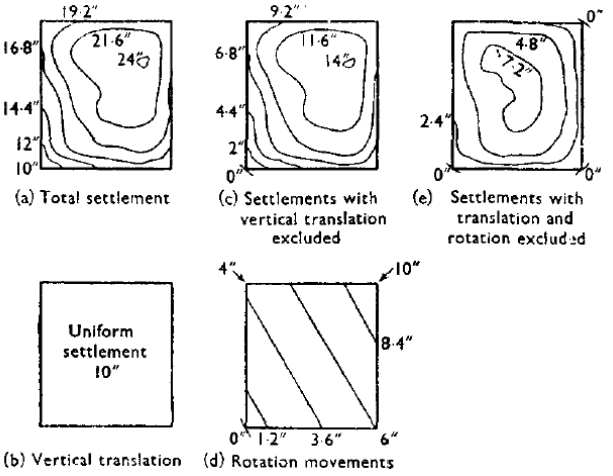


Figure 2.20 Building deformation including uniform settlement and tilt (Skempton and McDonald, 1956)

2.4 Interaction soil – building for shallow foundations

2.4.1 Introduction

So far, in this study, all excavation–induced displacements considered are green field displacements. These displacements are usually directly projected on the building, leading to bending and shear strains as discussed above. It is however known that the presence of the buildings also influences the settlement trough and the interface between building and soil influences the way the displacements are transferred to the building. This section deals with this interaction problem.

The following aspects of the buildings' presence are important to take into account:

- Building stiffness
- Building weight
- Interface between building and soil.

2.4.2 The effect of building stiffness

Potts and Addenbrooke (1997) produced a standard work on the influence of the building on tunnelling induced displacements. They present results of a parametric study in which the width of the structure, its bending and axial stiffness, its position relative to the tunnel and the depth of the tunnel are considered. The study is valid for typical London situations and typical tunnel dimensions and depths. Potts and Addenbrooke introduced relative stiffness parameters, which combine the bending and axial stiffness of the structure with the stiffness of the soil. Franzius et al. (2006) recommended modifications to the definitions of relative building stiffness in order to reduce the scatter in the data and to take 2D and 3D situations into account. Their revised bending stiffness and axial stiffness are defined as:

$$\rho^*_{mod} = \frac{EI}{E_s\ z_0 B^2 L}$$

$$\alpha^*_{mod} = \frac{EA}{E_s BL}$$

where
E is the stiffness of the building, E_s is a representative soil stiffness at 0.01% axial strain at half the tunnel depth, B is the width, L is the length of the building and z_0 is the depth of the tunnel.

Design curves were established for the likely modification to the green field settlement trough caused by a surface structure based on deflection ratio (DR) and horizontal strain. These modification factors M are the ratio between deformation of the building and the green field displacement (denoted with g) for various aspects:

- for sagging: $M^{DRsag} = DR_{sag}/DR^g_{sag}$
- for hogging: $M^{DRhog} = DR_{hog}/DR^g_{hog}$
- for horizontal strain in compression: $M^{\varepsilon hc} = \varepsilon_{hc}/\varepsilon^g_{hc}$
- for horizontal strain in tension: $M^{\varepsilon ht} = \varepsilon_{ht}/\varepsilon^g_{ht.}$

Goh (2010) modified the relative stiffnesses by Potts and Addenbrooke for deep excavations to:

$$\rho^*_{exc} = \frac{EI}{E_s L^3}$$

$$\alpha^*_{exc} = \frac{EA}{E_s B}$$

where EI is the building stiffness, Es a representative soil stiffness and L the length of the building in either hogging or sagging based on the greenfield settlement trough. EA is the axial stiffness of the building and B is the total length of the building.

The bending stiffness of the building can be assessed by taking into account the base slab, the floors and/or the walls and the amount of interaction between them.

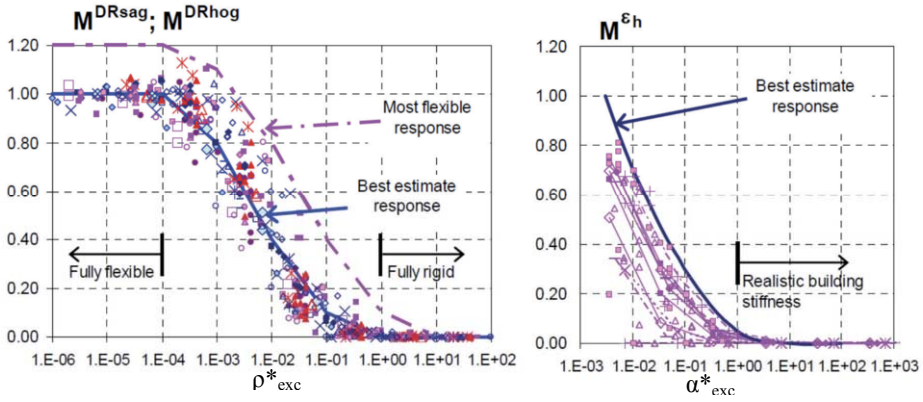


Figure 2.21 Design curves from Goh (2010) based on modified modification factors

2.4.3 The effect of building weight

Franzius et al. (2004) also included the effect of building weight. A parametric study in which combinations of building load and stiffness were considered, showed that the effect of the building weight is small since M_{DR} and $M_{\varepsilon h}$ increased with building load but decreased due to the larger stiffness of the building. Horizontal strains are influenced more by the building load; tensile strains doubled and compressive strains increased by 50%. Franzius et al. (2004) showed that this could be explained by two effects:

- the increase in stiffness in the top level reduces the horizontal movement, but
- the soil will be more able to transfer the strains to the building, resulting in a net increase in the building strains.

2.4.4 The effect of the interface between building and soil

Franzius and Potts (2006) varied the soil-structure interface and performed 3D FE analyses. For smooth interfaces, the horizontal strain in the building reduced dramatically, while M_{DR} values showed only a small reduction. When horizontal relative movements between the soil and building were allowed in a smooth soil-structure interface, there was a large reduction in $M\varepsilon h$ values whilst the M_{DR} values were less affected.

Several cases in the Jubilee Line Extension project have been investigated in this respect. Well known cases include the Treasury building, Elizabeth House and Neptune House (Mair, 2003). These cases showed that the deflection ratio of the buildings is often modified from the green field situations, except for very flexible buildings, and that buildings are less stiff in hogging than in sagging. Horizontal deformations usually are less for buildings than in green field situations, but also here exceptions exist, such as in case of foundations with individual footings. Dimmock and Mair (2008) reviewed cases in Moodkee Street (Neptune House, Murdoch House and Clegg House) and Keatons Estate and found that compared to the original Class A predictions (Mair and Taylor, 2001) the following adaptions to the modification factors by Potts and Addenbrooke (1997) would improve the results:

- In hogging use the bending stiffness of the foundation only
- Reduce the calculated bending stiffness in sagging by about one order of magnitude to include the effect of window and door openings.

The bending stiffness in hogging would thus be:

$$EI = EI_{foundation} = \frac{bd^3}{12} \tag{2.9}$$

Where

$E_{foundation}$ is $E_{concrete}$ (about 16,500 MPa) or $E_{masonry}$ (about 10,000 MPa)

b is 1 m for plane strain calculations

d is the thickness of the foundation slab.

This effect was studied in an experimental way by Elshafie (2008), who performed centrifuge tests on model buildings subject to excavation-induced ground displacements, see Figure 2.22. The tests included buildings made from micro-concrete with various stiffnesses, weights and with either a rough or smooth interface. Elshafie concluded that larger curvature of the building is found with decreasing bending stiffness, especially for a rough soil/building interface. Slip between the buildings and the soil surface was found and the horizontal displacement of the soil surface is significantly affected by the axial stiffness of the blocks. The effect of building weight (up to 40 kPa) was small (maximum about 10% increase in deflection ratio) as long as a high factor of stability (> 1.4) of the wall was maintained. The effect of the interface between the soil and the building is seen especially for buildings with low bending stiffness. Stiff buildings tend to tilt regardless of the interface. Horizontal displacements are clearly influenced by a smooth interface, leaving the green field soil displacements intact, even for higher axial stiffness. Rough interfaces restrained the horizontal movements of the building. Buildings with individual spread footings experience large differential deformations, because footings outside the zone of influence do not follow the influenced part of the building. This results in significant distortions and tensile strains concentrating at the weak parts of the buildings. The modification factors found in the centrifuge were confirmed by FE-analysis and are shown in Figure 2.23.

Mair (2011) showed that field data from Goh (2010) and Farrell (2010) confirmed the trend found from FE analyses and centrifuge modelling for the modification factors versus relative bending stiffness according to Goh (2010), see Figure 2.24.

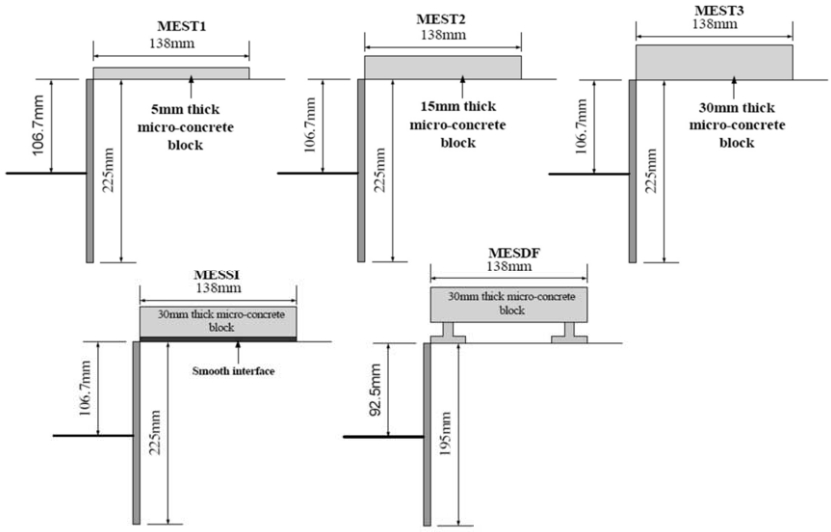


Figure 2.22 Buildings and interfaces used in centrifuge tests (Elshafie, 2008)

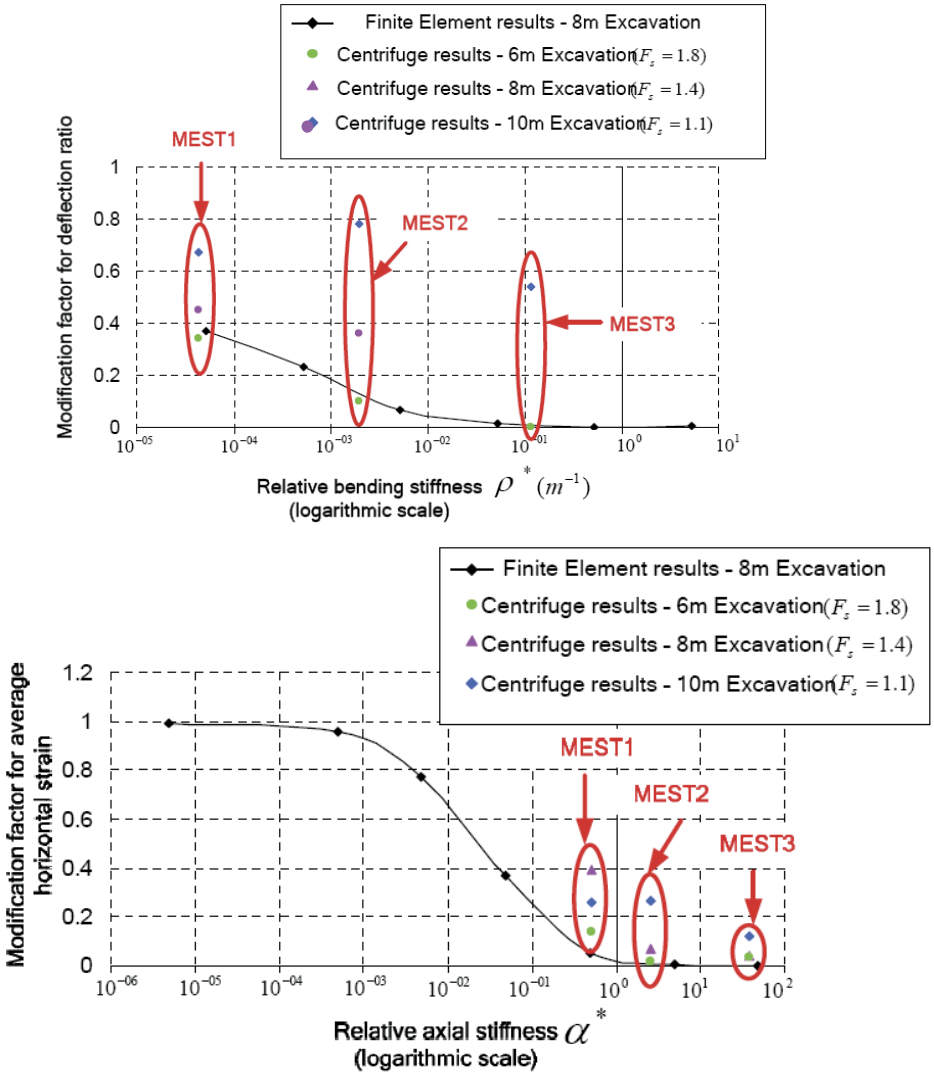


Figure 2.23 Modification factors for deflection ratio (top) and horizontal strain (bottom) from FEM and centrifuge tests (Elshafie, 2008)

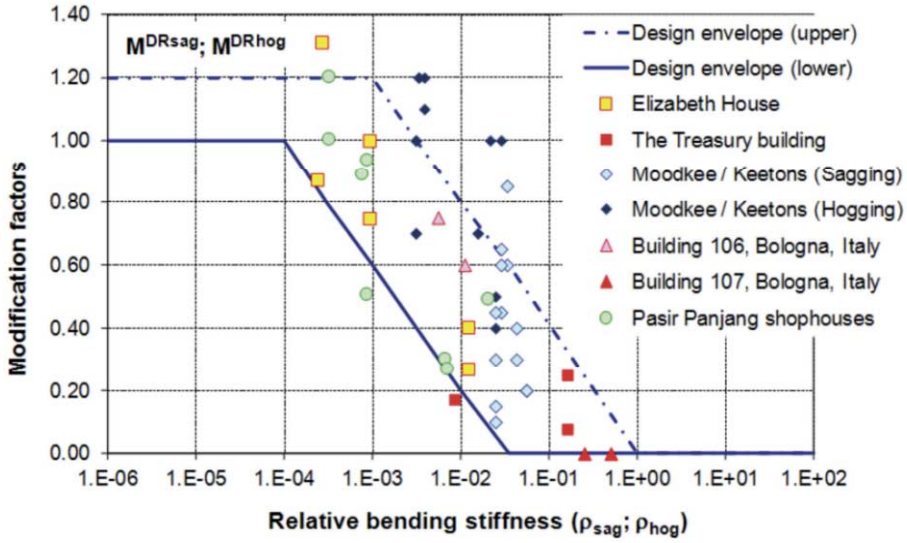


Figure 2.24 Field data of modification factor versus relative bending stiffness according to Goh (2010), Farrell (2010) and Mair (2011)

2.5 The response of pile foundations near deep excavations

2.5.1 Pile behaviour

The behaviour and capacity of piles under loading is governed by complex mechanisms such as installation effects and include negative and positive skin friction and base capacity. Both contributions to the capacity depend on the displacement of the pile relative to the soil. The elasticity of the pile itself can also play a role. The load displacement behaviour of the piles depends on the single pile capacity as well as the displacements transferred from other piles or the soil beneath the pile (group effect).

The settlement of the pile head is determined by the combination of the effects described above, according to::

$$s = s_b + s_{el} + s_2 \qquad (2.10)$$

with:

s is the settlement of the top of the pile, in mm;

s_b is the settlement of the pile tip due to the load on the pile, in mm;

s_{el} is the settlement of the top of the pile due to elastic compression of the pile, in mm.

s_2 is the settlement due to compression of the soil under the pile tip due to other effects than the load on the pile, in mm.

The Dutch Additional guidelines for Eurocode 7 NEN9997 published by NEN (2011) give a normalised pile-load curve for the base load and the skin friction separately, see Figure 2.25. In contrast to other methods (such as for example given by Tomlinson and Woodward (2008) and Fleming et al. (2009)), the shaft friction development is described independent of the pile diameter D.

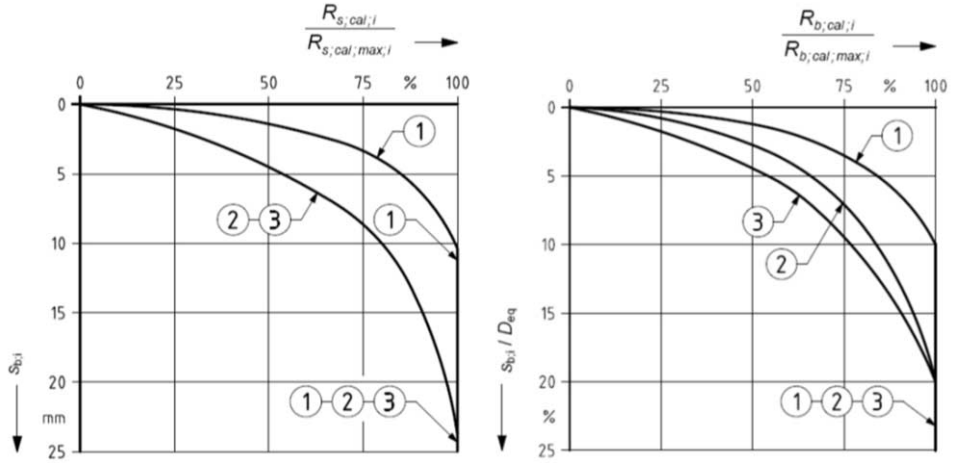


Figure 2.25 Normalised pile load curves for (1) driven piles, (2) auger piles and (3) bored piles, base load (Rb) on the left and skin friction (Rs) on the right

One of the most important aspects of piles affected by soil displacement is the development of negative skin friction. Common calculations methods for negative skin friction result in an additional load, which should be added to the working load on the pile to find a realistic pile settlement. The neutral level is the level at which the interface shear stress changes from negative to positive. The maximum force in the pile is found at this level. The negative skin friction can be determined by a total stress approach (α –method), effective stress approach (β-method) or directly and empirically from in –situ test results such as CPT.
The α method assumes the negative skin friction to be a percentage (given by the factor α) of the undrained shear strength c_u of the soil, according to:

$$Fs = \text{thickness layer} * O_s * \alpha * c_u \qquad (2.11)$$

With the slip (or β) method *(Eurocode 7)* it is possible to calculate the negative skin friction resulting from horizontal effective stress along the shaft. For single piles, piles in a row or pile groups with a large centre to centre distance the following formula is valid:

$$F_{nk} = O_{s;avg} \times \sum_{j=1}^{j=n} d_j \times \beta \times \frac{\sigma'_{v;j-1} + \sigma'_{v;j}}{2} \qquad (2.12)$$

With:

β is $(1 - \sin \varphi) \tan\delta_j$ for normally consolidated clay

F_{nk} is the load due to negative skin friction in kN

O_s is the pile circumference in m;

n is the number of soil layers attributing to the negative skin friction

d_j is the thickness of soil layer j, in m;

$K_{o;j}$ is the neutral soil pressure factor in layer j, assuming a horizontal green field level and no overconsolidation.

φ_j is the friction angle in layer j

δ_j is the friction angle between soil layer j and pile shaft with

— In situ cast concrete piles: $\delta_j = \varphi_j$

— precast concrete, timber and steel piles: $\delta_j = 0.75 \times \delta_j$

with a minimum of 0.25 for the combined value of $K_0 \times \tan \delta_j$

$\sigma'_{v;j;}$ is the vertical effective stress at the bottom of layer j, based on the volumetric weight of the layer (γ'_j) and the overburden stress p_{sur}.

p_{sur} is the overburden load on the surface, in kPa;

The pile spacing is considered large if the distance is larger than √ (10*D*d), with D is the pile diameter and d is the depth of the weak soil layers causing the negative skin friction.
Several opinions on the development of skin friction are available in literature. Some, such as Fellenius (1972), Bjerrum et al. (1969) and Alonso et al. (1984) have found that negative skin friction is already fully mobilized at a few millimetre differential displacement. Others, like Fukuya et al. (1982), Indraratna et al. (1992) and Clemente (1981) reported field cases in which the negative skin friction continued to increase with increasing ground settlement up to several hundreds of millimetres. Leung et al. (2004) confirmed this with centrifuge experiments and Shen (2008) investigated this effect in more detail using the centrifuge as well, assuming that the increasing negative skin friction resulting from consolidation of the soil around the pile is caused by the increase in effective stress. This effect can not be seen in laboratory tests such as presented by Alonso et al. (1984). Shen (2008) found in his tests that long, slender, flexible piles do not fully mobilize the negative skin friction along the pile. This depends on the pile-soil flexibility factor as defined by Samuel (1994) as the ratio between the elastic compression of the pile due to the drag load (caused by the negative skin friction) and the relative displacement necessary to eliminate the negative skin friction. The latter in this thesis is indicated by D_z, the relative displacement to reach full slip along the shaft. The soil pile flexibility factor is:

$$f = \frac{\bar{F}_{NSF} \cdot \frac{L}{E_p A_p}}{D_z} \tag{2.13}$$

If f > 8, as was the case in tests by Fellenius (1972) and Bozozuk (1972), Shen (2008) concludes that live loads in the pile are not transferred to the neutral level of the pile due to the flexibility. Shen's tests with f=0.7 show a degree of mobilisation 39%, 58% and 83% for piles that are respectively 100% end bearing, socketed (embedded 0.5 D in stable sand layer) or floating piles. For the typical piles in Amsterdam, f is in the order of 0.3 with F_{NSF} 85= kN, L = 12.5 m, EA_p = 250000kN and Dz= 15mm. Even though the timber piles have a relatively

low Young's modulus, most of the negative skin friction is transferred along the pile, since the soil stiffness is small. The degree of mobilization of the negative skin friction to be expected is thus even higher than of Shen's tests. Shen (2008) also stated, based on test data, that the β-method usually gives better results than the α-method.

For single piles, the negative skin friction is primarily controlled by the free field subsoil settlement profile and the mobilisation of the pile shaft resistance. For a pile group, interior piles will have less negative skin friction and external piles will have relatively more negative skin friction, due to redistribution between the piles. Zeevaert (1959; 1983) presented a method of calculating the negative skin friction for pile groups based on the reduction of the effective overburden stress caused by the soil "hanging" on the pile. DeBeer (1966) developed design charts based on Zeevaert's method. For piles in a pile group (with pile spacing smaller than $D \le \sqrt{10 \times D \times d}$) the negative skin friction can be calculated according to this method. In this method, a reduction of vertical effective stress is considered in the deeper layers, due to the transfer of load from the soil to the piles. This also diminishes the horizontal effective stress and the shear stress between soil and pile. The difference between the original vertical effective stress and the reduced value is the negative skin friction value and can be calculated by:

$$F_{\mathrm{nk}} = A \times \sum_{j=1}^{j=n} \left(\sigma'_{\mathrm{v};j;\mathrm{sur}} - \sigma'_{\mathrm{v;m};j} \right) \tag{2.14}$$

With:

$$\sigma'_{\mathrm{v};j;\mathrm{sur}} = \sigma'_{\mathrm{v;m};j-1} + d_j \gamma'_j + p_{\mathrm{sur}}$$

$$\sigma'_{\mathrm{v;m};j} = \frac{\gamma'_j}{m_j} \times \left(1 - \exp[-m_j \times d_j]\right) + \sigma'_{\mathrm{v;m};j-1} \times \exp[-m_j \times d_j]$$

$$m_j = \frac{O_{\mathrm{s;gem}}}{A} \times K_{0;j} \times \tan \delta_j \quad \text{and } K_{0;j} = (1 - \sin \varphi_j);$$

In which the following symbols are used in addition to the ones defined for the slip method (eq 2.12)

A is the surface area influencing the pile considered, in m^2;

$\sigma'_{\mathrm{v;m};j}$ is the reduction of the effective vertical stress in layer j, caused by the negative skin friction transferred to the pile group, in kPa;

$\sigma'_{\mathrm{v;sur};j}$ is the effective vertical stress in layer j caused by the weight of the soil above and the overburden load p_{sur} without the influence of the other piles, in kPa;

Table 2.8 shows several methods to determine the different percentages of negative skin friction within a group of piles. In general, the total negative skin friction imposed on the pile group should not be greater than the total imposed fill weight inducing the subsoil settlement within the effective coverage of the pile or group piles. The results in this table have been collected by Shong (2002).

Table 2.8 Negative skin friction for corner, edge and interior piles in pile group

Pile Location	Briaud et al (1991)	Broms and Badholms (1976)	Combarieu (1974)
Corner	¾ × $F_{n(\infty)}$	$S\times L\times c_u$ $+q\times(S\times L/4+L^2/16)$	$7/12\times F_{n(S)}+5/12\times F_{n(\infty)}$
Edge	½ × $F_{n(\infty)}$	$S\times L\times c_u + q\times S\times L/4$	$5/6\times F_{n(S)}+1/6\times F_{n(\infty)}$
Interior	$q\times S^2$	$q\times S^2$	$F_{n(S)}$

with:
S : Pile Spacing
L : Depth of Neutral Plane
q : Increase of Vertical Effective Stress in Subsoil
c_u : Undrained Shear Strength
$F_{n(\infty)}$: NSF in Single Pile
$F_{n(S)}$: NSF for Pile with spacing of S

2.5.2 Response of piles to tunnelling

Since very few papers describe the response of pile foundations related to excavations, first an overview is given of the developments in the field of the response of pile foundations to tunnelling. For piles subjected to tunnelling, Selemetas (2004) compared the results of a field test by Kaalberg et al. (2005) and centrifuge modelling by Jacobsz (2002) and Bezuijen and Van der Schrier (1994).

From the tests by Jacobsz (2002) it is found that piles directly above the tunnel settle more than the surface, whereas piles just next to the tunnel (at an angle of maximum 45 degrees from mid-tunnel, see Figure 2.26) settle about the same as the surface. Piles outside the line of 45 degrees from mid tunnel do not settle at all (or at least significantly less than the green field) according to Kaalberg et al. (2005). The settling piles experience a reduction in base load, while in some cases the shear stress and thus the shaft friction increases. This is due to larger horizontal stresses above and beside the excavated tunnel than at rest, which cause an increase in shear stress and shaft capacity. Also, the normal stresses increase due to the dilation of the soil-pile interface (Jacobsz, 2002).

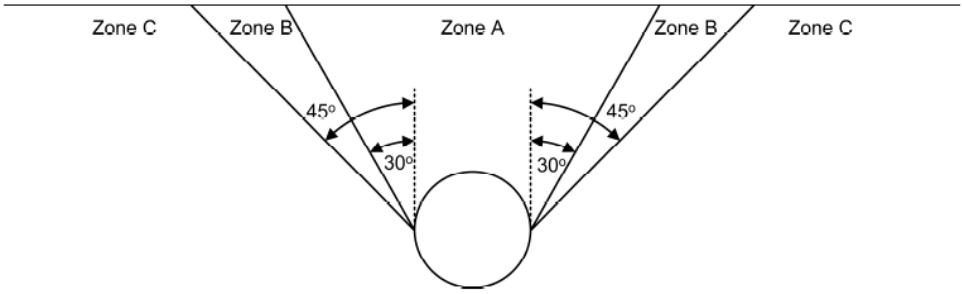


Figure 2.26 Pile toe influence zones (Kaalberg et al., 2005)

From centrifuge tests at GeoDelft (Deltares) (CUR, 1995) similar results have been found. The pile capacity has been reduced in the zones of influence (A and B).

Kaalberg et al. (2005) describes the results of an extensive programme in the Netherlands to find the influence of tunnelling on piles, for which measurements and a field test where performed at the Second Heinenoordtunnel. They showed that settlement of piles due to tunnelling consists of two phenomena, which have to be added together:

- Settlement of the soil layer around the pile toe and
- Pile settlement caused by stress relief around the pile toe.

3D FEM analysis showed that stress relief would be negligible for piles within one diameter from the tunnel (confirmed in the field test) or even 0.25 D (based on FEM only).
CPT tests and static load tests performed before and after tunnelling showed no significant changes, and pile capacities after tunnelling were almost unchanged, which indicates that no significant stress relief occurs. Time dependent settlement of the piles and surface are about 15% of the settlement immediately after passage of the TBM.

Jacobsz et al. (2005) concluded, based on three case studies in the Channel Tunnel Rail Link project, that a difference is found between end bearing and friction piles. End bearing piles follow the green field settlement at the pile base for small volume losses. Friction piles alter the green field subsurface displacements and follow more or less the surface settlements as a conservative approach. At the Renwick Road bridge, see Figure 2.27, end bearing driven piles are located with their base above the tunnel. It was assumed that the pile settlement would be governed by the movement of the soil at pile base level. During the driving of the first tunnel, the surface settlement (at 2m offset of the tunnel-axis) was 5.5 mm. The bridge abutment settled 7 mm, which was equal to the green field settlement predicted at pile base level. During passage of the second tunnel the pier deformation (piles) was just a few millimetres less than the surface settlement.

At the Ripple Road Flyover, see Figure 2.27, the piles extended to 25 m below surface, which was only 1 m above the tunnel crown. To reinforce the piles, grouting of the Terrace gravels took place. The prediction as well as the measurements showed that the piles settled the same as the surface (but less than at pile base level).

At a third location, the A406 viaduct, 23.5m long friction piles support the viaduct while the tunnel is constructed 4 m below the pile base. It was predicted that the piles would act as slender elastic members within the soil. Vertical and horizontal movement along the shaft was calculated and converted to strains in the piles. The measurements showed that the piles settled about the same as the surface.

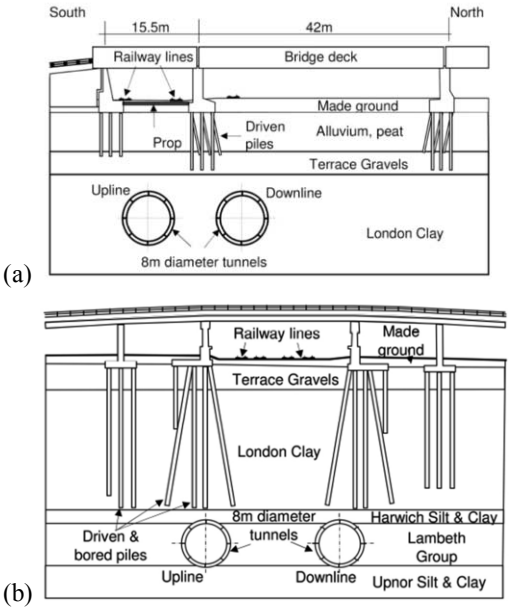


Figure 2.27 Renwick Road bridge (a) and Ripple Road Flyover (b)

Chen et al. (1999) present an analytical method to determine the influence of tunnelling on a single pile or a pile group for tunnels located above the base of the pile. They separately discuss lateral and axial effects. The lateral response of the pile is calculated by the PALLAS program, based on elastic soil and an elastic beam. Plastic behaviour can be simulated by a maximum pile-soil interaction stress. The axial response is calculated by the program PIES, based on the pile being simplified as an elastic column and the soil as elastic continuum. Slip at the interface pile-soil is possible. Chen et al. (1999) concluded that lateral pile deflections are very similar to the soil deflections and that the pile-head settlement is less than the maximum vertical soil settlement.

A coupled analysis is performed by Xu and Poulos (2001) using the GEPAN program. In this analysis, the soil is assumed to be an ideal homogeneous isotropic elastic weightless half space. The behaviour of the pile in axial and lateral loading are influenced by the ratio between pile and soil stiffness represented by the Young's moduli and the dimensionless ratio:

$$\frac{E_p I_p}{E_s / L^4} \tag{2.15}$$

Ep and Ip are the piles' Young's modulus and the moment of inertia, Es is the soil's Young's modulus and L is the length of the pile. The results seem to represent the 3D behaviour better than the uncoupled analysis, but no calculations of tunnels or excavations were given with this program.

Mroueh and Shahrour (2002) compared their three dimensional finite element modelling with simpler analytical models. The model used is a fully elasto –plastic (Mohr-Coulomb), with simulation of the initial pile loading and the tunnelling process by excavation and activation of the lining. The Young's modulus of the soil is 35 Mpa and for the pile it is 23.5 GPa with 1mx1m cross section. The pile deflection is slightly less than the lateral soil displacement in conditions without the piles present, see Figure 2.28. This means that there could be a minor stiffening effect, reducing the soil displacements when the piles are present or that the pile stiffness plays a role.

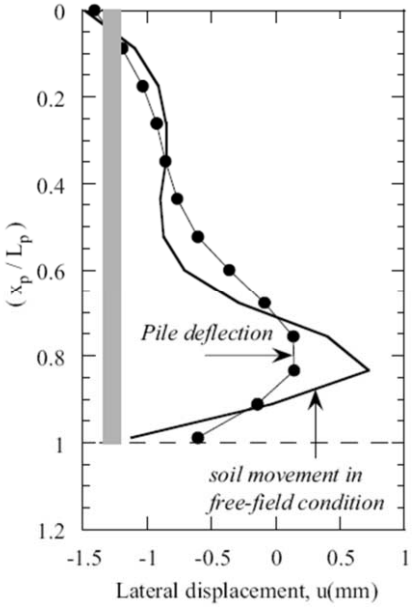


Figure 2.28 Lateral deformation of pile compared to soil with depth
(Mroueh and Shahrour 2002)

The following similarities and differences between the effects due to tunnelling and those due to deep excavations are fundamental:

- The general movement of the pile towards the tunnel or excavation and downwards is similar
- The 3D effect for a passing TBM is not present for deep excavations, but other 3D effects such as due to construction sequence, corners or the limited size of the building could still be significant.
- Installation effects of retaining walls present extra changes of stress in the case of deep excavations (unloading in case of excavation for diaphragm wall or bored piles, loading due to concrete pressures or densification due to vibrations).

2.5.3 Response of piles to deep excavations

Due to excavation-induced changes, the interface between the pile and the soil changes. For pile foundations behind excavations, it is important to understand the stress changes behind the excavation, as for example shown in Figure 2.29.

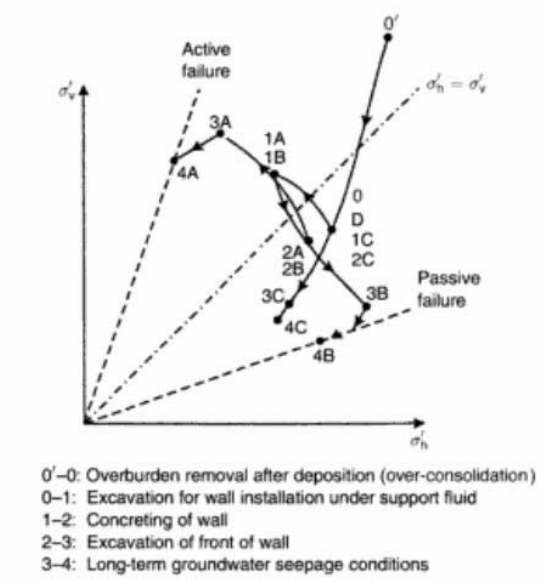


Figure 2.29 Stress changes in four locations in an over-consolidated clay with diaphragm wall; A at the active side, B at the passive side, C in the centre of the excavation and D at large distance from the excavation (Puller, 2003)

The soil around the piles is subject to vertical and horizontal displacements, similar to the ground surface. In stress terms the vertical and horizontal stresses around the pile decrease within a certain influence zone from the excavation.

Specifically related to piles near deep excavations, the work of Poulos and Chen (1997) and Zhang (2010) should be mentioned. Poulos and Chen (1997) adopted a two stage approach in which they determine the green field soil displacements with FE analysis and later determine the soil-pile interaction with a boundary element method (BEM).

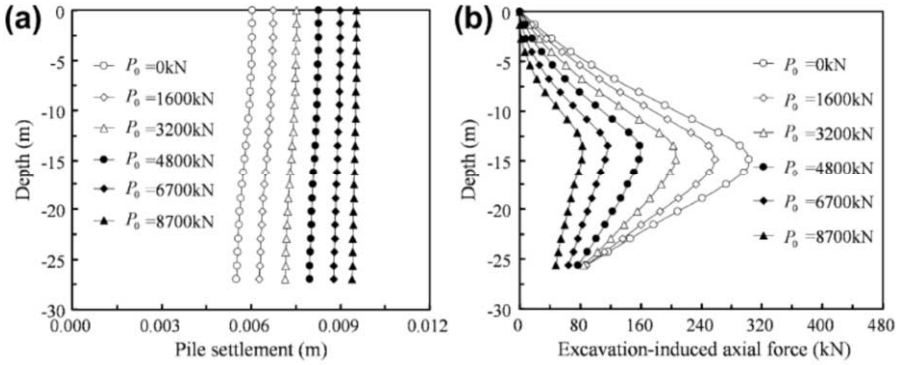


Figure 2.30 Zhang (2010) model for lateral and axial excavation induced effects with a) pile deformation with depth and b) pile axial force, both for different working loads (P_0)

Zhang (2010) developed a similar two-stage approach, in which the deflection of the retaining wall is determined by a beam on elastic spring method and the soil displacement behind the wall by the source-sink method described by Sagaseta (1987). Zhang then uses hyperbolic description of the friction behaviour between pile and soil, with unloading hysteresis to describe the soil-pile interaction. This requires the pile to be divided in segments and a solution with boundary conditions and linearization of the equations, while taking into account the presence of a working load on the pile. Zhang verified his work by comparing his results with solutions from BEM from Chen et al. (1999) and centrifuge test data from Loganathan et al. (2000) with satisfying results. Zhang (2010) concluded that the working load initially present on the pile before the excavation takes place is an important factor to take into account. An increasing working load means an increasing pile settlement related to the excavation and a decreasing additional axial force to be developed. Ultimately, for a pile in failure, no additional axial force can be mobilized. The work of Zhang (2010) also includes the lateral effect on the piles. Results of the effect of the working load are given in Figure 2.30.

Ong (2004) determined in centrifuge experiments that the development of bending moments and deflection in piles adjacent to deep excavations is time dependent. His results support the finding of Hull et al. (1991) that the limit soil pressure/soil strength ratio for piles subject to soil movement is significantly less than that of piles with loading at the pile head, in particular when the magnitudes of soil movement are large. For pile groups in clay the induced maximum bending moment found by Ong (2004) was always lower than that of the corresponding single pile. The induced bending moment of the front pile, which experiences greater soil movement, is moderated through the pile cap.

2.6 Summary of literature

The following conclusions are drawn from the literature survey regarding response of (piled) buildings to excavation-induced displacements.

2.6.1 Green field displacements

Empirical methods have shown that the displacements to be expected depend very much on the soil type and the type of construction. The shape of the settlements is most clearly related to the shape of the deformed wall and the soil type. No clear dependencies have been found however by most authors, because a complex combination of factors, such as workmanship or installation effects, can not be captured well in these general databases. For soft clays Moormann and Moormann (2002) show that little improvement has been made in the amount of settlements behind the wall compared to the early work of Peck (1969) and that displacements in the range of 1% of the excavation depth should be expected for soft soil conditions.

From the relevant literature sources, one should expect for a deep excavation in clay:

- Wall deflection 0.5 – 1.0%H (for an average system stiffness and sufficient basal stability)
- Better results are possible (0.2-0.5%H) for diaphragm walls with good supports, as long as the excavation effect is the main cause and installation and other effects are controlled sufficiently.
- Settlements behind the wall are about the same as wall deflections and may reach over a distance of 0.75H from the wall and decrease to 0 at 2-3H away from the wall.
- Settlements due to installation of a diaphragm wall can be limited to 5-10 millimetres in cases where a high factor of safety for trench stability is assured.
- 50%-100% margins should be expected around the values presented.

There is a lot of experience in modelling green field behaviour. Usually the wall deformations are predicted within 25-50% of the measured values. Settlements behind the wall are often under predicted. Deviations are usually related to the details of the construction process, such as the installation of struts and anchors and consolidation effects.

2.6.2 Building deformations and damage

Damage in structures is not always related to construction, but also temperature, creep and shrinkage are major attributes. Deformations due to construction activities have to be separated from effects of self-weight, temperature, moisture content etc.

The relationship between cracks or crack width and strains in a building depends on several aspects, such as material details, building dimensions and deformation modes. Usually low values of tensile strains (0-0.05%) are used as the onset of cracking. In general, buildings that experience more curvature, show more damage than buildings that tilt rather than bend or shear.

Some buildings are more susceptible to damage than others:

- Given the same vertical deformation, frame structures can accommodate differential displacements by deformation of the beams, whereas load bearing walls need to

deflect, which leads to cracking more easily. This leads to a 20-25% lower tolerable relative rotation and deformation for load bearing walls.

- Buildings subjected to relatively fast deformations (construction activities usually occur rather fast, which is more damaging than slow deformations)
- Buildings with structural discontinuities
- Building subject to hogging shaped deformations are usually more damaged than in sagging shapes.
- Buildings with deep foundations could be more sensitive to intolerable deformations (deformations are considered intolerable at smaller values), because differential deformations might be more localized than for shallow foundations. Tolerable relative rotations and deformations for deep foundations are about half those for shallow foundations according to Zhang and Ng (2007).

Damage to buildings can be assessed by several damage criteria. The use of relative rotation and deflection ratio are both widespread, but also widely discussed. Relative rotation is favoured more for shear deformation and deflection ratio more for bending deformation. Some authors, e.g. Mair et al. (1996) and Burland et al. (2004), prefer the deflection ratio method for simplicity of the calculation.

Rigid body rotation or building tilt, is a very important parameter when discussing excavation induced damage. Real rigid body rotation should be assessed in three dimensions and it should always be made clear exactly if and in what way tilt is considered.

Damage assessment procedures usually work from simple, conservative approaches to more detailed and specific procedures. The first step usually includes very simple damage criteria. In the second step strains are calculated, but without soil-structure interaction. Only if a third step is necessary, more detailed calculations are made including interaction and/or mitigating measures.

2.6.3 Soil-structure interaction

Part of the soil-structure interaction for excavation-induced displacements includes the effect that the presence of the structure will change the pattern of soil displacements. The building weight usually only has a minor influence on the deflection ratio, but more effect on transfer of the horizontal strains as shown by Elshafie (2008). Especially for large localised stresses such as for highly loaded deep foundations, this effect should be taken into account. Furthermore, the amount of displacement transferred to the building depends on the stiffness of the building in axial and bending modes and the interface between soil and foundation and between foundation and building. The stiffer the building, the larger the difference between the greenfield ground displacement and the building deformation will be. Very flexible buildings do not alter, but follow, the green field displacements. The interface between the soil and the building depends on the foundation type. Rough interfaces transfer a larger part of the soil strains and displacements to the building than smooth interfaces.

The presence of a pile foundation changes the soil-structure-interaction. Most methods to assess this effect are derived for tunnelling and distinguish between end-bearing and friction piles. Also for deep excavations, the soil displacements cause changes in the positive and negative shaft friction along the pile, depending on the pile and soil stiffness, the working load on the pile and the soil displacements. Most methods to assess the pile-soil interaction include a two-stage approach, first finding the green field displacements and then relating them to the pile-soil interface. Modelling soil and building in a combined calculation is still not well developed. So-called coupled models either have simple soil models or simple building models. Full non-linear coupled models are not likely to be available for practical use in the near future.

CHAPTER 3 PREVIOUS CASE HISTORIES

3.1 Introduction

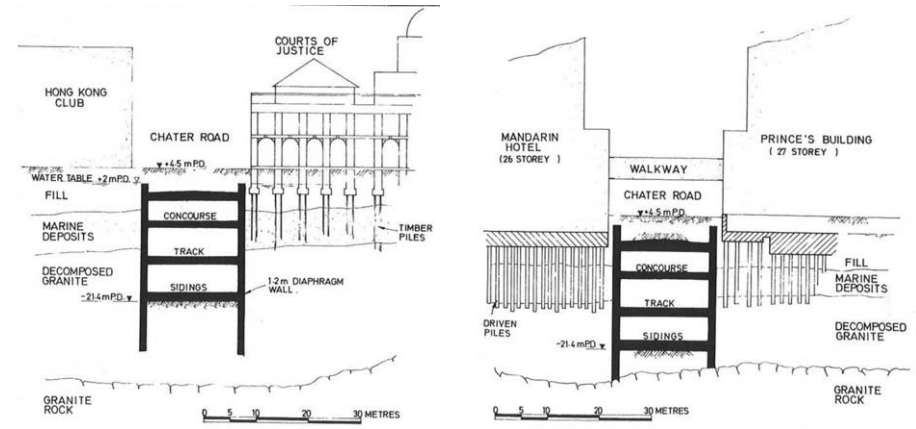
The case histories in this chapter have been selected for the insight they provide in the soil – structure interaction caused by deep excavations especially related to piled foundations. This chapter provides four documented case histories, in which both ground deformations and building deformations have been measured. The case histories have been re-analysed to investigate the soil-structure interaction related to the foundation.

3.2 Chater Station, Hong Kong (Davies and Henkel, 1982)

3.2.1 Situation

The construction of Chater Station, part of the Hong Kong Mass Transit Railway in the years 1976-1980 was performed in a congested urban area of reclaimed land. Old colonial buildings and new high rise blocks were nearby. Ground conditions include loose reclamation fill and marine deposits overlying a layer of silty sand. At about half the excavation depth the top of a layer of decomposed granite is found. High water tables are present in the area. The excavation was 27 m deep, 400 m long and about 20 m wide. Diaphragm walls of 1.2 m thick were constructed, after which the roof was constructed ('top down' construction)

The deep excavations were situated at some metres from the older buildings and even closer to the high-rise blocks. The Courts of Justice building is founded on timber piles under individual footings. Depth of the pile foundation is about 16 m. The Prince's Building and the Mandarin hotel are founded a concrete slab with driven piles to 19 m. Swire House, 22 storeys high, is founded on small individual pile caps with 6 driven piles each reaching into the decomposed granite at 15-18 m below ground surface. Cross sections over the excavation and the location and foundation of the buildings is shown in Figure 3.1.



(a) (b)

Figure 3.1 Section through Courts of Justice (a), Mandarin hotel and Prince's Building (b)

3.2.2 Effects of the construction

The construction of the diaphragm walls involved excavating and concreting a series of panels between 2.7 and 6.1 m long and up to a depth of 37 m. Measured settlements during construction were considerably larger than expected (38 mm at Hong Kong Club, 78 mm at Courts of Justice and 21 mm at Princes Building) and progressed to a distance of 50 m away. Settlements did not occur during single panel installation (which would be expected in case of instability) but during construction of a series of panels. Also observed was a rise in the water table after construction of the north wall, resulting in a lower effective pressure.
Near Swire house changes were made (shorter panels, higher density slurry; effective slurry pressure being 100 kN/m^2), and raising of the slurry level above the surface with high guide walls). These changes resulted in smaller movements (14 mm horizontal and 30 mm vertical of the building, of which half was due to dewatering).

Davies and Henkel concluded that the high water table in the decomposed granite resulted in low effective slurry pressures and subsequent large horizontal movements (40-60 mm at 1 m distance from the panels). The author's opinion is that part of this could also be explained by the construction of a series of panels close to each other (adjacent panels were not yet hardened). The actual panel width would then be larger and the stability much lower.

Lowering of the ground water table causes settlements and several variations in drawdown have been calculated for this case history. A marked variation of ground-water lowering outside the excavation was found. The settlements were linearly related to the amount of drawdown, see Figure 3.2. A groundwater recharge system reduced the settlements to 60% of the values without recharge. The settlement due to dewatering caused negative skin friction at the pile shafts, especially in the end bearing piles with shallow penetration into the bearing stratum. This explains the relatively large settlements of the buildings.

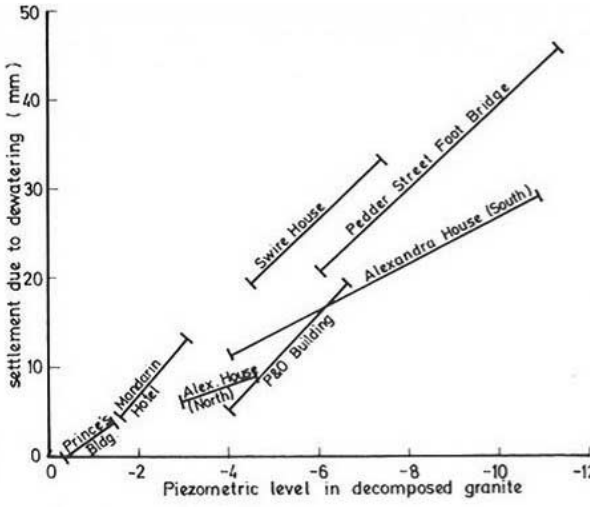


Figure 3.2 Settlement of high-rise buildings due to dewatering

Expected settlements due to excavation stages were 0.15-0.2% of the depth (27 m; resulting in 40 mm - 50 mm) with an influence zone of at least the 27m away from the excavation. The observed displacements were maximum 40 mm horizontal and 60 mm vertical, see Figure 3.3. The wall deflection is thus 0.15% of the excavation depth. The settlement is 1.5 times the wall deflection (during excavation only).

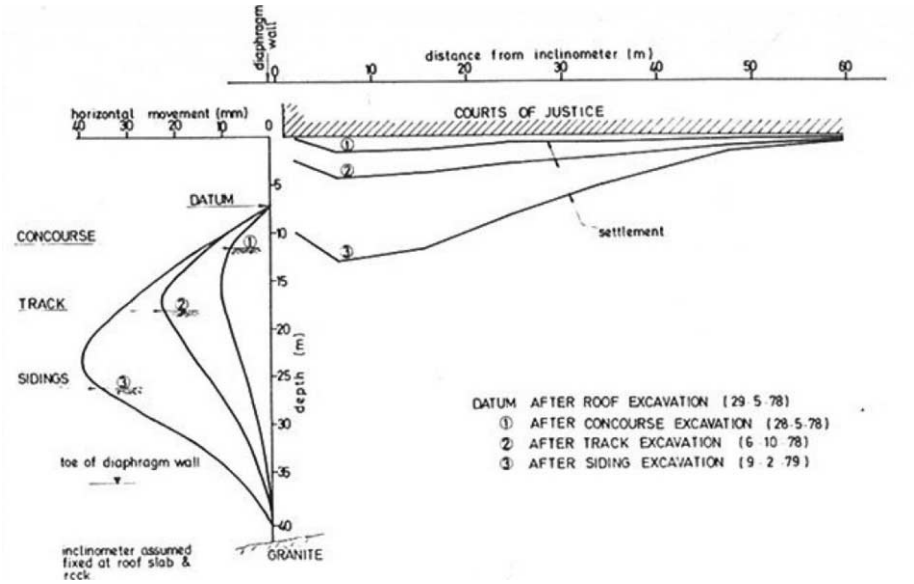


Figure 3.3 Horizontal and vertical deformations during excavation (West façade)

3.2.3 Final deformations and damage

Most buildings exhibited overall settlements and a slight tilt towards the excavation. Measured distortions were relatively small and very little damage occurred. One exception was the Courts of Justice building, at which 50 m from the retaining wall a hinge occurred between two sections of the building, resulting in large cracks (the size was not described by the authors).

Final deformations for the Courts of Justice building are presented in Figure 3.4. The final settlement of the building is 4.5 times the wall deflection and 0.7% of the excavation depth. These high values relate to the drawdown and diaphragm wall installation rather than the excavation itself. As seen in Figure 3.4 it seems that the building behaved as two rather stiff units.

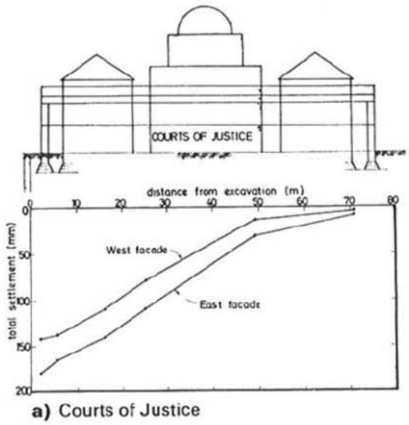


Figure 3.4 Building deformations (final stage, East and West perpendicular to excavation)

Based on the information given in the paper by Davies and Henkel (1982) it was not possible to find the influence of the pile foundation on the results, because no measurements of the ground displacements were given. It is however clear that the piles experienced serious settlements due to negative skin friction caused by the lowering of the water table. Since the settlements of the building behind the wall during excavation were already 1.5 times the deflection of the wall, it seems that the piles might have followed the green field rather than the pile tip level, but this can not be verified.

If reasonably large percentages of horizontal displacement are transferred to the building, this could possibly explain the amount of damage. On the other hand, based on the construction details, it is clear that the building is not a homogenous beam, but is rather formed by two (or even possibly even three) connected parts. The two rigid body units are connected through a hinge at about 50 m from the façade (at the corridor). Since damage was concentrated in the joint, it is possible to calculate the crack occurring if the two units behave independently. Assumed that the building height is about 15m at the corridors, the crack that would occur between the two units will be 0 mm at the bottom and 25 mm at the top. This would be considered a large crack and matches the damage description from the original

data. The individual building parts will experience hardly any bending and an unknown amount of horizontal strain.

3.2.4 Conclusion from Chater station case history

Piled foundations adjacent to deep excavations can experience serious settlements due to negative skin friction caused by the lowering of the water table. The settlement of the building behind the wall during excavation was about 1.5 times the maximum deflection of the wall. Settlements due to diaphragm wall installation are significantly influenced by the stability of the trench. Installation of several panels close to each other in a short time and/or high ground water pressures during construction will increase the ground displacements behind the wall.

All of the buildings settled a fairly large amount, mostly in the form of an overall settlement and slight tilt towards the excavation. The distortion in the buildings was small, with the exception of the Courts of Justice, where a large crack occurred between two building parts. This damage can not be explained by the curvature of the building, but can if rigid body tilt is taken into account. Considering the methods for damage assessment, it is clear that it is very significant to understand whether a building will rotate like a rigid body or deform by bending and shearing. The difference will be that tilting will not cause damage within a unit, but gaps might occur between building units.

This case history shows the importance of the rigid body tilt if two or more stiff units are connected through a flexible joint. Because no information is presented on the ground displacements, the interaction effect between soil and pile foundation could not be determined.

3.3 KPE Singapore (Lee et al., 2007)

3.3.1 Introduction

This case history describes the result of a building damage assessment for a Multi-propped excavation in Singapore for the Construction of Kallang Paya Lebar Expressway (KPE). Special attention is given to the soil-structure interaction for a building with a piled foundation. Figure 3.5 shows the cross section with the geological profile.

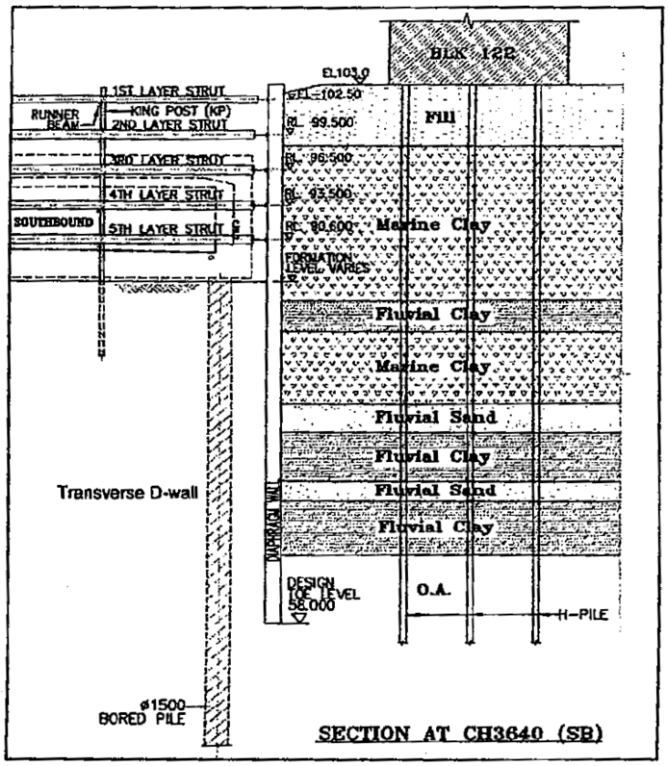


Figure 3.5 Cross section with the geological profile

At 6 m behind the diaphragm wall, a 12-storey building (a reinforced concrete frame structure) founded on 37m long, driven steel H-piles, is the main point of interest of this case history. The building length is 8.5 m, its height 36 m, which results in L/H = 0.25.

3.3.2 Damage prediction and results

Lee et al. (2007) used the prediction method from the Gaussian curve adopted from the one Peck previously presented for tunnelling in Peck (1969), see section 2.2.3. They used the estimation of the trough width from Bowles (1988). This means the trough is constructed from the depth of zero moment in the wall at an angle of 45- φ'/2 to the vertical line to the ground surface. Lee et al. (2007) took an angle of 45° for soft clay to construct this line. The total trough width was predicted at 30 m and the maximum settlement at 50 mm.

Horizontal deformations were taken as

$$H(x) = \frac{dh}{ds} \cdot \left(1 + \frac{2x}{W}\right) \cdot S(x) \tag{3.1}$$

with $\frac{dh}{ds}$ = 0.5 for the situation with a diaphragm wall.

The damage prediction was made according to Burland (1995), but with relative rotation instead of deflection ratio. The prediction of the settlements was based on the settlements and horizontal deformations at pile toe level, see Figure 3.6. In the calculation of the relative rotation, tilt was excluded (so β = slope – tilt (ω)). Tilt in the prediction was defined by the straight line between the settlement points of the building at pile toe level.

Both building and ground deformations were measured, inclinometers installed and tape extensometers used to check the relative horizontal building movements. Slope measurements were installed to monitor overall movement in parallel and perpendicular to the wall of the excavation. The results showed (Figure 3.6) that the actual wall deformation was very close to the predicted one. The settlement behind the wall was somewhat higher (about 10 mm) than predicted and extended further from the wall.
Characteristic numbers derived for this case history:

- Deflection wall/excavation depth = 16mm/16.5 m = 0.1%
- Settlement behind the wall / deflection wall = 30mm/16 mm = 1.9
- Width of the surface settlement trough / excavation depth = 50 / 16.5 =3.0
- Width of surface settlement trough / depth of deforming layers = 50 / 35 = 1.4.

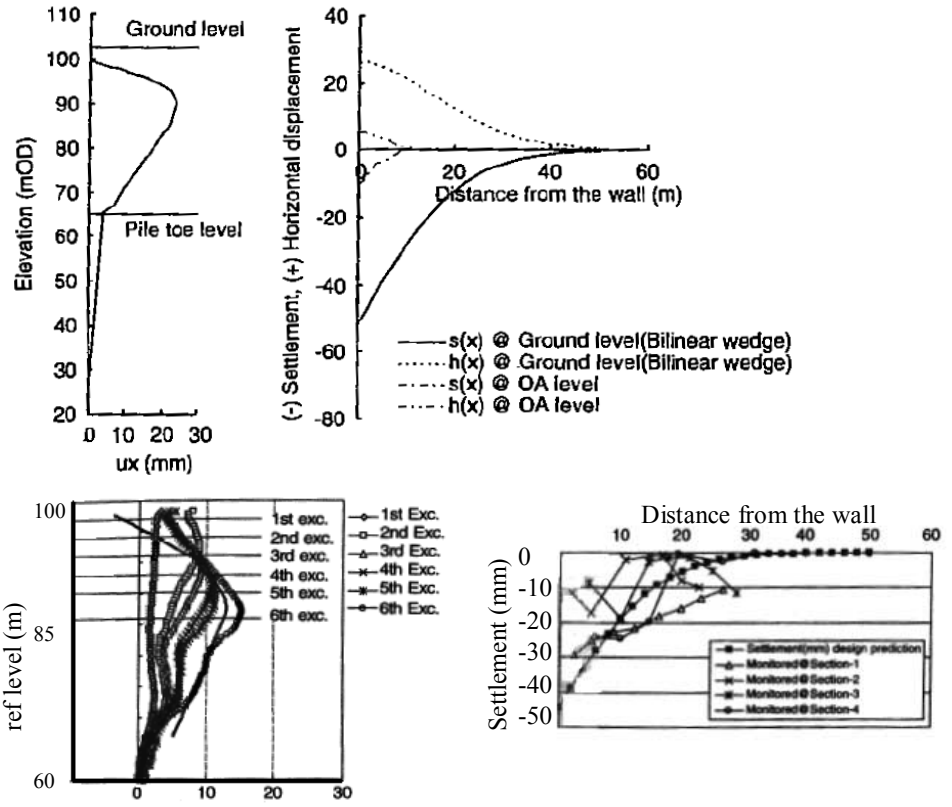


Figure 3.6 Predicted (above) and measured (below) deformations (Lee et al., 2007)

Table 3.1 Comparison of prediction with measurements (Lee et al., 2007)

	Results of the prediction	**Results of the measurements**
(Burland, 1995), with β instead of Δ/L	$\varepsilon_{h,ground}$ = 0.0835% and β_{ground} = 0.0354%	n.a.
	$\varepsilon_{h,toe}$ = 0.0835% and β_{toe} = 0.0462%	$\varepsilon_{h,building} \approx$ 0.075% and $\beta_{building} \approx$ 0.05%, all < 0.1%
(Burland and Wroth, 1974)		$\varepsilon_{bmax} \approx$ 0.08% and $\varepsilon_{dmax} \approx$ 0.08%

Table 3.1 clearly shows that the horizontal strain is the most important factor causing the prediction to assess a category "slight" amount of damage. Due to the small L/H factor in this direction (perpendicular to the deep excavation), the building behaves in a relatively stiff manner.

3.3.3 Conclusion from Lee et al. (2007) case history

A 15-17 m deep excavation caused (minor) pile tip settlement due to an increase in negative skin friction. Monitoring results were in general 80-100% of the prediction in green field conditions. The soil displacements and wall deflections were within the band widths of Clough and O'Rourke (1990).

The effect of horizontal strain was significant in the measurements of the building and in the derivation of the damage indicators. The differential horizontal deformation is 0.075%*8500mm = 0.6 mm. Differential horizontal green field deformations are about 3.0 mm equivalent. This indicates that, 0.6/3.0 = 20% of the horizontal ground strain was transferred to the building.

The assumption that the building follows the vertical deformations of the pile toe level worked well in this case history, although due to the small deformations and the lack of measurements at depth this can not be confirmed.

3.4 Excavation next to Xavier Warde School, Chicago (Finno et al., 2002)

3.4.1 Situation and construction works

Finno et al. (2002) describe observations made during the excavation and construction of the Chicago Avenue and State Street Subway renovation project in Chicago. Figure 3.7 shows a top view of the location, the deep excavation and the adjacent Warde School with the instrumentation.

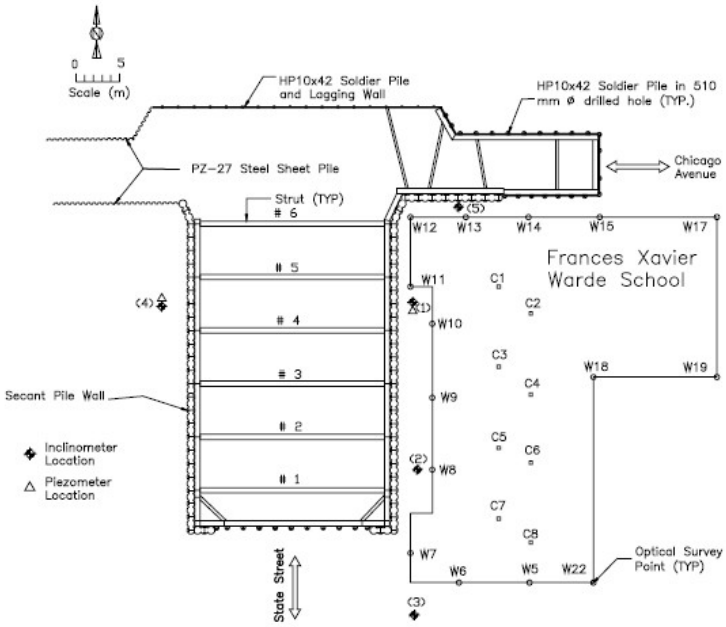


Figure 3.7 Top view of Chicago Avenue and State Street Subway renovation project

The school was built in the late 19-sixties and is a 3-storey reinforced concrete frame structure. An approximately 1.2 m wide continuous footing supports the basement wall. The interior columns are supported by reinforced concrete spread footings. The average depth of the footings is approximately 3.7 m below ground surface. The school is located approximately 2 m from the excavation. The soils found at the site are primarily lightly overconsolidated glacial clays, increasing in stiffness and strength with depth, see Figure 3.8.

The excavation was supported by a secant pile wall, approximately 18.3 m deep, with three levels of support. The excavation along State Street was approximately 40 m long, 24 m wide and reached an average final depth of 12.2 m. The excavation along Chicago Avenue was approximately 24 m long and 7 m wide and advanced to a depth of 8.2 m.

The construction at the site was separated into three stages; wall installation, support system installation and excavation, and station renovation and backfill.

3.4.2 Deformations and building damage

Displacements of the retaining wall, ground level and the Warde school building are analysed per construction phase. During the wall installation lateral soil movements and settlements of the school reached a maximum of 9 mm. They extended to a distance from the

wall equal to the depth of the secant pile wall. Lateral wall movements during the excavation is 28 mm, which is about 50% of the final deformation.

The Warde School settled as much as the soil displaced laterally, with the settlement extending as far behind the excavation as the secant pile wall extended below the bottom of the school's foundation, see Figure 3.8. The adjacent settlements were virtually identical to the lateral movements within the soft clay. Finno et al. (2002) also calculated the deflection ratio and relative rotations with time. The rigid body tilt of the building was 1:15000 on Day 116 (final excavation depth reached) and 1:3900 by the end of the project. These values are small and therefore neglected in the calculation of the relative rotations (and deflection ratios). The actual damage observed in the Warde School can be characterized as "negligible" to "slight" according to the damage severity classification presented by Burland et al. (1977). This was the case for both the calculated and observed damage.

Finno et al. (2002) did not include horizontal strains in the damage estimation. If we assume that the horizontal deformations in the building are equal to the vertical deformations, the damage category would have been 'very slight' for most building parts, but 'moderate' for the sagging zone in the East West direction. By including all of these horizontal strains in the building, the damage category would have been overestimated. It is more likely that only a portion of the horizontal deformations was transferred to the building.

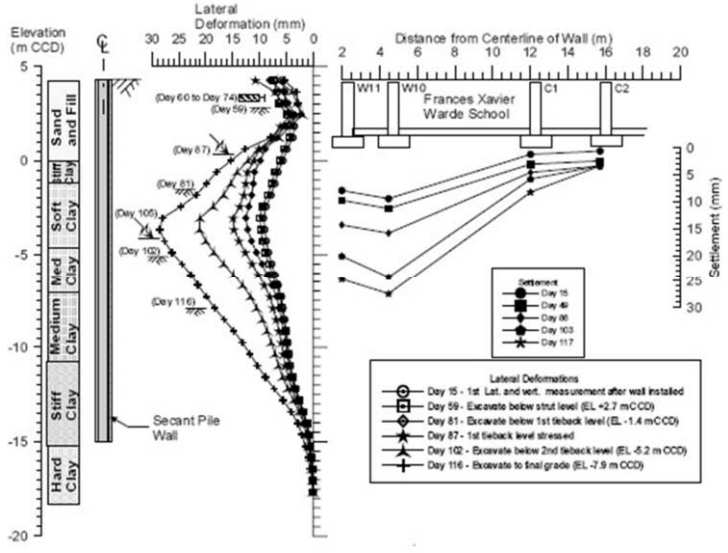


Figure 3.8 Comparing settlements and inclinometer data at the end of the excavation (Inclinometer 1)

3.4.3 Conclusion from Xavier Warde School case history

This case history showed the amount of deformations and damage a three-dimensional excavation caused to a frame building with basement, founded on spread footings.

Some characteristic numbers for wall deflection over excavation depth have been derived for this case history:

- State street (12.2 m deep), excavation phase = 28 mm/12.2 m = 0.23%
- State street (12.2 m deep), total deformation = 41 mm/12.2 m = 0.34%

Note: lateral displacement from inclinometer 1.

- Chicago Avenue (8.2 m deep), excavation phase = 14 mm/ 8.2 m = 0.17%
- Chicago Avenue (8.2 m deep), total deformation = 34 mm/ 8.2 m = 0.41%

Note: lateral displacement from inclinometer 5, resultant deformation.
The ratio of wall deflection over settlement behind the wall for this case history is generally about 1.0 for all phases of the construction.

The settlement trough width (measured by the deformation of the building) reached to about the same distance as the depth of the piled wall. This value seemed not to be affected by the depth of the excavation. The trough width was about 1.6 times the deepest excavation depth. It is concluded that this deep excavation follows the patterns and indicative values suggested by Clough and O'Rourke (1990). The three-dimensional behaviour of the excavation and the building resulted in smaller deformations close to the corners (even at the inward corner) of the excavation.

Depending on the amount of horizontal strain in the building, the damage category expected based on the measurements would have been under predicted (using deflection ratio without horizontal strain) or over predicted (using deflection ratio and horizontal deformations equal to vertical deformations). Using relative rotation without rigid body tilt or horizontal strain resulted in values comparable to the damage experienced. If horizontal strain (>80% of vertical deformations) would have been included, the damage would also have been overestimated. Due to the lack of horizontal measurements, it will not be possible to state which of the damage indicators gives the most appropriate results. Since no ground deformations were presented it was also not possible to find the modification factors of the building depending on its stiffness.

3.5 Willemspoortunnel – White House Rotterdam

3.5.1 Introduction and soil conditions

Several papers by Van Tol and Brassinga (1991, 1992, 1993) and Sarlemijn et al. (1993) report on the construction of the Willemspoortunnel in Rotterdam. This deep excavation of 18 m deep is located near the 'Witte Huis' (White House) 11-storey high rise building, dating from the end of the 19th century. The building is founded on wooden piles in the Pleistocene sand layer.

This case history is studied because it gives information on the response of piled buildings to deep excavations in soft soils. The study especially looks into the response of the building to the induced soil displacements. The precise origin of the soil displacements is not the main concern.

The soil conditions are rather typical for Rotterdam and the Western part of the Netherlands. The high phreatic level is found at 1-2 m below ground level (NAP[1] +3.0 m). About 2-7 m of sand is found as the top layer, underlain by clay and peat layers to a depth of about 20 m (NAP -17 m). Below that the Pleistocene sand layer, commonly used as a foundation layer for piles, is found. Figure 3.9 shows a typical CPT and soil profile with parameters.

3.5.2 Details of the White House building

The White House, see Figure 3.10, 11-storey high rise building was built in 1897/1898. The size of the building is 20x20 m square and 43 m high. Details of the construction are difficult to find. According to Top010 (2009) the construction is made from masonry. The facades are covered with white tiles and natural stone. The roof is made out of iron.

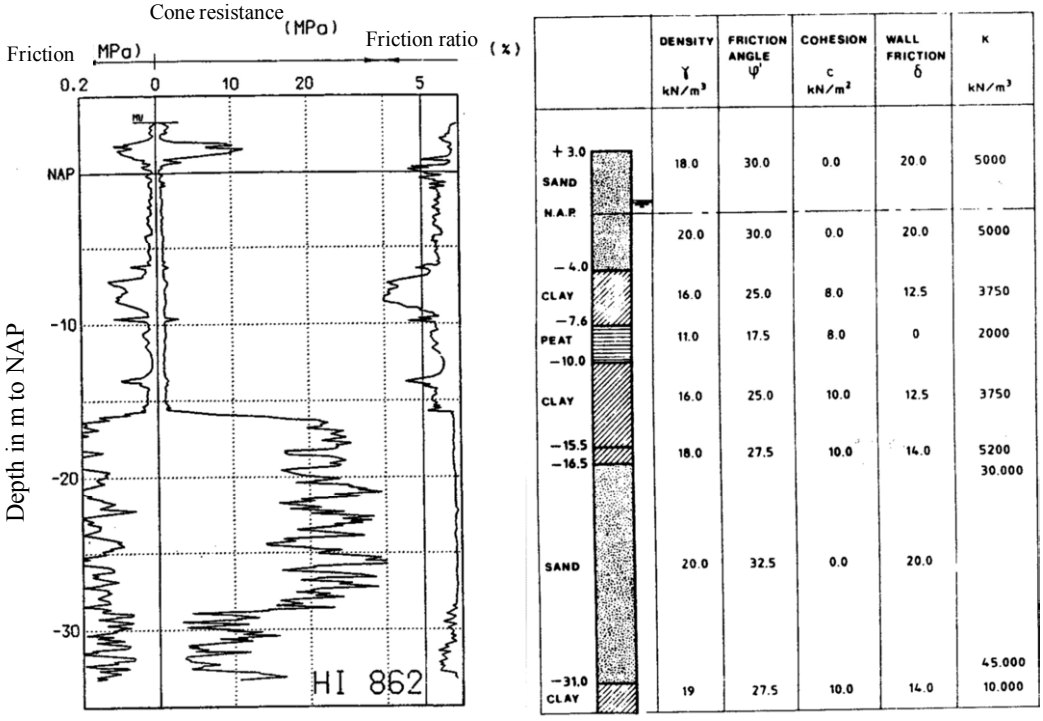


Figure 3.9 Typical CPT near White House and soil parameters used for design (Brassinga and van Tol, 1991)

[1] All levels are related to NAP, which is the Dutch reference level

The building is found on wooden piles in the Pleistocene sand layer, with a pile diameter of about 250 mm. The design drawing in Figure 3.11 shows about 750 piles for the foundation. The piles are located in rows of 2-4 under the main walls, with a centre-to-centre spacing of 450 – 500mm. Almost 9% of the total foundation area was filled with piles. During installation of the piles, a significant heave of the ground level of about 1.0 m was reported in Wikipedia (2009).

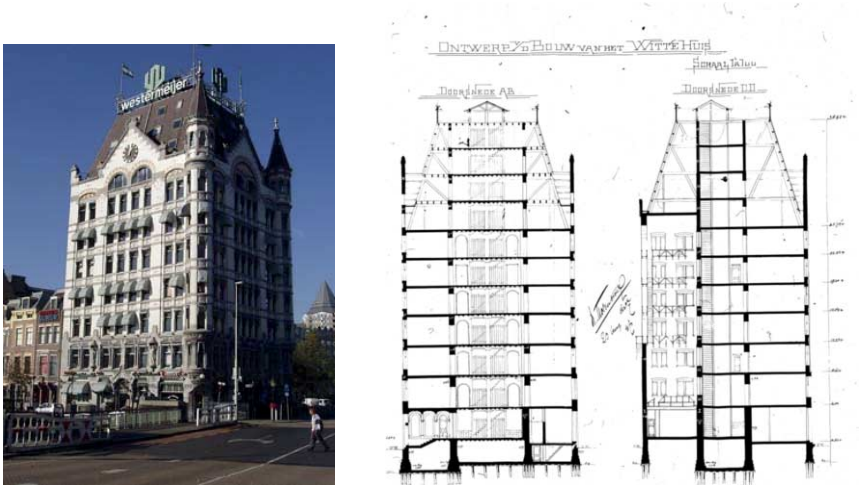


Figure 3.10 The White House in Rotterdam
(with recent picture on the left and design drawing from 1895 on the right)

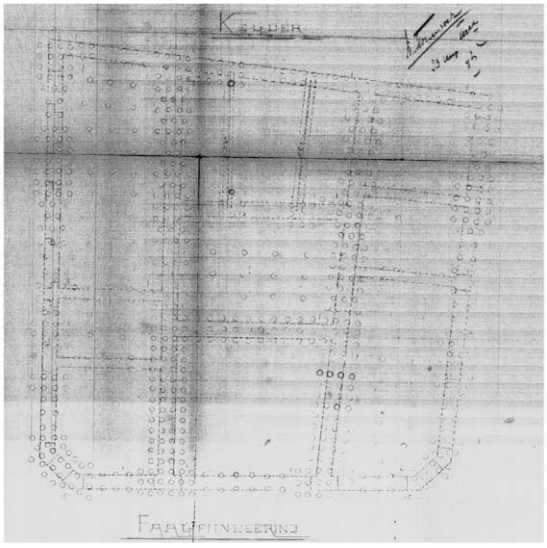


Figure 3.11 Design drawing of the White House pile foundation (1895)

Brassinga and van Tol (1991) report that the foundation had a low factor of safety before construction started. However, in the past no significant differential settlements of the White House were noticed.

3.5.3 Construction characteristics for Willemspoortunnel

Near the White House (at 10 m from the 36m deep, 1.2 m thick D-wall) the cut-and-cover tunnel crosses a canal from the harbour, leading to unequal loads on both sides of the trench, see Figure 3.12 and Figure 3.13. This caused horizontal displacements of the building, even though a cofferdam was built for that matter. The excavation reached to 20 m (NAP -17m), just at the base of the pile foundation of the White House.

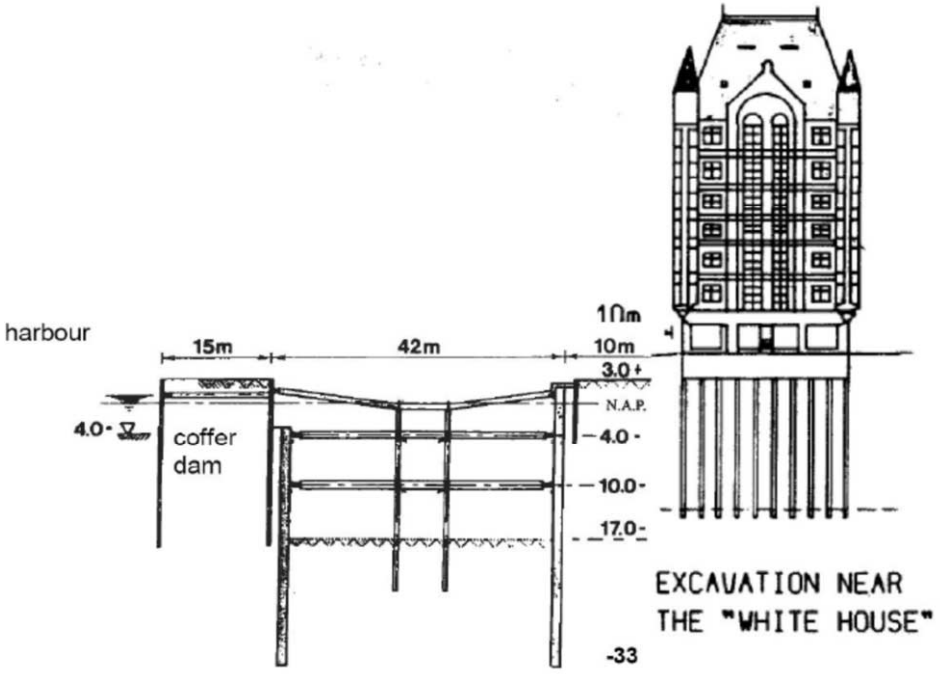


Figure 3.12 Excavation near the Witte Huis (Sarlemijn et al, 1993)

The wall deflection was not measured near the White House. Inclinometers were placed at other locations, where the loading on both sides was equal, showing displacements of around 20mm maximum and about 0 mm at the top. These measurements can not be used to evaluate the interaction with the White House due to the unequal loading at that specific location. Ground surface settlements unfortunately were not measured. See Figure 3.14 for the development of the settlements of the four corners of the building with time.

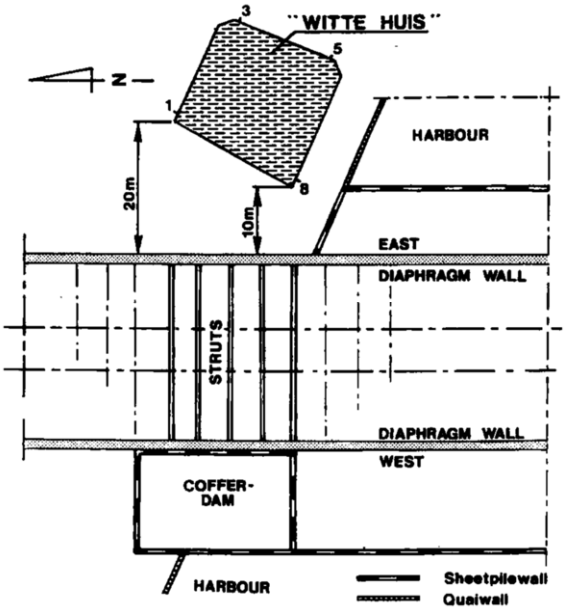


Figure 3.13 Top view near the White House (Brassinga and van Tol, 1991)

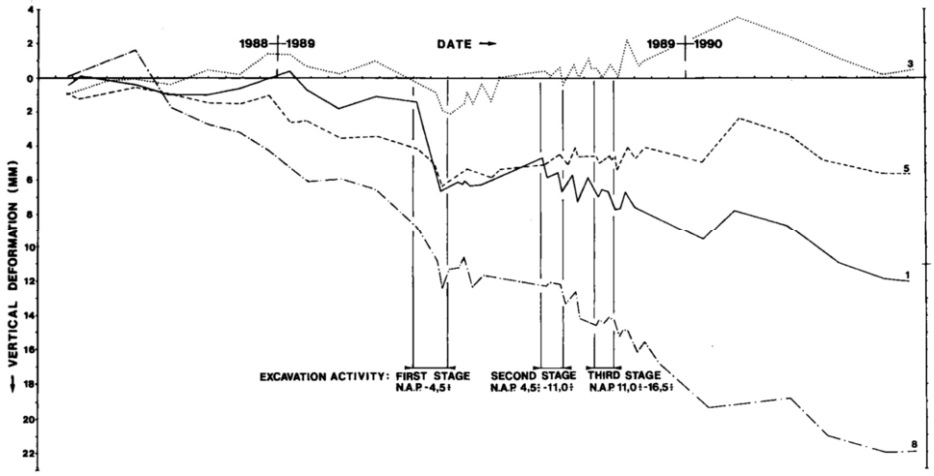


Figure 3.14 Vertical deformations versus time for White House (Brassinga and van Tol, 1991). Numbers relate to the settlement markers shown in Figure 3.13.

3.5.4 Response of the 'White House'

The building settled 6 mm during the D-wall construction, 12 mm in total including the first excavation phase (to NAP -4m) and after extra prestressing of the struts an additional 5 mm (17 mm total) during the rest of the excavation.

The measured deformation of the building in the first stage of the excavation is compared with the calculated green field settlement over the soil depth in Figure 3.15. During this stage the settlement of the White House was 6 mm in measuring point 8 and 5 mm in point 1. The soil deformation was calculated by FEM using the wall deflection as input. The level of the neutral point was determined matching the calculated vertical ground deformation at the subsequent levels with the measured deformation of the building. Vertical settlements of the building occur due to the combination of the deformation of the pile tip level and an increase in negative skin friction. Due to a low factor of safety of the original pile foundation, the settlement of the piles follows the deformation of the soil at the neutral point along the pile shaft (where negative and positive skin friction meet). Vertical soil displacements calculated using FEM equal to the pile settlement were found at NAP -12 m at both distances from the wall. This is assumed to be the level of the neutral point, which was used to predict for the further excavation stages, see Figure 3.15. It should be noted that the calculated ground settlement with depth in the soil turned out to be very sensitive to the assumed stiffness of the struts. This makes it difficult to define the neutral level accurately.

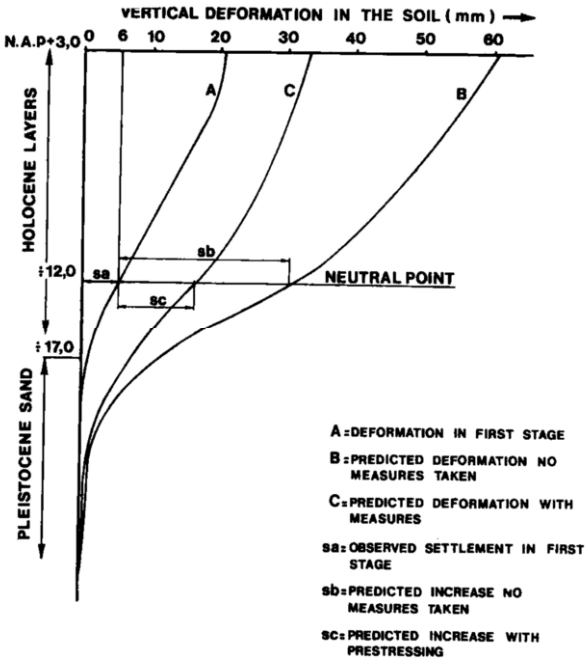


Figure 3.15 Calculated soil deformations with depth White House (Brassinga and van Tol, 1991)

Deformations after this stage (between August and November 1989) for the building were 10-12 mm. This value compares well with the calculated values based on the neutral point, which was 11 mm.

Figure 3.16 shows the settlement of the building at the points 1, 3, 5 and 8 of the two stages: halfway down the full excavation depth and at full depth. Based on the regular distance between the lines of equal settlements, it is concluded that the building mostly tilted, without sagging or hogging deformation. The tilt is not exactly in the direction of the deep excavation due to the unequal loading on the harbour side, where the ground level is at NAP – 4m. Due to the extra struts in the second stage of the construction, the tilt at this stage is directed more towards the diaphragm wall. The measured deflection is very small. No actual damage due to the deep excavation was observed in the building.

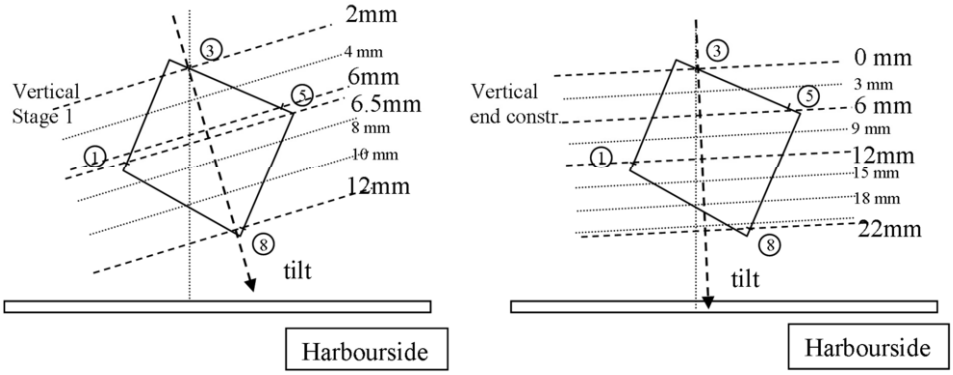


Figure 3.16 Vertical deformation of White House (left after stage 1, right at end of construction) with direction of tilt indicated

Horizontal deformations are not available anymore, but were larger than expected due to the translation of the deep excavation in the direction of the cofferdam. No damage was observed as a consequence, so it is expected that the building moved rather uniformly. It translated more than it strained horizontally. The maximum calculated horizontal deformation at point 8 was 20mm after stage 1 and 25mm at the end of construction. If the rear of the building did not move at all, the horizontal strain would have been 20 mm / 28 m (after stage 1) = $7*10^{-4}$ or 25 mm/ 20 m = $1.2*10^{-3}$ based on the FEM results. The L/H ratio of the high rise is 20 m / 43 m = 0.47. Combined with negligible deflection this would have resulted in 'very slight' or 'slight' damage respectively following Mair et al (1996) and Cording et al. (2001).

The building shows no signs of bending in the structure, which means the building is relatively stiff compared to the soil. The relative stiffness is defined as the stiffness of the building relative to the stiffness of the underlying ground. The bending stiffness of the building can be assessed using different methods; by taking into account the base slab, the floors and/or the walls and the amount of interaction between them. In this case the masonry walls, with a width of over 1 m in the basement and about 0.4 m at the top of the building, provide most of the stiffness. Based on an average width of 0.6m, a height to the roof of 30m and 2 walls in the 20 m building, the EI of the building would be $810*10^6$ kNm2/m.

If a correction is made for the openings in the wall, based on Dimmock and Mair (2008), the actual stiffness would be about one order of a magnitude lower at about $80*10^6$ kN m^2/m. If only the stiffness of the slab and the floors is considered, the EI would be about a thousand times smaller at 100 $*10^3$ kNm^2/m. The estimated relative bending stiffness values are calculated and presented in Table 3.2 and Figure 3.17.

Table 3.2 Calculated (relative) bending stiffness White House

Description	**Calculated value**
Number of storey's	11 + basement, floor slabs 0.2m
Width building	20 * √2 = 28m
Length of building	20 * √2 = 28m
Foundation	Slab cement/masonry 0.3 m + piles
E soil	$E_{0.01\%}$ = 3 MPa Soft clay
E slab and floors / wall	10 GPa / 6 GPa
I building m^4/m: - Slab + floors - 2 walls 0.6 m	 1m $*0.3^3/12$ + 11x$0.2^3/12$ = 0.01 2* b_{wall} / $b_{building}$* H_{wall}^3 /12 = 2* 0.6 / 20 * 30^3 /12 = 135
ρ^*_{Goh} = EI / E_s L^3 - Slab + floors - 2 walls 0.6 m	 $1.5*10^{-3}$ 1.2 (including reduction for openings)

In reality very little hogging deformation was observed, which is consistent with the estimated relative bending stiffness based on the walls (allowing for openings) leading to a modification factor of 0. The interaction based only on the individual slabs and floors underestimates the relative bending stiffness for this building. Methods for frame structures such as presented by Goh (2010) and Potts and Addenbrooke (1996) are not considered realistic for this type of masonry bearing structure.

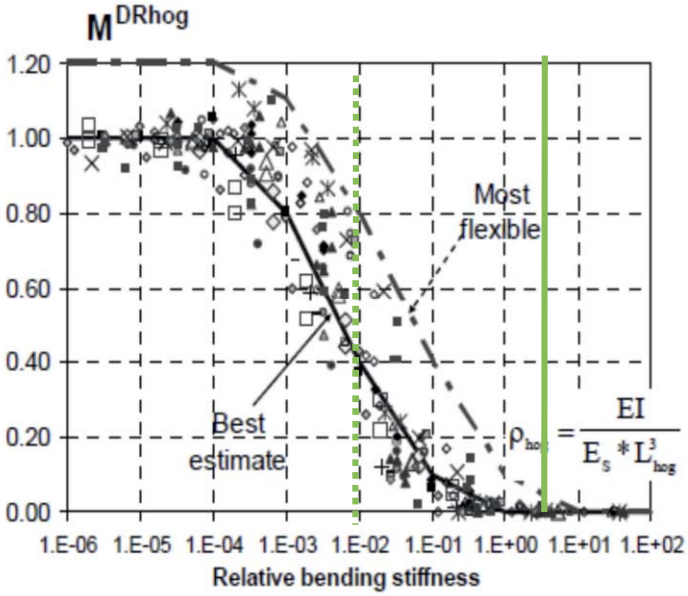


Figure 3.17 Design curves from Goh (2010) for hogging, modified modification factors with result for White House in green lines (solid for walls, dashed for slab and floors)

3.5.5 Conclusions

Deformation of the White House as a result of the deep excavation mainly caused tilt in the building. The amount of differential settlement (and associated deflection ratio) was negligible and so was the corresponding damage.

The effect of the pile foundation could only be evaluated by the use of FEM, because no deformations of the wall were measured. These calculations indicate that the timber piles follow the soil deformations at about NAP -12 m, while the bearing layer is situated at NAP -17 m. This would mean that the neutral level is found at NAP -12m. The neutral level, based on this analysis, did not change between stage 1 and the end of construction.

Horizontal deformations were not available any more at present, but were larger than expected at the point closest to the excavation due to the translation of the whole deep excavation in the direction of the cofferdam. Based on Mair et al (1996) the expected damage of the White House based on the maximum assumed horizontal strain in stage 1 would have resulted in 'very slight' with a central point load calculation or 'slight' according to the FEM analysis.

The building shows no signs of bending in the structure at all. This means it is relatively stiff compared to the soil, which is confirmed by Goh (2010) for the upper bound of EI values calculated for the building based on the stiffness of the walls (allowing for openings).

3.6 Conclusions from previous case histories

This collection of case histories shows that the topic of soil-construction interaction in the case of piled buildings related to the construction of deep excavations in soft soils can be improved if certain aspects related to soil displacements, building damage and interaction with the foundation are taken into account.

Settlements due to diaphragm wall installation are significantly influenced by the stability of the trench. Installation of several panels close to each other in a short time and/or high ground water pressures during construction will increase the ground displacements behind the wall. Deep excavations and the adjacent buildings are never two dimensional. The three-dimensional behaviour may cause a reduction in absolute deformations (if a stiff corner and support system is in place) but increases differential settlement.

The case histories presented confirm the general trends presented in Chapter 2 that for stiff clays, residual soils and sands, as suggested by Clough and O'Rourke (1990), a maximum horizontal wall deflection of about 0.2% H and for soft clays up to 1-2% H, reaching to a distance of 2 times the excavation depth should be expected.

- Warde School, Chicago: wall deflection is 0.23% H (excavation only) and 0.41% H after total construction
- Chater station, Hong Kong: wall deflection is 0.15% H (excavation only), building settlements are 0.7% after total construction
- KPE, Singapore: wall deflection is 0.1%H (excavation only), ground settlements behind the wall are 0.2%H after total construction.

The ratio between the wall deflection and the settlement behind the wall in these case histories falls within the general band of 0.5-1.5. In special circumstances (such as extreme ground-water lowering outside the excavation) this ratio might increase. The settlement trough of these case histories extends to 1-2 times the excavation depth from the wall. The Chicago case history showed that, based on building deformations, the settlement trough width remained constant at about the length of the retaining wall. This effect was not found in the other case histories.

The case histories proved that actual green field displacements were in general larger than the predicted ones, mainly caused by installation effects, ground-water lowering or other effects not accounted for. The effect of the excavation itself is generally predicted rather well. The three-dimensional behaviour of the excavation and the building resulted in smaller deformations close to the corners (even at the inward corner) of the excavation.

There are very few case histories available with both green field and building deformations, especially for buildings founded on piles. The limited evidence available shows that the assumption that the building follows the deformations of the pile toe level in the Singapore case worked well. There is an even greater lack of case histories with sufficient data on horizontal deformations of the building compared to green field and subsoil deformations.

Depending on the amount of horizontal strain in the building, the damage category expected may vary over more than one category. Most damage to buildings can be explained by the deflection of the building, but if several stiff building units or parts are flexibly connected rigid body tilt can cause substantial damage as well. If buildings are homogeneous taking into account rigid body tilt may limit the damage expected.

CHAPTER 4 FIELD DATA NORTH SOUTH LINE

4.1 Introduction

In Amsterdam a 9.5 km long new metro line is under construction, of which 3.8 km is built underground by two bored tunnels with three large cut and cover stations in the historic centre, the North South Metroline (original Dutch name being 'Noord/Zuidlijn'). The line starts above ground in the North of Amsterdam, continues under the river IJ and Amsterdam Central Station and continues with two bored tunnels under the streets Rokin, Vijzelgracht, Ferdinand Bolstraat and the Scheldestraat. At the RAI area the railway line still runs underground. The North South Line comes above the ground in the mid section of the ring road A10 between RAI and WTC. The bored tunnel is 3.1 km long. The tunnel boring machines follow the existing street pattern as closely as possible. Two tunnels are constructed under the historical centre, one for each underground railway track. In total five underground stations are built along the line, see Figure 4.1. For the construction of the most centrally located underground stations (Central Station, Rokin, Vijzelgracht and Ceintuurbaan) the top-down method is used. The stations are realised to a maximum depth of approx. 30-33 m. below surface level.

This Chapter describes the soil characteristics, the building types and the construction works involved in the North South Metroline. This information is used for the analyses described in Chapters 5 – 10. The work presented in this chapter is an abstract of work performed in cooperation with others, which was published in COB (2011a, 2011b, 2011c and 2011d). The author of this thesis was the lead author of those publications.

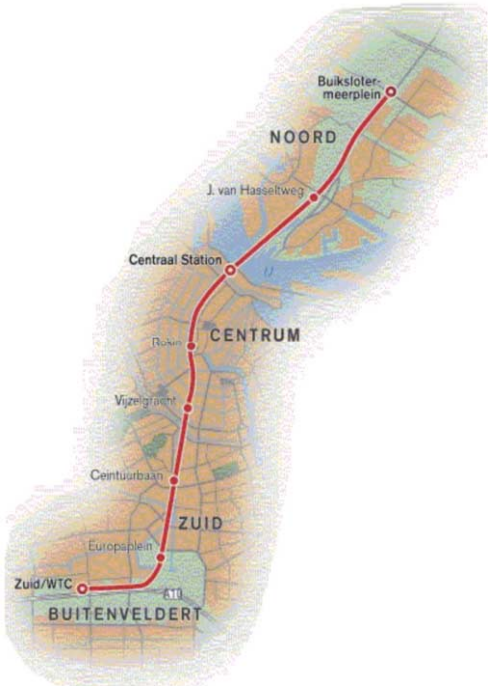


Figure 4.1 Overview of the North South Line and its stations

4.2 Soil characteristics

4.2.1 Geology and geohydrology

The geology of the Amsterdam subsoil, taken from ABNZL (2000) and Lange et al. (1999), is of interest for the analysis of the field data from the surface level to the base sand layer (called 3rd sand layer) at about 50 m deep. All stratigraphies of interest are part of the Quaternary Period, consisting of both Pleistocene and Holocene deposits.

A glacial basin was formed during the last stages of the previous ice age as a lateral moraine (Saalien age, about 150.000 year ago). The depth varies over the city centre between 50-60 m deep, but is much shallower to the south of the city centre and much deeper to the North. The basis of the basin consists of the Third Sand layer, which is formed by coarse river sands and fines upward towards the top of the layer. Above this layer, the moraine and fluvio-glacial deposits of the Saalien consist of laminated clay deposits (Warven clay) with a thickness of 5 to 30 m. Glacial deposits of Aeolian, very fine, sands are found over the Warven Clay; which are part of the Intermediate Sand layer. On top of that layer, the Eemclay layer is found with 0 to 30 m thickness over Amsterdam (from South to North, on average about 15 m around the deep stations), see Figure 4.2. This Eem clay layer consists of a variation of laminated clay, fissured clay and massive clay. The clay is generally stiff to very stiff, silty, from marine origin and rather homogeneously consisting mainly of quartz, calcite and illite.

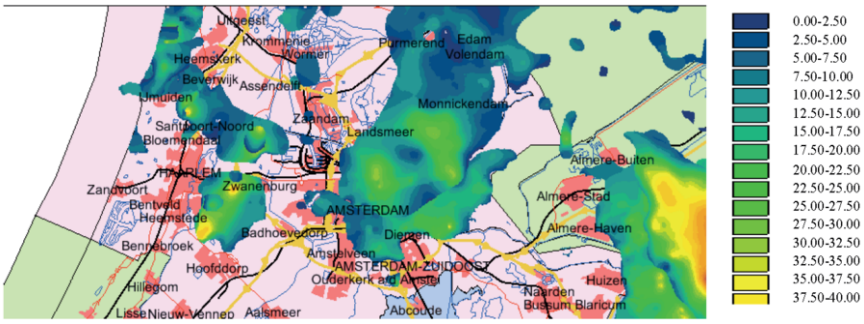


Figure 4.2 Location and thickness of the Eem Clay Formation around Amsterdam (TNO DINO Regis 2008)

More recent deposits were formed in the Weichselian period of the last ice age, in which The Netherlands was not covered with ice. During this period the First and Second sand layers were formed, consisting of Aeolian sands from sediments running of the moraines. The Second Sand Layer consists of fine to medium coarse sand. On top of this layer the silty sandy, firm clay layer of the Allerød is found, which results from river deposits. The First Sand Layer has the same characteristics as the Second, but was eroded in some areas. The Holocene deposits determined the shape of the western and northern part of The Netherlands, under conditions of rising temperatures and sea-level. A large variation of layers is found, starting with the base-peat layer (Basisveen), followed by a soft marine Hydrobia clay. After this period, a brackish environment formed the Wad-deposits, a sand layer previously used as foundation layer (also called 'farmers sand') underneath the soft Old Sea clay and the very soft Holland Peat. The youngest layers are the soft Young Sea Clay and the man-made 'Ophooglaag' (fill). In some locations (especially at Rokin Station), tidal channels were formed during the Holocene period, eroding the Holland Peat and/or the Base Peat layer.

The first aquifer for a geohydrological schematization is usually addressed as the combination of the first and second sand layer including the Allerød. The second aquifer is formed by the third sand layer. The hydrological conditions are influenced by the deep polders surrounding the city (such as Haarlemmermeerpolder, Bijlmermeer and Watergraafsmeer). The piezometric level in the first aquifer is about NAP–3 m and fairly constant over the project (max. difference 0.5m). The rather impermeable deepest Holocene layers prevent that the phreatic level is influenced by the level in the first aquifer.

4.2.2 Soil profile

The typical soil profile at the three deep station locations consists of a man-made top layer, followed by soft Holocene clay and peat to a level of about NAP –11.0m (ground level around NAP +0.4m). Then the Weichselian deposits are found, starting with the "first sand layer", as it is called, found between NAP – 11.0 m and NAP – 14m, a dense, fine to medium sand layer. Beneath it lays a heterogeneous layer of very sandy clay, very clayey sand and silt (the Allerød). The 2nd sand layer is found at about NAP –16m, extending to NAP – 24 m

and comprises a dense to very dense, fine to coarse sand. Below the 2nd sand layer a stiff to very stiff clay layer of about 15m total thickness (the Eem clay and Drente clay) is found, sometimes separated by the Intermediate sand layer. The base is formed by the highly permeable 3rd sand layer. A more detailed overview of the depth of the layers is given in Table 4.1 for each of the deep stations. A typical CPT for each station is given in Annex A. More detailed information on the soil profiles for each monitoring section can be found in the three station reports COB (2011b, 2011c and 2011d). For the most relevant layers, also the permeability is given, based on direct measurements in the lab (falling head on clay/silt and constant head on sandy samples) and indirect measurements, being oedometer tests.

Table 4.1 Soil profiles, more details in COB (2011b, 2011c and 2011d)

	Permeability k_v ABNZL (2004)	**Typical cross section Rokin**	**Typical cross section Vijzelgracht**	**Typical cross section Ceintuurbaan**
	Average [m/s]	**Top [m to NAP]**	**Top [m to NAP]**	**Top [m to NAP]**
Fill man made (aanvulling)		+0.5	+1.0 to +1.3	+0.4
Peat (Hollandveen)	$1 * 10^{-8}$	-4.8 to -5.1	-2.5 to – 5.0	-2.3 to -3.0
Old Seaclay	$1.5 * 10^{-9}$	-5.5/-9.8 South, not in North	-4.5 to– 5.0	-5.0
Waddeposit, with sand	$1 * 10^{-7}$	-8.4 to -10.7	-6.7 to -7.0	-6.4
Hydrobiaclay	$1 * 10^{-9}$	-10.2 to -10.3	-9 to -10.5	-10.3 to -11
Peat (Basisveen)	$1 * 10^{-8}$	-11.2 to -12.2	-11.3 to -12	-10.5 to -11.5
First sandlayer	$1.5 * 10^{-4}$	-11.6 to –12.6	-11.5 to -12.5	-11.0 to –12.0
Allerød	$3 * 10^{-5}$	-14.3 to 15.7	–13.7 to – 15	-14.0
Second sand layer (local occurrence of clay layers)	$1 * 10^{-4}$	-16.3 to -18.2	-16 to –17	-15.5 to -16.0
Eemclay	$2*10^{-9}$	-24.2 to - 26.3	-20.5 to - 25.7	-24.7 to - 25.0
Harting layer		-43.2	–40.7	x
Intermediate sand layer		x	–41.3	-38.0 to -38.2
Glacial Drente clay		-41.9 to -43.8	-42.5 to –43	-41 to -42
Glacial Warven clay		-49.9 to –-52.1	-50	-45.5 to –49 (local occurrences of sand)
Third sand layer	$1 * 10^{-4}$	-51.8 to –54.1	-52.5	-47.3 to –50

4.2.3 Soil parameters

An overview of all soil parameters derived for the North South Line project is included in Annex B and more extensively reported in COB (2011a) and ABNZL (2000).

Standard triaxial tests have been used to determine the soil strength. The tests were performed strain controlled, consolidated and undrained with 38 mm and 65 mm samples, with $K_0 = 0.5$. Post peak strengths are taken at 15% strain and other values at 0.5% for clay and 1.0% for sand. A variation coefficient for the angle of internal friction is found of about 10%.

Cohesion (c') of the Eemclay is 10-15 kPa, angle of internal friction post peak (φ') is 32-34 degrees and at 0.5% strain 28-30 degrees. For the Eemclay, the average value of E'_{50} determined from triaxial tests is 27 MPa , according to ABNZL (2000) and for the FEM calculations the $E'_{50,ref}$ has been determined at 10-14 MPa. All reference stresses are 100 kPa. A large variation in E'_{50} exists (35-50% variation coefficient). E'_{50} is determined as 48-80 MPa according to Pound (1999). Oedometer tests have been performed to determine low characteristic values for E_{oed}. The high characteristic values have been determined using a correlation with the cone resistance $E_{oed;ref} = 8\ (q_c - \sigma_{v;0})$ taken from Lunne et al. (1997). The resulting average of $E_{oed;ref}$ for the Eemclay layer is 3-4.5 Mpa.

The second sand layer shows very consistent values of the friction angle of 34.5 degrees. $E_{oed;ref}$ for sand has been found using similar correlations with the cone resistance q_c according to Lunne et al. (1997) as:

- $E_{oed} = (2 * q_c + 20)$ for sand with $q_c > 10$ MPa and
- $E_{oed} = 3 * q_c$ for silt.

E'_{ur} has been determined using several methods, including oedometer tests with relaxation, triaxial unloading (Consolidated Undrained Anisotropic Extension CAUE) tests, cyclic triaxial tests and CPM tests, as well as several correlations based on cone resistance and void ratio.
The values in the parameter set are based on the CPM tests according to the following correlation:

- $E_{ur;ref} = 2\ G\ (1 + \nu_{ur})$, with $\nu_{ur} = 0.15$.

The resulting $E_{ur;ref}$ for the Eemclay is 40-55 Mpa.

The Poisson ratio used is based on Biarez and Hicher (1994) and Carter and Bentley (1991):

- Clay: 0.3 – 0.33.
- Peat: 0.35.
- Sand: 0.25.

All layers below the second sand layer (Eemclay and deeper) are overconsolidated. The overconsolidation ratio (OCR) is between 1.0 and 2.5, with 2.0 as average value for the Eemclay. The Holocene layers are lightly overconsolidated due to ageing effects. The

Overconsolidation Ratio (OCR) is about 1.05 to 1.1. The angle of dilatancy is taken as the friction angle minus 30 degrees. The earth pressure coefficient for neutral conditions (K_0) is about 0.5.

4.2.4 Subsidence in Amsterdam

The presence of soft soil layers combined with historical raising of the ground level causes subsidence in the city of Amsterdam due to consolidation and creep of the Holocene layers and even the Eemclay at larger depth. Over 100 years ago, usually small scale fills were used at construction sites. Most of the large scale fills (the man-made top layer) were placed 50-100 years ago and included the largest deposition of 4-5 m of sand in the area south of Ceintuurbaan (Oversteegen, 1998). Old cities in the western part of the Netherlands in general experience ground surface settlements of about 10 to 20 mm/year. Buildings on average (usually piled buildings) settle about 2 to 4 mm /year, if they are related to the settlement markers (NAP –levels).

The city of Amsterdam operates a net of reference bolts (NAP-levels), placed on buildings and other structures. Hogenes (1998) assessed the stability of 794 NAP-levels and found an average settlement of these NAP-levels of 0.9 mm/year over the period 1927 to 1998. These levels are placed on various types of buildings, resulting in values between +2.4 and - 7.9 mm/year, with 95% of the settlement values smaller than 2.4 mm/year. Figure 4.3 shows the settlements in mm / year throughout the city as well as zoomed in on the location of the deep stations, which are also shown. These settlements have been derived by comparing the NAP –levels with 33 underground reference points; consisting of concrete piles (11) or deep CPT-rods (22) founded in the second sand layer. Due to creep of the Eem clay these reference points can also settle; values up to 0.3 mm/year have been found for this effect (Hogenes 1998). No reference points deeper than the 3rd sand layer are used. The 3rd sand layer is assumed to be the stable base level. In total, the settlement of the buildings relative to the 3rd sand layer on average would be around 4 mm/year, with 95% of the settlements smaller than 7 mm/year.

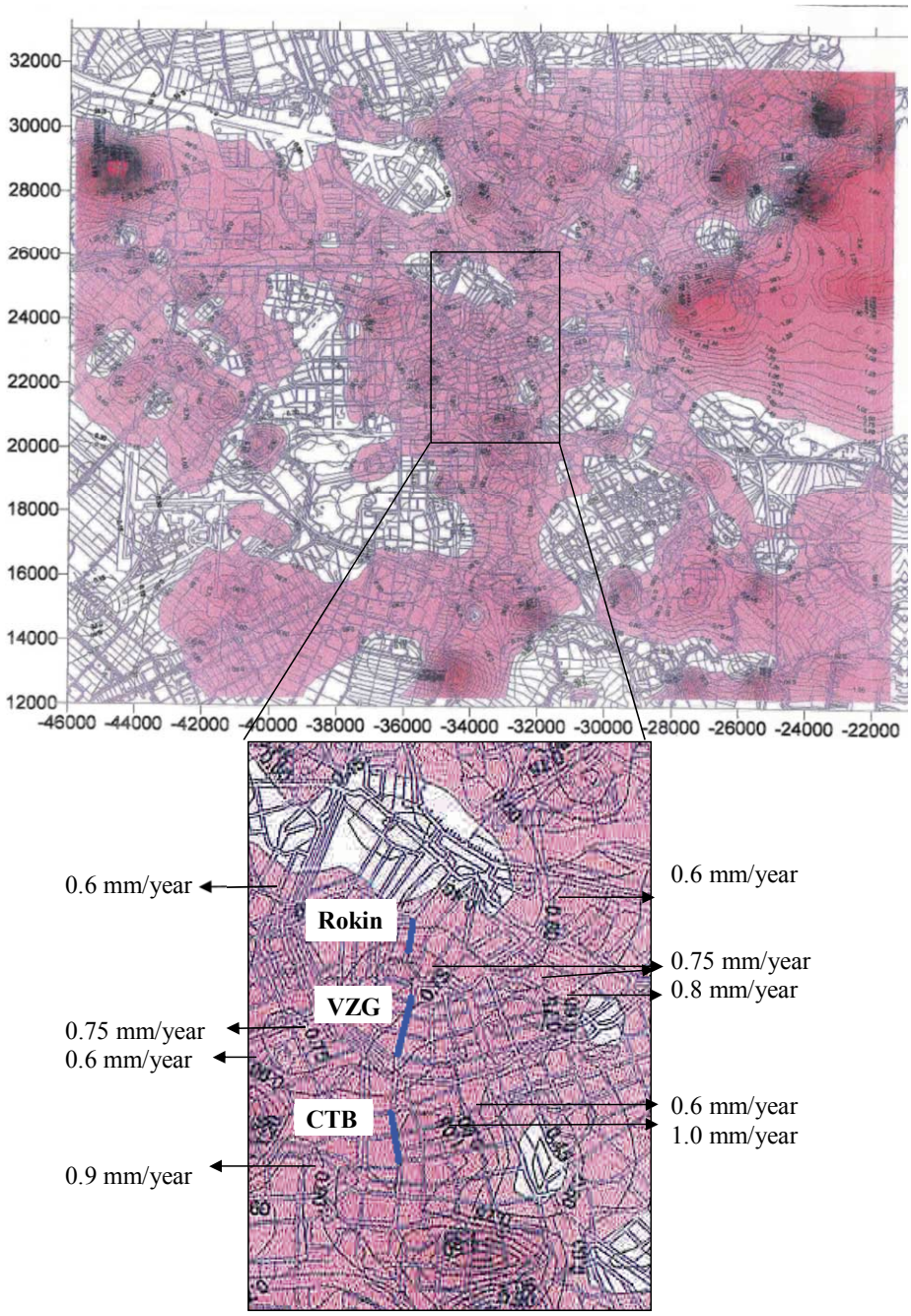


Figure 4.3 NAP –levels and their settlement in mm/year referenced to the second sand layer and their settlement in mm/year at location of deep stations (Hogenes, 1998)

4.3 Building characteristics

4.3.1 Buildings in Amsterdam

Most buildings in the historic centre of Amsterdam are built from masonry and/or concrete. Three types of constructions are common:

- Old buildings (from 1600-1900) with masonry walls, wooden floors and timber pile foundations. This type of building is common in the older inner cities, such as Amsterdam and Rotterdam.
- Recent buildings for 1-4 storey houses, built with concrete walls and floors, prefabricated concrete or steel piles and usually a roof that is a little lighter, for example made of wood and tiles.
- Recent buildings (more than 3 storeys), made of concrete or steel frames with infill walls and usually prefabricated concrete floors. Foundations are usually deeper than in the other cases.

The geometry and structure of typical buildings before 1940 is shown in Figure 4.4. The masonry walls and facades are slimmest from the top to the first floor (220 mm), average at ground level (330 mm) and widest below ground level (440mm) (TNO, 1995).

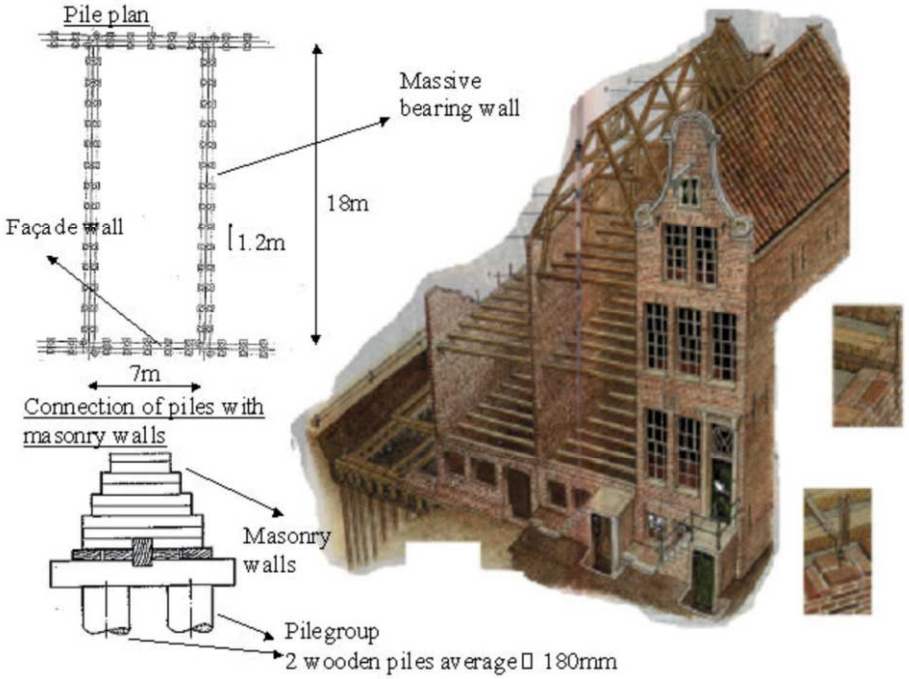


Figure 4.4 Typical structure for historical buildings (mostly around Rokin) TNO (1995)

The average pile load, excluding negative skin friction, is about 90 kN/pile for the walls and 35 kN/pile for the facades as derived by Frankenmolen (2006).

4.3.2 Typical timber foundations

The oldest pile foundations still present in Amsterdam (and rather typical for the old cities in the Western part of The Netherlands) date from the 17th century. Most of the buildings around the deep stations rest on a foundation of timber piles in the First Sand Layer (Eerste Zandlaag). Pile installation was done by hand using a tripod and weight lifted by several men at that time. Since approximately 1870 steam engines were used, see Figure 4.5.



Figure 4.5 Installation of wooden pile by steam engine (picture taken in 1891 by Jacob Olie)

The wooden piles are installed in pairs with 0.8m between the pairs. Average diameter of the piles is 180 mm or according to a historic source (Zantkuijl, 1993) “not less than 200 mm at the thicker end or 85 mm at the thin end”. These piles were driven between oak beams present at either side of a trench, after which other oak beams were laid across at regular spaces: the so called “cross beams”. Each cross beam has a thickness of about 3 ‘thumbs’ (old Dutch measure, equivalent of an inch, about 0.025 m). Cross beams have been used since the second half of the 17th century. Over these cross beams, foundation plates of 4 thumbs (about 0.1m) thick are installed to spread the weight of the wall over the piles. Since the 18th century, a piece of quarter sawn timber was used to prevent shifting of the masonry wall (see Figure 4.6).

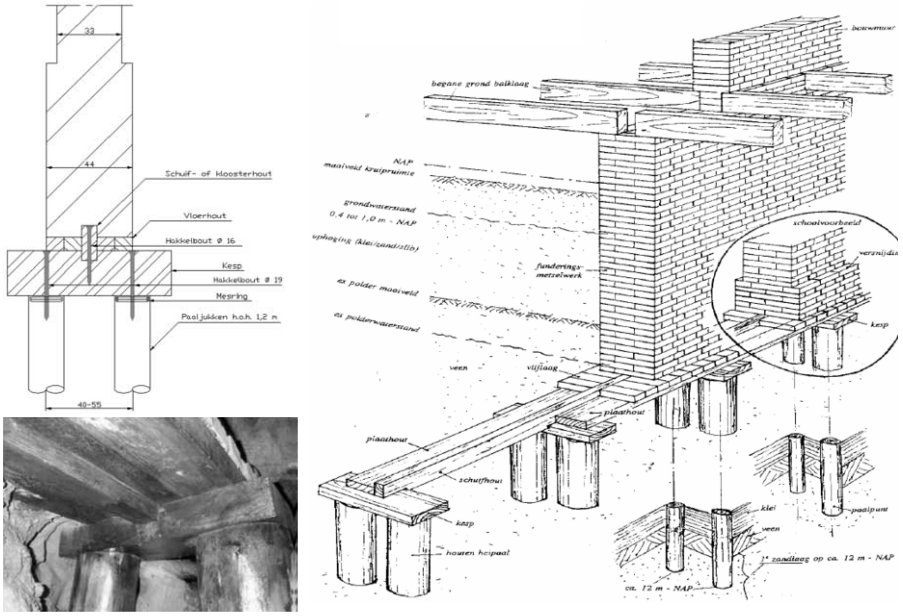


Figure 4.6 Typical Amsterdam pile system (Zantkuijl, 1993)

Buildings built between 1860 and 1925 usually have a so-called Amsterdam foundation with the double row of piles as shown in Figure 4.6. Pile diameters for the timber piles vary from 160 – 300 mm (typical 180-200 mm) at the head and usually diminish by 8 mm/m to about 70-200 mm (typical 120-140 mm) at the toe. From the 20th century, piles were driven more easily and deeper due to the development of pile driving equipment like diesel hammers.

Buildings between 1920 and 1940 usually have a single row of piles with a reinforced concrete beam on top. Pile lengths were usually taken similar to those chosen for adjacent structures. After 1945 other pile types were introduced, especially the driven prefabricated concrete pile. Around this time, soil investigations started to take place to determine the pile lengths. From about 1965, it became common to account for negative skin friction in the design, although this effect was often underestimated until the 1980s (van Tol, 1994). Based on several pile load tests in the historic centre it is known that the wooden pile foundations have low factors of safety. As piling technology developed further, the more recent structures tend to have concrete or steel piles which are installed to the deeper, more stable 2nd sand layer.

4.3.3 Foundation quality assessment method Amsterdam

Van Tol (1994) described the percentage of pile foundations in Amsterdam and Rotterdam that are not up to standards, as a function of the age of the building, see Figure 4.7. These numbers were derived from large scale investigations in both cities and clearly show a trend that foundations perform better when they are newer, between 1900 and 1930. Van Tol warned that the absolute values are not very reliable, since for Amsterdam and Rotterdam

different methods of determination are used and the overall selection of inspected buildings is not completely random. Nevertheless, the overall conclusion is that the foundation quality increases over time for these specific years of construction.

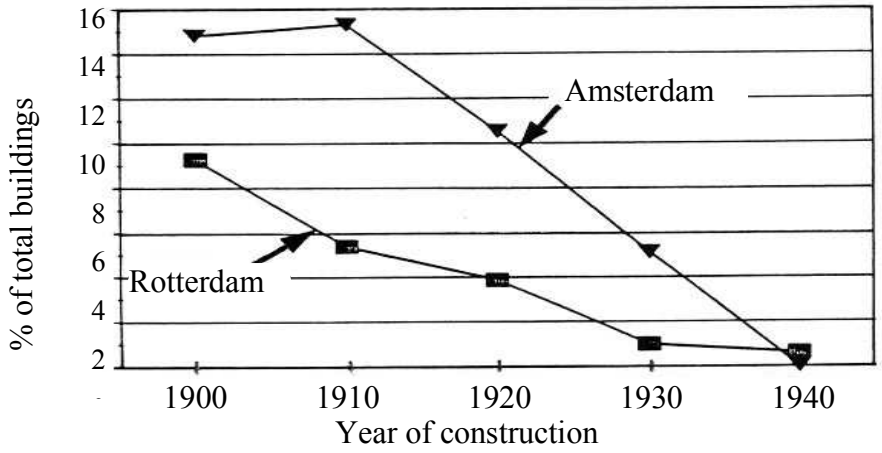


Figure 4.7 Percentage foundations with insufficient foundation quality (van Tol, 1994)

Problems with the timber piles can have two types of causes; the first group of causes is related to the construction itself. The quality of the wood, the cross beam on top of the piles and/or the connection to the walls. The second group of problems is related to the geotechnical pile capacity.

Timber pile foundations can deteriorate due to decay of the wood. Decay can be caused by bacteria, fungi or mould and usually occurs due to lowering of the phreatic groundwater table. This can result in collapse of the cross beam on top of the piles, which causes a sudden loss of foundation capacity (the foundation load is not transferred to the piles). This effect is shown in Figure 4.8. The pile shafts can also deteriorate, leading to smaller effective diameter of the pile.

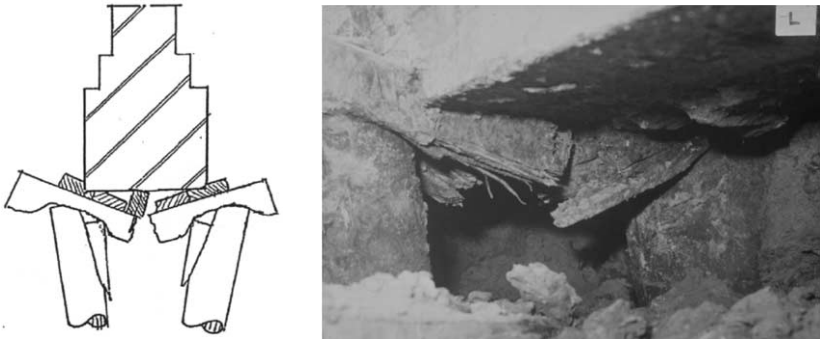


Figure 4.8 Foundation failure due to collapse of the cross beam

All buildings in the influence zone of the North South Line have been surveyed and categorised in four different quality classes based on the state of the foundation.

Table 4.2 Quality class for Amsterdam foundations (from city of Amsterdam)

Quality class	Criterion
Class I	Structure-foundation good; Time to renewal at least 40 year.
Class II	Structure-foundation good or reasonable; Time to renewal at least 25 year.
Class III	Structure-foundation moderate; Time to renewal at least 15 year.
Class IV	Structure-foundation in bad condition; Unacceptable settlements may occur any time. No advised time to renewal. No immediate need to demolish unless stated.

The quality class, see Table 4.2, is determined by an optional inspection of the foundation, characteristics of the structure of the building and its present damage and needs to take into account the mechanism of deterioration. If the foundation is overloaded, the settlement with time is much smaller than in case the timber has decayed. The assessment method of the city of Amsterdam (Oversteegen, 1998) includes a scoring system based on three indicators:

- The maximum rotation of the building (θ).
- The maximum speed of settlement (S_v/year).
- The maximum difference in speed of settlement (Δv).

4.3.4 Pile capacity and load-settlement behaviour

The capacity of the foundation piles can be determined by the combination of the skin friction and the tip resistance. Both contributions to the capacity depend on the displacement of the pile relative to the soil. The elasticity of the pile itself can also play a role. The load settlement behaviour of the piles depends on the single pile capacity as well as the deformations transferred from other piles or the soil beneath the pile (group effect). The Dutch Additional guidelines for Eurocode 7 NEN9997 (NEN, 2011) give a normalised pile-load curve for the base load and the skin friction separately, see Figure 2.25.

Subsequent raising of the street level over the last 100 years caused the piles under the facades to attract most of the external loading. The man made layer (Fill) is usually thicker in the streets than under the houses, leading to larger negative skin friction and also horizontal displacements at the position of the facades. Negative skin friction can be calculated according to the Zeevaert - de Beer or the slip method (NEN, 2011).

Most piles in the historic centre of Amsterdam will already have experienced the maximum negative skin friction possible over time. Due to low factors of safety of the pile foundations, there can also be a development of positive skin friction to balance the negative skin friction. Kaalberg et al. (2005) shows that timber piles generally find between 80 % and according to

Van der Stoel (2001) even 90 % of their theoretical capacity at the tip, although the analysis in Chapter 6 gives other results. The high horizontal flexibility assures that the piles can move rather easily with the soil in horizontal direction, compared to concrete piles.

For further analysis in Chapter 8, the most common foundations around the deep stations in Amsterdam have been characterized into different groups, see Table 4.3.

Table 4.3 Pile group characterization Amsterdam

Type of foundation	Foundation layer	Material	Age group [year]	Foundation Class
1a	First sand	wood	Before 1860	I, II, III or IV
1b	First sand Amsterdam 2 rows	wood	1860-1925	I, II, III or IV
1c	First sand, single row	wood	1920-1940	I, II, III or IV
1d	First sand	wood	1940-2010	I, II, III or IV
1e	First sand	Concrete/steel	-	I, II, (III or IV)
2a	Second sand	Concrete/steel	-	I
3a	Third sand	Concrete/steel	-	I

4.4 Rokin Station

4.4.1 History

The Rokin area used to be a wide canal until 1936. The old river bed of the Amstel river (one of the tidal channels) and the canal shown in Figure 4.9 have been filled with sand, clay, peat and debris.



Figure 4.9 Rokin, picture BMA dated around 1900 (BMA, 2009)

4.4.2 Station overview

Rokin Station is the first of the Deep Stations for the North South metro Line in Amsterdam, following the line south from Central Station. The station is 24.5 m wide and reaches a maximum depth of NAP - 26 m, see Figure 4.10. It is built by means of a top down construction, with 1.2 m thick diaphragm walls extending to a depth of NAP - 39 m. Adjacent buildings are found at 3.0 m from the diaphragm wall or further away.

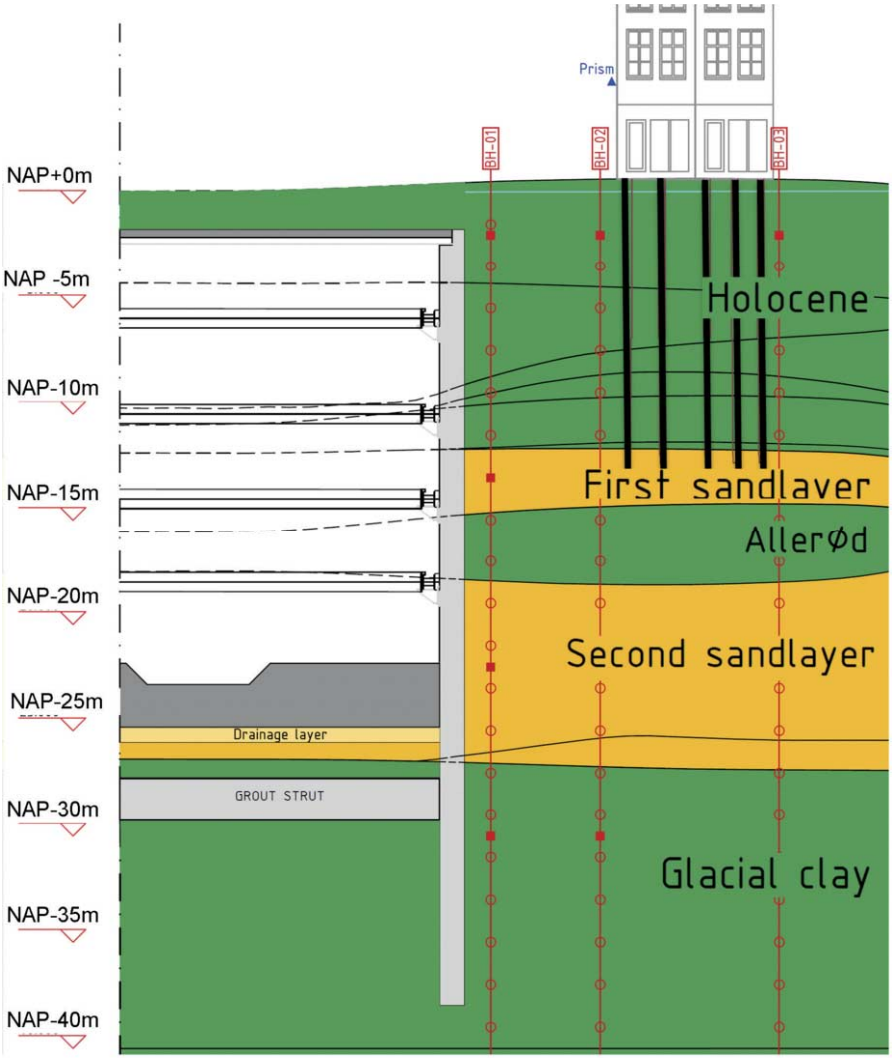


Figure 4.10 Cross section of Rokin Station (at km 11212)

Rokin Station has four arrays of subsurface measurements perpendicular to the station (numbered 11233, 11192, 11212 and 11131), see Figure 4.11.

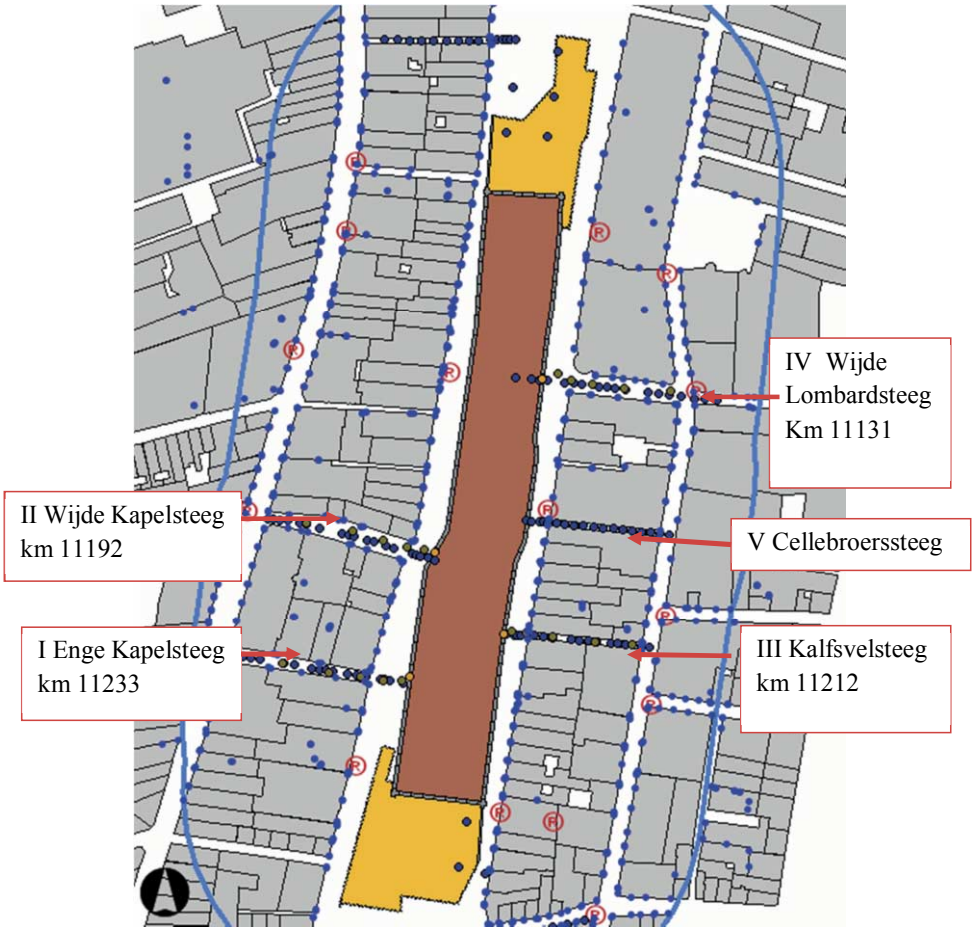


Figure 4.11 Locations of cross sections with subsurface monitoring

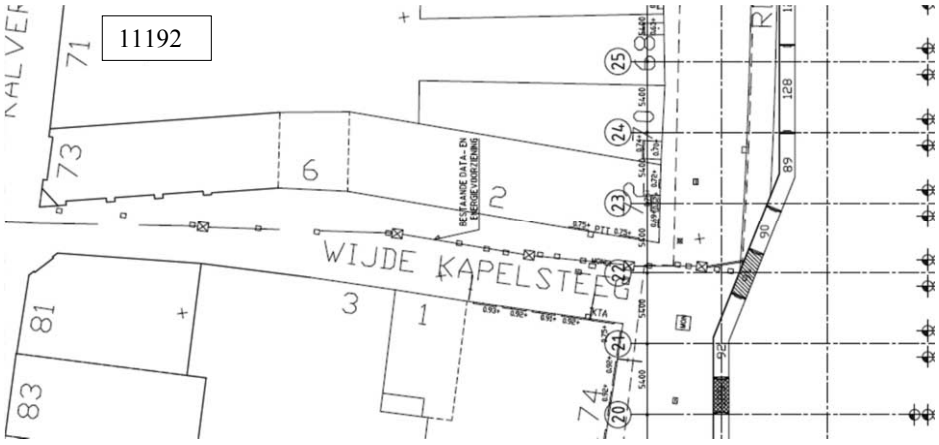
Details on the soil profile and parameters are given in COB (2011b). The ground water pressures for Rokin are presented in Table 4.4.

Table 4.4 Phreatic and piezometric levels

SLS during construction	**Layer indication in measurements**	**Minimal piezometric head [m NAP]**	**Average piezometric head [m NAP]**	**Maximal piezometric head [m NAP]**
Phreatic layer	A	-0.95 (5%)	-0.25	-0.07 (5%)
First sandlayer	C	-2.06	-1.84	-1.61
Second sandlayer	D	-2.10	-1.89	-1.68
Third Sandlayer	F	-3.12	-2.76	-2.40

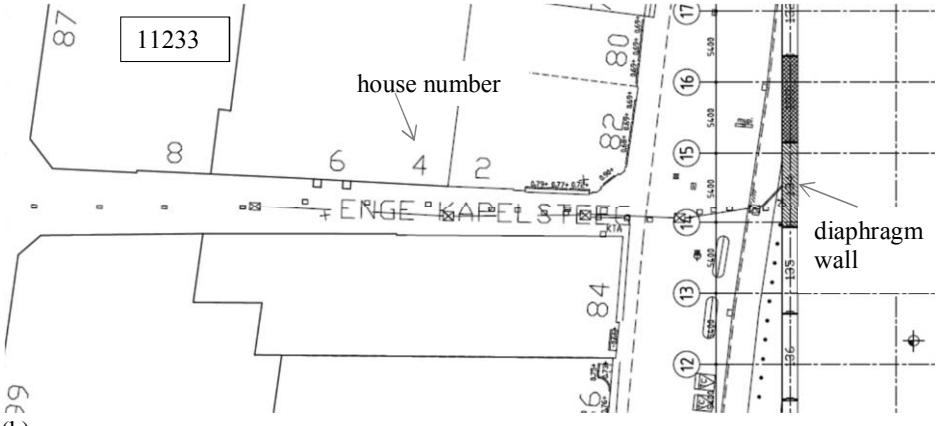
4.4.3 Cross sections

The maximum depth of the excavation is NAP-24.8m. A drainage layer of 0.5 m will be put in place below this depth. The top of the deepest floor is NAP - 22.8m. The width of the excavation including the diaphragm walls is 29.1 m in most sections and 24.5m in section 11131. Details of the cross sections are shown in Figure 4.12 and in COB (2011b).



(a)

⊠ inclino/extensometer point
□ surface measurement point



(b)

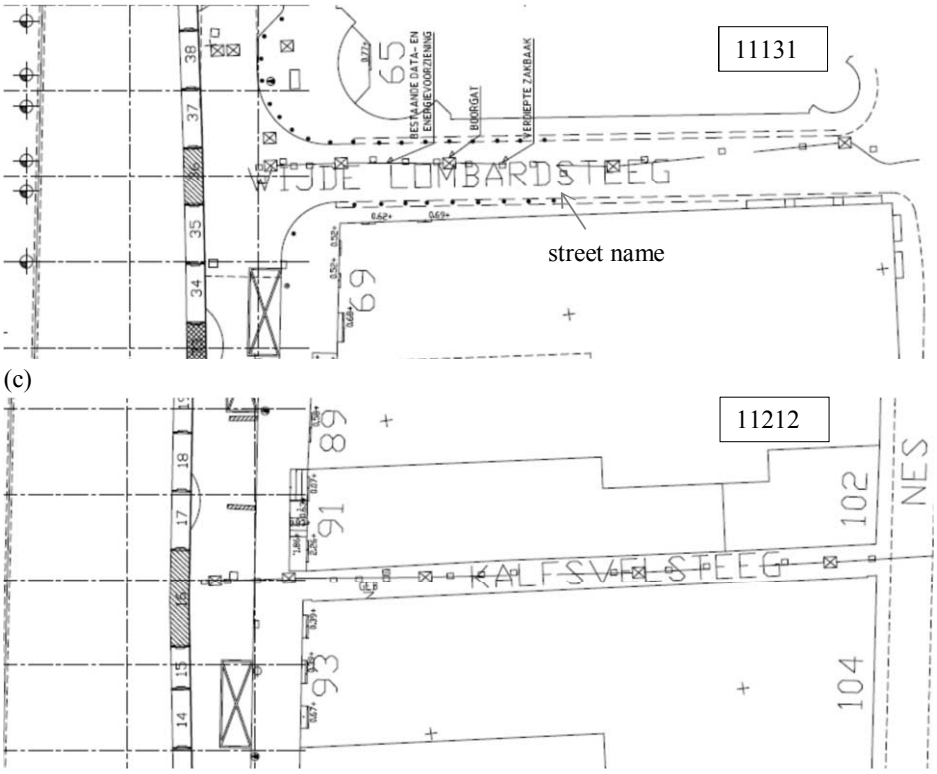


Figure 4.12 Top view of monitoring cross sections 11192, 11233, 11131 and 11212 with inclinometer/extensometer borehole locations and surface measurement points

4.4.4 Diaphragm wall and excavation supports

The diaphragm walls consist of panels with lengths of approximately 2.8m to 5.2m. Traditional grabs and steel stop ends (CWS-type) with water bars (PVC strips) (Puller 2003) are used to a depth of NAP–36m to provide waterproofing. The Eem-clay layer below NAP–26m provides a seal for the bottom of the excavation. Ground improvement works took place along the line of the diaphragm walls in order to remove obstacles in the Holocene deposits before installing the walls. The diaphragm wall characteristics for all cross sections are given in Table 4.5.

Steel struts (permanent and temporary) are located at NAP -5.5m , NAP -10m, NAP -14m and NAP -18m. Prestressing forces per metre are respectively 600 kN, 1200 kN, 900 kN and 600 kN. Both the roof and the floors act as struts during top-down construction. Most of the roof (top at NAP -1.5m) is constructed with precast beams with a floor of 400 mm. Floors are located at NAP -17m and NAP -27 m.

Table 4.5 Characteristics of diaphragm wall

Parameter	Value
Top [m+NAP]	-0.2
Bottom [m+NAP]	-38
Width [mm]	1200
Quality	B25
E'_b [kN/m^2]	10 x10^6 – 30x10^6
EA [kN/m]	average 1.2 10^7 upper 1.8 10^7 lower 9.6 10^6
EI [kNm^2/m]	average 1.4 10^6 upper 2.2 10^6 lower 1.2 10^6
Volumetric weight [kN/m^3]	23

The deepest strut consists of jet grout columns that were installed from the surface. The strut was not completely closed, some of the columns were deliberately left out to obtain the optimum overall stiffness of the strut. A detailed as built drawing of the strut is shown in COB (2011b). The grout strut has a thickness of 2000 mm and is located at NAP –27.25 m (top). There are not many gaps in the grout strut for Rokin station (90% closed). The average equivalent stiffness used in the design is 2300 N/mm^2*0.9*0.65(creep factor)=1350 N/mm^2 as given by ABNZL (2008). The characteristics of the grout strut as derived from tests have been summarized in Table 4.6.

Table 4.6 Properties of the grout strut

	Compressive strength [MPa]	Tensile strength [MPa]	Elasticity modulus [MPa]	Poisson's ratio [-]	Vol. weight [kN/m^3]
Average values PIP (Van der Stoel 2003)	12.6	0.86	2800	0.3	17.1
Selected test results grout strut (Delfgaauw et al, 2009)	12.6 MPa		4000 MPa		17.1
Average test results grout strut (Delfgaauw et al, 2009)	6-9 MPa		E/UCS is 320, so 1920 – 2880 MPa		15 - 16

4.4.5 Buildings around Rokin Station

Typical buildings at Rokin are shown in Figure 4.13.



Figure 4.13 Typical buildings at Rokin Station (left Rokin 73, centre Rokin 84, right Rokin 55-65)

Buildings around Rokin Station usually house shops (with large openings) at street level and residential users in the upper floors. Information about the initial condition of the buildings, details of the foundation class and the buildings in general are given in COB (2011b).

4.4.6 Construction activities and timelines

The construction of Rokin Station is divided in 7 main stages:
Stage 0 Preparations, diaphragm wall, construction of the roof and pumping test
Stage 1 Excavation to NAP –6.4m.
Stage 2 Excavation to NAP –10.9m.
Stage 3 Excavation to NAP –14.9m.
Stage 4 Excavation to NAP –18.9m.
Stage 5 Excavation to NAP –26.3m.
Stage 6 TBM passing through.
In stage 0 the following activities took place:

Removal of obstacles
Identified obstacles at Rokin are old quay walls, abutment, foundation beams, sewers and foundation piles. In the North-East and far South-East part of the station, obstacles were removed using shallow excavations. At some locations (Salet, 2004) a large diameter crushing machine was used. Deep obstacles (piles) are removed by pulling or vibrating.

Over the rest of the diaphragm wall route, the obstacles were removed with two rows of intersecting columns (1.2m diameter, see Figure 4.14) filled with lean concrete; a mixture of cement, sand, water and fly ash. At the East wall the soil is replaced to a depth of NAP -14 to -15 m, for the West wall this level was reduced to NAP -13 m.

Sand fill
The green field level is raised by 0.5 m of sand to provide working level for the installation of the diaphragm walls. The distance of the sand layer to the buildings is about 3 m.

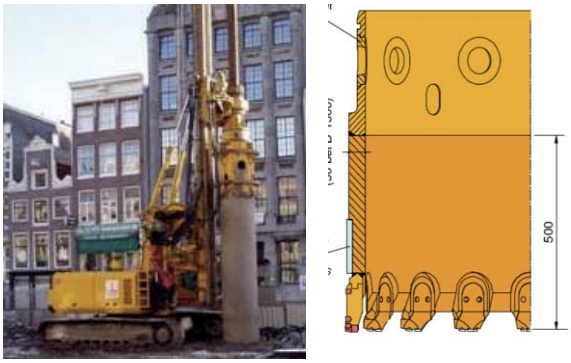


Figure 4.14 Equipment for removal of obstacles with large diameter drilling

Construction of diaphragm walls

The diaphragm walls were constructed in panels, see Figure 4.15. The individual panels have a width of 1.2m and a length of about 3.6m-6.6m along the wall, the bottom level is found at NAP-38m. The stabilizing fluid (bentonite) has a volumetric weight of about 10.5kN/m^3 minimum.



Figure 4.15 D-wall construction and jet grout strut installation

Jet grout strut

A grout strut was constructed to prevent settlement of the surroundings at a depth of (top) NAP-27.25m (in the Eem clay layer). The strut has a thickness of 2.0m. The installation was performed from the surface. As it is constructed in different phases and activated after excavation the time-dependency of the grout stiffness is important. The period between installation and activation differs for the eastern and western side of the station.

Before jet grouting obstacles were removed by predrilling.

Roof of the station
The roof is constructed by first excavating to a depth of NAP -2m (locally to NAP –3.5m at the beams near the roof openings). The total thickness of the roof is 0.9 m. After hardening of the concrete, the roof is covered with sand to surface level and asphalt on top to open the street again for traffic.

Stages 1 - 5 include the excavation of the station. The excavation below the level of strut 1 is reached at NAP – 6.4 m. Strut level 1 is prestressed to 600 kN/m. Dewatering of the station takes place to the level of NAP -11m. Pictures of the roof and struts are shown in Figure 4.16.

The excavation below the level of strut 2 is reached at NAP – 10.9 m. Strut level 2 is prestressed to 1200 kN/m. The excavation below the level of strut 3 is reached at NAP –14.9 m. Strut level 3 is Prestressed to 900 kN/m. Dewatering of the station takes place to the level of NAP - 19m. The construction activities were postponed at this stage from 2008-09-11 until 2009-11-23 due to the leakage incidents at Vijzelgracht (see Chapter 10). Further stages of excavations are not included in this study.
A detailed timeline for each cross section is given in COB (2011b). For the monitoring evaluation, the dates that mark the different stages of construction are given in Table 4.7:

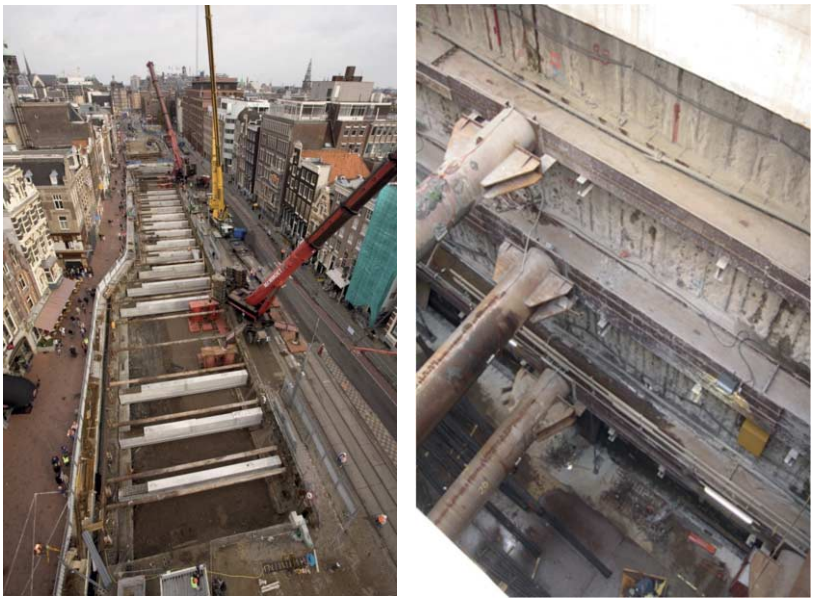


Figure 4.16 First excavation (left) and strut layers (right)

Table 4.7 Overview of Rokin monitoring dates

Stage	Dates 11233	Dates 11192	Dates 11212	Dates 11131
Start measurements Back ground monitoring	2001-10-10 / 2002-04-01	2001-10-10 / 2002-04-01	2001-10-10 / 2002-04-01	2001-10-10 / 2002-04-01
Start stage 0	2003-05-01	2003-05-01	2003-05-01	2003-05-01
Stage 0 -> 1	2007-12-01	2007-12-01	2007-12-01	2007-12-01
Stage 1 -> 2	2008-06-13	2008-06-27	2008-06-06	2008-06-20
Stage 2 -> 3	2008-08-12	2008-08-12	2008-08-12	2008-08-12
End activities	2008-09-11	2008-09-11	2008-09-11	2008-09-11
End data	2010-05-01	2010-05-01	2010-05-01	2010-05-01

4.5 Vijzelgracht Station

4.5.1 Station overview

Vijzelgracht Station is the second of the Deep Stations for the North South metro Line in Amsterdam. The station is 250 m long, 22 m wide and reaches a maximum depth of NAP - 29.5 m. It is built by means of a top down construction, with 1.2m thick diaphragm walls extending to a depth of NAP - 44.5 m. Adjacent buildings are found at 3.2m from the diaphragm wall or further away. Station Vijzelgracht has two arrays of measurements perpendicular to the station (numbered 12270 and 12197), see Figure 4.17.

4.5.2 Cross section 12197

This section is located between grid lines 44 and 46, closest to 45.

The maximum depth of the excavation at this section is NAP- 29.85m. A drainage layer of 0.6 m will be put in place below this depth. The top of the deepest floor is NAP- 27.35m. The width of the excavation including the diaphragm walls is 20.35 m (or 18.0 m between the walls). Details of the cross section are shown in Figure 4.18 and COB (2011c).



Figure 4.17 Locations of cross sections with subsurface monitoring

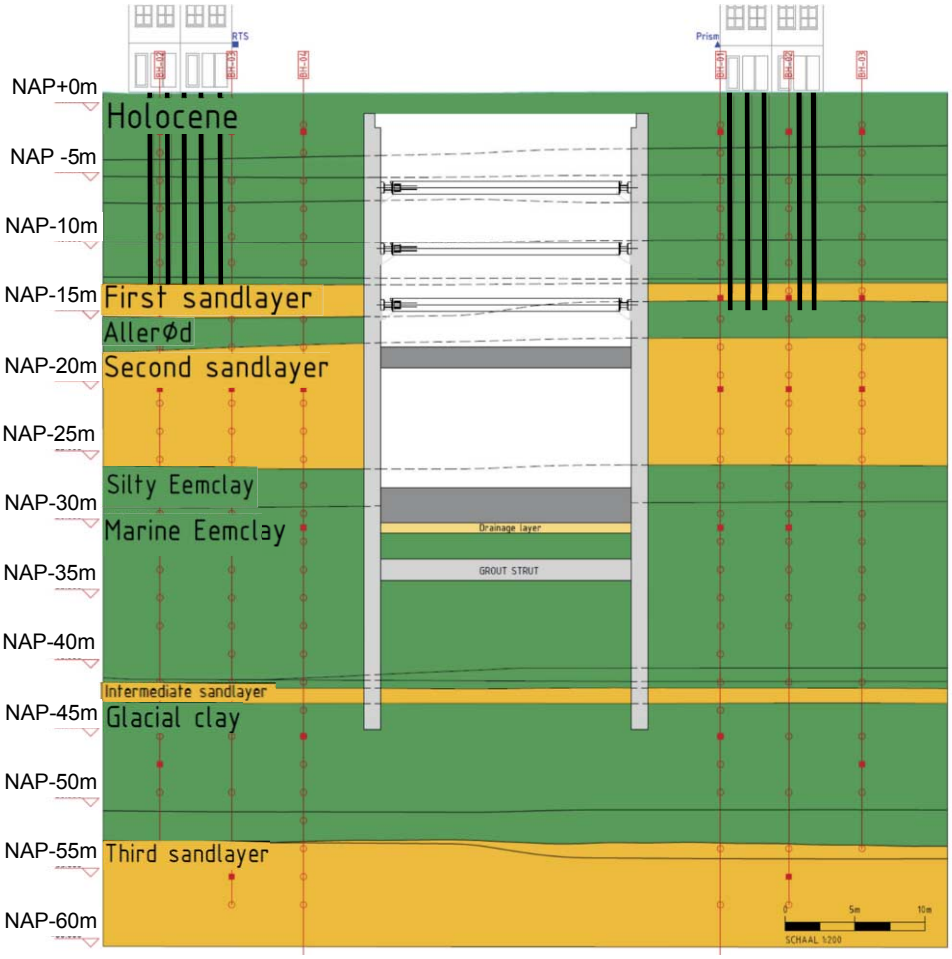


Figure 4.18 Cross section 12197

4.5.3 Cross section 12270

This section is located between grid lines 24 and 25. The maximum depth of the excavation at this section is NAP- 29.7m. A drainage layer of 0.6 m will be put in place below this depth. The top of the deepest floor is NAP- 27 m. The width of the excavation including the diaphragm walls is 20.4 m (or 18.0 m between the walls). Details of the cross section are shown in Figure 4.19 and COB (2011c).

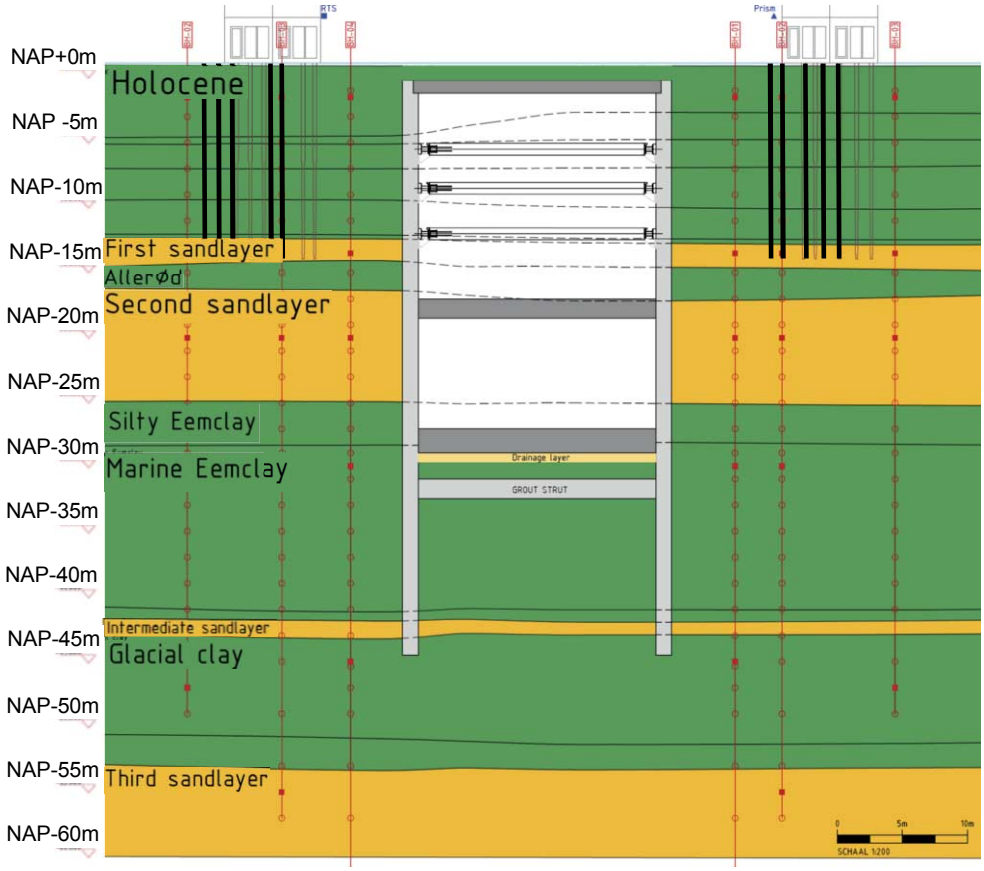


Figure 4.19 Cross section 12270

4.5.4 Diaphragm wall and excavation supports

The diaphragm wall at Vijzelgracht station has similar characteristics as for Rokin station, see Table 4.5. At Vijzelgracht however, the wall reaches to NAP -45m.

Six layers of support are present in the excavation, in the form of both steel tubes and concrete floors. Steel struts are located at NAP -5m, NAP -9m, NAP -13m. The prestressing force per metre is respectively 1000 kN, 1500 kN and 1500 kN. The instrumented struts in cross section 24-25 and 45 have the numbers 18 and 40 (numbered according to ABNZL) respectively. Both the roof and the floors act as struts during top-down construction. The top of the roof is found at NAP -0.2m with a thickness of 1.0m. The thickness of the floor at NAP -17m is 1.5 m and the deepest floor at NAP -27m is 2 m thick for cross section 12270. For cross section 12197 the second floor is located at NAP -18.25 m.

The deepest strut consists of jet grout columns that were installed from the surface. The strut was not completely closed, some of the columns were deliberately left out to obtain the optimum stiffness of the strut. A detailed as built drawing of the strut is shown in COB

(2011c). The grout strut has a thickness of 1500 mm and is located at NAP – 31.0 m (top). The characteristics of the grout strut have been summarized in Table 4.6. Close to the diaphragm wall a larger thickness (2.5 m) is realized to obtain a good load transfer to the diaphragm wall.

4.5.5 Buildings around Vijzelgracht Station

A typical picture for Vijzelgracht is given in Figure 4.20.



Figure 4.20 Typical historic building at Vijzelgracht Station

Buildings around Vijzelgracht Station usually house shops (with large openings) at street level and residential users in the upper floors. Information about the initial condition of the buildings, details of the foundation class and the buildings in general are given in COB (2011c).

4.5.6 Construction activities and timelines

The construction of Vijzelgracht Station is divided in 7 main stages:
Stage 0 Preparations, diaphragm wall, construction of the roof and pumping test, inclusive of excavation to NAP - 3.5m
Stage 1 Excavation to NAP – 5.5m / NAP- 7.0 m (locally)
Stage 2 Excavation to NAP – 9.5m.
Stage 3 Excavation to NAP – 13.5m.
Stage 4 Excavation to NAP – 16.9m.
Stage 5 Excavation to NAP – 22m / NAP -20.5m.
Stage 6a Excavation to NAP -22.9 m / NAP -23.5 m
Stage 6b Excavation to NAP -26 m
Stage 7 Excavaton to NAP -30 m
Stage 8 TBM passing through.

In stage 0 the following activities took place:

Removal of obstacles

Identified obstacles at Vijzelgracht are quay walls, abutment, sewers and foundations. Some of the obstacles were removed using shallow excavations to a maximum depth of NAP -1.5m (see COB (2011c)). Deep obstacles (piles) are removed by pulling or vibrating, this is done from a small excavation as well. Over the rest of the diaphragm wall route, the obstacles were removed with a bored casing of 1.2 m diameter. The specific effects of this activity have been described by Korff et al. (2011a). The casing is filled with a mixture of cement, fly-ash, sand and water, called Softmix. The East wall the soil is replaced until a depth of NAP -14 to -15 m, for the West wall this level was reduced to NAP -13 m.

Sand fill

The green field level is raised by 0.7 m of sand to provide working level for the installation of the diaphragm walls. The distance from the sand layer to the buildings is about 3 m.

Construction of diaphragm walls

The diaphragm walls were constructed in panels. The individual panels have a width of 1.2m and a length of about 2.6m (panels 21 and 43) or 3.7m (the other panels) along the wall, the bottom level is found at NAP - 45m. The stabilizing fluid (bentonite) has a volumetric weight of about 10.5kN/m^3 minimum. Figure 4.21 shows the equipment and the guide walls used for the diaphragm walls.

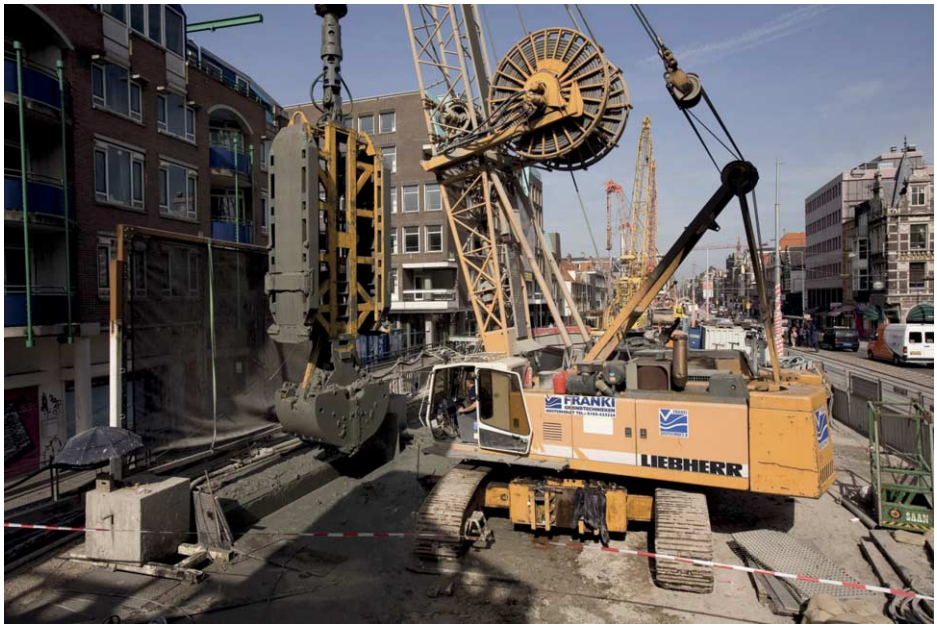


Figure 4.21 Construction of D-wall Vijzelgracht Station

Installation of jet grout strut

A grout strut was constructed to prevent settlement of the surroundings at a depth of (top) NAP - 31.0m / NAP - 32.5m (in the Eem clay layer). The strut has a thickness of 1.5m. The installation was performed from the surface, see Figure 4.22. Before jet grouting obstacles were removed by predrilling.



Figure 4.22 Installation of the jet grout strut (left) and construction of the roof (right)

Roof of the station

The roof is constructed by first excavating to a depth of NAP – 1.2m. The total thickness of the roof is 1.0 m. After hardening of the concrete, the roof is covered by sand to surface level with asphalt on top to open the street again for traffic.

Installation sheet pile

A sheet pile has been installed at cross section 12197 to a depth of NAP - 17.00m. The location of this temporary sheet pile is indicated in Figure 4.23.



Figure 4.23 Sheet piles for entrance of Vijzelgracht Station (photo Hollandse Hoogte)

Stages 1 - 5 include the excavation of the station. The excavation below the level of strut 1 is reached at NAP – 5.5 m. Strut level 1 is prestressed. Dewatering of the station takes place to the level of NAP - 11m. Also some activities by other parties have influenced the measurements, such as foundation renewal and pumping actions. The excavation below the level of strut 2 is reached at NAP – 9.5 m. Strut level 2 is prestressed. The excavation below the level of strut 3 is reached at NAP – 13.5 m. Strut level 3 is prestressed. Dewatering of the station takes place to the level of NAP - 19m. The construction activities were postponed at this stage from 2008-09-11 until 2009-11-23 due to leakage incidents (see Chapter 10).

A detailed timeline for each cross section is given in COB (2011c). For the monitoring evaluation, the dates that mark the different stages of construction are given in Table 4.8.

Table 4.8 Overview of Vijzelgracht dates monitoring dates

Stage	Dates 12197	Dates 12270	Dates used for building movement 12197	Dates used for building movement 12270
Start measurements Back ground monitoring	2001-10-24	2001-10-24	2001-10-24 until 2001-10-31	2001-10-24 until 2001-10-31
Start stage 0	2003-10-01	2003-10-01	2003-10-01 until 2003-10-07	2003-10-01 until 2003-10-07
Stage 0 ->1	2007-11-09	2007-11-09	2007-11-09 until 2007-11-16	2007-11-09 until 2007-11-16
Stage 1 -> 2	2008-03-17	2008-03-17	2008-03-17 until 2008-03-20	2008-03-17 until 2008-03-20
Stage 2 -> 3	2008-05-12	2008-06-06	2008-05-12 until 2008-05-18	2008-06-06 until 2008-06-13
End stage 3	2008-06-24	2008-08-15	2008-06-24 until 2008-06-26	2008-08-15 until 2008-08-22
Start no activities	2008-10-25	2008-10-25	2008-10-25 until 2008-10-31	2008-10-25 until 2008-10-31
End activities reported	2009-07-01	2009-07-01	2009-06-24 until 2009-07-01	2009-06-24 until 2009-07-01

4.5.7 Incidents

For more information about the leakages which happened at the dates and locations described in Table 4.9 can be found in Chapter 10 and Bosch and Broere (2009).
Current state of excavation during the incidents was NAP – 13m.

Table 4.9 Date and location of the leakages

leakage	Date	location
1st Leakage	June, 16 2008	12197 E
2nd Leakage	June, 18 2008	12197 W
3rd Leakage	September, 10 2008	12270 W

4.6 Ceintuurbaan Station

4.6.1 Station overview

Ceintuurbaan station is the third deep station (starting from Central Station), it is 210 m long and is the narrowest station of only 10.5 to 11.5m wide. The maximum excavation depth is 31 metre. Ceintuurbaan Station has two arrays of (subsurface) measurements perpendicular to the station, which are called cross section 13044 and cross section 13110. The location of the cross sections is shown in Figure 4.24.

4.6.2 Cross section 13044

This section is located between grid lines 38 and 39. The maximum depth of the excavation at this section is NAP-30.9 m. A drainage layer of 0.6 m will be put in place below this depth. The width of the excavation including the diaphragm walls is 13855 mm (or 11455 mm between the walls). For more details see Figure 4.25.

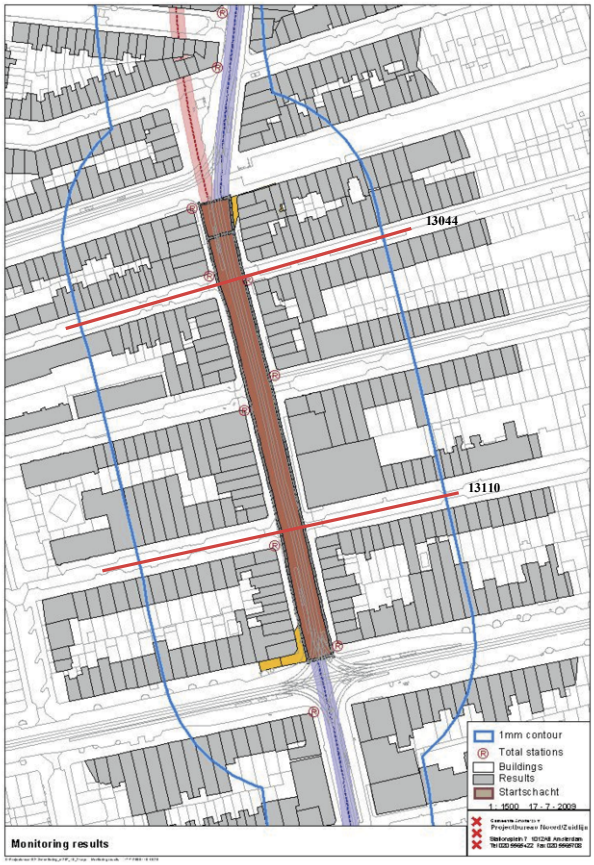


Figure 4.24 Locations of cross sections with subsurface monitoring

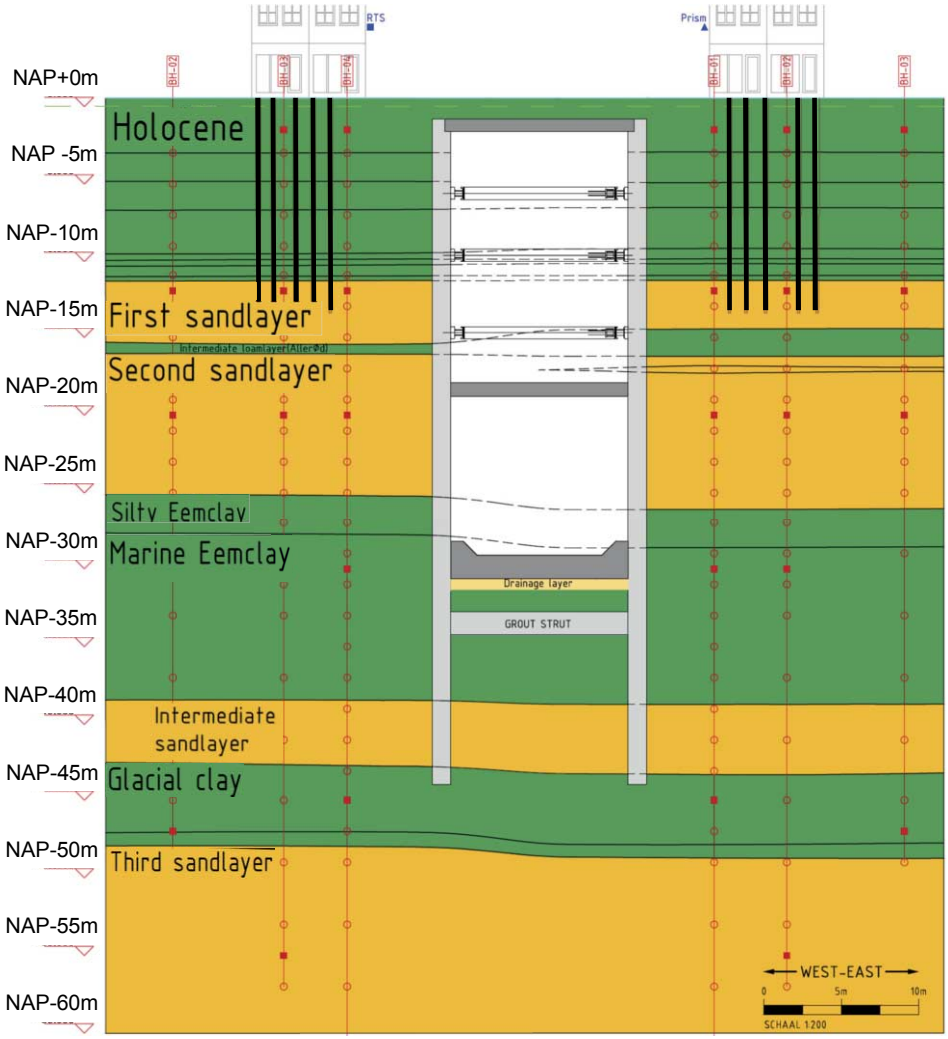


Figure 4.25 Cross section 13044

4.6.3 Cross section 13110

This section is located between grid lines 13 and 15, closest to 14. The maximum depth of the excavation at this section is NAP-29.75 m. Along the diaphragm wall locally a depth of NAP-30.5 m will be reached. A drainage layer of 0.6 m will be put in place below this depth. The top of the deepest floor is NAP-27.5 m. The width of the excavation including the diaphragm walls is 12752 mm (or 10372 mm between the walls). The cross section is presented in Figure 4.26.

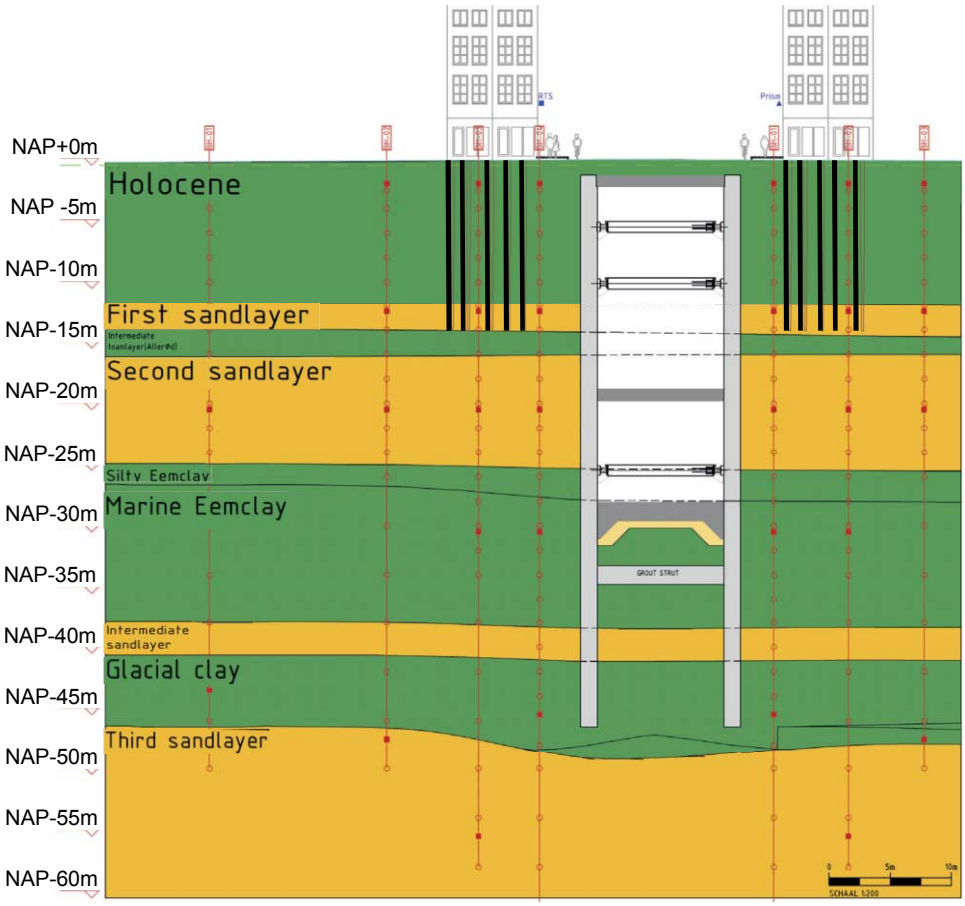


Figure 4.26 Cross section 13110

4.6.4 Diaphragm wall and excavation supports

The diaphragm wall characteristics for both cross sections are given in Table 4.5. The top of the wall at Ceintuurbaan station is found at NAP -0.8m, the bottom at NAP -45 to -46 m.

Six layers of support are present in the excavation, in the form of both steel tubes and concrete floors. Steel struts are located at NAP -5.6m, NAP -9.6m, NAP -14.7m and NAP -25m. The prestressing force per metre is respectively 600 kN, 1100 kN, 1650 kN and 800 kN. The instrumented struts in grid lines 13-15 and 38-39 are numbered 14 and 40 (according to ABNZL) respectively. Both the roof and the floors act as struts during top-down construction. The top of the roof is found at NAP -0.8m with a thickness of 0.8m. The thickness of the floor at NAP -6.45m is 0.7 m, at NAP -18.35m it is 0.9m and close to the wall 1.5 m and the deepest floor at NAP -27.58m is 1.5 m thick in the middle and 3.0 m near the wall. The deepest strut consists of jet grout columns that were installed from the surface. The strut was not completely closed, some of the columns were deliberately left out to obtain the optimum stiffness of the strut. The grout strut has a thickness of 1500 mm and is

located at NAP – 33.5 m (heart line). The characteristics of the grout strut have been summarized in Table 4.6. The gap factor in the grout strut for Ceintuurbaan station is 0.61-0.77. The grout strut's equivalent E-modulus ranges from 2000 to 3800 MPa based on back analysis of the diaphragm wall deflection by Delfgaauw et al. (2009).

4.6.5 Building characteristics around Ceintuurbaan Station

Information about the initial condition of the buildings is given in COB (2011d) in the form of an indication of the amount and severity of any cracking, quality class, details of the foundation and the building. A typical historic building is shown in Figure 4.27.



Figure 4.27 Typical historic building at Ceintuurbaan Station

4.6.6 Construction activities and timelines.

The construction of Ceintuurbaan Station is divided in 8 main stages:

Stage 0 Preparations, diaphragm wall, construction of the roof and pumping test
Stage 1 Excavation to NAP –6.2m.
Stage 2 Excavation to NAP –10.3m.
Stage 3 Excavation to NAP –15.3m.
Stage 4 Excavation to NAP –19.4m.
Stage 5 Excavation to NAP –25.6m.
Stage 6 Excavation to NAP –31.1m (with air pressure).
Stage 7 TBM passing through.
In stage 0 the following activities took place:

Removal of obstacles

At Ceintuurbaan Station only cables and lines have been identified and removed as obstacles. Max depth of removal is NAP - 1 m. This is done from May 2003 (and was finished before 2003-11-15).

Sand fill

The green field level is raised by 0.7 m of sand to provide working level for the installation of the diaphragm walls, see Figure 4.28. The distance of the sand layer to the buildings is about 3m.



Figure 4.28 Back fill at Ceintuurbaan Station

Construction of diaphragm walls

The diaphragm walls were constructed in panels. The width of the panels is about 1.2 m, the individual elements have a length of circa 2.6m (panels 22, 57 and 73) or 3.8m (the other panels) along the wall, the bottom level is found at NAP-45m. The stabilizing fluid (bentonite) has a volumetric weight of about 10.5 kN/m^3 minimum.

Jet grout

The jet grout strut installation took place from the surface level. The grout strut is located at a depth of NAP –33.5 m (heart line) and has a thickness of 1500 mm in the centre and 2500 mm at the connection with the wall.

Pumping test

A pumping test was performed in March and April 2006 by lowering of the phreatic level to NAP-5m in the 1st, 2nd and intermediate sand layer within the excavation after all diaphragm walls were installed.

Construction of the roof of the station

The roof is constructed by first excavating to a depth of NAP –1.95m, see Figure 4.29. The total thickness of the roof is 0.8 m. After hardening of the concrete, the roof is covered with sand to the bottom of street level at circa NAP+0.5m and asphalt on top of it to open the street again for traffic. Also some activities by other parties have influenced the measurements, such as foundation renewal and pumping actions.



Figure 4.29 Construction of the roof (top) and back fill above the roof (bottom)

The excavation took place in stages. The exact dates at which the excavation was reached is given in Table 4.10. The excavation below the level of strut 1 is reached at NAP –6.2 m. Strut level 1 is prestressed. Dewatering of the station takes place to the level of NAP -10m. The excavation below the level of strut 2 is reached at NAP –10.3 m. Strut level 2 is prestressed. The excavation below the level of strut 3 is reached at NAP – 15.3 m. Strut level

3 is prestressed. Dewatering of the station takes place to the level of NAP -19m. The excavation below the level of the air pressure floor is reached at NAP –19.6 m. The designed mitigating strut at NAP –16.5 m was not installed. The air pressure floor at NAP -18.35 m (top) is constructed. Dewatering of the station takes place to the level of NAP -26.92m. The strut at NAP -14.7 is removed.

The deepest excavation without air pressure is reached at NAP –25.6 m. Dewatering of the station takes place to the level of NAP -26.92m. The strut at NAP -25 m is prestressed to 800 kN/m. A pumping test was performed in the intermediate sand layer on February, 26-27 2009. Dewatering of the station takes place to the level of NAP -29.39 m. On 4 March 2009 a preliminary test with the air over pressure equipment was performed to 0.5 bar. Final excavation takes place to a depth of NAP – 31.2m (with air pressure). At the end of the period studied (July, 1st 2009) the excavation reached the level of NAP – 24 m (cross sections 1-5) and NAP – 25.6m in the rest of the station. From April 15, 2009 an over pressure of 0.5 bar was available in the station. Figure 4.30 gives an impression of the excavation at Ceintuurbaan Station.

A detailed timeline for each cross section is given in COB (2011d). For the monitoring evaluation, the dates that mark the different stages of construction are given in Table 4.10.



Figure 4.30 Excavation and supports at Ceintuurbaan Station

Table 4.10 Overview stages and dates of construction and monitoring at Ceintuurbaan Station

Stage	Prisms 13044	Prisms 13110	Surface 13044	Surface 13110	Levelling 13044	Levelling 13110
Start measurements Back ground monitoring	2001-06-01	2001-06-01	2002-05-31	2002-05-31	2002-01-14	2002-01-14
Start stage 0	2003-11-01	2003-11-01	2003-11-10	2003-11-10	2004-05-18/ 25	2004-05-18/ 25
Stage 0 ->1	2007-04-01	2007-04-01	2007-04-18	2007-04-18	2007-06-29/ 07-03	2007-06-29/ 07-03
Stage 1 -> 2	2007-09-13	2007-08-24	2007-08-21	2007-08-21	2007-06-29/ 07-03	2007-06-29/ 07-03
Stage 2 -> 3	2007-12-10	2007-11-07	2007-12-28	2007-11-16	2007-06-29/ 07-03	2007-06-29/ 07-03
Stage 3+ 4 ->5	2008-03-01	2008-03-01	2008-03-19	2008-03-19	2008-07-08/ 10	2008-07-08/ 10
End stage 5 + 6	2009-07-01	2009-07-01	2009-06-19	2009-06-19	2009-07-16/ 17	2009-07-15

4.7 Monitoring system

4.7.1 Introduction monitoring system

A full description of the monitoring system in Amsterdam is given in COB (2011a). Relevant to the response of piled buildings are the following devices:

- prism measurements with Robotic Total Stations; these measurements are related to reference buildings outside the area influenced by construction activities
- manual levelling of the buildings; measurements relate to deep datums in the 3rd sand layer
- manual levelling of the surface points; measurements relate to deep datums in the 3rd sand layer
- extensometer measurements of the surface, NAP -1.5m, at the 1st sand layer and deeper; measurements relate to the deepest sensor in the 3rd sand layer or in the Glacial till.

In order to determine the displacement of the historic structures along the deep stations an extensive, mostly automatic monitoring system is installed in the city centre. Robotic total stations measure prisms attached to the façades in the influence zone. The displacement of the prisms is measured in three directions (x, y and z). In order to handle the large amount of monitoring data software applications have been developed by the client. The applications use the Geographical Information System (GIS) as the user interface. The GIS has been developed to store, analyse, structure and visualise the data used in settlement risk management. From each building within the influence zone numerous facts are stored, such as state of the foundation, photograph of the original state with prism locations, owner details and details of its use. General data stored in the system include settlement predictions, settlement risk assessment studies, defect studies and site investigations.

4.7.2 Deformation measurements for buildings

An automatic or primary monitoring system follows the buildings in the influence zone of the project. Primary instrumentation comprises of 74 Robotic total stations (RTS, see Figure 4.31) installed on key building facades, which take readings from the prisms on the buildings. These buildings are selected for their good quality foundation, but are in the influence zone. Measurements made with the RTS are related to other RTS locations outside the zone of influence. These again are related to stable reference points, with their foundations either in the second or third sand layer. Prisms are located on the fronts and the sides of the buildings, usually a minimum of 4 per building. Each robotic total station monitors about 50 to 100 prisms. Prisms are usually made of glass and have a diameter of 25 mm, see Figure 4.31.



Figure 4.31 Robotic Total Station and prism

The conventions used in x/y/z direction are shown in Figure 4.32. The positive z-direction is the upward direction. The y-direction is taken parallel to the stations (for the side streets this is the displacement perpendicular to the façade, positive values going North). The x-direction is taken perpendicular to the station (or in plane of the facades for the side streets) and is taken positive to the east.

The required accuracy of the measurements in the contract is 0.5mm over 75m distance. Each prism is measured by at least 2 total stations. Based on Cooke (2006) it is known that degradation to actual values of +/- 1.5 mm is possible in non-optimal conditions. Several types of RTS have been used, such as the Leica TCRA2003, TCA1800 and TCRA1201 as well as Zeiss meters.

Secondary instrumentation comprises of precise levelling points installed on structures being monitored primarily by robotic total stations. Precise levelling is made to deep datums in the Third Sand Layer outside the zone of influence for the extensometer heads and building levelling points. The secondary system is mainly used as a backup system and

measured at intervals of 6-12 months. The precise levelling points have been attached to the buildings with a stainless steel socket, fixed with epoxy (see Figure 4.33). At the start of the project problems were noticed with the accuracy of the manual levelling points, which contractually should be 1.0mm maximum. These problems were solved later on and the data of the precise levelling points could be used in the analysis.

4.7.3 Surface measurements

The surface settlement points have been installed with a vertically fixed system. The ground levelling points are made of a galvanised steel plate (300*300mm) on which a vertical bar is fixed, see Figure 4.34. The depth of the plate is about 800 mm below the surface. The surface points are situated in lines in the side streets perpendicular to the diaphragm wall and measured at 6 week intervals.

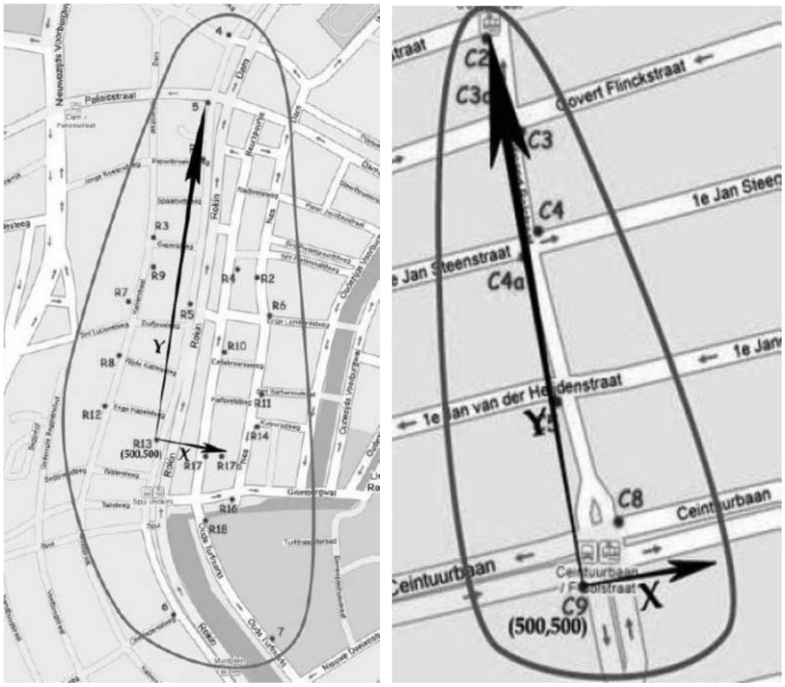


Figure 4.32 Conventions Rokin Station (left) and Ceintuurbaan Station (right)

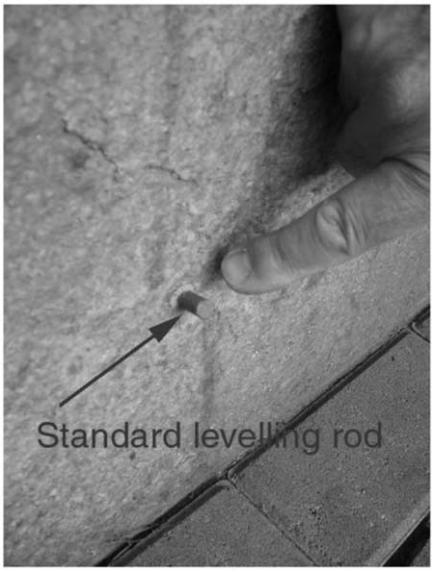


Figure 4.33 Manual levelling point

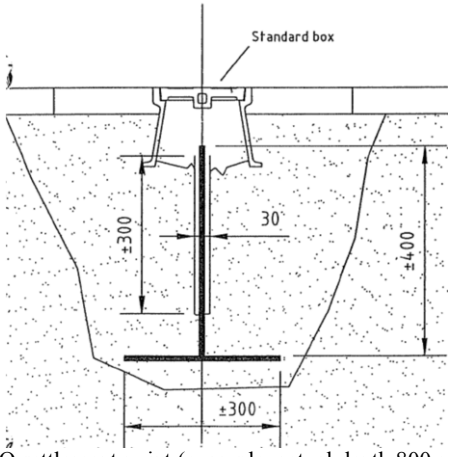


Figure 4.34 Bornes FENO settlement point (example, actual depth 800 mm instead of 400 mm)

4.7.4 Extensometers

For each station, four measurement arrays are installed with sub surface monitoring by means of extensometers and inclinometers. The extensometers (see Figure 4.35) have packers fixed at several depths. The displacement of the packers is monitored precisely relating fibre glass sticks leading freely to the top of the instrument with a reference block. This reference point itself is regularly checked against the deepest anchor (about 60 m deep) to obtain absolute displacements.

The products used for these measurements are the Interfels Multi-Point Borehole Exentsometer (MPBX) and the IPI Chain extensometer. The specified resolution is 0.01% FS (potentiometer) or 0.025% FS (vibrating wire), with FS is Full Scale of 100 mm. This would result in an accuracy of less than 1mm. De Nijs and Buykx (2009) state that in practice the accuracy will be around 2-5 mm due to the combination of the extensometer instrument, the precise levelling process and the friction that might occur between the instruments. The location of the packers in depth can vary about 0.5 m from the theoretical depth as given in Figure 4.39. The extensometers relate to the third sand layer, except for the 2 boreholes furthest from the excavation, which have their foundation in the second sand layer. At these locations a back ground settlement of approximately 2 mm/year should be expected.

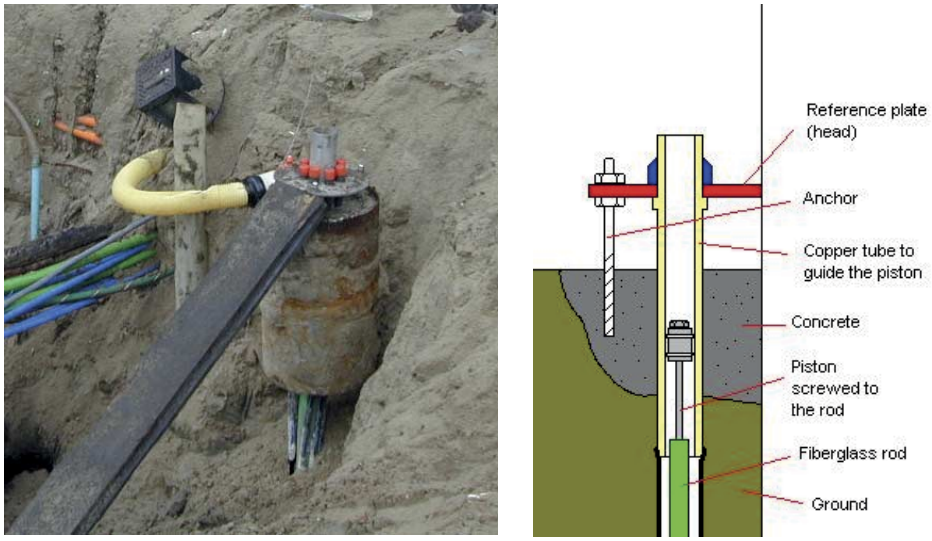


Figure 4.35 Extensometer (left) and illustration of measurement system (right)

4.7.5 Inclinometers

Automatic inclinometers are placed along the same locations and depths of the extensometers, see Figure 4.39. A combined inclinometer/extensometer system is used, see Figure 4.36 and Figure 4.36.

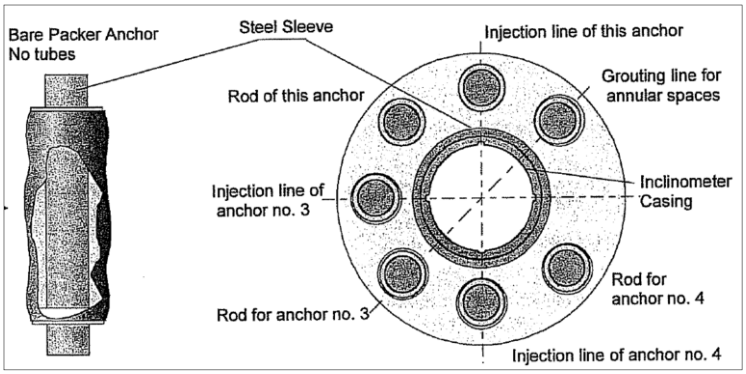
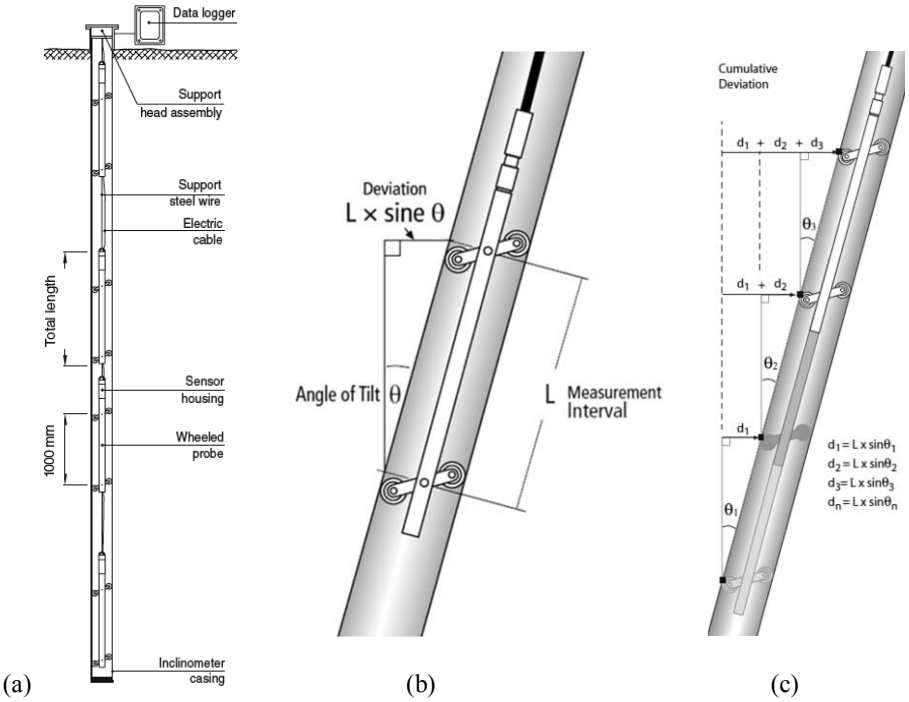


Figure 4.36 Combined inclino- and extensometer cross section (source Boart Longyear', Interfels)



Figure 4.37 Combined inclino- and extensometer (a) and assembled inclinometer instrument (b)



(a) (b) (c)

Figure 4.38 'In-place inclinometers' SISGEO (2009) (a) and Slopeindicator (2009) (b,c)

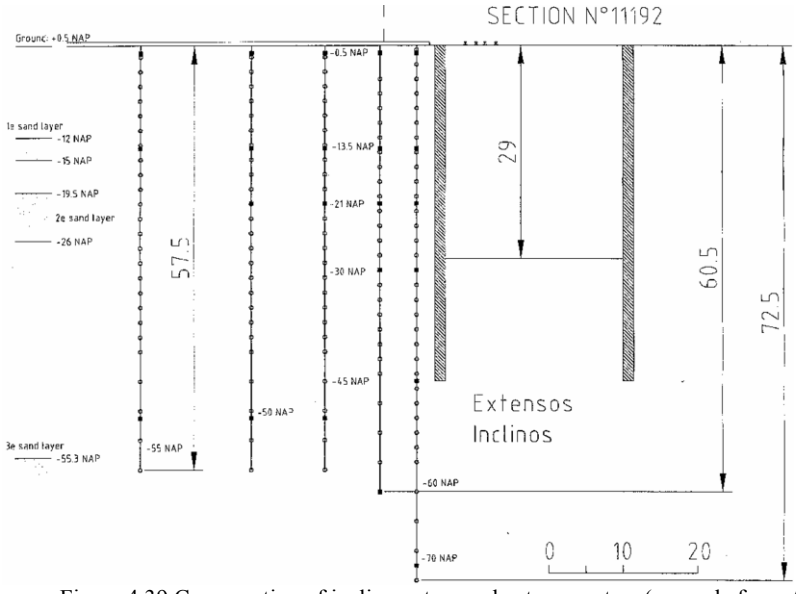


Figure 4.39 Cross section of inclinometers and extensometers (example from ABNZL)

The subsurface monitoring is automated. In addition manual inclinometers are placed in the heart line of some of the diaphragm wall panels, see Figure 4.40.

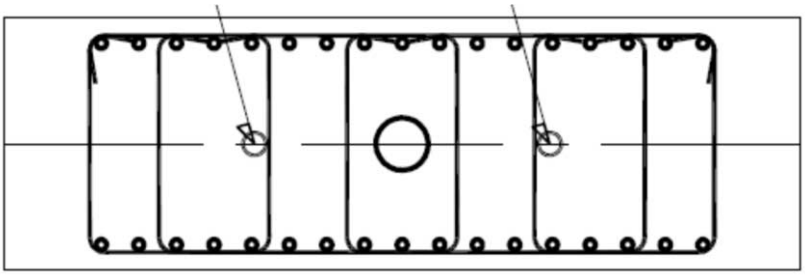


Figure 4.40 Position of inclinometer tubes in diaphragm wall panel

It should be noted that up to 2010 the top of the diaphragm wall inclinometers is not surveyed independently against the XY-references to determine the absolute displacements. This means relative values are found. Standard procedures assume the base of the inclinometer to be fixed.

The type of inclinometers used are the Inplace SISgeo with magneto resistive sensor and the IPI Monoaxial Chain. The specified accuracy is smaller than 0.5% Full Scale (FS = 10 degrees angle). This would mean a deviation of over 50 mm for 60 m total depth and 3.5mm on a 4 m individual instrument length. In practice a maximum error in the order of 2-3% is found, leading to much larger deviations.

The sensors (sensor length 1.0m) have been put in strings with 2 m distance between the sensors. The accuracy is determined mainly by the sensor (0.2% F.S.), the positioning of the grooves (spiralling) and the number of measurements taken. For a string of measurements (See Figure 4.41), with a sensor each 2m (and sometimes 4m) the accuracy decreases further. The practical system accuracy of the inclinometer is +/- 7mm per 30m, based on a large number of datasets. This consists of a systematic error and a random error combined. The grooves of the casings have as much as possible been aligned with the project axes. All of the data is presented with the positive direction to the East. Deviations of these positions have been determined by a spiralling survey.

Temperature measurements are preformed in two boreholes per cross section (the one closest to the diaphragm wall and one in the middle of the section) and each in two depths (the first chain from the surface and the string at about 2/3 of the maximum depth).

4.7.6 Other equipment

Not all monitoring equipment available has been used in this thesis. Some of the remaining systems can be found in COB (2011a). They include several types of piezometers, both vibrating wire types and special BAT piezometers. Standpipes are also located around the

station boxes. To determine the strut loads vibrating wire strain gauges have been installed on some of the struts.

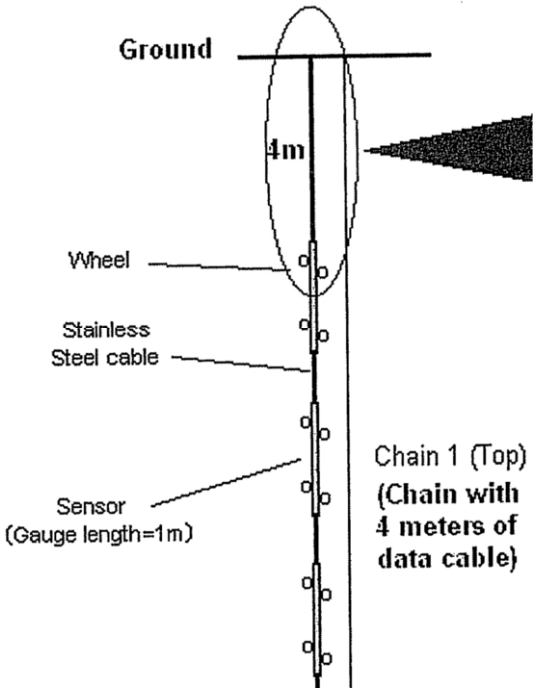


Figure 4.41 String of inclinometer sensors

4.7.7 Corrections for background settlement

Amsterdam is currently sinking by between 1mm and 3mm a year, depending on the exact location in the city. The surface settlement is a result of the on-going consolidation process of Holocene Layers related to the continuing placement of fill at street level and creep of the Eem Clay Layer. Around Ceintuurbaan station, where houses are about 100 years old, the rate of settlement is higher than in the historic centre (around Rokin).

Due to this effect, buildings will settle even without construction taking place. This is called the 'background settlement' and is a result of two separate phenomena:

- Settlement of the foundation layer, usually the First Sand Layer, a result of creep of the Eem Clay Layer.
- Piles subjected to negative skin friction related to the constant compression of the Holocene Layer.

This effect is important while studying deformations due to construction activities. The average subsidence of the surface around Ceintuurbaan Station is about 3.5 mm per year. The background settlement of the buildings varies between 0.5 and 2 mm per year as found

by Hogenes (1998). The specific current value per building can derived from a combination of the automatic and manual measurements. Some prisms show positive values (heave) because they settle less than the reference building of the RTS, see Figure 4.42. This phenomenon is studied in more detail in Chapter 9.

The building on which the RTS is located is influenced by the construction activities. The prism reading is the combined result of the deformation of building 1 to the RTS +/- the relative displacement of the RTS to the reference building. This means the settlement of building 1 consists of the natural settlement in the area (equal to the settlement of building R) plus the construction effect. The prism reading gives the construction effect only.

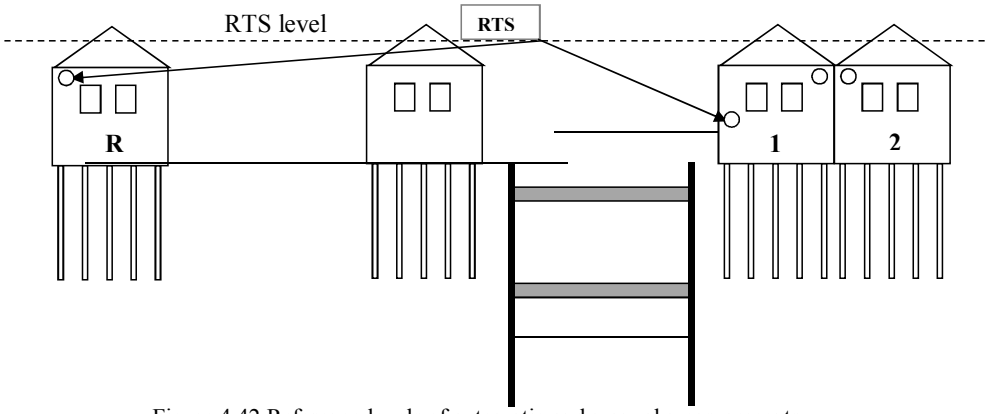


Figure 4.42 Reference levels of automatic and manual measurements

4.7.8 Reference of inclinometers in the wall

Chao et al (2010) give a method for correcting inclinometer results when the tip of the wall is not fixed. Their solution is the fix the deformation of the wall at the level of the first strut after prestressing of the strut. FEM calculations support this method. For Rokin Station this effect has been studied in Figure 4.43 Inclinometer results with different fixation levels

The figure on the left is the original wall displacement with assumed fixed tip level, while the figure on the right is the wall displacement if we assume that the grout strut at -30 m is fixed. It is clear that the maximum displacement increases by this change and the displacement with time show more consistency with the expected values as the excavation progresses. If we assume the roof (NAP -2m) as fixed (centre) the results do not seem realistic.

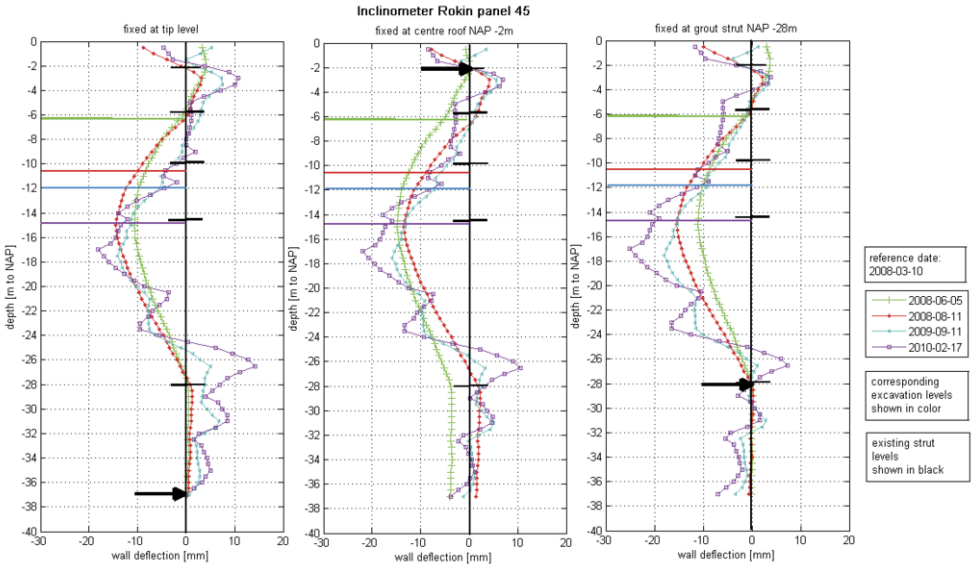


Figure 4.43 Inclinometer results with different fixation levels

CHAPTER 5 GROUND DISPLACEMENTS

5.1 Ground Settlement response

The assessment of the response of buildings to excavation-induced displacements involves a combination of geotechnical and structural aspects. The first step is to determine the effects, such as deformations and stress changes, that the excavation imposes on its surroundings in so-called 'green field' or 'free field' conditions, see figure 5.1.

In this chapter, the monitoring results at the three stations for the North South Line are analysed with respect to the green field displacement. The results are compared with some of the prediction methods for the ground displacement.

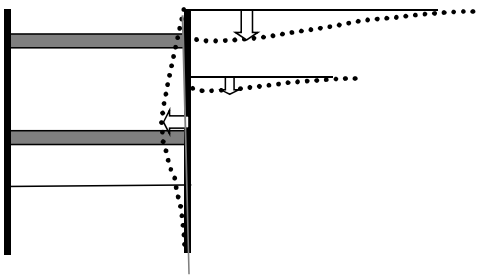


Figure 5.1 Simplified interaction between excavation and vertical ground displacement

5.2 Green field prediction models for surface displacement

The first step in the prediction of excavation-induced displacements is to predict the green field displacements. Current prediction models provide an estimate of green field displacements for two or three-dimensional situations.

In the Amsterdam cases, the following construction effects contributed to the displacement of the ground surface:

- Installation of diaphragm wall including preliminary activities such as predrilling and raising of the ground level / embankment
- Excavation of the station box

- Some lowering of groundwater levels outside the excavation due to imperfections in and permeability of the diaphragm wall
- Consolidation effects due to all activities mentioned above.

The resulting ground surface displacements are presented for various moments in time, each representing a certain construction stage, in Annex C. The effect of the leakage incidents at Vijzelgracht Station (see Chapter 10) are not included in the analysis of this chapter. Unless stated otherwise, the effects of the incidents have been excluded from the results.

The results of the measurements are first compared with the envelopes of Peck (1969), see Figure 5.2. The application of Peck's model gives an overall surface settlement, including all construction activities. For the Amsterdam condition, with the soil consisting of soft clay, hard clays and sand, Zone I should be an appropriate estimate of the surface displacements. This means the maximum settlement directly beside the wall is 1% of the excavated depth (H) and reaches to a distance of about 2H. In the Amsterdam cases, this would be 50-60 m away from the diaphragm wall.

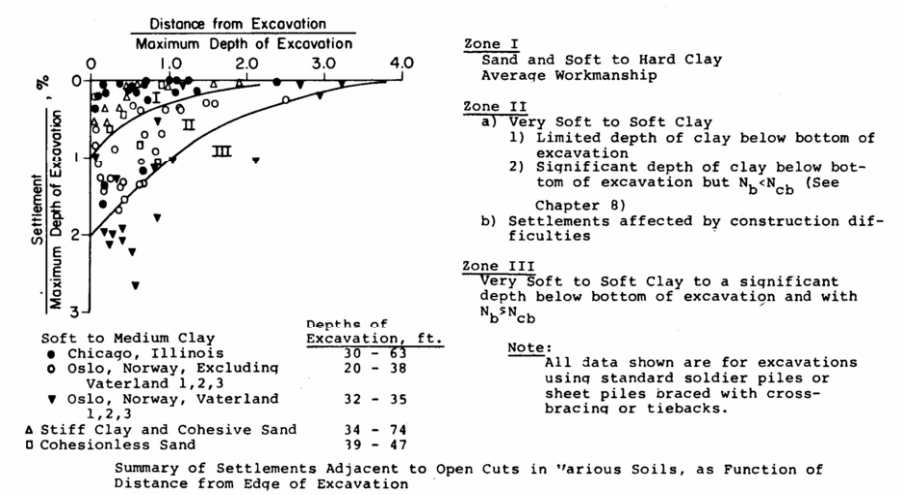
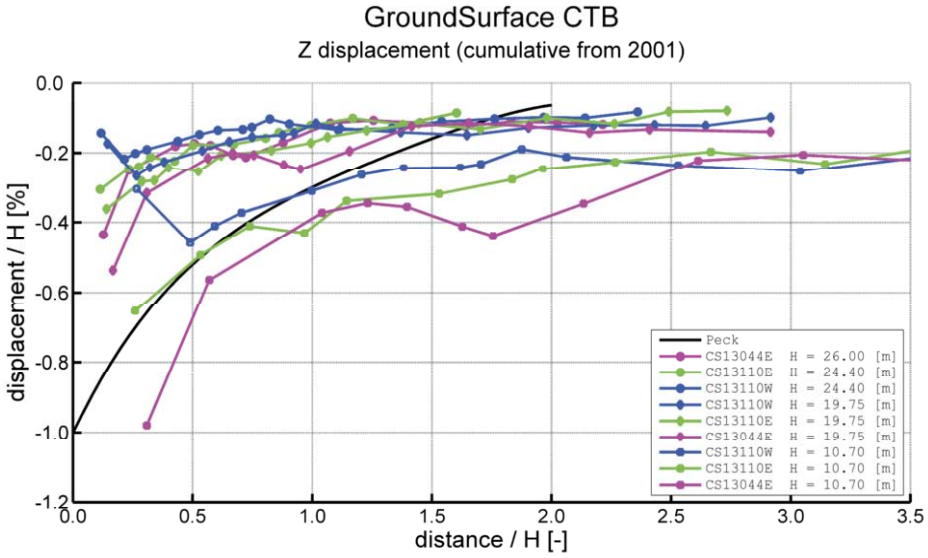
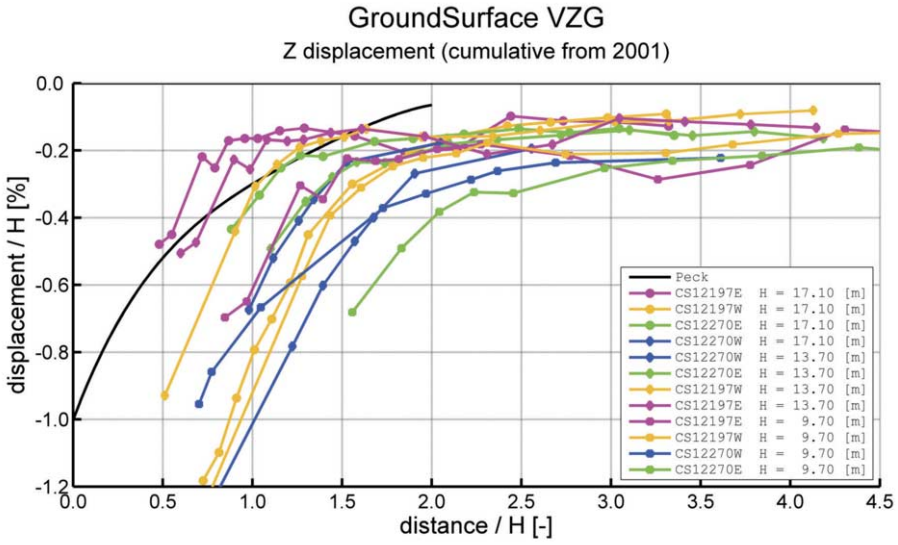


Figure 5.2 Settlements caused by all activities relating to deep excavations in various soils by Peck (1969)

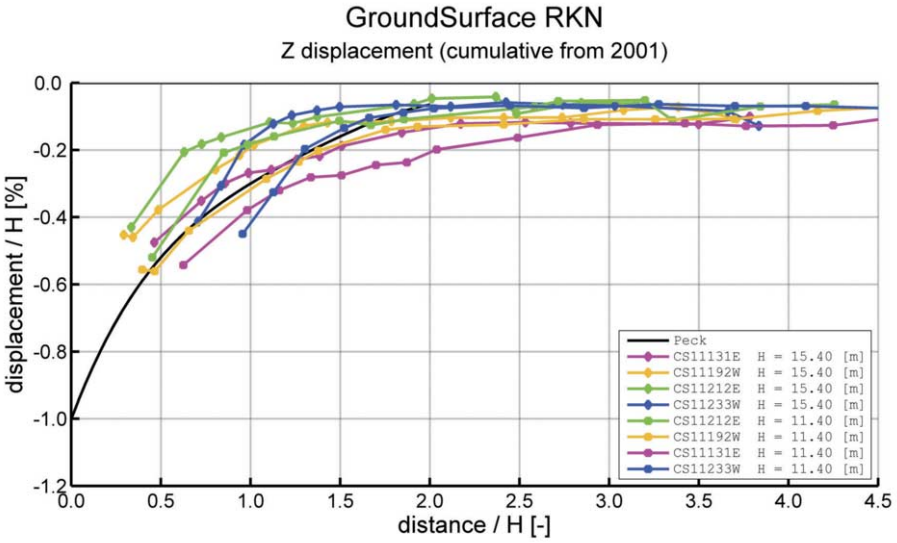
Figure 5.3 shows the measurement results for the ground surface for all three stations, Rokin, Vijzelgracht and Ceintuurbaan, at various depths of the excavation. It should be noted that the excavations had not finished at the time these measurements were taken and thus the long-term consolidation settlement is not completely included. The total period of the displacement measurements was over 6 years (from 2003-2009). This included all preliminary activities, such as diaphragm wall and grout strut installation, predrilling for obstacles and raising of the ground level. The excavation sequence is described in Chapter 4.


GroundSurface CTB
Z displacement (cumulative from 2001)
displacement / H [%]
distance / H [-]
Peck
CS13044E H = 26.00 [m]
CS13110E H = 24.40 [m]
CS13110W H = 24.40 [m]
CS13110W H = 19.75 [m]
CS13110E H = 19.75 [m]
CS13044E H = 19.75 [m]
CS13110W H = 10.70 [m]
CS13110E H = 10.70 [m]
CS13044E H = 10.70 [m]

(a)


GroundSurface VZG
Z displacement (cumulative from 2001)
displacement / H [%]
distance / H [-]
Peck
CS12197E H = 17.10 [m]
CS12197W H = 17.10 [m]
CS12270E H = 17.10 [m]
CS12270W H = 17.10 [m]
CS12270W H = 13.70 [m]
CS12270E H = 13.70 [m]
CS12197W H = 13.70 [m]
CS12197E H = 13.70 [m]
CS12197E H = 9.70 [m]
CS12197W H = 9.70 [m]
CS12270W H = 9.70 [m]
CS12270E H = 9.70 [m]

(b)



(c)

Figure 5.3 Soil displacements normalized with excavation depth H, compared with envelopes by Peck (1969) for Ceintuurbaan Station (a), Vijzelgracht Station (b) and Rokin Station (c)

From Figure 5.3 it is concluded that the ground displacements found in Amsterdam falls within the limit of Zone 1, as described by Peck, with the surface displacement falling within 1% of the (largest) excavated depth. The main displacements occur within 2 times the excavation depth as also predicted by Peck. More significant however is the effect of the excavation depth itself. In all three of the Amsterdam cases, the largest effect on the ground surface can be attributed to the preliminary activities, which took in total about 4 of the 6 years presented. The actual excavation stage caused only about 25-30% of the surface displacements and fell within 0.15% of the excavated depth.

For each station, the average contribution of the preliminary activities to the surface displacements has been determined in Table 5.1. The percentage shown is the amount of displacement caused by preliminary activities in 2003-2007 compared to the overall displacement between 2003-2009 or 2003-2010.

Table 5.1 Percentage of ground displacements caused by preliminary activities

	Surface displacements caused by preliminary work/total displacements
Ceintuurbaan	70%
Vijzelgracht	55%
Rokin	74%

The values at Ceintuurbaan and Rokin are comparable, the values at Vijzelgracht are influenced by the first incident (the points influenced by the second incident have been disregarded), showing a little larger effect during the period after 2007. The percentages for all the stations are somewhat higher than the actual values would be if the displacements at the end of construction (after 2012) had been taken into account, although additional displacements between 2009-2012 have been very small.

Such a high percentage of the settlements caused by preliminary activities was also reported by Fernie et al. (2001), who described a case study in London (Harrods). The deflection of the retaining wall in a top-down construction, caused only a small fraction of the overall ground movements. The installation of a contiguous piled wall of bentonite-cement caused up to 40% of the total movement.

Clough and O'Rourke (1990) evaluated the maximum displacement that should be expected behind different types of retaining walls based on a number of cases. In stiff clays, residual soils and sands the maximum ground displacement behind the wall is about 0.15% - 0.5% of the excavation depth, see
Figure 5.4. The Amsterdam cases are plotted in a similar way in Figure 5.5.

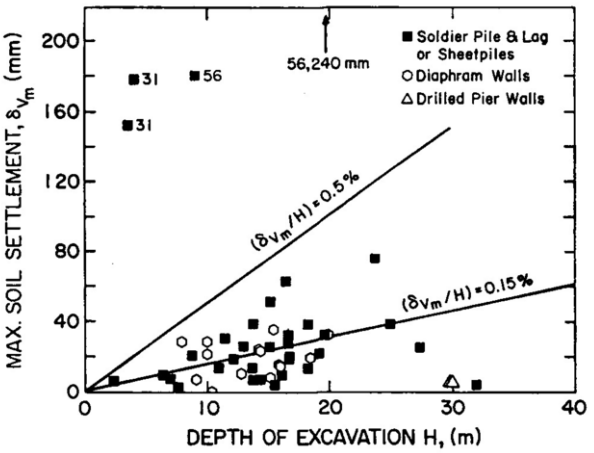
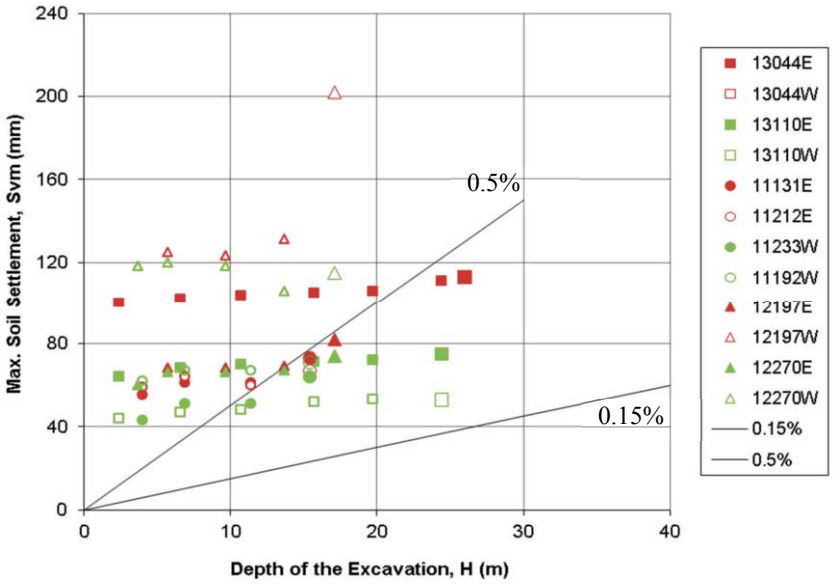
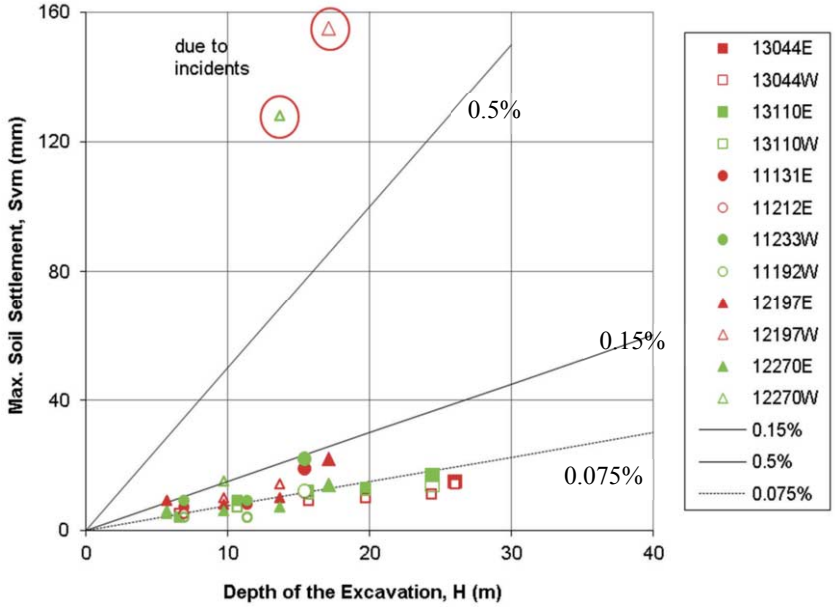


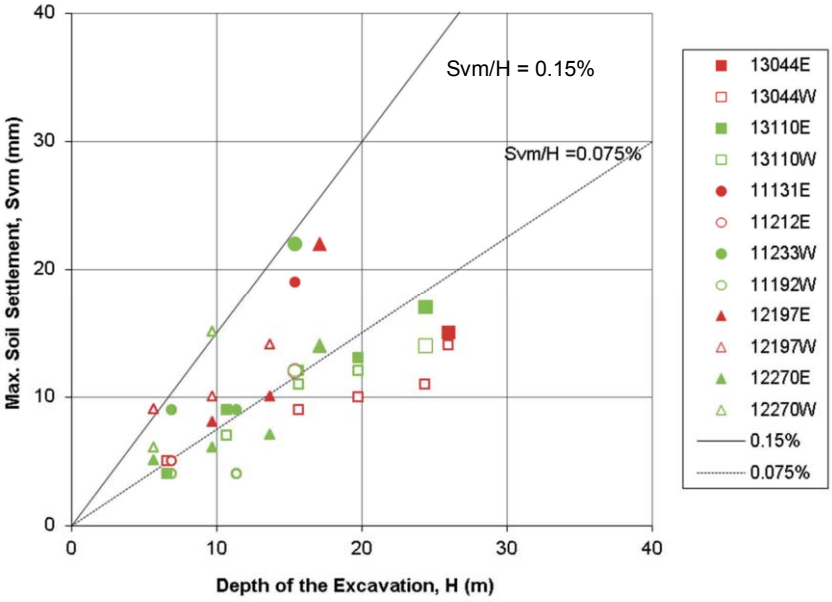
Figure 5.4 Observed maximum wall deflection and settlements for stiff clays, residual soils and sands (Clough and O'Rourke, 1990)


Max. Soil Settlement, Svm (mm)
Depth of the Excavation, H (m)
0.5%
0.15%
13044E
13044W
13110E
13110W
11131E
11212E
11233W
11192W
12197E
12197W
12270E
12270W
0.15%
0.5%

(a)


due to incidents
Max. Soil Settlement, Svm (mm)
Depth of the Excavation, H (m)
0.5%
0.15%
0.075%
13044E
13044W
13110E
13110W
11131E
11212E
11233W
11192W
12197E
12197W
12270E
12270W
0.15%
0.5%
0.075%

(b)



(c)

Figure 5.5 Observed maximum surface settlements in Amsterdam for a) all construction effects (including preliminary activities), b) for excavation only and c) as b) without incidents.

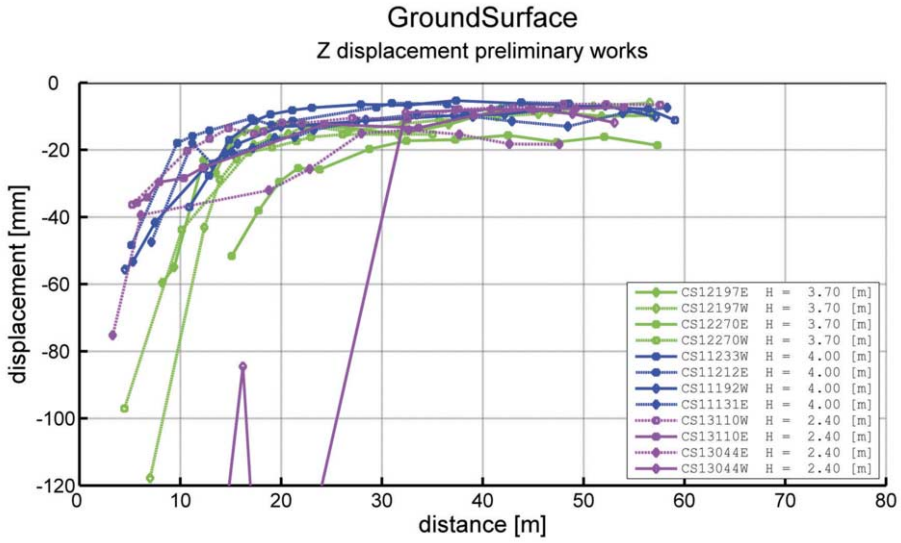
At the time of the end of the measurements presented, the surface displacement falls within the band of 0.15-0.5% times the excavation depth as determined by Clough and O'Rourke (1990), except for 2 incident locations (12197W and 12270W). During the early stages of construction, the surface displacement is approximately 1% of the excavated depth. This can be attributed to the significant impact of the preliminary activities, mainly due to the presence of highly disturbed soil conditions and the long duration of the works. The final values (shown slightly bigger in Figure 5.5a) for the surface settlement average to 0.3 to 0.45% of the excavation depth, with 0.3% for Ceintuurbaan Station which had almost reached full depth and 0.45% for Rokin and Vijzelgracht Station, which were both excavated about halfway down. The additional displacement due to the deeper excavation steps thus is small compared to the preliminary activities.

If the preliminary stages are not taken into account, the values are given in Figure 5.5b look much more like the values found by Clough and O'Rourke. The surface settlement, due to excavation of the stations, is less than 0.15% of the excavated depth, with an average of 0.07%. This value is achieved through the use of the very stiff diaphragm wall in combination with a large number of struts, including the deep grout strut. Long (2001) and later Moormann and Moormann (2002) extended the work of Peck to over 500 cases. The Amsterdam cases at the end of construction perform better than the values by Moormann and Moormann (2002), but the settlements due to the preliminary activities in the soft clay could have easily lead to a similar or even higher percentage if the excavation had for example been only 10m deep.

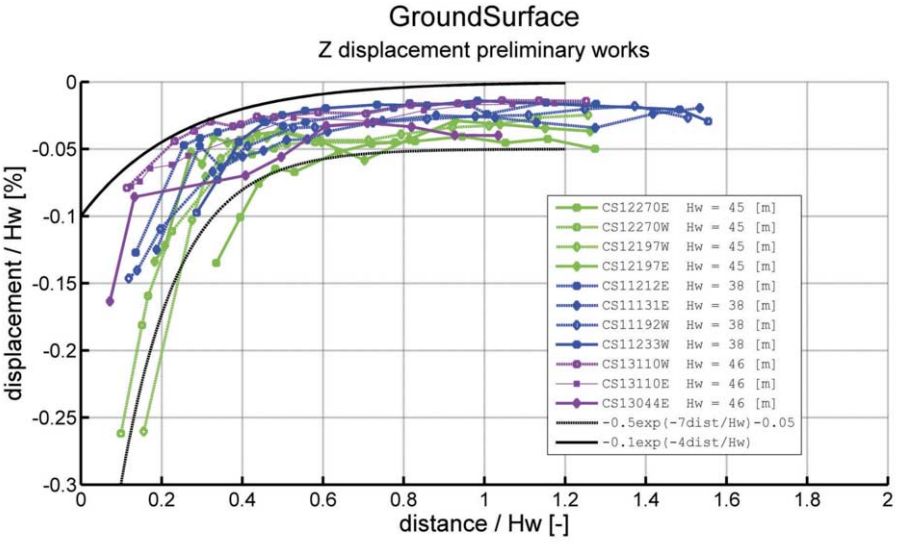
To evaluate the shape of the surface displacements as presented in the literature (See Chapter 2) with the Amsterdam results, the work of Peck (1969), Clough and O'Rourke (1990) and Hsieh and Ou (1998) is used. For a multi-propped wall, such as in Amsterdam, a concaved displacement profile should be expected, where the maximum ground surface displacement is found at a distance of approximately half the excavated depth away from the wall. The shape of the ground surface displacement for all three predictions methods is shown in Figure 5.7. In Peck's envelopes, the surface has a hogging shape, whereas in the other method's hogging occurs at larger distance from the wall, while closer to the wall the profile has a sagging shape. Other shapes which are used in practice to determine the shape of the displacement curve are the parabolic shape, such as by Bowles (1988) or the Gaussian curve, both being strictly hogging for deep excavations.

Figure 5.6 shows the shape of the surface displacement during the preliminary activities that caused most of the displacements.
Figure 5.7 shows the surface displacements during the excavation period only.

It can be seen that during the preliminary activities a hogging displacement profile similar to that seen above tunnels fits the measurements reasonably well. Most of the displacement in this stage is caused by predrilling and raising of the ground level for the purpose of the installation of the diaphragm wall, both having the largest impact on the top layers, thus resulting in this curved profile.

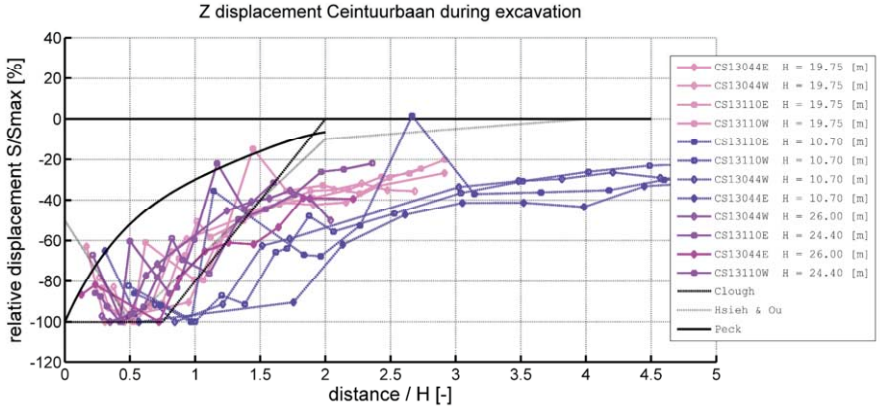


(a)

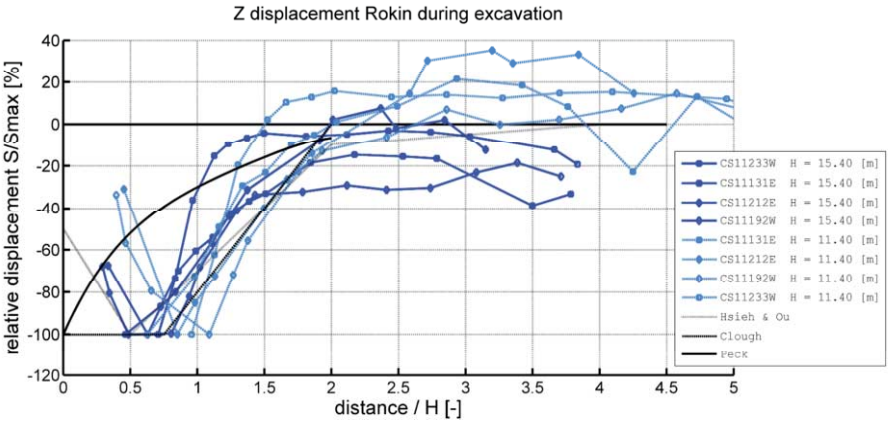


(b)

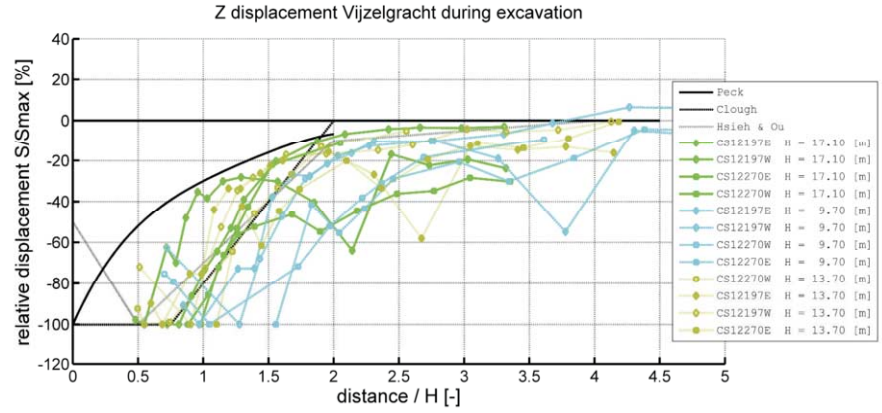
Figure 5.6 Measured surface displacements (a) and normalized surface displacements with wall depth Hw (b) for Amsterdam deep stations during preliminary activities



(a)



(b)



(c)

Figure 5.7 Measured surface displacements normalized with excavation depth H for three Amsterdam deep stations during excavation of the stations, compared to settlement envelopes proposed by Peck (1969), Clough and O'Rourke (1990) and Hsieh and Ou (1998).

During the excavation itself, the shape of the surface displacement consists of both hogging and sagging parts. The sagging part could not always be captured, because some settlement markers close to the excavation were lost in the process of construction. During the early excavation stages, the shape of the displacement profiles differs more from literature than in later stages. To show this, the results of all three stations are combined in Figure 5.8 for the deepest available excavation stage at the time of the data collection (2009-07-01). The shape of the surface displacement profile suggested by Hsieh and Ou (1998) fits the curve reasonably well, although the actual ground displacements sometimes extends further away from the wall.

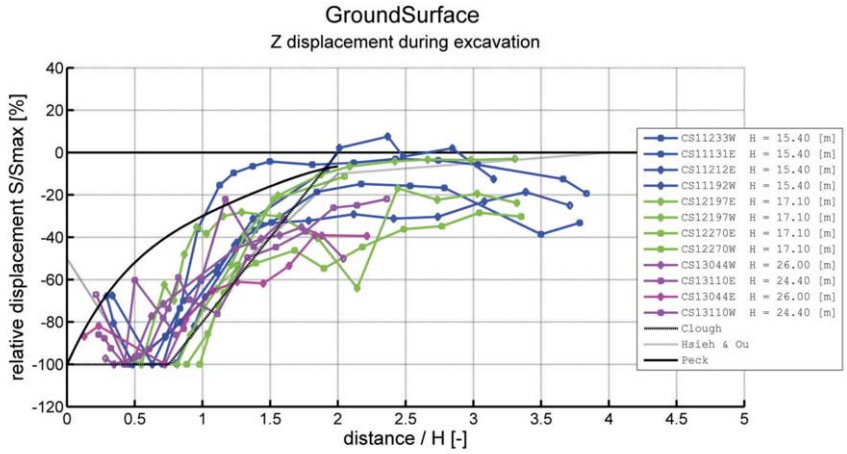


Figure 5.8 Measured surface displacements normalized with excavation depth H for three Amsterdam deep stations at the deepest excavation level available, compared to settlement envelopes proposed by Peck (1969), Clough and O'Rourke (1990) and Hsieh and Ou (1998).

The distance to which the displacements are found also depends on the excavation depth, according to the prediction methods described above. This assumption is tested for the Amsterdam deep excavations. In Figure 5.9, the maximum distance to which the displacement is found (or becomes horizontal) is shown for all three deep excavations.

A comparison is made in Figure 5.10 for the same values, now normalized with the excavation depth, either including all the construction stages or the excavation only. As discussed before, the largest impact on the ground surface displacement occurred during the early stages of the construction, leading to an almost constant distance to which the displacements are found. For the excavation stages, one could see a correlation between the distance and the excavated depth, but it is not as strong as might have been expected. For the initial excavation depths, usually larger relative distances are found, especially if all construction activities are taken into account. The distance to which the surface displacements reach might be related to more constant factors, such as the depth of the diaphragm wall or the depth of the soft soil layers. This effect can not be studied in the Amsterdam cases, because diaphragm wall depths and soil profiles are fairly uniform between the three cases.

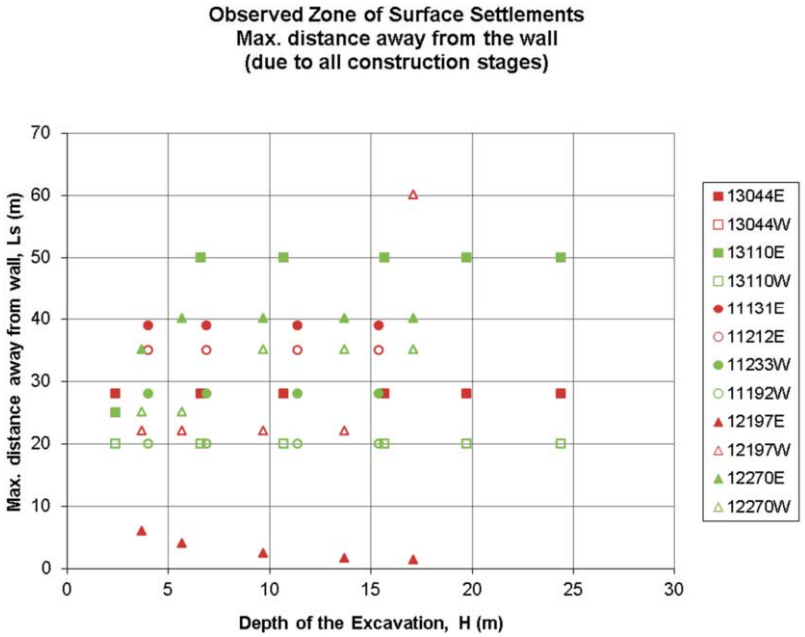


Figure 5.9 Maximum distance away from the wall to which the displacement is found in Amsterdam deep excavation, data from all construction stages.

The width of the settlement trough is also given by Caspe (1966) as a function of the angle of internal friction

$$W_{caspe} = \left(H + H_d\right) \cdot \tan\left(45 - \frac{\varphi'}{2}\right) \qquad (5.1)$$

$H_d = 0.5 \cdot B \cdot \tan\left(45 - \frac{\varphi'}{2}\right)$ for soils with $\varphi' > 0$ or

$H_d = B$ for cohesive soil

where H is the excavation depth and H_d is the influence depth below the excavation; φ' is the internal friction angle of the soil and B is the width of the excavation.

For the Amsterdam deep excavations, the resulting widths are presented in Table 5.2.

Table 5.2 Width of the settlement trough according to Caspe (1966) for sand and clay

	H*	B	Wclay	Wsand**	Wmeasured (all data)	Wmeasured (excav. only)
CTB	26	11	60	21	33	48
VZG	17	22	63	21	31	40
RKN	15	18	54	18	39	31

* H is excavated depth considered, this is not final depth, see Chapter 4

**With φ' = 30 degrees for Wsand

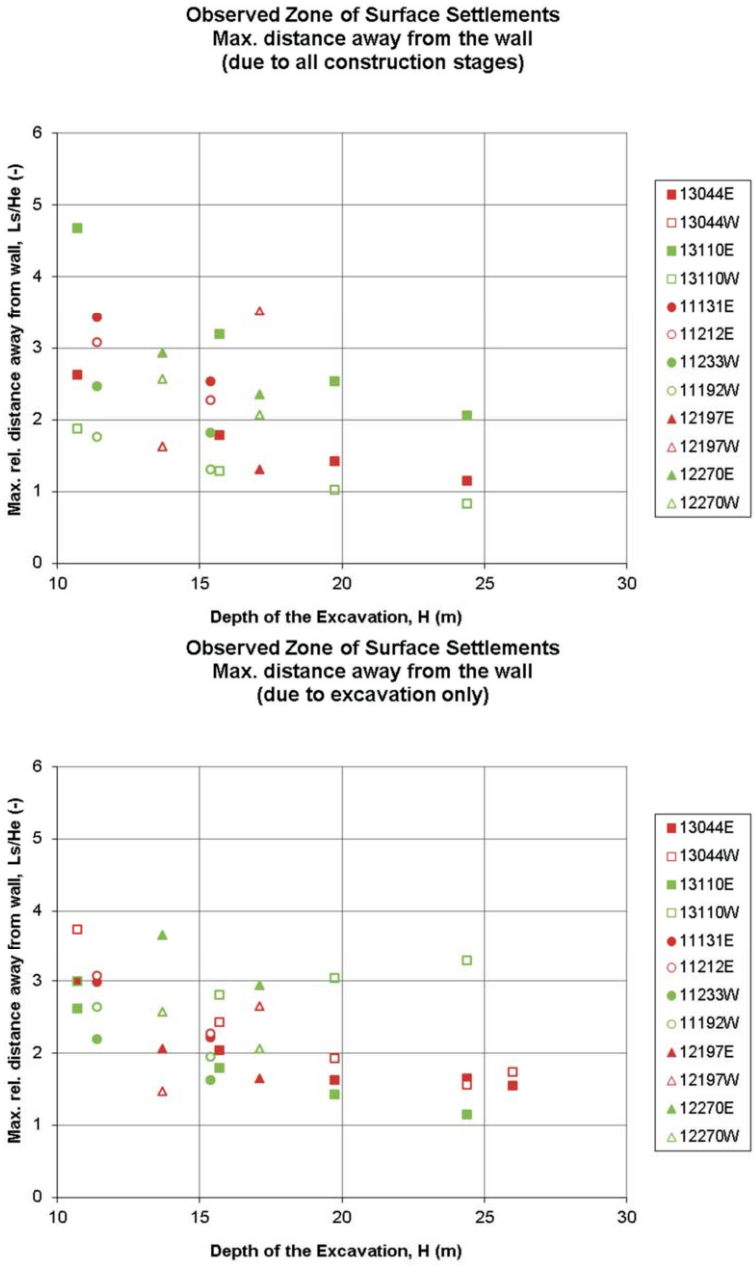


Figure 5.10 Maximum distance away from the wall (normalized with the excavation depth) to which the displacement is found in Amsterdam including preliminary activities (top) and for excavation only (bottom).

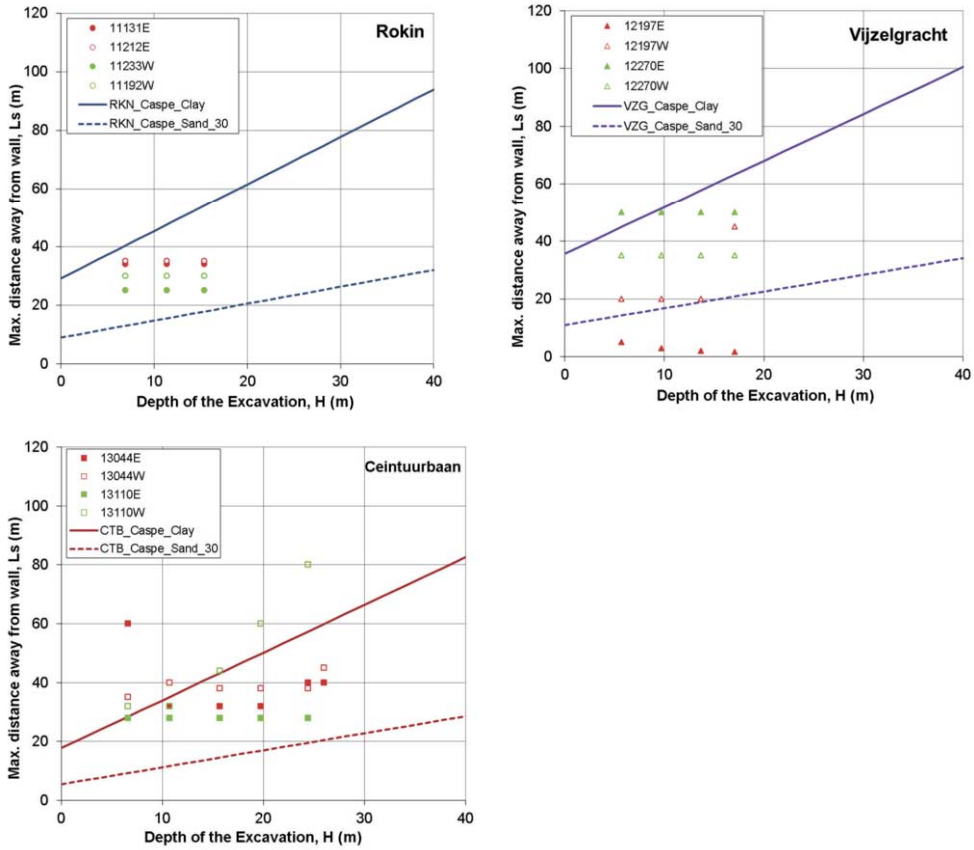


Figure 5.11 Maximum distance away from the wall to which the displacement is found compared to Caspe's prediction model for the excavation stages for each of the three stations

For clay soils, this means that the distance of the influence zone increases with the width of the station. This effect is not seen in the Amsterdam cases, since the narrowest station (CTB) shows a similar influence zone as the much wider stations RKN and VZG. Since the Amsterdam soil is a mixture of both sand and clay, the actual average zone of influence is something between the sand and clay values, see Figure 5.11. No evidence of substantial precision is found in the Amsterdam cases for the width defined by Caspe.

As the relationship with the excavation depth by Caspe (1966) does not fit the Amsterdam data very well, a more constant factor is used to determine the length of the zone of influence. Figure 5.12 shows the maximum distance to which surface displacements are found related to the depth of the wall. It can be concluded that the maximum distance to which displacements are found is about 0.6 – 1.0 times the depth of the wall, with an average of 0.8. The variation coefficient of 0.4 is however rather large.

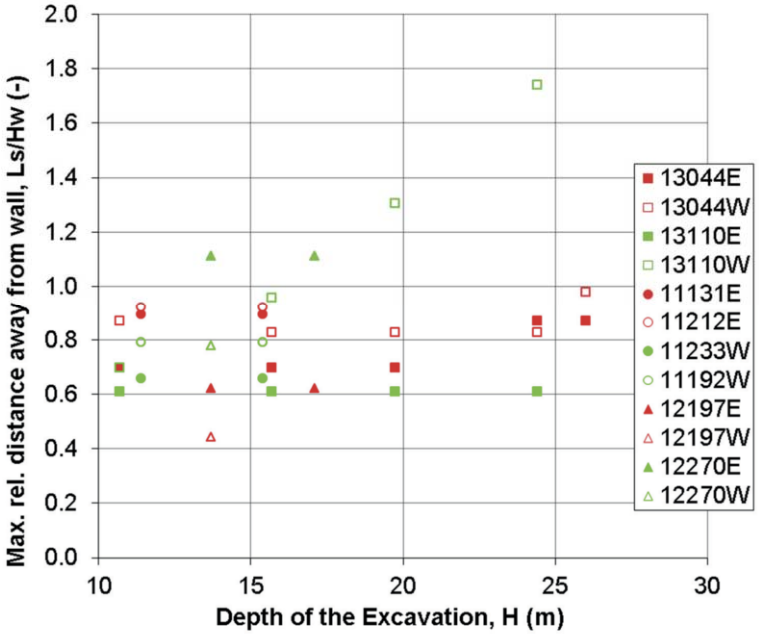


Figure 5.12 Maximum distance away from the wall to which the displacement is found normalized with the depth of the wall due to the excavation stages for the three stations

Using the depth of the deforming layers (Lam and Bolton, 2011) as the reference depth, the excavations at Ceintuurbaan show good correlation with the depth to the stable Third Sand layer (52 m) with an average zone of influence of 48 m. For Vijzelgracht and Rokin the excavation depths are smaller, but the depth to the Third Sand Layer is similar. The measured influence zones of 40 m and 31 m respectively (see Table 5.2) are smaller than this depth. It appears that both the excavation depth and the depth of the deforming layers contribute to the width of the settlement trough.

5.3 Ground displacements at depth

Not only do the surface displacements matter, but especially for buildings with deep foundations, the displacements at deeper levels in the ground determine the influence on these buildings. Figure 5.13 and Figure 5.14 show measurements of the vertical ground displacement at the surface and as much as possible also from the extensometers at depth. Since not all extensometers and inclinometers in the D-wall show good results, just three cross sections from Ceintuurbaan and two from Rokin have been analysed in full with wall deflection and ground displacement. In the figures, the corresponding excavation levels are shown as well.

For Ceintuurbaan, the maximum surface displacement is 11 mm, at the first sand layer (NAP-12m) it is 9 mm and at the second sand layer (NAP -20m) it is 6 mm. The wall deflection at the corresponding time (6 June 2009) shows only 10 mm of deflection. This value is likely to be incorrect as the deflection at smaller excavations levels is larger (20 mm), that is why Figure 5.13 shows the previous value available at 28 April 2009. The inclinometer is assumed to be fixed at the tip level (see Chapter 4 for discussion on this topic).

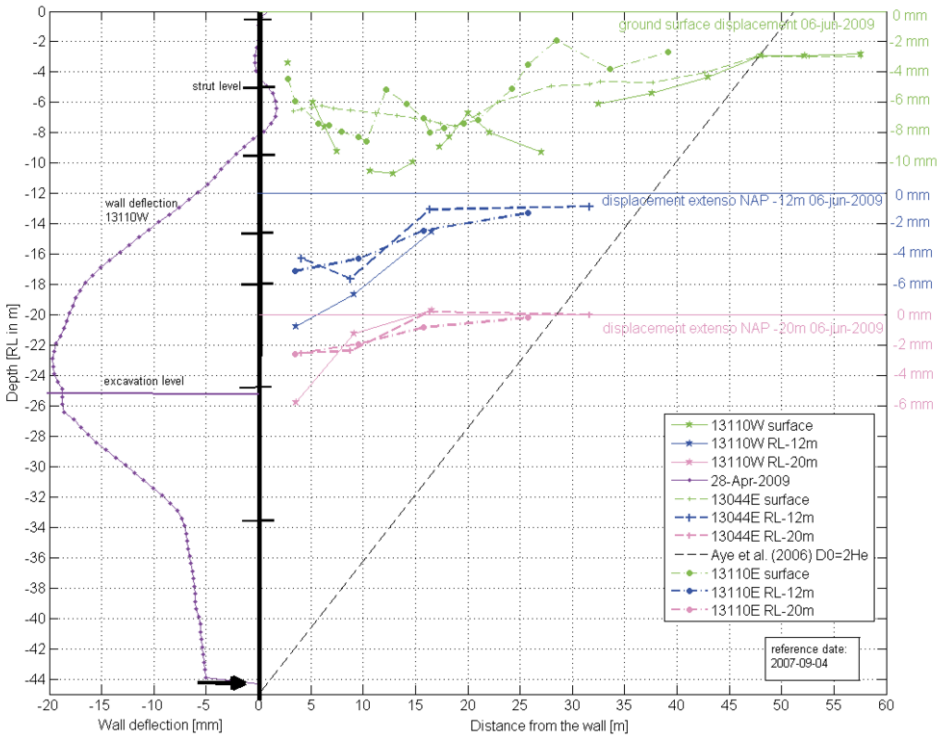
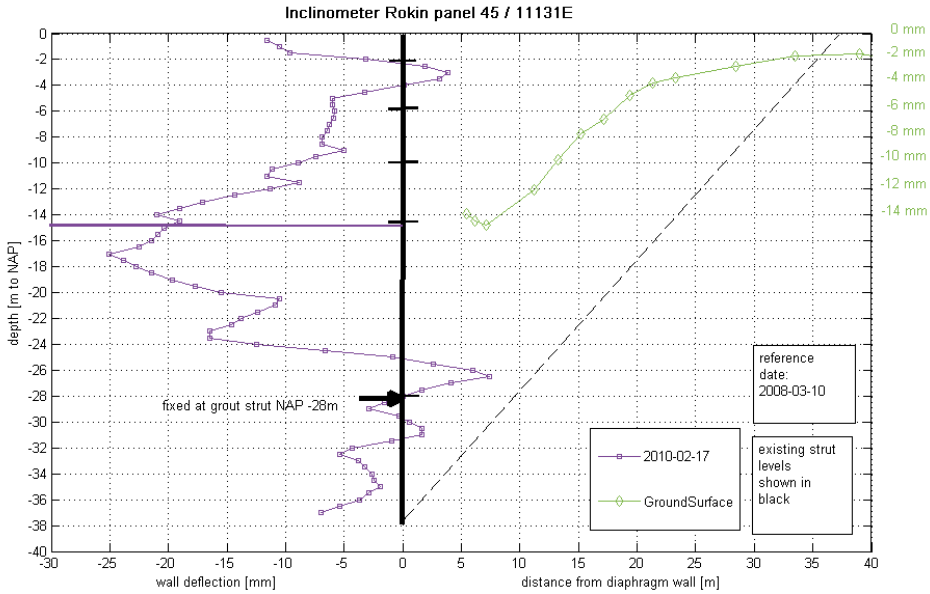
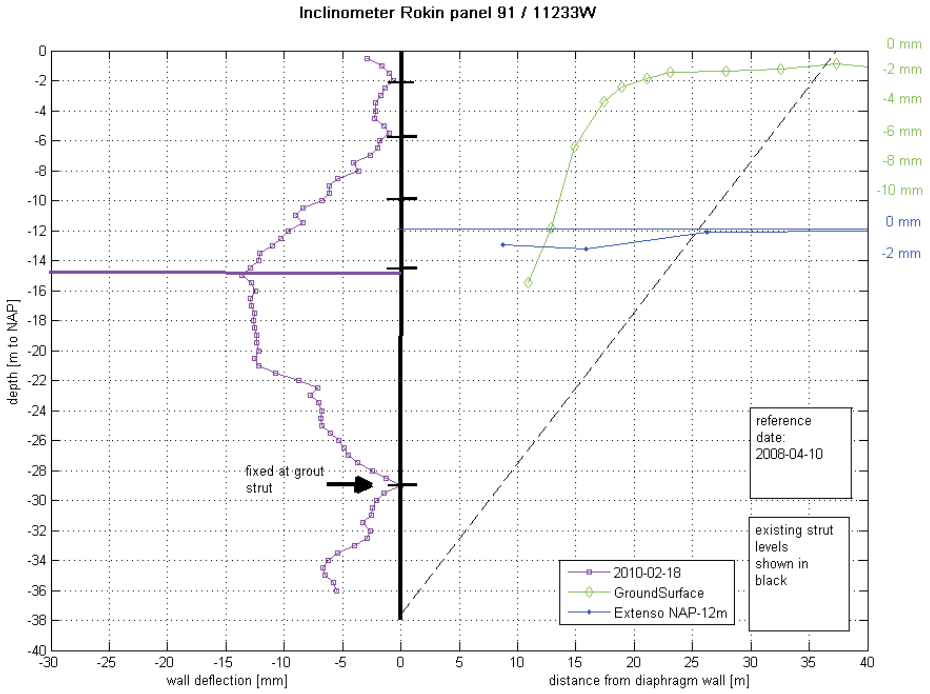


Figure 5.13 Measured deflection Dwall (horizontal) and ground displacement at different levels (vertical) for three cross sections at Ceintuurbaan Station. Influence zone as described by Aye et al. (2006) but with D_0=2He instead of 2.5He is shown in black striped diagonal line.

At Rokin Station two wall deflection curves are presented, with the one at 11131W being rather irregular. Both inclinometer results have been fixed at the level of the grout strut, which gives the most realistic result in combination with the other strut levels. Not all extensometers are reliable here, which is why only the ground surface and for one cross section the first sand layer results have been given.



(a)



(b)

Figure 5.14 Measured deflection Dwall (horizontal) and ground displacement at different levels (vertical) for two cross sections at Rokin Station. Influence zone as described by Aye et al. (2006) with D_0= 2.5He is shown in black striped diagonal line.

First, the assumption is tested that ground displacements at depth take place mainly within the active zone behind the retaining wall. Müller-Breslau (1906) assumed the active zone to fall within a straight line from the base of the wall with an angle of : $\pi/4 + \varphi'/2$ as minimum or $\pi/4 - \varphi'/2$ as maximum, see Figure 5.15. For an angle of internal friction φ' of 30º, this results in an influence area of 0.6 to 1.75 times the length of the wall (H_w, denote L in Figure 5.15). The active area determined according to this method results in an influence zone between 22 and 65 m from the wall for Rokin Station and between 26 and 78m for Vijzelgracht and Ceintuurbaan Stations, with respectively a length of the wall of 38 m and 45 m. The measured zones of surface displacements are between 30 and 50 m wide at maximum, which is clearly smaller than the outer values found from the angles of the active zone. This means the soil displacements do take place within the zone described by Müller-Breslau (1906), but the outer boundary is set too far away. A maximum distance of about once the depth of the wall is more realistic, as shown in Figure 5.12

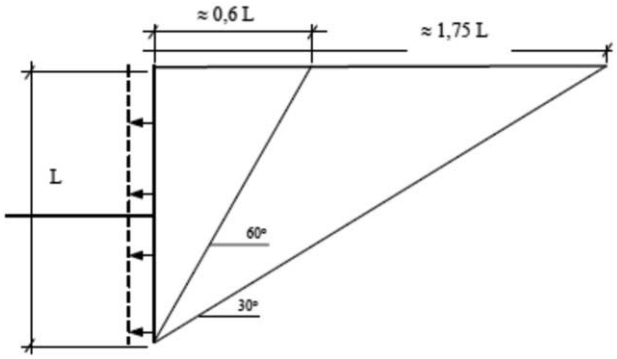


Figure 5.15 Limits of active zone according to Müller-Breslau (1906) for φ' is 30º

There are not many methods to determine the ground displacements at depth. Aye et al. (2006) introduced a simplified method in which the length of the zone of influence behind the wall is estimated to be 2.5 times the excavation depth for the surface and a linear relationship between the volume of the deflected wall shape and the volume of the settlement trough at any depth within the settlement influence zone.

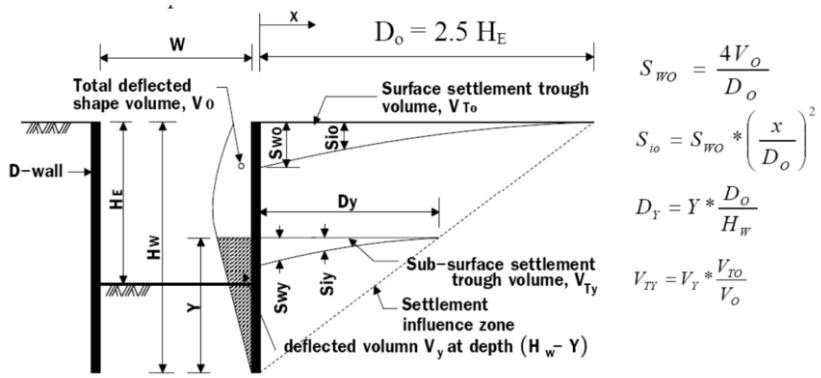


Figure 5.16 Surface and subsurface settlement prediction from diaphragm wall deflection values according to Aye et al 2006

NB: The formula for the displacement along the distance x from the D-wall should be:

$$S_{i0} = S_{w0} \cdot \left(\frac{D_0 - x}{D_0}\right)^2 \tag{5.2}$$

By rewriting Aye's formulae and integrating the displacement trough between x=0 and x=D_0, it is possible to determine the ratio of the displacement at depth Y over the surface displacement (S_{wy}/S_{w0}).

$$\frac{S_{wy}}{S_{w0}} = \frac{V_y \cdot D_0}{V_0 \cdot D_y} = \frac{V_y \cdot H_w}{V_0 \cdot Y} \tag{5.3}$$

For the measurements presented, these ratios have been determined and compared to the prediction by Aye et al. (2006) in
Table 5.3.

Table 5.3 Comparison of measured and predicted values for displacement at depth Y compared to the surface according to Aye et al. (2006)

		13110W NAP-12m	**13110W NAP-20m**	**11233 NAP-12m**
Y	m	45-12 = 33	45 – 20 =25	38-12 = 26
Hw	m	45	45	38
Vy /V0 meas	-	0.95	0.7	0.8
Swy/Sw0 calc	-	0.95*45/33=1.3	0.7*45/25=1.3	0.8*38/26=1.2
Swy/Sw0 meas	-	0.8	0.6	0.6
D0 calculated	m	64	64	37.5
D0 measured	m	45	45	25
Dy calculated	m	47	36	26
Dy measured	m	21	16	15-26*

* extensometer present at 15 m clearly shows displacement, marker at 26m does not show displacement. No information or trend is available between those markers.

It seems that due to the large number of struts in the upper part of the excavation, a relatively large percentage of the deflection takes place at larger depth. The presence of the grout strut does not seem to influence the results significantly. Scaling the total volume of displacement (V_{ty}/V_{t0}) does not work well in the sense that the measured displacements at depth are much smaller than the predicted values. At the surface (D_0) the measured distance is about 60-70% of the predicted distance, while this difference is even larger for D_y (40-50%). The relative values of the predicted and measured D_y/D_0 values do not match as well. The distance D_y at depth Y is scaled linearly with Y/H_w, while the volume of displacement at depth V_{ty} is scaled with the volume of the wall deflection V_y/V_0. This causes the method to predict relatively larger displacements at depth, while in practice smaller displacements at depth have been found.

If D_0 would be determined by 2 times the excavated depth and the ratio of S_{wy}/S_{w0} is scaled with V_y/V_0 directly, the corresponding S_{wy} and D_y fit the Amsterdam cases better, see Table 5.4 and Figure 5.17.

This means:

$$\frac{S_{wy}}{S_{w0}} = \frac{V_y}{V_0} \tag{5.4}$$

and

$$D_y = \frac{Y}{H_w} D_0 \tag{5.5}$$

Table 5.4 Comparison of measured and predicted values for displacement at depth Y compared to the surface with modified method

		13110W NAP-12m	**13110W NAP-20m**	**11233 NAP-12m**
Y	m	45-12 = 33	45 – 20 =25	38-12 = 26
H_w	m	45	45	38
V_y/V_0 meas	-	0.95	0.7	0.8
S_{wy}/S_{w0} calc	-	0.95	0.7	0.8
S_{wy}/S_{w0} meas	-	0.8	0.6	0.6
D_0 calculated	m	51	51	30
D_0 measured	m	45	45	25
D_y calculated	m	24	15	14
D_y measured	m	21	16	15-26

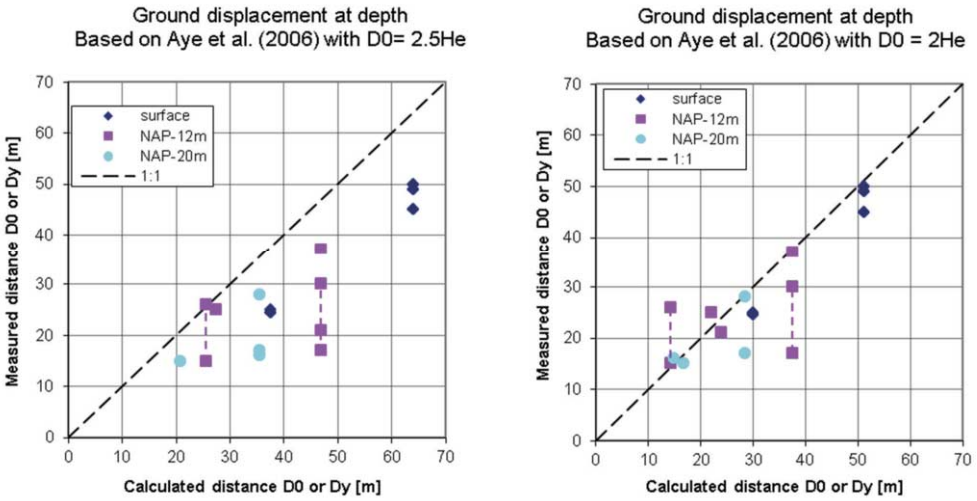


Figure 5.17 Comparison between measured and calculated influence distance a) for D_0=2.5He and b) for D_0=2He

MSD (Bolton et al. 2008) as described in Chapter 2 gives displacements of the ground behind a retaining wall based on a cumulative method of energy conservation, see Figure 5.18.

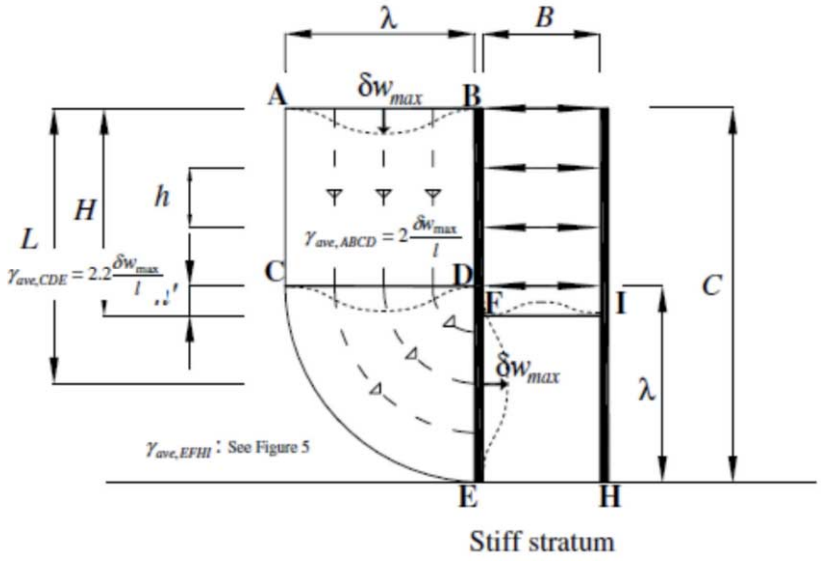


Figure 5.18 Incremental displacement field for narrow excavations (Bolton et al., 2008)

The displacement is negligible at distance λ behind the wall, where λ originally is defined by O'Rourke (1993) as the distance between the lowest strut and the level at which the wall is effectively fixed in a stiff underlying layer. Lam and Bolton (2011) found from 110 cases

that λ is limited by the depth of the soft clay stratum. They define it as the distance between the lowest prop level and the base of the clay stratum. For a multi-prop excavation, the average wavelength is λave ≈ C – (H –h)/2, in which C is the depth of the clay layer(s), H is the ultimate excavation depth and h is the average vertical prop spacing.

Results for the Amsterdam deep excavations are given in Figure 5.5 The method indeed predicts small distances compared to the measurements as shown earlier by Lam and Bolton (2011). If for the wall height the length from the top of the wall to the bottom/heart of the grout strut would be taken, the difference between measurement and MSD method would be even larger. Better results may be obtained for Ceintuurbaan Station if the value for C is not limited by the wall depth but extends below the excavation to the base of the Eemclay at approximately 52 m. For Rokin Station, with a shallower excavation depth this would however lead to overestimating the zone of influence. For the Amsterdam cases, the influence zone clearly decreases with depth also in the zone above the lowest strut. The MSD method can be used to predict the ground displacements below the surface for deep excavations if a stepwise approach is taken and deformation patterns for subsequent stages are added together. The minimum width of the influence trough however, is the value given in Table 5.5, which overpredicts the measured trough at NAP-12m and deeper in Amsterdam. The complications in using the MSD method arise mainly due to the presence of the sand layers in the soil profile.

Table 5.5 Comparison of measured and predicted values MSD method

		CTB 13110W 28 Apr 2009	**RKN 11233**
C	m	45	38
H	-	25.6	15
h	m	25.6/5 = 5	15/3 = 5
λave calculated	m	35	33
$\lambda_{O'Rourke}$ calculated	m	26	28
λ measured surface	m	45	25
λ measured NAP-12m	m	21	15-26*
λ measured NAP-20m	m	16	x

* see comment Table 5.3

5.4 Presence of the buildings

All ground displacements presented in the previous sections have been determined from measurement points located in the side streets of the three stations. Some of these streets are narrow, some wider, but in all cases the closest buildings are present at a distance of about 2-3 m from the instruments. It is assumed that the displacements can be considered 'free field' displacements. To check this assumption, the displacement profiles are related to the distance to the nearest facades along the side street (X1 in Figure 5.19) to see whether the distance from the façade plays a role.

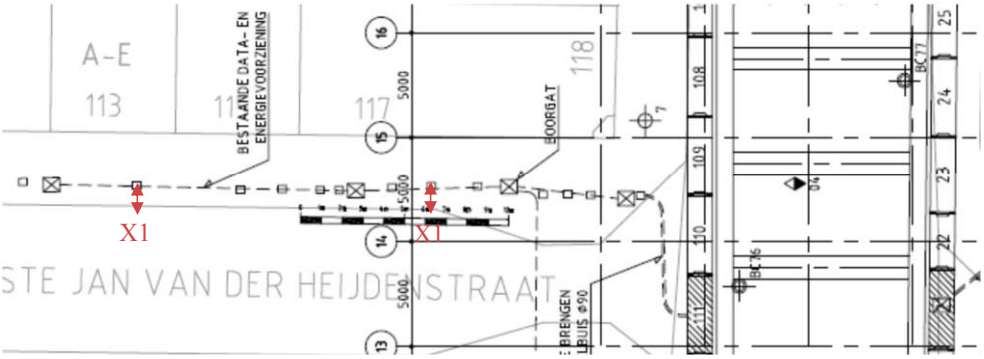


Figure 5.19 Example of location of measurement points in cross section

The distance as mentioned in Figure 5.19 is given by two values; the first being the distance close to the deep excavation and the second the distance further into the side street. The ground surface displacements for the cross sections are shown in Figure 5.20. The narrowest streets (and the measurement sections closest to the facades) show slightly less settlement than in the wider streets and larger distances to the facades. The effect however is small and not consistent for all cross sections.

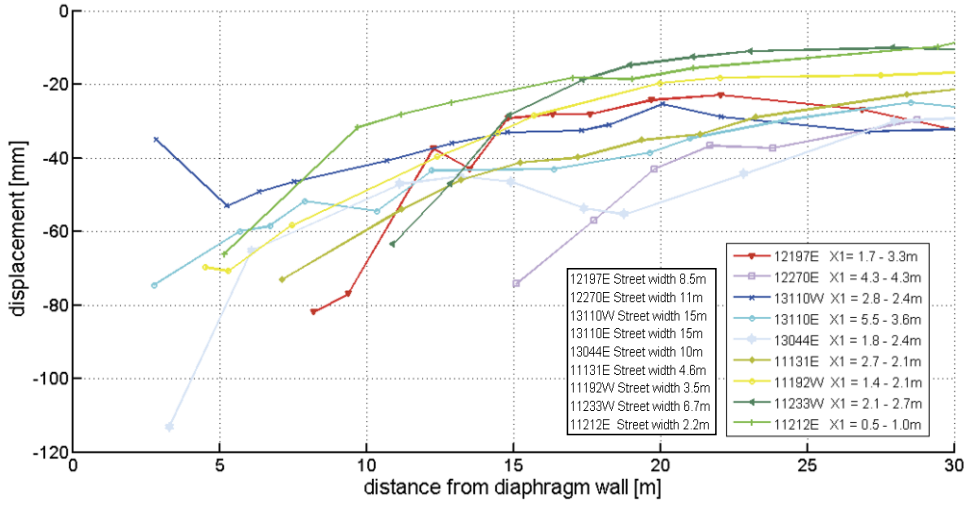


Figure 5.20 Measured surface displacements in periods 2001/2002 – 2009/2010for three Amsterdam deep excavations with distance X1 to facades and street widths, excluding incident locations at Vijzelgracht.

A second analysis for the influence of the distance between the diaphragm wall and the facades parallel to the station also did not show a clear relationship. It is concluded that although the ground settlements might not be completely free field, the impact of the variations in construction is larger than the effect of the presence of the buildings.

5.5 Conclusions on ground displacements due to deep excavations

The ground displacement measurements for the Amsterdam cases have been compared to several, mostly empirical, relationships to determine the green field surface displacements and displacements at depth. Most methods assume that the shape of the displacements is related to the shape of the deformed wall and the soil type. The effect of the relative flexibility or stiffness of the system (wall and supports) compared to the soil stiffness, the safety against basal heave and the duration of the excavation could not been assessed due to a lack of variables present in the deep excavations studied.

From the Amsterdam cases it is concluded that the surface displacement behind the wall is 0.3 – 1.0% (for an average system stiffness and sufficient basal stability). Better results are possible (0.2-0.5%H) for diaphragm walls with good supports, if installation effects are controlled sufficiently. Surface displacements behind the wall can be much larger than the wall deflections, as proved in the Amsterdam deep excavations, and may reach over a distance of 0.75H from the wall and become negligible at 2-3 times the excavated depth away from the wall. The shape of the displacement fits the profile of Hsieh and Ou (1998) best.

In all three of the Amsterdam cases, the largest effect on the ground surface displacement can be attributed to the preliminary activities, which took in total about 4 of the 6 years presented. The actual excavation stage caused only about 25-35% of the surface displacements, with 55-75% attributed to the preliminary activities.

The main displacements caused by the excavation and its construction works take place within about 2 times the excavated depth at the surface level. At larger excavation depths, the influence zone is significantly smaller. Most prediction methods overestimate the influence zone at depth compared to the measured values for the deep stations. It must be mentioned that not all extensometers show trustworthy results, which means that this conclusion is based on a limited number of cross sections. At the sections presented however, this effect is clearly shown.

The diagonal line from Aye et al. (2006) could be used as an estimate for the influence area, since it is a conservative line. The curvature of the displacement profiles from this method can also be considered conservative. For a better fit, the maximum distance from the wall for significant surface displacements (D_0) could be taken as 2 times the excavated depth (instead of 2.5 times as suggested by Aye et al. (2006)).

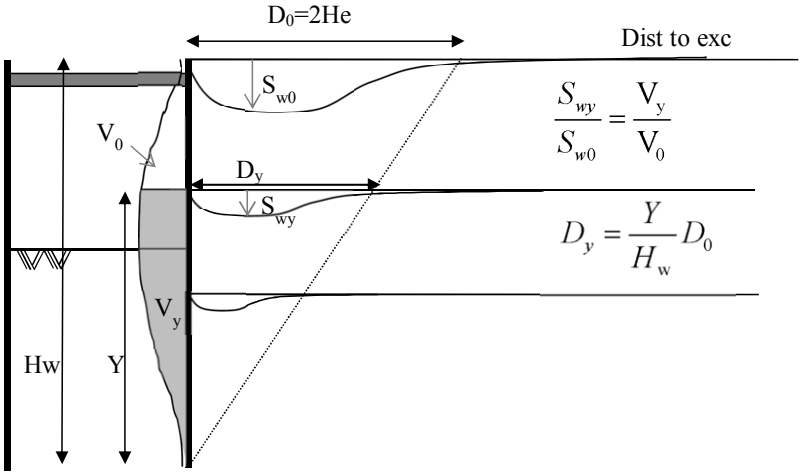


Figure 5.21 Proposed influence area for vertical soil displacements, modified from original Aye et al. (2006).

The influence distance D_0 could also be estimated from the MSD method by Lam and Bolton (2011) as the depth of the clay layers, which in the Amsterdam case (by coincidence) is equal to twice the final excavation depth.

Although the measurements are located at close distance (2-3m) of the nearest facades, no clear relationship is found between the amount or the shape of the settlements with the distance to the facades. The measured displacements can be considered as similar to 'free field' displacements.

CHAPTER 6 PILE LOAD TESTS DAPPERBUURT

6.1 Introduction tests Dapperbuurt Amsterdam

The initial condition of the piles in Amsterdam is determined with the help of an extensive test series (Hoekstra and Bokhoven, 1974) of piles in the "Dapperbuurt" neighbourhood in Amsterdam. The test location is located at the 2nd Van Swindenstraat, see Figure 6.1. In 1973, several pile load tests have been performed on piles from demolished houses in this street and on additionally installed (driven) piles. These houses had to be demolished due to large differential deformations, caused by foundation problems. Details on the tests are reported in sections 6.1 to 6.3. In sections 6.4 and onward the original test results have been reinterpreted and translated to more general conditions for the piles near the Deep Stations to be used in this thesis.

The original buildings were four storey's high with additional loft on top and sometimes a (semi-) basement. The buildings dated from 1876 – 1906, so the piles where about 70 – 100 years old at the time of testing. The houses before demolition are shown in Figure 6.2.

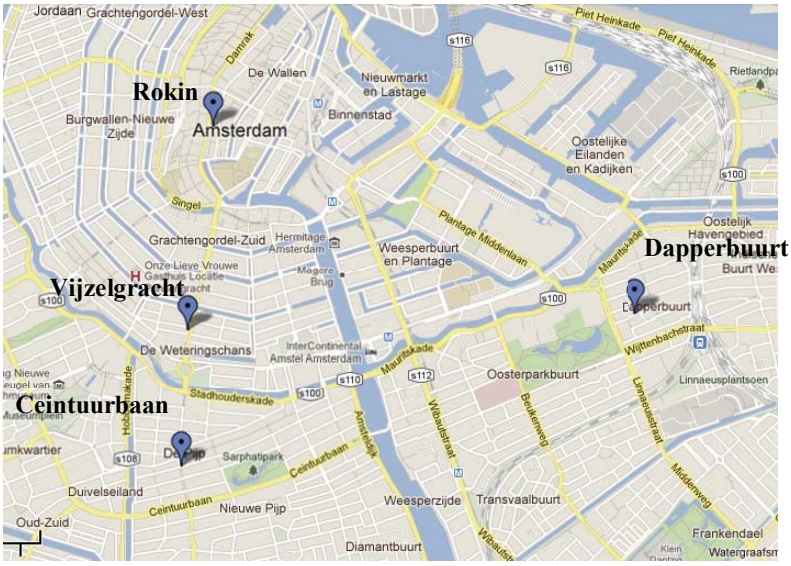


Figure 6.1 Dapperbuurt in Amsterdam, also shown are Rokin, Vijzelgracht and Ceintuurbaan



Figure 6.2 Typical façades Dapperbuurt / 2nd Van Swindenstraat (picture Martin Alberts 1981)

The average pile head diameter of the timber piles found in the test area is 220-225 mm and the average toe diameter is 110 mm. The resulting average tapering is about 10.5 mm/m. The average tapering in the Holocene layers is 9.1 mm/m.
All piles tested and reported here are made of Pine wood (or Scots Pine; in Dutch “grenen”, in Latin “pinus sylvestris”). Scots Pine wood is generally more susceptible to degradation than Spruce (Picea Abies), which is the other common type of timber pile in Amsterdam.

From the foundation plans, similar pile spacing is found under the facades compared to the walls. Since the walls bear larger loads, the average pile load under the walls is higher than under the walls. The average pile spacing is 0.6 m, with maximum values up to 0.9 m.

6.2 Soil conditions

The soil characteristics at the 2e van Swindenstraat are mainly taken from CPT and borings. The CPT’s are presented in Annex D. Surface level is found at NAP +0.3 to NAP + 0.7 m and close to NAP under the houses. Above NAP -4 m, which used to be the original green field level, a man made (fill) layer is found. Below this level 1.5 – 2 m of peat is found, underlain by 1-1.5 m of soft clay. From NAP -7 or -7.5 m a fine sand, with clay layer (called “wadzand”) of 2.5 m thickness is found. The foundation layer is the first sand layer, with the top at NAP -12 m on average, with the highest level found in the test area at NAP -11.7 m and the lowest level at NAP -13 m. Just above this first sand layers, a layer of peat is found, which separates the first aquifer from the phreatic levels above. Some characteristic soil parameters are given in Table 6.1.

Table 6.1 Characteristics of soil layers from tests by Hoekstra and Bokhoven (1974)

Number	**Top**	**γ;sat**	**φ'**	**Soil type**
	[NAP]	[kN/m^3]	[degrees]	
1	0	17	25	Sand, Fill
2	-4.0	11		Peat
3	-6.0	16		Clay
4	-7.0	18.5	27	Sand, clay
5	-9.5	15		Clay, peat
6	-12.0	11		Peat
7	-12.2	18	33	Sand

6.3 Test results

Tests were performed in axial compression and axial tension, see Annex D for locations of the piles and CPTs and for the results of the pile load tests. Tests reaction loads were provided by dead weight. Time steps of the loads were taken as 24 hours (some tests have been performed with 12 hour steps). Load steps were usually 25 kN – 50 kN. For the tests in tension, load steps of 25 kN – 50 kN for 0.5 hour periods (sometimes 12 hour periods) were used. The piles reported here were tested in compression first, except for pile 5 and pile 6.

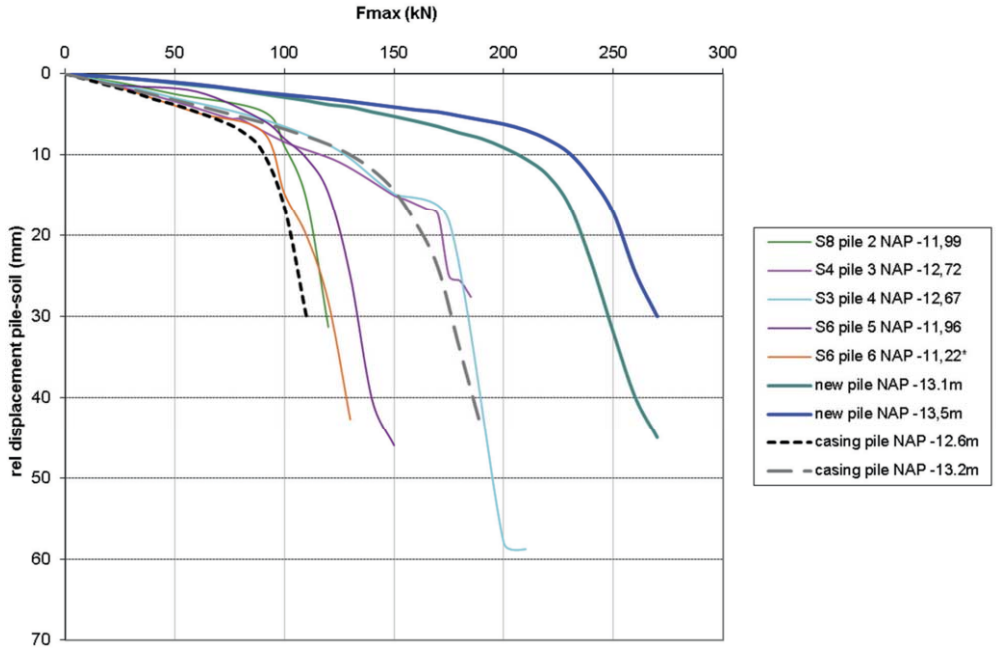
Figure 6.3 shows the results of the pile load tests in compression and in tension. Table 6.2 gives the resulting pile capacities for the 'old' piles if failure is assumed at displacements of 10-15 mm. Higher ultimate values can be found for larger displacements, as shown in Table 6.3.

Table 6.2 Failure capacity for single piles in kN (at 10-13 mm head displacement)

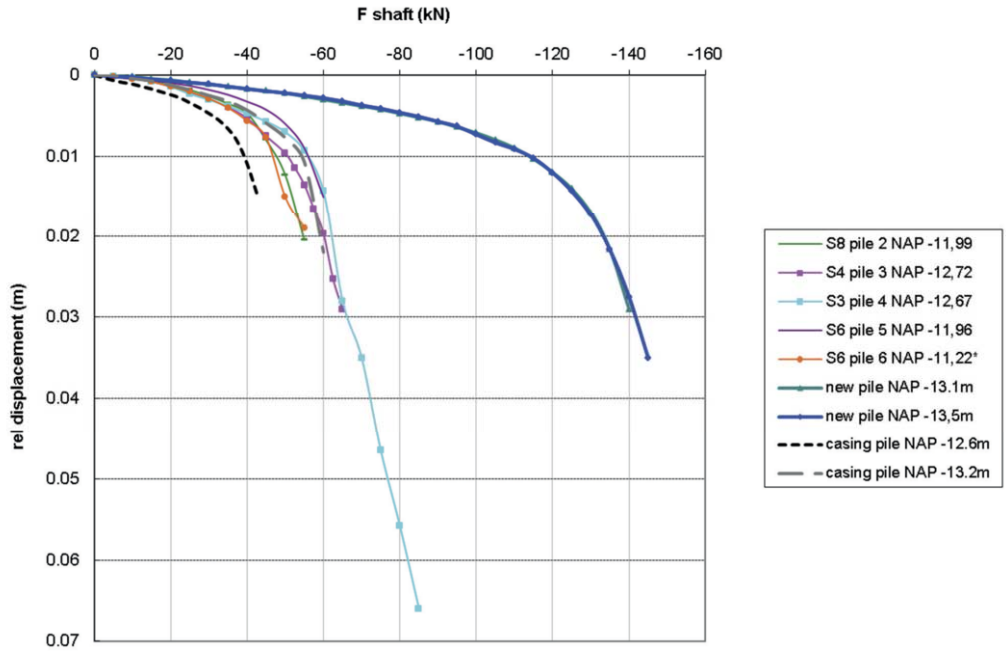
	Pile 2 Toe NAP -11.99m	Pile 3 Toe NAP -12.72m	Pile 4 Toe NAP -12.67m	Pile 5 Toe NAP -11.96m	Pile 6 Toe NAP -11.22m
Tension (test)	55	59	62	60	48
Compression (test)	111	171	176	120	98

Table 6.3 Failure capacity for single piles in kN (at ultimate displacements)

	Pile 2 Toe NAP -11.99m	Pile 3 Toe NAP -12.72m	Pile 4 Toe NAP -12.67m	Pile 5 Toe NAP -11.96m	Pile 6 Toe NAP -11.22m
Tension (test)	55	65	85	60	55
Compression (test)	115	185	210	150	130



(a)



(b)

Figure 6.3 Results pile tests in compression shown in (a) for shaft + base, and in tension shown in (b) (shaft capacity)

All piles were extracted from the soil. Piles 2, 5 and 6 were reported as broken at the end of the pile. This explains the toe level being above the foundation sand layer. It is assumed that the piles had been broken due to overloading of the piles before they were extracted. The low pile base capacity calculated for these three piles is most likely due to the failure of the pile itself.

A special set of (new) piles was installed at the test location to compare the pile capacity with and without the soft Holocene layers. One pile was installed as reference pile (called 'new pile') and one with a casing to NAP -11 m. Inside the casing the soil was removed, to exclude the contribution of the soft layers to the test. Both piles were tested in compression to failure first, than in tension to failure. After these tests, the piles were driven to a deeper level and tested again in compression and tension. Both piles had the same dimensions (pile toe diameter 0.13m) and are located within 1.5 m from each other. CPT's 01, 108A and 108B were located close to the piles, with 01 closest to the casing pile and the other two CPT's closer to the reference pile, see Annex D.

The results for the pile load tests are given in Table 6.5 as well as Figure 6.1 and Figure 6.2. If the maximum capacity is limited to a displacement of 10mm along the shaft and 10% of the diameter at the toe, the pile capacities are reduced to the values in Table 6.4.

Table 6.4 Failure capacity for special piles in kN for 10 mm (shaft) and 13 mm (base) displacement

	Pile with casing		New pile	
	Toe NAP -12.6m	Toe NAP -13.2m	Toe NAP -13.1m	Toe NAP -13.5m
Tension / shaft (test)	41	56	123	122
Compression (test)	95*	145	221	240

Table 6.5 Ultimate failure capacity for special piles in kN

	Pile with casing		New pile	
	Toe NAP -12.6m	Toe NAP -13.2m	Toe NAP -13.1m	Toe NAP -13.5m
Tension / shaft (test)	45	60	140	145
Compression (test)	110*	190	260	270

*The cased pile with toe level NAP -12.6 m has extremely low test results, which might be due to the limited embedment in the foundation layer (0.4 m) combined with possible loosening of the sand when the soil was removed from the casing. The results of this test are not used in further analysis.

6.4 Analysis of special piles with/without casing

Since the piles of these tests were not instrumented, the shaft friction in the foundation layer, the shaft friction in the Holocene layer and the base capacity have to be separated by comparing the results of the different tests. In all further analyses, it is assumed that the soil conditions do not vary over the test location (which is only a few metres wide and long).

6.4.1 Shaft friction in Holocene layer

Comparing the two tests with similar pile toe level of NAP -13.1/-13.2 m, a maximum of 80 kN (140 – 60 kN) of shaft friction in tension is mobilized in the soft layers above the level of NAP -11 m for the ultimate values. A similar value of (123-56=) 67 kN is found if failure is assumed at 10-13 mm relative movement.

Based on a calculation with the slip method (β-method) the maximum negative skin friction, which acts in the same direction of the tension loading, is 68 kN, based on the pile tapering from 0.23m to 0.15m and a friction coefficient K * tanδ of 0.25 (minimum value for skin friction to be adopted according to NEN (2011). The amount of shaft friction in the Holocene layers can also be assessed by the α-method based on Tomlinson and Woodward (2008) as being:

$$Rs = \tau * \pi * D * \text{layer thickness, with } \tau = \alpha * c_u \quad (6.1)$$

The undrained shear strength of the Holocene varies between 20-30 kPa according the North South Line dataset, but is more likely in the order of 12-15 kPa based on correlations with the cone resistance by Lunne et al. (1997). α is usually 1.0 for soft clays and the length of the pile in the Holocene is about 9 m (NAP -2 m to NAP -11 m). With an average diameter of the pile of 0.2 m this leads to a total shaft friction estimated of 1.0 * 12-15 kPa * 3.14 * 0.2 * 9 m = 67-84 kN. Both the β-method and the α-method give similar results as the values taken from the pile load tests.

The value of shaft friction found for tension/negative skin friction is used also as downward friction. This is consistent with Tomlinson and Woodward (2008), who report that the Imperial College method (ICP) uses the same value for shaft friction for clays in tension compared to compression. Compared to sands, clays do not experience significant degradation of the soil particles at the pile–soil interface. API (1993) also state a factor of 1.0 between tension and compression can be used.

6.4.2 Shaft friction in foundation layer

Table 6.6 and Table 6.7 show the derived friction values in the foundation layer based on comparisons of the cased and new pile.

Table 6.6 Shaft friction in first sand layer based on failure at 10-15 mm relative displacement

	Pile with casing		New pile	
	Toe NAP -12.6m	Toe NAP -13.2m	Toe NAP -13.1m	Toe NAP -13.5m
Tension / shaft (test) (kN)	41	56	123	122
Shaft capacity to NAP -11 m (kN)	0	0	67	67
Shaft capacity NAP -11 m to NAP -12.2 m (kN)	=1.2 m* 67 kN / 9 m = 9 kN	9	9	9
Net resistance in 1st sand (kN)	32	47	47	46
Depth in 1st sand layer (m)	0.4	1	0.9	1.3
Shaft friction sand (D=0.13 m) (kN /m)	80	47	52	35
Shaft friction sand (kN/m^2)	196	115	128	87

Table 6.7 Shaft friction in first sand layer, based on values at failure

	Pile with casing		New pile	
	Toe NAP -12.6m	Toe NAP -13.2m	Toe NAP -13.1m	Toe NAP -13.5m
Tension / shaft (test) (kN)	45	60	140	145
Shaft capacity to NAP -11 m (kN)	0	0	80	80
Shaft capacity NAP -11 m to NAP -12.2 m (kN)	=1.2 m* 80 kN / 9 m = 11 kN	11	11	11
Net resistance in 1st sand (kN)	34	49	49	54
Depth in 1st sand layer (m)	0.4	1	0.9	1.3
Shaft friction sand (D=0.13 m) (kN/m)	86	49	55	42
Shaft friction sand (kN/m^2)	210	121	134	102

Based on the depth in the first sand layer, the shaft friction in tension in the sand is 35 – 52 kN/m pile (average 45 kN/m), as can be seen from Table 6.6 or even 42-55 kN/m for larger displacements if the pile at NAP -12.6m is excluded (see Table 6.7, average 49 kN/m).

The calculated shaft resistance in the sand according to Meigh (1987) for a driven timber pile in cohesionless soil is:

$Rs = q_c / 80 * A_s$ (6.2)
with q_c is the average cone resistance of the embedment.

This is very similar to the Dutch Annex to Eurocode 7 by NEN (2011) where:
$R_s = A_s * \alpha_s * q_{s;z}$ (6.3)
With:
$A_s = \pi * 0.13$ m per metre pile
α_s is the pile shaft factor = 0.012 for tapered timber piles in compression
with $q_{c;z}$ for CPT 01 is 12 MPa for the pile toe level of NAP -13.2m.

$Rs;compression = \pi * 0.13 * 0.012 * 12000 = 59$ kN/m.
These design values are for piles in compression, while the test result presented is in tension. NEN (2011) gives $\alpha_s = 0.007$ in tension, leading to $Rt = \pi * 0.13 * 0.007 * 12000 = 34$ kN/m. This large difference between the shaft friction in tension compared to compression according to NEN (2011) is probably caused by the tapering of the timber piles. The difference between shaft friction in tension and compression is most clearly present in sands, while this was not the case for clays as described in section 6.4.1. De Nicola and Randolph (1993) concluded based on numerical results, that both contraction of the shaft and a change in the loading direction are responsible for a lower shaft friction in compression than in tension for sands.

Based on their formulae:
$Rt/Rc \approx (1- 0.2 \log_{10} (100/ (L/D))* (1- 8 \eta + 25\eta^2)$ (6.4)
and
$\eta = \nu_p (L/D) (G_{ave}/E_p) \tan\delta$ (6.5)

with
Rt/Rc is the reduction factor for tension loading
L/D is the slenderness of the pile (Length over Diameter of the pile)
ν_p is Possions ratio of the pile
G_{ave} is the average shear modulus of the sand
E_p is the Young's modulus of the pile
δ is the angle of friction between pile and soil

The following reduction factor is found for the Dapperbuurt piles (and most typical timber foundations in Amsterdam): $Rt/Rc \approx 0.9$
The following values are used to obtain this result:
L/D = 12/0.2 = 60
G/E = 12.5 MPa / 15000 MPa = 0.00083
$\tan\delta$ = tan 28 degrees = 0.53
$\nu_p = 0.37$ for timber piles.

De Nicola and Randolph's method does not consider the effects of interface dilation or volume change arising from rotation of the principal stress directions when the loading direction is changed. In other literature, values between 1.0 and 0.8 are given as a factor between tension and compression loading. For example, Toolan et al. (1990) indicate 0.8 as factor, UWA05 as described by Lehane et al (2007) states 0.75 should be used. The IC method as described by Tomlinson and Woodward (2008) gives Rt/Rc = $(\Delta\sigma'_{rd} + 0.8\ \sigma'_{rc}) / (\Delta\sigma'_{rd} + \sigma'_{rc})$ which leads to a factor of 0.8-1.0 as well.

In further analysis, the shaft friction in compression is taken as 1.2 times the value in tension for the 1st sand layer. The measured shaft friction in tension is 49 kN/m for upward friction in sand for new piles with toe diameter 130 mm. The value for compression is taken as 1.2 times 49 kN/m = 59 kN/m, which is about the same as the values resulting from the design methods based on CPT measurements.

6.4.3 Base capacity in foundation layer

With the results from the previous sections, the base capacity of the piles can be derived based on the test results and the assumed factor of 1.2 between tension and compression for shaft friction in the sand layer. The values are given in Table 6.8. For example the value of the new pile with toe at NAP -13.5 m at failure is determined by 270 (ultimate capacity in compression including base and shaft) – 91 kN * 1.0 for shaft friction in clay – 54 kN * 1.2 for shaft friction in sand = 114 kN.

Table 6.8 Base capacity

	Pile with casing		New pile	
	Toe NAP -12.6m	Toe NAP -13.2m	Toe NAP -13.1m	Toe NAP -13.5m
Pile base capacity [kN] at failure	-	120	110	114
Pile base capacity [kN] at 10-15 mm relative displacement	-	80	89	109

The calculated pile base capacity for a circular tapered pile with toe diameter of 130 mm according to Dutch Annex to Eurocode 7 by NEN (2011) is:

$$R_{b;max} = A_b * \alpha_p * q_{b;max} \qquad (6.6)$$

With:

A_b is the cross section of the pile at the toe (base), this is $\pi * 0.13^2 / 4$

α_p is the pile base factor, which is 1.0 according to the NEN (2011)

$q_{b;max}$ is the average cone resistance according to the Dutch method by Van Mierlo and Koppejan (1952) and De Ruiter and Beringen (1979); it is the average of the cone resistance 0.7 – 4 diameters under and up to 8 diameters above the pile toe level.

$q_{c;av}$ for CPT 01 is about (13 + 12)/2 = 12.5 MPa under the pile toe and 6MPa above the pile leading to an average cone resistance of 9 MPa for a pile toe level of NAP -12.7m.
$R_{b;max}$ is the calculated maximum base capacity, which results in $\pi * 0.13^2 / 4 * 1 * 9000 =$ 120 kN.
Tomlinson and Woodward (2008) for a pile in sand give the following alternative method:

$$Rb = Nq * \sigma'_{v0} * A_b \quad (6.7)$$

where σ'_{v0} is the effective overburden pressure at pile base level, Nq is the bearing capacity factor. The factor Nq depends on the ratio of the depth of penetration of the pile to its diameter and on the angle of shearing resistance φ of the soil. For the first sand layer at NAP -12 m the average vertical effective stress will be 6 kN/m^3 * 12 m = 72 kN/ m^2, the average cone resistance over 1.5 m above and below the pile base is q_c = 8 Mpa and the angle of internal friction after pile installation φ' is about 38 degrees in this situation. This leads according to Berezantzev et al. (1961) to Nq is about 120 and Rb = 120 * 72 * 0.13^2 * 3.14 / 4 = 115 kN.

According to the IC method described by the same authors the base capacity is a factor times q_c, the average cone resistance over 1.5 pile diameters above and below the toe. This factor depends on the pile diameter D compared to the CPT diameter D_{cpt} according to:

$$q_b = q_c * [\ 1\text{-}0.5 \log (D/D_{cpt})] \quad (6.8)$$

This leads to q_b = 8.2 * (1-0.5 log (0.13/0.036) = 8.2 * 0.72 = 5.9 MPa. This is about the same result as Fleming et al. (2009) gives in his Figure 4.4 following Bolton (1986), which states q_b is 6-8 MPa for these conditions. This leads to $R_b = q_b * A_b$ = 5.9 * 0.132 * 3.14 / 4 = 78 kN.

The base capacity calculated by various international methods varies between about 78 – 120 kN. The calculated and measured base capacities are within this range for the new piles that are taken into account.

6.4.4 Mobilization of negative skin friction / shaft capacity

The tests performed in tension provide insight in the development of shaft friction along the pile, which can be compared to the situation in which negative skin friction occurs. In both cases, the soil moves down compared to the pile / the pile moves upward compared to the soil.

Figure 6.3 shows the results of the pile load tests, for the combined friction for the first sand layer and the Holocene layer, except for the piles with the casing, where mostly the first sand layer provided friction. The casing pile tests can be used to derive the friction development curve for the first sand layer. Figure 6.4 shows both pile tests on the casing piles normalized with the maximum pile capacity in tension. The shape of the curve is somewhat softer compared to the Dutch code NEN. The Dutch code is further combined with the elastic extension of the pile with the following characteristics:

- E of the timber is 2E7 kN/m, since the pile tests were performed on new piles.
- The average pile diameter is 180 mm
- The maximum tension load in the pile is 60 kN at the top while 0 at the bottom, leading to 30 kN on average.

The best fit for the mobilization of friction in the sand layers is found if the theoretical shaft friction development according to NEN is reduced by a factor of 1.3 in stiffness and the elastic extension is taken into account. This means all relative displacements are increased by this factor 1.3 while the percentage of the maximum capacity remains the same.
In sand, the shaft friction development according to NEN reduced by 1.3 will be used in future analysis. For all piles, the elastic extension has to be taken into account, with for new piles a pile Young's modulus of $2*10^7$ kN/m^2.

For the Holocene layers, the shaft friction development can be obtained if we assume the friction in the sand develops according to the shape in Figure 6.4 and described above as the Dutch code reduced by a factor 1.3. The pile tests in tension have been recalculated for the remaining capacity in the Holocene layers.

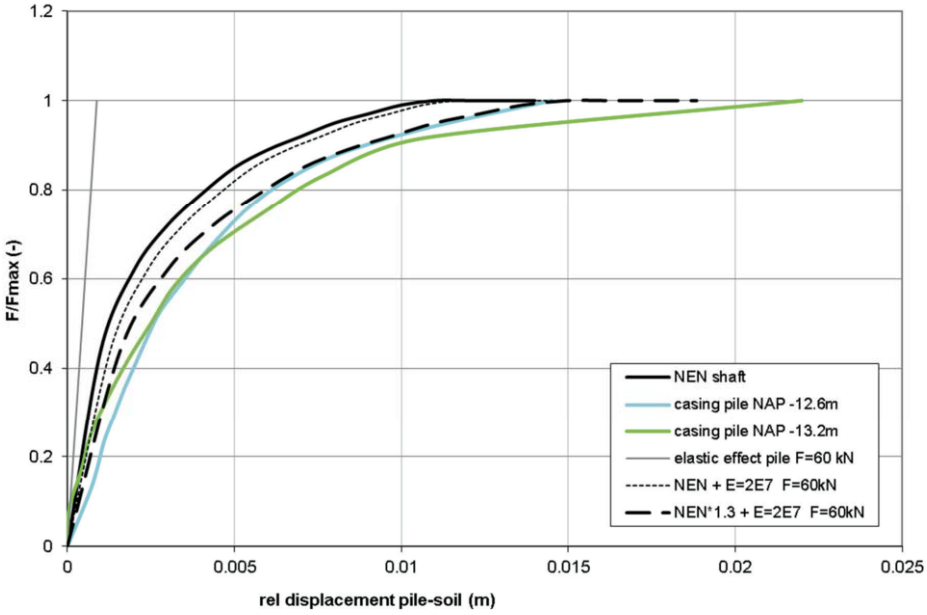


Figure 6.4 Shaft friction in sand; measured in tension test for casing pile and calculated according to Dutch code NEN for displacement piles

For the new piles without casing (pile toes at NAP -13.1 and NAP -13.5 m) the best fit is found if for the Holocene layers the NEN curve is reduced by a factor of 2.5. Figure 6.5 shows the results of the tension test on the new pile at NAP -13.1 m, with the combination of curves for sand (factor 1.3) and clay (factor 2.5). Based on the respective contributions of the

shaft friction in the sand (49 kN, see Table 6.8) and clay (140 – 49 = 91 kN), the average factor is (49* 1.3 + 91 * 2.5) / 140 = 2.1.

Based on the tests with the new piles (with and without casing), the average shaft friction in the Holocene layers was 67 kN from NAP-11 m to NAP -2 m, resulting in 7.4 kN/m, or at larger displacements 80 kN over 9 m, resulting in 8.8 kN/m.

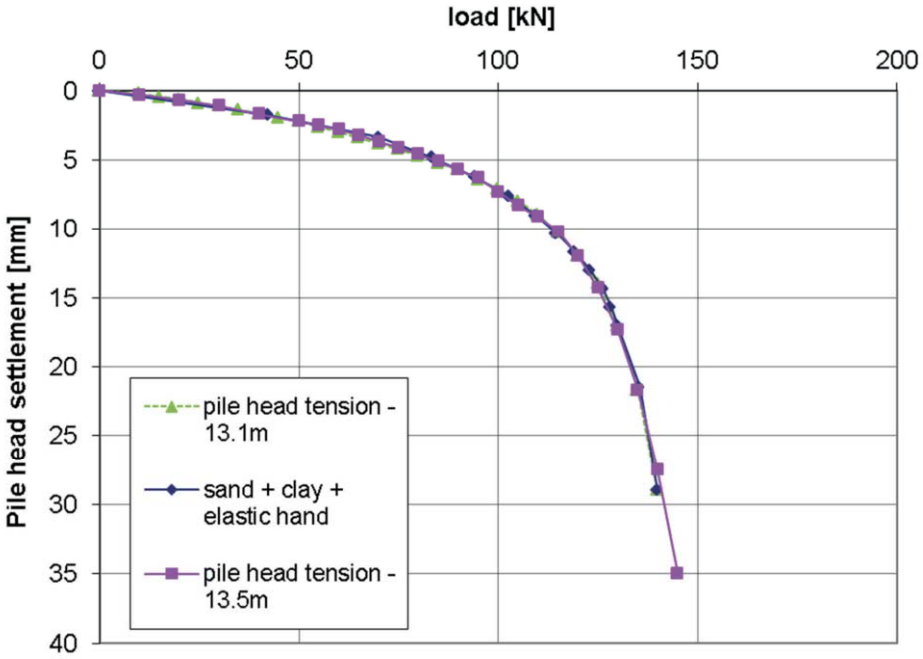


Figure 6.5 Shaft friction in new piles with NAP -13.1 m and NAP -13.5m (tension tests) and fit with NEN curve factored 2.1 times

Alternatively, other curves could be used to match the measured shaft friction. For example, the method proposed by Vardanega et al (2011) describes a curve based on shear strain developed to mobilise 50% of the shear strength. The resulting curve is valid for pile loads upto 50% of the maximum capacity and fits well with the curve according to NEN for realistic pile diameters as present in Amsterdam.

6.4.5 Mobilization of base capacity

The tests on the new piles can also be used to derive the base load displacement curve. In Figure 6.6 the results of the base load displacement curves are shown, determined for the new pile (without casing) at two different depths. The curves are found by subtracting the tension test from the compression test after correcting the displacements for the elastic compression and using the factor 1.2 for the compression versus tension in the sand layer. The weighted factor for compression over tension becomes 1.08 for both piles. For the

elastic compression a Young's modulus of $2*10^7$ kN/m^2 and an average pile diameter of 180 mm is used. Based on Figure 6.6, the assumed pile base curve according to the Dutch standard fits well for the first test (NAP -13.1 m). The second test (on the same pile) shows a much stiffer response, which can be explained by the effect of reloading.

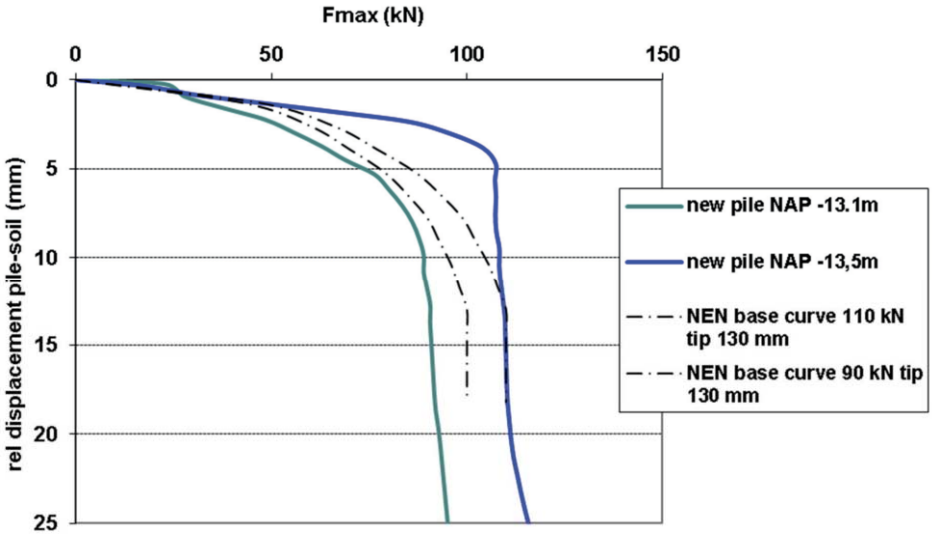


Figure 6.6 Base load displacement curve for new piles

For the new piles, the NEN load displacement curve for the base is used for further calculations. The new piles have also been calculated by the non-linear, uncoupled spring model (cap model) in DPileGroup with the assumptions described in Table 6.9. For details on DPileGroup see Bijnagte and Luger (2010).

Table 6.9 Average values for pile capacity and load-displacement curves used for new piles

	Maximum value	T-Z curve (load – displacement)
Holocene shaft friction tension and compression	8.8 kN/m	NEN curve * 2.5
Sand layer shaft friction tension	49 kN/m	NEN curve * 1.3
Sand layer shaft friction compression	59 kN/m	NEN curve * 1.3
Pile base	90/110 kN	NEN curve

Figure 6.7 shows reasonable agreement of the calculated average values with the specific test data. Due to a large variation in results for both the shaft and base capacity and stiffness, there is some scatter in the data when the overall average values are used.

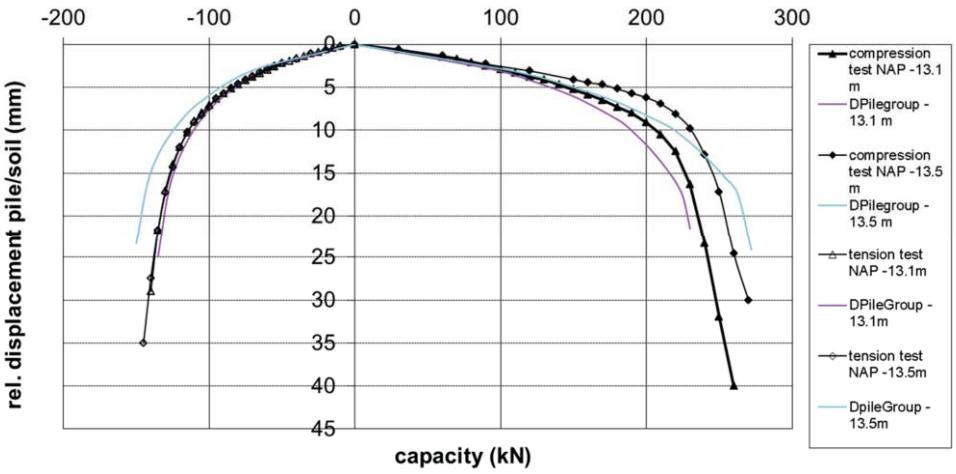


Figure 6.7 DPilegroup results based on average shaft friction and load- displacement values, compared to load displacement curves of new piles in compression and tension

6.4.6 Neutral level for new piles

Based on the average pile capacities, the neutral level for the new pile can be calculated through the following two equations:

$$W + \tau_s * \pi D * L_{neg} = R_{base} + R_{pos;sand} + \tau_s * \pi D * L_{pos} \quad (6.9)$$

$$L_{neg} + L_{pos} + L_{sand} = L_{pile} \quad (6.10)$$

Combining both equations results in:

$$L_{neg} = (R_{base} + R_{pos;sand} + \tau_s * \pi D * (L_{pile}-L_{sand}) - W) / (2* \tau_s * \pi D) \quad (6.11)$$

Where

W is the external load on the pile in kN

$\tau_s * \pi D$ is the shaft friction per metre pile in the Holocene layer in kN/m (assumed to have been fully mobilized)

L_{neg} is the depth of the neutral level in m from the top of the pile (see Figure 6.8)

R_{base} is the pile base capacity in kN (assumed to have been fully mobilized)

$R_{pos;sand}$ is the shaft friction in the sand layer in kN (assumed to have been fully mobilized)

L_{pos} is the depth of the Holocene under the neutral level in m

L_{sand} is the length of the pile in the sand layer in m

L_{pile} is the total length of the pile in m

If for the pile at NAP -13.1 m the following values are taken:

W =100 kN; $\tau_s * \pi D$ = 8.8 kN/m; R_{base} =100 kN; $R_{pos;sand}$ = 49 kN (from test); L_{sand} =0.9m and L_{pile} = 11.3 m; than the neutral level is found at NAP -9.8 m.

If for the pile at NAP -13.5 m the following values are taken:
W =100 kN; $\tau_s * \pi D$ = 8.8 kN/m; R_{base} =125 kN; $R_{pos;sand}$ = 54 kN (from test); L_{sand} =1.3m and L_{pile} = 11.3 m; than the neutral level is found at NAP -11.7 m.
The neutral level is found relatively deep in the Holocene, because the pile capacity (260-270 kN in compression) is larger than found for most older piles (see section 1.4). For larger pile loads of 150 kN, the neutral level shifts to NAP -6.9 m and NAP -8.8 m respectively.

Figure 6.8 as an example shows the neutral level for the new pile at NAP -13.1 m for a pile load of 100 kN, 125 kN and 150 kN. Both shaft (positive and negative) and pile base capacity are assumed as fully developed in this figure for simplicity.

The same pile is calculated with DPileGroup (Bijagte and Luger, 2010), including pile elasticity and the load displacement curves as described in Table 6.9. If a soil displacement of 0.1 m is assumed at the top of the pile and 0 m at the top of the sand layer, the neutral level is found in Figure 6.9 to be similar to the result in Figure 6.8. The transition zone in which positive and negative friction are not fully developed is (for this soil displacement pattern) about 2.8 m above and below the neutral level. Over about 1.1 m above and below the neutral level a distinct reduction in shaft friction is found of at least 20%. In an even smaller zone of 0.5 m each direction the shaft friction is reduced by at least 40%.

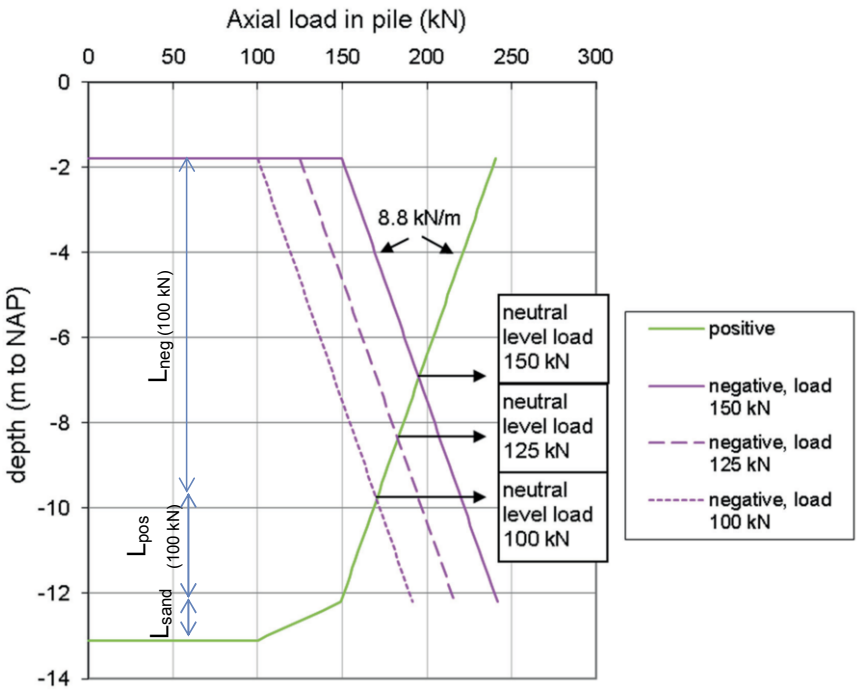


Figure 6.8 Neutral level for the new pile with pile tip at NAP -13.1 m for different pile loads.

Annex D shows the full results of the DPileGroup calculation with the development of the shaft friction over the depth of the pile and the pile displacement. The pile displacement before development of negative skin friction (pile load 150 kN) is 6 mm at the head and 3 mm at the pile toe. In the pile test the head displacement was 5 mm at 150 kN load. After development of the negative skin friction, it is 56 mm (for 100 mm soil displacement) at the head and 52 mm at the toe.

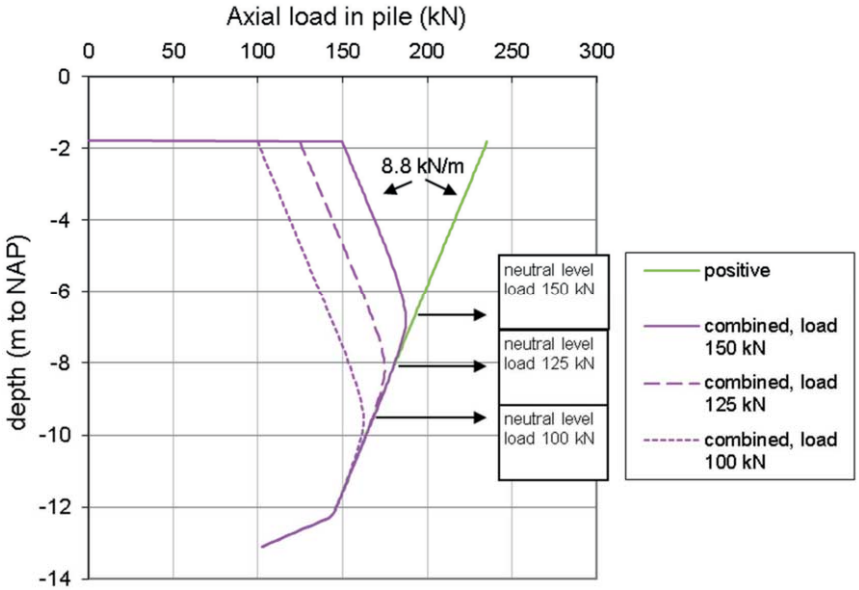


Figure 6.9 Neutral level for the new pile with pile tip at NAP -13.1 m for different pile loads with DPileGroup.

Note: for the DPileGroup calculation the shaft friction in the sand is taken from Table 6.9 instead of from the test (59 kN/m * 0.9 m = 53 kN versus 49 kN). The resulting difference in neutral level is approximately 0.3m.

It is concluded that the neutral level can be determined realistically when the external pile load is known or estimated. Based on the load-displacement curves found in the tests for the new piles, the neutral level will be a rather distinct level between the surface and the top of the first sand layer. The transition zone between positive and negative skin friction is 2 m long for a reduction at least 20% of the maximum value and a linear soil displacement profile with depth.

6.5 Old timber piles

The results of the old piles compared to the new pile show a few remarkable differences (see Figure 6.3):

- low pile base capacity for the broken piles (pile 2, pile 5 and pile 6), piles are excluded from further analysis

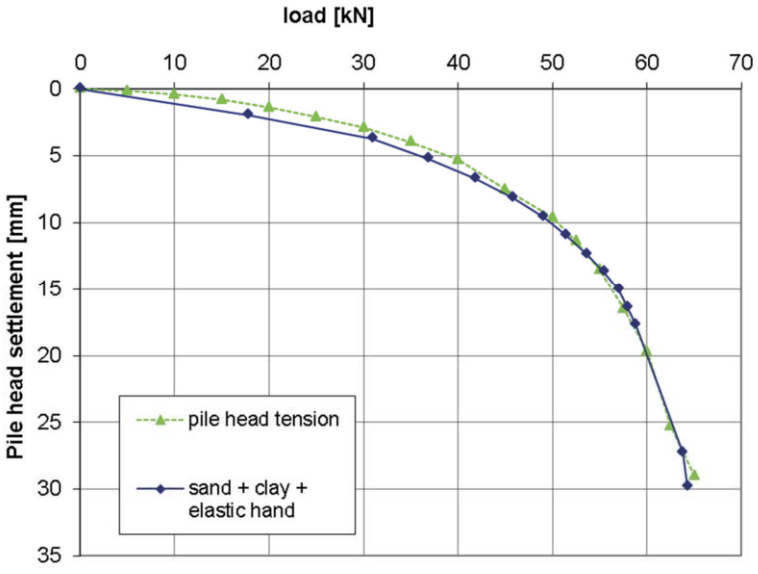
- similar pile base capacity for the piles that were not broken compared to the new piles
- lower stiffness load displacement curves
- lower capacity of shaft friction in both sand and clay compared to new piles
- pile load tests have been performed including unloading-reloading cycles.

6.5.1 Mobilization of negative skin friction / shaft capacity

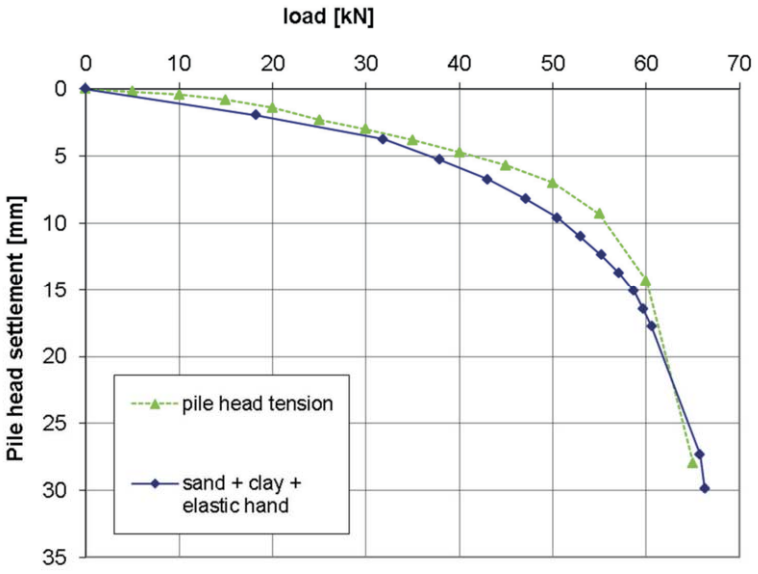
Figure 6.10 shows the results of the pile load tests in tension for the two piles that were not broken (Pile 3 and Pile 4). The old piles are assumed to have the same load-displacement curve, but clearly have lower capacities in both the clay and the sand. The shaft friction in both sand and clay had to be reduced by 40% to obtain a fit with the test data as shown in Figure 6.10. In addition, the shaft friction in the Holocene layers is reduced for the actual diameter of the shaft. The elastic modulus of the pile is assumed to be $6*10^6$ kN/m^2 for the old piles.

This leads to a shaft friction in the Holocene layers of 8.8 * 0.6 = 5.3 kN/m for an average pile diameter of 180 mm. The shaft friction in the sand layers is 49 * 0.6 = 29 kN/m. All values are derived for tension loading.

The shaft friction in the three broken piles (pile 2, pile 5 and pile 6) is assumed to be present in the Holocene layers only. Back calculating the results of the tension tests for these piles shows that 5.1 – 6.5 kN/m shaft friction is developed for the average diameter of 180 mm (for smaller and larger average diameters a correction is included in this number). The test results however do not resemble piles in clay, but show a much stiffer response. Since it is not known how deep the piles were in the sand, the shaft capacity can not be used from these tests.



(a)



(b)

Figure 6.10 Shaft friction in pile 3 (top) and pile 4 (below) from tension tests compared to fit with similar curves as for new piles (elastic Young's modulus of pile $6*10^6$ kN/m^2)

6.5.2 Mobilization of base capacity

The base capacity of the old piles can be derived based on the test results and the assumed factor of 1.2 between tension and compression for shaft friction in the sand layer. In compression the shaft friction in sand is assumed to be 29 * 1.2 = 34 kN/m. The overall

factor of compression over tension is 1.04-1.06, based on the amount of shaft friction in both layers respectively. The values are given in Table 6.10.

Table 6.10 Base capacity old piles

	Pile 2 Toe NAP -11.99m	**Pile 3 Toe NAP -12.72m**	**Pile 4 Toe NAP -12.67m**	**Pile 5 Toe NAP -11.96m**	**Pile 6 Toe NAP -11.22m**
Pile base capacity [kN] at failure	60	115	115	90	75
Pile base capacity [kN]at 10-15 mm relative displacement	56	108	111	60	50

The measured base capacities for the piles that are not broken (pile 3 and 4) are similar to the values found for the new piles.

In Figure 6.11 the results of the base load displacement curves are shown. The curves are found by subtracting the tension test from the compression test after correcting the displacements for the elastic compression. For the elastic compression, a Young's modulus of $6*10^6$ kN/m^2 and a realistic average pile diameter is used per pile. The Young's modulus is taken from lower bound values given for Pine in literature. Based on Figure 6.11, the assumed pile base curve according to the Dutch standard fits well. The results of the pile tests show that the final value of the displacement of the toe (13 mm, 10% of the pile diameter) gives a realistic value, although it might be even a bit lower due to the reloading effect.

For the old piles, the NEN load displacement curve for the base is used for further calculations. The old piles have been calculated by DPileGroup with the assumptions presented in Table 6.11.

Table 6.11 Average values for pile capacity and load-displacement curves used for old piles

	Maximum value	**T-Z curve (load – displacement)**
Holocene shaft friction	5.3 kN/m	NEN curve * 2.5
Sand layer shaft friction	29 kN/m	NEN curve * 1.3
Sand layer shaft friction compression	34 kN/m	NEN curve * 1.3
Pile base	115 kN	NEN curve

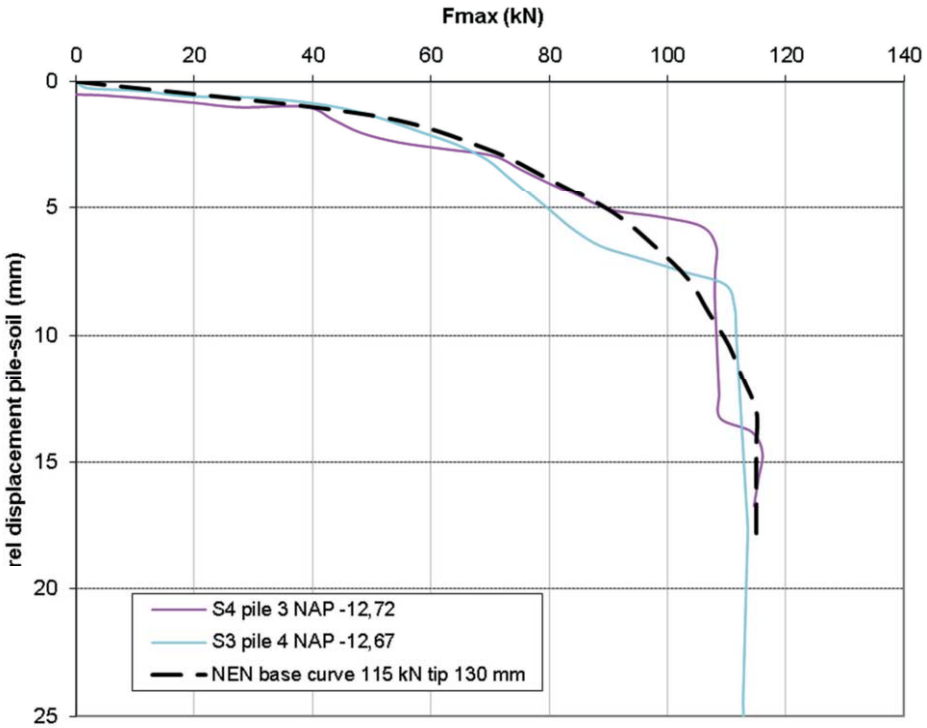


Figure 6.11 Base load displacement curves for Pile 3 and Pile 4 (old piles, not broken)

A constant pile diameter of 165/170 mm is assumed for the elastic compression. The Young's modulus is $6*10^6$ kN/m^2 for pile 3 and $8*10^6$ kN/m^2 for pile 4 (for a better fit). Figure 6.12 shows quite good agreement of the calculated average values with the specific test data.

The old piles have a lower Young's modulus of about 0.6-0.8 $*10^7$ kN/m^2 compared to $2*10^7$ kN/m^2 for the new piles. The same load-displacements curves can be used as for the new piles, but with 40% reduction for shaft friction both in sand and in clay.

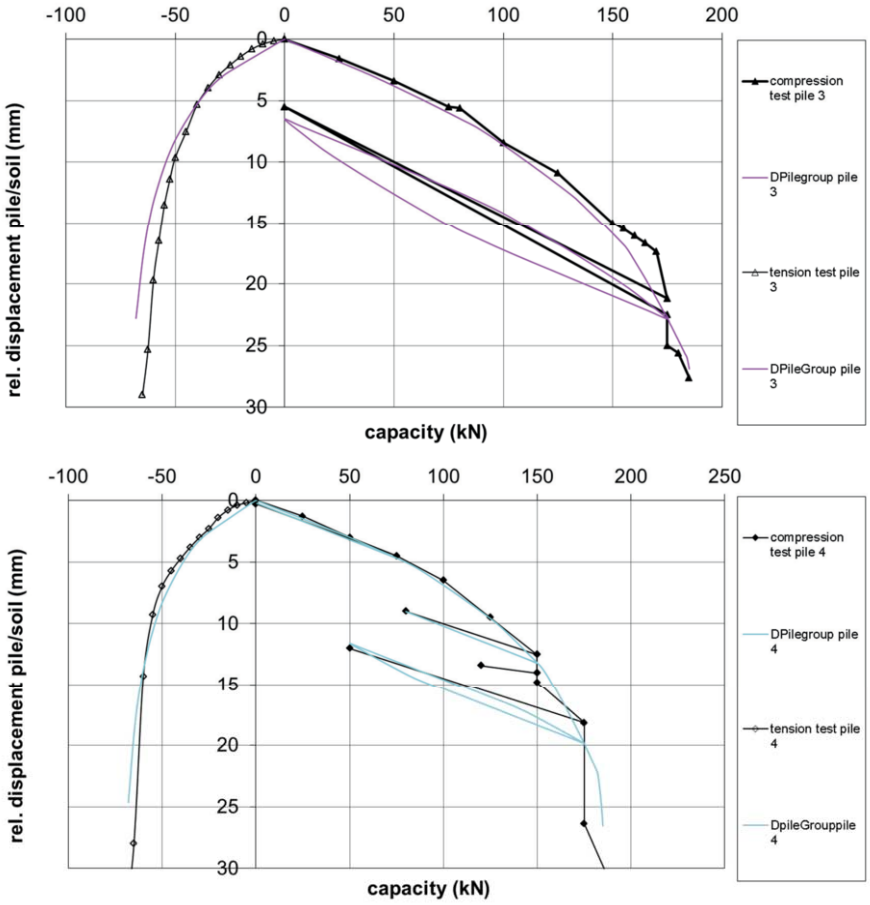


Figure 6.12 DPilegroup results based on average shaft friction and load- displacement values, compared to tests in compression and tension for old pile 3 (top) and pile 4 (below).

6.5.3 Neutral level for old piles

Based on the average pile capacities, the neutral level for the old piles can also be calculated through equation (3). If for pile 3 and pile 4 at NAP -12.7 m the following values are taken: W =100 kN; τ_s * O = 5.3 kN/m; R_{base} =115 kN; $R_{pos;sand}$ = 17.4 kN; L_{sand} =0.5m and L_{pile} = 10.4 m; than the neutral level is found at NAP -10.0 m. For a larger pile load of 120 kN, the neutral level shifts to NAP -8.2 m. All values between NAP -7 and NAP -12 m can be considered realistic.

Figure 6.13 shows as an example the neutral level for old piles for a pile load of 100 kN, 120 kN and 140 kN. Both shaft (positive and negative) and pile base capacity are assumed as fully developed in this figure for simplicity.

The same piles are calculated with DPileGroup, including pile elasticity and the load displacement curves as described in Table 6.11. If a soil displacement of 0.1 m is assumed at the top of the pile and 0 m at the top of the sand layer, the neutral level is found in Figure 6.14 to be similar to the result in Figure 6.13. The transition zone in which positive and negative friction are not fully developed is (for this soil displacement pattern) about 3.0 m above and below the neutral level. Over about 1.1 m above and below the neutral level a distinct reduction in shaft friction is found of at least 20%. In an even smaller zone of 0.6 m each direction the shaft friction is reduced by at least 40%.

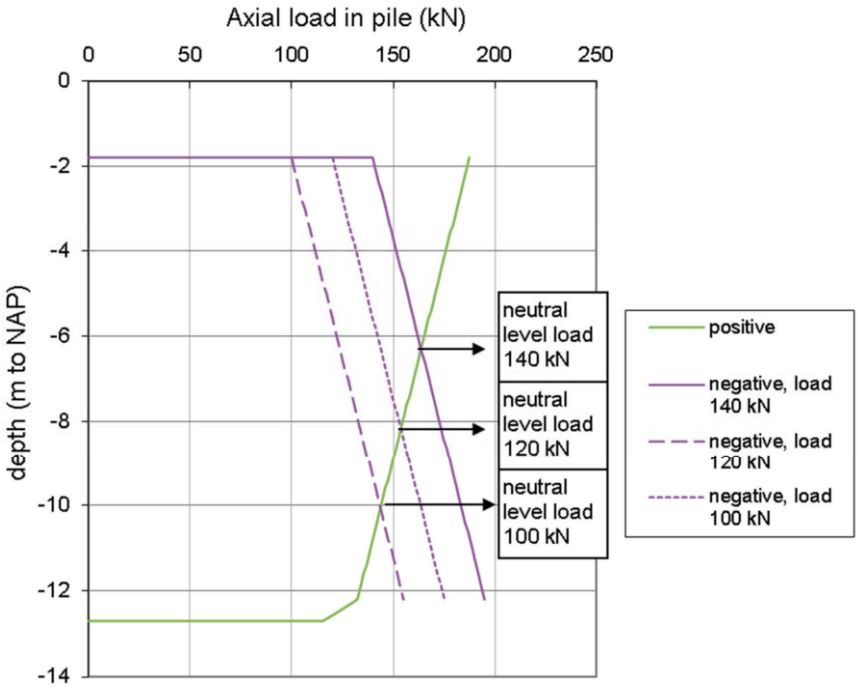


Figure 6.13 Neutral level for the old piles for different pile loads.

Annex D shows the results of the DPileGroup calculation with the development of the shaft friction over the depth of the pile and the pile displacement. The pile displacement before development of negative skin friction (pile load 120 kN) is 9 mm at the head and 3 mm at the pile toe. In the pile tests the head displacement was 9-10 mm at 120 kN load. After development of the negative skin friction the pile displacement is 45 mm (for 100 mm soil displacement) at the head level and 37 mm at the toe level.

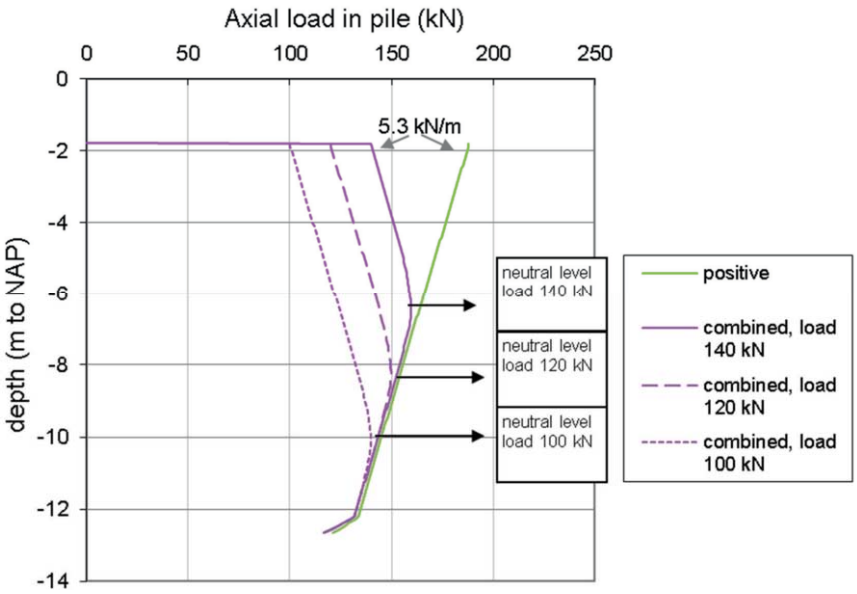


Figure 6.14 Neutral level for the old piles for different pile loads with DPileGroup.

6.6 Conclusions based on test results Dapperbuurt

Since most piles under the building along the North South Line are old timber piles, the results of the old piles are most relevant for the future analyses. Compared to the new piles, the old piles show lower shaft friction (40% reduction compared to new piles), but similar base capacity and load-displacement curves. Both old and new piles have shown that in clay the maximum shaft friction develops at about 25 mm and in sand at about 15 mm. The maximum base capacity for piles with 130 mm diameter is reached at about 10% of the diameter, as can be found in common design methods.

The Young's modulus is $2*10^7$ kN/m^2 for the new and 6 to 8 $*10^6$ kN/m^2 for the old piles.

The shaft resistance in the sand is 29 kN/m for the old piles and 49 kN/m for the new piles in tension and 1.2 times this value in compression. This relates to the design values for the capacity by using:

$R_{s;max} = O\ pile * \alpha_s * q_{s;z}$ (6.12)

With:

O pile = $\pi * 0.13$

$q_{c;z}$ for CPT 01 is about 12.0 MPa for a pile toe level of NAP -13.2m.

$q_{c;z}$ for CPT 01 is about 10.6 MPa for a pile toe level of NAP -12.7m.

Rs;sand;old = $\pi * 0.13 * 0.008 * 10600 = 35$ kN/m

Rs;sand;new = $\pi * 0.13 * 0.012 * 12000 = 59$ kN/m.

The shaft friction factor for compression in the sand is thus 0.008 for old piles and 0.012 for new piles. The shaft friction in the Holocene is 5.3 kN/m for 180 mm pile diameter, which can be compared to $K_0 * \tan\delta * \sigma'_{0v}$ with $K_0 * \tan\delta = 0.17$ instead of 0.25 (upper limit). This means $\delta = 0.65 * \varphi$ if φ is 25 degrees in the Holocene clay. For new piles, the negative skin friction is close to $0.25 * \sigma'_{0v}$.

The old piles find in failure 60% of their capacity at the toe, 10% as friction in the sand layer and 30% as friction in the Holocene layers.

6.7 Combination of two piles (Amsterdam foundation)

Some extra tests (not reported here) have been performed in the Dapperbuurt Amsterdam during the previous test sequence, with a set of 2 piles close to each other, as is the usual foundation lay out for the Amsterdam foundations. The results of the combined pile tests did not show completely different results from the single tests. The combined maximum load per pile is at least the same as the individual load, as can be seen in Table 6.12.

Table 6.12 Results of pile load tests with single or combined test

Pile	Single max applied load	In combination Max. applied load per pile
2e van Swinden pile 5	150 kN	183 kN / 170 kN
2e van Swinden pile 6	140 kN	148 kN / 150 kN
Wijttenbach pile 6	100 kN	97 kN
Wijttenbach pile 7	90 kN	100 kN

6.8 Timber characteristics

The allowable compression of timber piles is 10-12.5 N/mm^2 (old piles) or 15-19 N/mm^2 for new piles. If the average pile load is 80 kN, the average negative skin friction is 65 kN, the total axial load is 145 kN. If the diameter at the toe is 120 mm, the stress in the wood is smaller than 12.5 N/mm^2. Larger external loads may easily cause overstressing the piles in compression.

Boutelje and Bravery (1968) showed that timber piles over time deteriorate due to decay by bacteria and fungi. The compressive strength, the bending capacity and the Young's modulus reduced over time. The Young's modulus (or modulus of Elasticity) for Scots Pine reduced from $1.2*10^7$ kN/m^2 to $0.3 – 0.6*10^7$ kN/m^2. Also creep of the wood could play a role, which makes it reasonable that the Young's modulus decreased as was shown in the results of the old piles in section 6.5.

6.9 Results Dapperbuurt compared to other pile load tests

Other pile load tests on timber piles in Amsterdam have been reported by TNO (1995) and Van der Stoel (2001).

TNO assumed for a typical timber pile in Amsterdam 30 kN shaft capacity and for the base 150 kN, as shown in a combined load displacement curve in Figure 6.15. TNO (1995) also stated that the timber piles give 80-90% of the capacity through the pile base and only 10-20% from the shaft. This can only be true if the shaft capacity of the Holocene layers is not taken into account. The old Dapperbuurt piles find in failure 60% of their capacity at the base, 10% as friction in the sand layer and 30% as friction in the Holocene layers.

Van der Stoel tested piles (before performing grouting at the base) which are shown in Figure 6.16. The piles in these tests have not been taken completely to failure, which results in rather linear load-displacement curves. Van der Stoel's piles had similar dimensions as the Dapperbuurt piles (head diameter 230 mm, toe diameter 130 mm, toe depth NAP -13.5m). Van der Stoel assumed 75-85% of the ultimate bearing capacity came from the toe and 15-25% from the shaft.

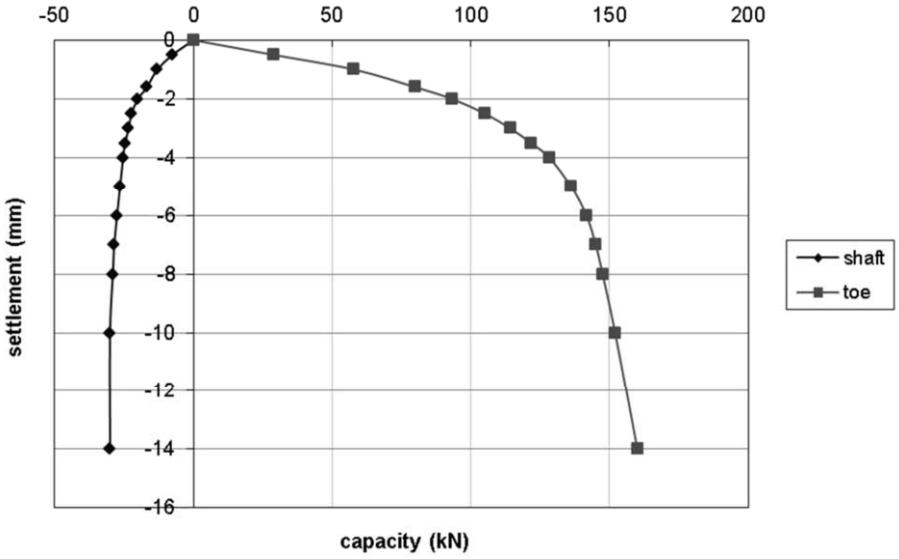


Figure 6.15 Pile load results according to TNO (1995)

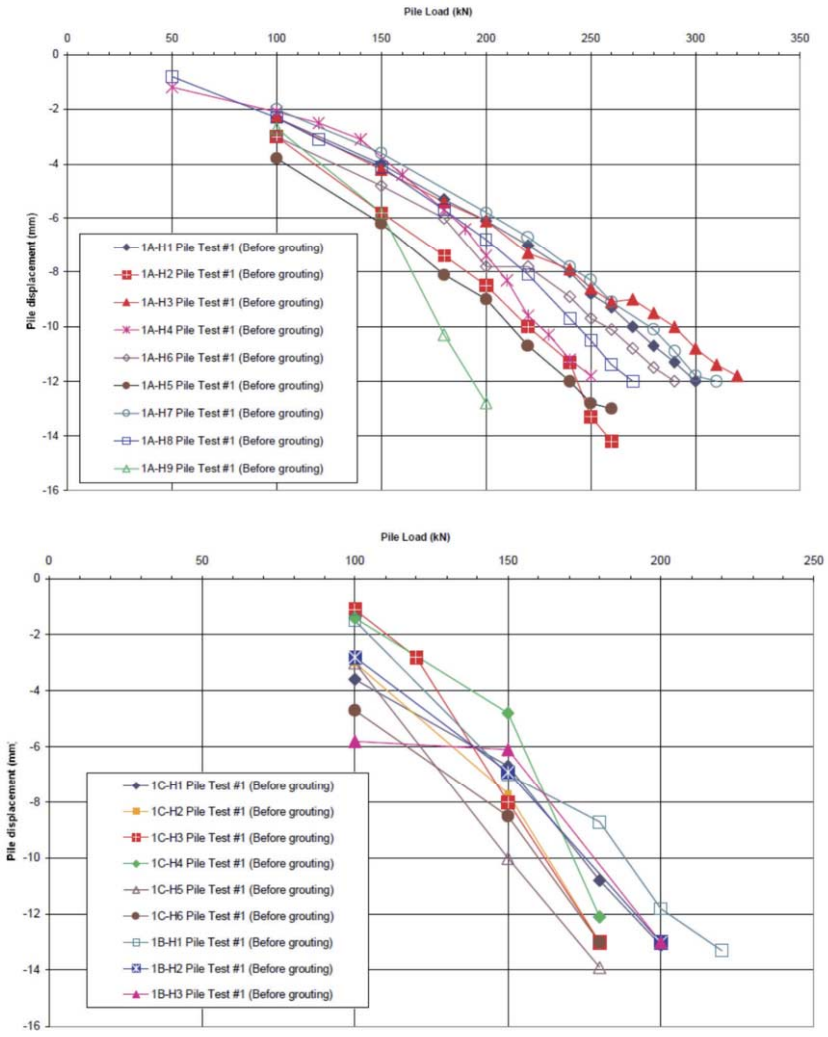


Figure 6.16 Pile load tests from Van der Stoel (2001)

Figure 6.17 shows all three series of tests in one figure. The (new!) piles by Van der Stoel show similar behaviour as the new piles in the Dapperbuurt and are even stronger, because they do not show failure at the maximum displacements. The TNO result somewhat deviates from the test data.

For the load-displacement behaviour, the results from the Dapperbuurt fall within the range for medium soil (for the sand layer) and soft soil (for the Holocene clay) as given by Van Weele and Riethoff (1982).

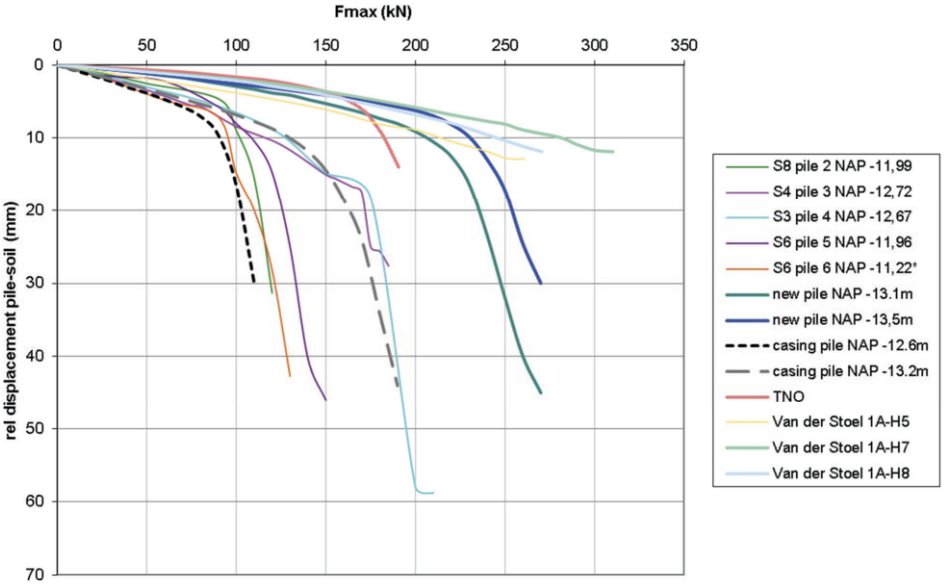


Figure 6.17 Pile test results in compression from TNO, Van der Stoel and Dapperbuurt combined

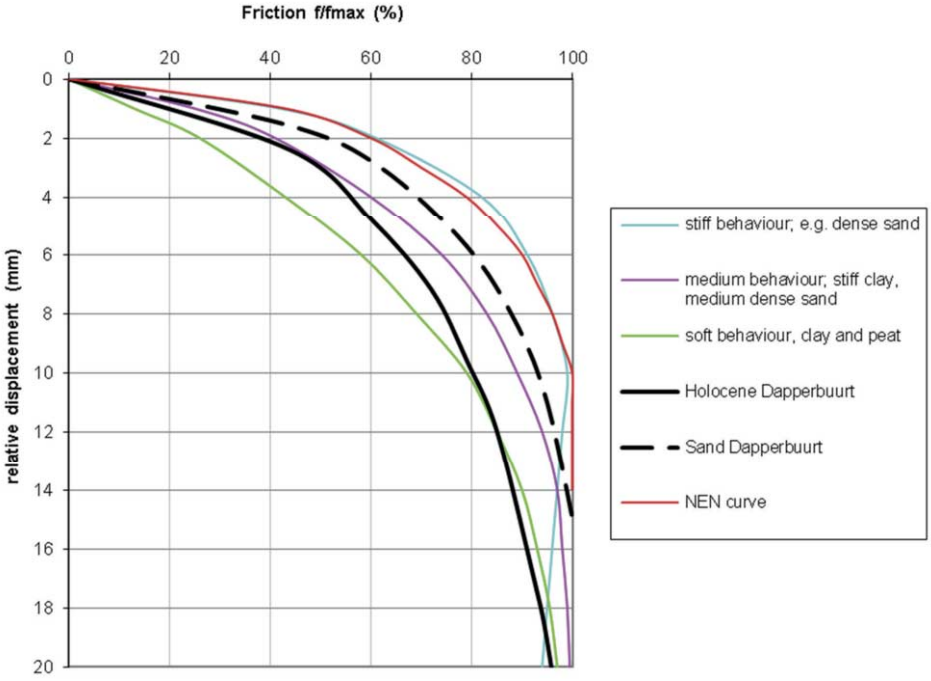


Figure 6.18 Shaft friction development based on Dapperbuurt and Van Weele and Riethoff (1982)

The results of the Dapperbuurt piles have been used to explore the typical conditions of Amsterdam pile foundations in section 6.10.

6.10 Initial condition piles in Amsterdam

The situation of the piles in Amsterdam is evaluated for their initial condition (prior to the excavation or tunnelling). The soil around the piles is known to settle continuously under the weight of an overburden layer of sand placed prior to the construction of the houses (see Chapter 4) and for the piles at the edge of the structures also due to subsequent street level reconstructions. This means negative skin friction is developed along the pile prior to the excavation.
The current factor of safety of the pile foundation can be determined according to the Eurocode 7 procedure for the Ultimate Limit State. In this case, the negative skin friction should not be a part of the load on the pile, since at failure the shaft friction can only be positive. The safety margin for the pile according to EC7 would thus be: $(R_b + R_{s;pos}) / (F_c)$, which in EC7 should be based on design values. Rb;d and Rs;pos are determined from Rb;cal, with factors γ;b and ξ_3 being 1.2 and 1.39 for the Dutch Annex, NEN (2011), for a single CPT. The design load is determined from the dead load G and the live load Q. For Q = 0, the design load Fd equals 1.35 times the calculated load Fc. In Amsterdam, the old pile foundations commonly do not comply with these factors. The pile bearing capacity is determined based on the Dutch annex to Eurocode 7 by NEN (2011). Input for the calculation are the following characteristics:

- CPT 4414w for Vijzelgracht Station, as shown in Figure 6.19.
- Tapered timber pile: diameter base is 130 mm, average shaft diameter 170 mm
- Pile tip level NAP -13.5m
- Surface level NAP +0 m
- Phreatic level NAP -1 m
- Soil profile and characteristics in Table 6.13 and Table 6.14.

Table 6.13 Soil layers

Number	Top	$\gamma_{;dry}$	$\gamma_{;sat}$	φ'	Soil type
	[R.L.]	[kN/m^3]	[kN/m^3]	[deg]	
1	0.000	15.00	18.40	30.00	Sand
2	-5.000	11.00	16.00	25.00	Clay
3	-12.500	4.00	11.70	21.00	Peat
4	-13.000	16.80	19.80	33.00	Sand
5	-14.250	14.40	18.50	28.00	Loam
6	-16.500	15.90	19.80	33.00	Sand
7	-25.500	13.00	17.90	29.00	Clay

Table 6.14 Soil layers and input values for two layer system

Soil type	**Top**	**$\gamma_{;dry}$**	**$\gamma_{;sat}$**	**φ'**	**c_u**	**K_0**	**α**
	[R.L.]	[kN/m^3]	[kN/m^3]	[deg]	kN/m^2]	[-]	[-]
1Clay holocene	0.0	11.00	16.00	25.00	30		0.4
2 Sand. 1st	-13.0	16.80	19.80	33.00		0.5	0.01

The top of the bearing layer (Pleistocene Sand, first sand layer) is found at NAP -13 m, just 0.5 m above the pile tip. All of the soil above this level is of Holocene nature and is not realistically providing any pile bearing capacity. This means the top of the positive friction zone for design purposes is taken at NAP -13.0m. The top of the positive friction zone for the Ultimate Limit State however is NAP + 0 m.

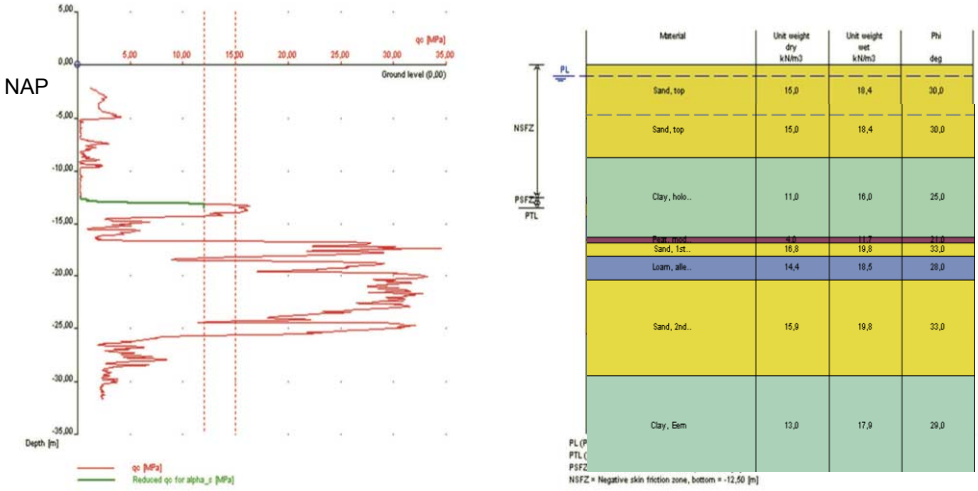


Figure 6.19 CPT and soil profile for Vijzelgracht station

The calculation of the negative skin friction is performed according to the Slip method (Eurocode 7) for single piles (see Chapter 2). The total negative skin friction between NAP+0m and NAP -12.5m is:

$F_{s;nk}$ =0.53 * [(5 * 0.25 * (0 + 49)/2) + (7.5 * 0.25 * (49 + 94)/2)] = 88 kN

Top sand layer: $K_0 \times \tan \delta_j$ = [1- sin(30)] * tan (0.75*30) = 0.22 < 0.25, thickness 5 m

Holocene layer: $K_0 \times \tan \delta_j$ = [1- sin(25)] * tan (0.75*25) = 0.20 < 0.25, thickness 7.5 m

σ'_v at 0m is 0 kN/m^2 , σ'_v at NAP -5m is 49 kN/m^2 , σ'_v at NAP -12.5m is 94 kN/m^2

O_s = 0.53 m average

The peat layer between NAP -12.5 m and NAP -13m is not expected to contribute to any positive or negative skin friction. Positive skin friction is taken from NAP -13.0 m to NAP -13.5 m and calculated based on the CPT method:

$R_{s;pos}$ = thickness layer * O_s * α_s *$q_{c;av}$

With

α_s = 0.01

$q_{c;av}$ = 13500 kN/m^2

This leads to $R_{s;pos}$ = 0.5 m * 0.53 m * 0.01 * 13500 = 0.5 m * 72 kN/m = 36 kN
The base capacity is calculated with the same method:
$R_{b;cal} = A * \alpha_b * q_{c;av}$ which leads to $R_{b;cal} = \pi/4 * 0.13^2$ m * 1.0 * 8000 = 106 kN
with $q_{c;av}$ = 8000 kN/m^2. The pile bearing capacity is $R_{tot;cal}$ = 36 + 106 = 142 kN.

The calculations above are performed with average values and without any partial factors. If the partial factors are included in the calculation according to NEN (2011) this pile would not be suitable for any external load. The ULS condition is not the problem, since Rd = Rcal / (ξ * y) = 142 kN / (1.39 * 1.2) = 85 kN. This pile would be suitable for an external design load of 85/1.35 kN = 63 kN (in case of dead weight only). However, in this case the pile would not fulfil the required deformation limits, because of the additional settlement caused by the negative skin friction. Even for smaller loads, the deformation requirements of GEO and SLS states can not be met if the design depth of the positive friction is chosen at NAP -13 m.

Accounting for the positive friction in the Holocene layers is not acceptable for these conditions in a design situation. If this would however be the case, the pile capacity would increase by 5.3 kN/m (see Dapperbuurt for Holocene layer) * 13 metre is 69kN to 142 kN + 69kN = 211 kN. A realistic pile load of 90 kN (characteristic) is to be expected for the piles in Amsterdam, which for characteristic values can be taken by the piles, but this does not comply to the Eurocode standard. This means the piles can only allow the actual load if over a large part of the pile positive friction is present.

If the partial factors are ignored, characteristic results are shown in Figure 6.20. If negative skin friction occurs due to the soil settling around the pile to a level of NAP -13 m, the maximum load on the pile is limited to Wmax = 73 kN, see Figure 6.20. The negative skin friction between NAP and NAP -13 m is 69 kN if a soil displacement larger than twice the relative displacement necessary to develop the shaft friction in the soil takes place, which in this case is 2 * 26 mm = 52 mm for the Holocene layers.

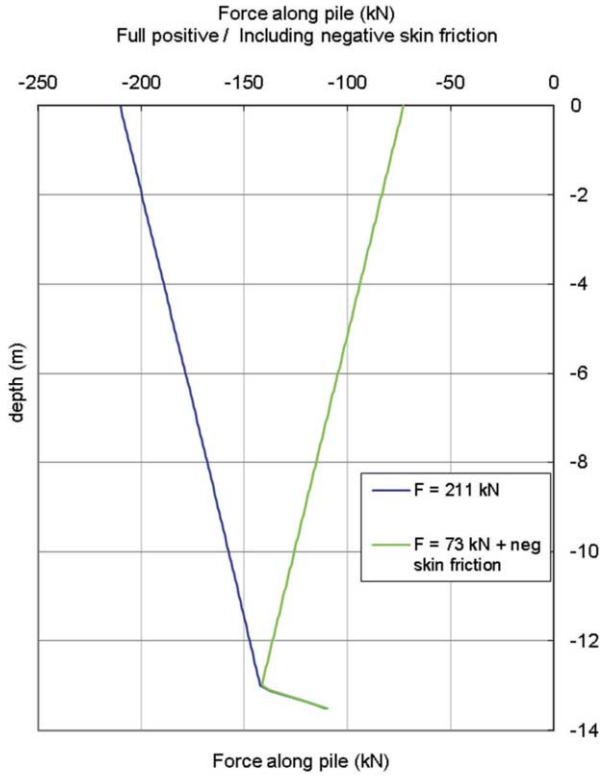


Figure 6.20 Actual timber pile with (blue) all layers positive friction and (green) negative skin friction to NAP -13m, base capacity 106 kN

CHAPTER 7 SOIL-PILE INTERACTION MODEL

7.1 Piles in influence zone of excavation

The response of piled buildings near deep excavations is governed by the effect of the deep excavation on the soil, the interaction between the soil and the pile and the interaction between the pile and the building.

The buildings in the influence zone of the excavation may experience several phenomena:
1. Reduction of pile capacity due to lower stress levels (S_1)
2. Settlement of the pile tip due to soil displacement below the base of the pile (S_2)
3. Development of negative (or positive) skin friction due to relative movements of the soil and the pile shaft (S_3)
4. Redistribution of pile load over the piles under the building slab, the building wall or a foundation cap or beam (S_4)
5. Horizontal deformations of the piles (causing bending of the pile).

The settlement of the pile head is determined by the settlement resulting from the first four effects described above:

$$s = s_1 + s_2 + s_3 + s_4 \qquad (7.1)$$

Since timber piles are rather flexible in horizontal loading, they tend to follow the soil deformations. This effect is not part of the interaction model.
S_1 for end bearing piles is expected to be significant if the pile tips are very close to the excavation. Stress relief around the pile tip can lead to additional mobilisation of positive shaft friction. If this situation occurs, a new load-displacement curve will be established due to relaxation at the tip. The amount of relaxation can be determined based on the method of Figure 7.1. The reduced bearing capacity of the tip can be related to the reduction of the cone resistance with the stress level determined from FE-analysis. For the deep excavations in Amsterdam, the reduction in stress level has not been measured. It could thus not be further evaluated separately.

S_2 may be calculated without interaction with the piles, for example with a FE-analysis or by using the Aye et al. (2006) method for deeper soil displacements due to excavations. This effect can directly be related to the displacement of the soil at the pile tip level from the extensometer measurements, see Chapter 8.

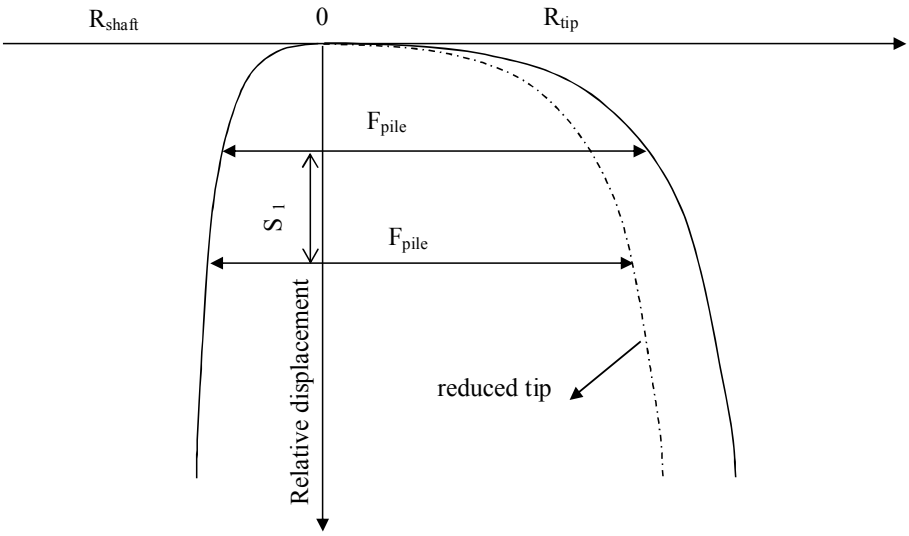


Figure 7.1 Load –displacement curve for a pile with constant load Fpile, and subsequent settlement S1.

S_3 is a true interaction component, which is different for friction piles and end-bearing piles. First, the situation in the case of pure friction piles is considered (no base resistance). If the soil has never moved along the pile (no natural settlement or even reconsolidation has taken place), the shaft friction along the pile is positive at every depth along the pile. If the soil displaces as a result of the excavation or tunnelling process, a new equilibrium has to be found, but the initial load on the pile is still present. This new equilibrium implies that any additional negative shaft friction must be balanced by additional positive shaft friction. In this chapter it is shown that piles with a large factor of safety (working load significantly smaller than load at which the pile fails) settle less due to the excavation or tunnelling than piles with a small factor of safety.

If the soil displaces an equal amount over the whole depth of the pile, the pile settles with this amount of soil settlement. Any other shape of soil settlement (either larger at the top as for excavations or larger near the pile toe as for tunnelling) will cause additional negative as well as positive shaft friction, since the pile will settle a certain amount between the minimum and maximum soil displacement found along the pile. If the settlement profile is irregular (low-high-low or high-low-high settlements with depth), the pile may experience two zones of either positive or negative shaft friction, which in total still have to balance.

For end bearing piles something similar happens, but now the additional negative shaft friction is balanced with additional positive friction plus additional base resistance. Depending on the relative displacement necessary to reach maximum shaft friction and maximum base resistance, the relative maximum percentages for each might be different. For example, the pile base capacity may be reached at much larger displacement than the shaft friction.

Figure 7.2 shows the axial load in the pile in case a soil displacement takes place and the maximum shaft friction is reached both for positive and negative friction. The corresponding shaft friction profile along the pile is shown in the same figure on the right. The pile is loaded by external load W and negative friction caused by a soil displacement that is largest at the surface and decreases towards the pile tip (excavation profile). The positive friction and base load balance the total downward forces.

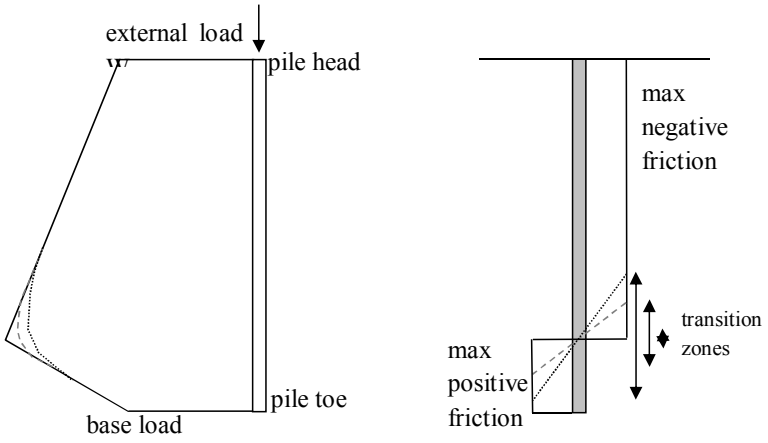


Figure 7.2 Theoretical axial load (left) and shaft friction (right) along pile for different lengths of the transition zone

The shaft friction along the pile is partially mobilized in the transition zone between maximum positive and maximum negative shaft friction. The relative displacement between soil and pile at failure in the soil layers is an important characteristic which determines the length of the transition zone between positive and negative shaft friction. If the relative displacement between soil and pile to reach failure is small compared to the soil settlement gradient, the shaft friction changes from positive to negative in a short section of the pile. For larger values, the transition zone significantly increases in length. If the transition zone length is larger than the length of the pile, the maximum shaft friction will not be reached.

The S_3 effect is described in more detail in section 7.2 which assumes no load redistribution amongst the piles. If the building does redistribute loads, S_4 needs to be determined together with S_3. This could occur if the piles closest to the excavation settle more than the piles further away. The building's stiffness will prevent it from following the different pile movements and the pile load will redistribute accordingly. If this happens, the external load on the pile changes, leading to a new equilibrium. This effect should be determined by a coupled analysis for a pile group, such as with a boundary element method as described by Xu and Poulos (2001) or with the DPileGroup model with a cap over the piles as described in Bijnagte and Luger (2010), see Figure 7.3. The Cap module from DPileGroup is used, which includes multilayered soils with non-linear springs. Cap interaction can be taken into account, but interactions between piles through the soil are not taken into account.

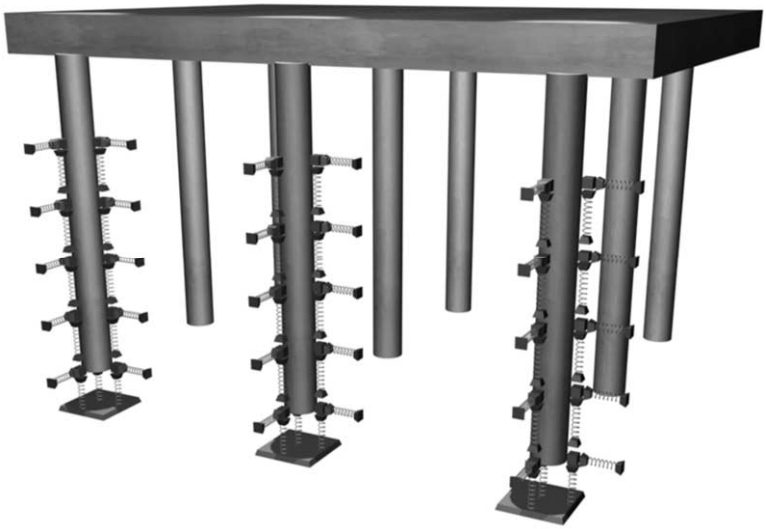


Figure 7.3 Cap interaction model DPileGroup, modified from Bijnagte and Luger (2010)

7.2 Axial interaction for single pile

7.2.1 Introduction

In this section, the interaction between the soil displacement and the pile displacement (S_3 based on axial interaction for single piles) is explored for both friction piles and end-bearing piles. The effect of the initial loading condition of the piles is studied by varying the initial pile load from 0% to 100% of the maximum capacity. The displacement of the pile is the main parameter to be determined as a consequence of the soil displacement resulting from the construction of the excavation or tunnel. The pile displacement can be described relative to the greenfield settlement of the soil by finding the depth z at which the pile displacement equals the soil settlement. The greenfield settlement is defined here as the settlement at the location of the pile, as if no pile or building were present. All soil displacements referred to in this chapter are greenfield values.

Based on the following axisymmetric conditions, the displacement of the pile (p) related to the displacement of the soil (S_z) can be determined. The vertical axis is called z (positive down along the pile). The pile is positioned from z=0 to z=Lp, with Lp is the length of the pile, see Figure 7.4. The working load W on the pile is constant (no redistribution between piles) and for friction piles balanced by the resulting forces of the positive and negative shaft friction along the pile according to equation (7.2)

$$W = \int_0^{L_p} \tau \cdot \pi \cdot D dz \qquad (7.2)$$

In which τ is the shaft friction in [kN/m^2] along the pile with diameter D in [m]. This basic equilibrium needs to be fulfilled at any time.

The shaft friction τ_z is a function g_s of the following variables:

$$\tau_z = g_s((S_z - p), D_z, \tau_{max}) \tag{7.3}$$

with:

τ_z is the shaft friction between pile and soil in [kN/m^2]

τ_{max} is the maximum shaft friction at the depth considered in [kN/m^2],

S_z is the soil displacement with depth z, S_z is a function of depth z in [m]

S_z –p the relative displacement between soil and pile in [m];

D_z is the relative displacement at which τ_{max} is reached in a bilinear approach in [m]

Working towards a dimensionless representation all variables are transformed by relating them to a characteristic dimension (for example the length of the pile), denoted by ' :

$$z' = \frac{z}{Lp} \text{ and } \tau' = \frac{\tau}{\overline{\tau}_{max}} \text{ and } \tau'_{max} = \frac{\tau_{max}}{\overline{\tau}_{max}} \text{ with}$$

$$\overline{\tau}_{max} = \frac{\int_0^{L_p} \tau_{max} dz}{L_p} \text{ , which leads to } W_{max} = \int_0^{L_p} \tau_{max} \cdot \pi \cdot D dz = \pi D L_p \overline{\tau}_{max}$$

$$S'_z = \frac{S_z}{D_z}, \; p' = \frac{p}{D_z} \text{ and } D_z' = \frac{D_z}{D_z} = 1$$

Transforming Equation (7.2) in dimensionless form to:

$$\frac{W}{W_{max}} = \int_0^1 \tau' dz' \tag{7.4}$$

The general shaft friction formula (see Figure 7.5):

$$\tau = \tanh\left(\frac{S_z - p}{D_z}\right) \cdot \tau_{max} \tag{7.5}$$

becomes in dimensionless form:

$$\tau' = \tanh(S'_z - p') \cdot \tau'_{max} \tag{7.6}$$

The initial stiffness k_s is the gradient of τ at $(S_z\text{-}p) = 0$:

$$k_s = \frac{\tau_{max}}{D_z} \tag{7.7}$$

During the initial loading of the pile (referred to as step 1) the shaft friction along the length of the pile can be found by solving equation (7.4) in combination with (7.6). The pile displacement p_1 will be found as a result, with the corresponding τ_1, when the initial soil displacement S_z=0.

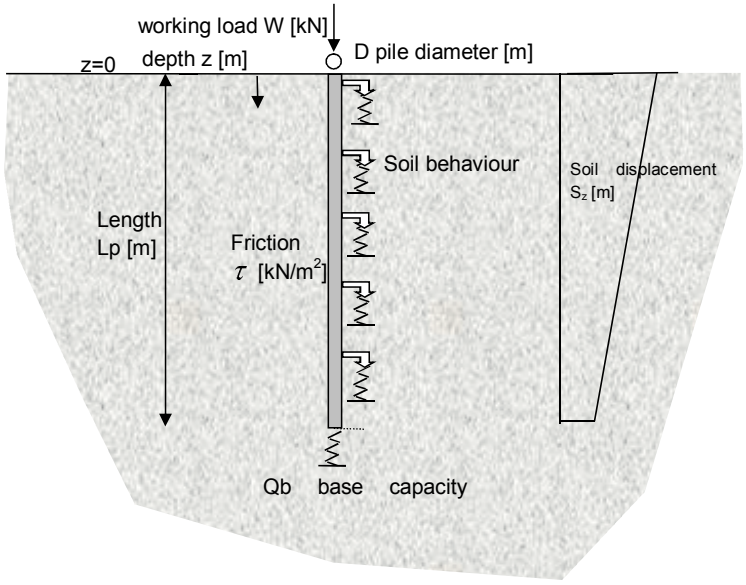


Figure 7.4 Model schematization and parameters

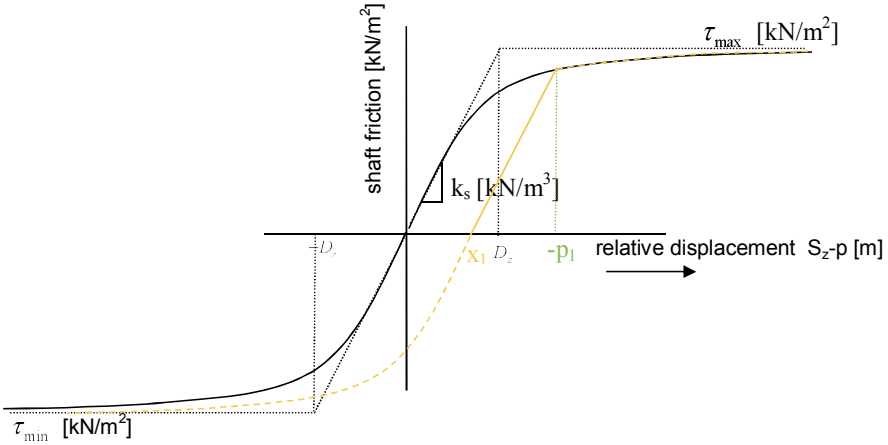


Figure 7.5 Shaft friction versus relative displacement between pile and soil

The next step is the external soil displacement initiated by the excavation (referred to as step 2). For step 2: the formula of the shaft friction is given in three parts, represented by the yellow line in Figure 7.5. The pile displacement after this step (p_2) can be found from:

$$\left.\begin{array}{ll} \text{if } (S\text{-}p_2) > -p_1 & \tau = \tanh\left(\dfrac{S_z - p}{Dz}\right)\cdot\tau_{max} \\ \text{if } x_1 < (S\text{-}p_2) < -p_1 & \tau = k_s\cdot(S_z - p - x_1) \quad \text{with } x_1 = -\dfrac{\tau_1}{k_s} - p_1 \text{ with } x_1 \geq 0 \\ \text{if } (S\text{-}p_2) < x_1 & \tau = \tanh\left(\dfrac{S_z - p - x_1}{Dz}\right)\cdot\tau_{max} \end{array}\right\} \quad (7.8)$$

Similarly in dimensionless form for step 2:

$$\left.\begin{array}{ll} \text{if } (S'\text{-}p'_2) > -p'_1 & \tau' = \tanh(S'_z - p')\cdot\tau'_{max} \\ \text{if } x_1 < (S'\text{-}p'_2) < -p'_1 & \tau' = k'_s\cdot(S'_z - p' - x'_1) \quad \text{with } x'_1 = -\dfrac{\tau'_1}{k'_s} - p'_1 \\ & \quad \text{with } x'_1 \geq 0 \text{ and } k'_s = 1 \\ \text{if } (S'\text{-}p'_2) < x'_1 & \tau' = \tanh(S'_z - p' - x'_1)\cdot\tau'_{max} \end{array}\right\} \quad (7.9)$$

The solution for the pile displacement p_2 for step 2 depends on the shape of the soil displacement and the shaft friction with depth, which are described in the following two sections.

The pile displacement caused by the greenfield soil displacement can be found by subtracting the pile displacement from step 2 and step 1:

$$\Delta p = p_2 - p_1 \quad (7.10)$$

7.2.2 Soil displacement profile

The shape of the soil displacement with depth along the pile is an important parameter for the interaction between pile and soil. For excavations, the settlement at the surface is usually larger than at the pile tip. For this analytical model, a linear shape of the soil displacement is assumed as:

$$S_{z2} = S_0 + \frac{\Delta S}{L_p}\cdot z \quad (7.11)$$

with:

S_0 is the soil displacement at z=0

S_{lp} is the soil displacement at z=Lp

$$\Delta S = S_{Lp} - S_0 \quad (7.12)$$

Written as a function of the dimensionless z', S_{z2} becomes

$$S'_{z2} = S'_0 + \frac{\Delta S}{D_z}\cdot z' \quad (7.13)$$

We already know that any soil displacement acting along the whole length of the pile, such as S_0, does not change the negative and positive friction and will be fully taken by the pile. So, for now we assume $S'_{z2} = \frac{\Delta S}{Dz} \cdot z'$ and we will later add S_0 to the pile displacement.

A different S_3 will be found for the same surface settlement and settlement of the foundation layer, when the 'shape' of the settlement with depth is not linear, for example due to the nature of the settlement origin, such as dewatering, tunnelling or excavation. See Figure 7.6.

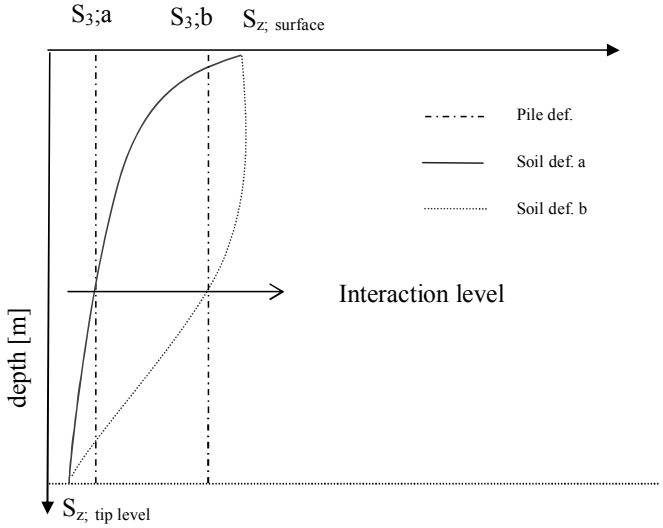


Figure 7.6 S_3 based on a non-linear settlement profile and known interaction level

Due to the S_3 settlement a small amount of extra shaft resistance could be obtained for the extra embedment in the bearing layer. When the cone resistance in the bearing layer is not constant, also the tip resistance might be affected. Both these effects are considered to be second order and should be neglected in normal conditions.

7.2.3 Analytical solution if shaft friction is constant with depth

In the simplest case, the maximum shaft friction τ_{max} is a constant value with depth along the pile. Inserting (7.9) in (7.4) results in:

$$\frac{W}{W_{max}} = \int_0^1 \tanh(S' - p') \cdot 1 dz' \tag{7.14}$$

Step 1: the initial condition with $S_{z1} = 0$ becomes:

$$\frac{W}{W_{max}} = \int_0^1 \tanh(-p'_1) dz' \; = \tanh(-p'_1) \tag{7.15}$$

Equation (7.15) can be solved into:

$$p'_1 = -\operatorname{arctanh}\left(\frac{W}{W_{max}}\right) \text{ and}$$

$$p_1 = -Dz \operatorname{arctanh}\left(\frac{W}{W_{max}}\right) \text{ which is equal to:}$$

$$p_1 = -\frac{1}{2} Dz \ln\left(\frac{1+\frac{W}{W_{max}}}{1-\frac{W}{W_{max}}}\right) \tag{7.16}$$

Step 2: the soil settlement takes place:
The normalized pile displacement p'_2 can be found by solving the following set of equations:

$$\frac{W}{W_{max}} = \int_0^1 \tau' dz' \tag{7.17}$$

with:

if $(S'-p'_2) > -p'_1$ $\qquad \tau' = \tanh\left(\frac{\Delta S}{Dz} \cdot z' - p'_2\right)$

if $x_1 < (S'-p'_2) < -p'_1$ $\qquad \tau' = \frac{\Delta S}{Dz} \cdot z' - p'_2 - x'_1$ with $x'_1 = -\tau'_1 - p'_1$ with $x'_1 \geq 0$

if $(S'-p'_2) < x'_1$ $\qquad \tau' = \tanh\left(\frac{\Delta S}{Dz} \cdot z' - p'_2 - x'_1\right)$

To obtain the pile displacement caused by the soil displacement p_2 is found by transforming back to dimensions:

$$p_2 = p'_2 \cdot D_z \tag{7.18}$$

We now have to add the minimum soil displacement that we took out of the equation earlier and add it to Δp to get:

$$\Delta p = S_0 + p_2 - p_1 \tag{7.19}$$

The interaction depth z_i/L_p at which Δp is equal to S_{z2} can be found for the linear soil displacement by solving:

$$\Delta p = S_0 + p_2 - p_1 = S_0 + \frac{\Delta S}{L_p} \cdot z_p \tag{7.20}$$

which leads to

$$\frac{z_p}{L_p} = \frac{p_2 - p_1}{\Delta S} \tag{7.21}$$

Figure 7.7 shows the numerical solution for the interaction depth z_i/L_p at which the pile displacement due to the excavation is equal to the soil displacement S_{z2}. This depth is the

neutral level. This depth is an interaction factor, because it determines the relative sensitivity of the pile to soil displacements along its shaft.

From Figure 7.7 it is concluded that friction piles settle with at least the average soil displacement along the pile (for very small loads on the pile) and at most the maximum soil displacement (for piles with very high initial loads). For excavations, where the maximum soil displacement is found at the surface, the interaction depth z_i/L_p decreases from halfway the pile depth to the surface (0.5 to 0). For tunnels, where the maximum soil displacement is found at the pile toe, the interaction depth z_i/L_p increases from halfway the pile depth to the pile toe (0.5 to 1). For soils with small initial stiffness k_s (and thus small D_z) compared to the gradient of the soil displacement, $\Delta S/D_z$ is large and the interaction depth changes linearly with increasing load on the pile. For smaller values of $\Delta S/D_z$, the pile settles less than that.

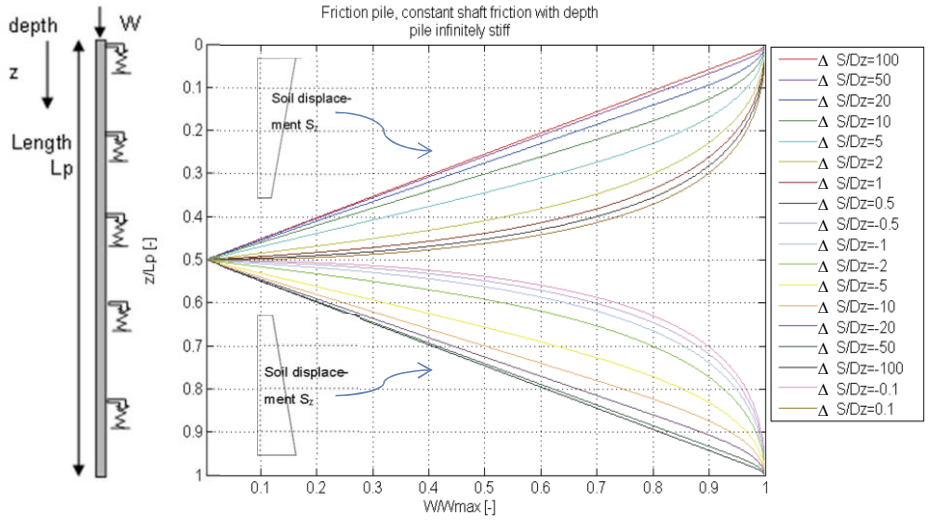


Figure 7.7 Relationship between z_i/L_p and W/Wmax for different values of $\Delta S/Dz$ for a friction pile with infinite stiffness and constant shaft friction with depth.
Positive values of $\Delta S/D_z$ are used for linearly decreasing soil displacement with depth, negative values of linearly increasing soil displacement with depth.

7.2.4 Analytical solution if shaft friction increases with depth

If we extend the work in section 7.2.3 to include an increasing τ_{max} with depth, we first assume it to be a linear function of z. τ_{max} is a known function h_s: $\tau_{max} = h_s(z)$.

$$\tau_{max} = \tau_{max;0} + \frac{\tau_{max;Lp} - \tau_{max;0}}{L_p} \cdot z = \tau_{max;0} + (\tau_{max;Lp} - \tau_{max;0}) \cdot z' \qquad (7.22)$$

with

$\tau_{max;0}$ is the maximum shaft friction at z=0

$\tau_{max;Lp}$ is the maximum shaft friction at z=Lp

In dimensionless form with $\bar{\tau}_{max}$ is the average shaft friction along the pile, (7.22) becomes:

$$\tau'_{max} = \frac{\tau_{max;0} + (\tau_{max;Lp} - \tau_{max;0}) \cdot z'}{\bar{\tau}_{max}} \tag{7.23}$$

With a constant value of D_z, the shaft friction for different depths along the pile is shown in Figure 7.8.

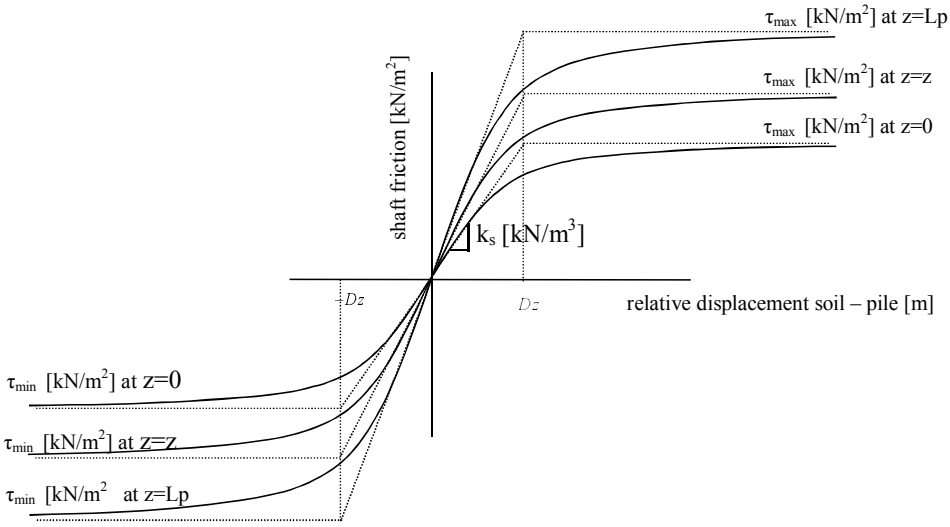


Figure 7.8 Shaft friction versus relative displacement between pile and soil, increasing with depth with constant D_z

The basic equation still is:

$$\frac{W}{W_{max}} = \int_0^1 \tanh(S' - p') \cdot \tau'_{max}\, dz' \tag{7.24}$$

Combining equation (7.22) with (7.23) leads to:

$$\frac{W\bar{\tau}_{max}}{W_{max}} = \int_0^1 \tanh(S' - p') \cdot (\tau_{max;0} + (\tau_{max;Lp} - \tau_{max;0}) \cdot z')dz' \tag{7.25}$$

For the initial condition with $S_{z1} = 0$ this leads to p'$_1$ by solving

$$\frac{W\bar{\tau}_{max}}{W_{max}} = \int_0^1 \tanh(-p_1') \cdot (\tau_{max;0} + (\tau_{max;Lp} - \tau_{max;0}) \cdot z')dz'$$

$$\frac{W\bar{\tau}_{max}}{W_{max}} = \tanh(-p_1') \cdot (\tau_{max;0} + (\tau_{max;Lp} - \tau_{max;0}) \cdot \frac{1}{2})$$

Since $\bar{\tau}_{max} = \tau_{max;0} + \frac{1}{2}(\tau_{max;Lp} - \tau_{max;0})$, the result is similar to the result in section 7.2.3.

$p'_1 = -\text{arctanh}\left(\frac{W}{W_{max}}\right)$ and $p_1 = -Dz\,\text{arctanh}\left(\frac{W}{W_{max}}\right)$ which is equal to:

$$p_1 = -\frac{1}{2} Dz \ln\left(\frac{1+\frac{W}{W_{\max}}}{1-\frac{W}{W_{\max}}}\right) \tag{7.26}$$

In the second stage, the soil displacement takes place. Again we use $S'_{z2} = S'_0 + \Delta S \cdot z'$ with S'$_0$ added to the pile displacement in a later stage.

$$\frac{W}{W_{\max}} = \int_0^1 \tau' dz' \tag{7.27}$$

Equation (7.27) now includes the shaft friction with depth including loading and unloading:

if (S'-p'$_2$) > -p'$_1$ $\quad \tau' = \tanh\left(\frac{\Delta S}{Dz} \cdot z' - p'_2\right) \cdot \frac{\left(\tau_{\max;0} + (\tau_{\max;Lp} - \tau_{\max;0}) \cdot z'\right)}{\overline{\tau}_{\max}}$

if x$_1$ < (S'-p'$_2$) < -p'$_1$ $\quad \tau' = \frac{\Delta S}{Dz} \cdot z' - p'_2 - x'_1$ with $x'_1 = -\tau'_1 - p'_1$ with $x'_1 \geq 0$

if (S'-p'$_2$) < x'$_1$ $\quad \tau' = \tanh\left(\frac{\Delta S}{Dz} \cdot z' - p'_2 - x'_1\right) \cdot \frac{\left(\tau_{\max;0} + (\tau_{\max;Lp} - \tau_{\max;0}) \cdot z'\right)}{\overline{\tau}_{\max}}$

To obtain the pile displacement caused by the soil displacement p$_2$ is found by transforming back to dimensions:

$$p_2 = p'_2 \cdot D_z \tag{7.28}$$

We now have to add the soil displacement S$_0$ which we took out of the equation earlier and add it to Δp to get:

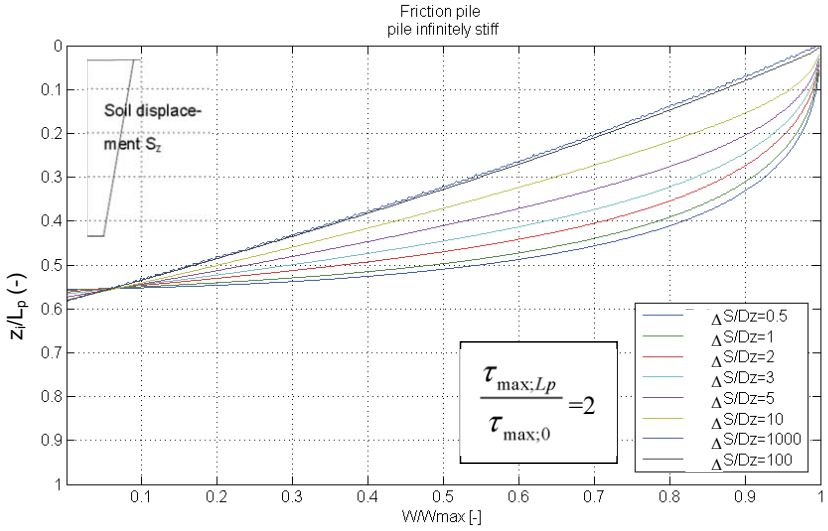
$$\Delta p = S_0 + p_2 - p_1 \tag{7.29}$$

The depth z$_i$ at which Δp is equal to S$_{z2}$ can be found for the linear soil displacement by solving:

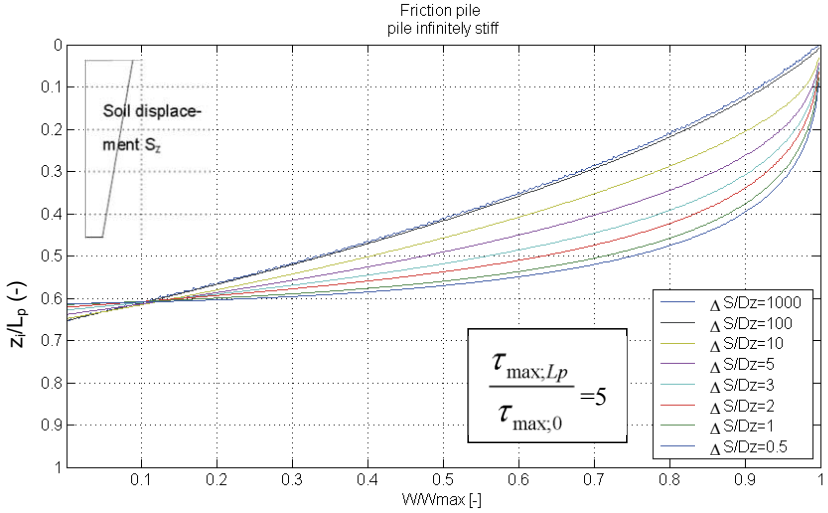
$$\Delta p = S_0 + p_2 - p_1 = S_0 + \frac{\Delta S}{L_p} \cdot z_i \tag{7.30}$$

$$\frac{z_i}{L_p} = \frac{p_2 - p_1}{\Delta S} \tag{7.31}$$

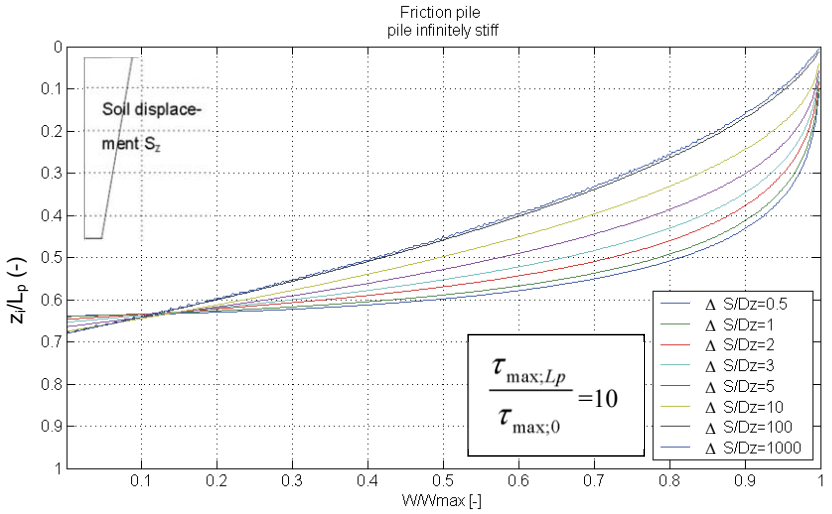
In summary, the pile displacement problem includes the following dimensionless parameters: $\frac{z_i}{L_p}$, $\frac{W}{W_{\max}}$, $\frac{\Delta S}{D_z}$, $\frac{\tau_{\max;Lp}}{\tau_{\max;0}}$. The result for different variations of these parameters is shown in Figure 7.9.


Friction pile
pile infinitely stiff
Soil displace-
ment S_z
$\frac{\tau_{max;Lp}}{\tau_{max;0}}=2$
ΔS/Dz=0.5
ΔS/Dz=1
ΔS/Dz=2
ΔS/Dz=3
ΔS/Dz=5
ΔS/Dz=10
ΔS/Dz=1000
ΔS/Dz=100
z_i/L_p (-)
W/Wmax [-]

(a)


Friction pile
pile infinitely stiff
Soil displace-
ment S_z
$\frac{\tau_{max;Lp}}{\tau_{max;0}}=5$
ΔS/Dz=1000
ΔS/Dz=100
ΔS/Dz=10
ΔS/Dz=5
ΔS/Dz=3
ΔS/Dz=2
ΔS/Dz=1
ΔS/Dz=0.5
z_i/L_p (-)
W/Wmax [-]

(b)



(c)

Figure 7.9 Interaction factor z_i/L_p for friction piles as a function of the initial pile load W/W_{max} for different values of $\Delta S/Dz$ and increasing maximum shaft friction with depth

Figure 7.9 shows three plots, each for a different increase in maximum shaft friction.
By comparing Figure 7.9 with Figure 7.7, it is concluded that for increasing maximum shaft friction with depth, the interaction depth at low initial loads (small W/Wmax) is found deeper along the pile. This leads to a smaller pile displacement compared to the situation with constant shaft friction. For constant shaft friction with depth, z_i/L_p started at 0.5, while for shaft friction increasing from 0 kN/m^2 to a certain number at depth $\tau_{max;Lp}/\tau_{max;0}$ is infinite, z_i/L_p starts at the lowest level of 0.707 = 1/2*√2 if also $\Delta S/D_z$ is infinitely large.

For that specific case:

$$\left.\frac{z_i}{L_p}\right|_{W=0} = \frac{\tau_{max;0} + (\tau_{max;L_p} - \tau_{max;0})\frac{1}{2}\sqrt{2}}{\tau_{max;L_p} + \tau_{max;0}} \tag{7.32}$$

Other combinations of W/W_{max}, $\Delta S/D_z$ and $\tau_{max;Lp}/\tau_{max;0}$ can be found in the corresponding graphs of Figure 7.9.

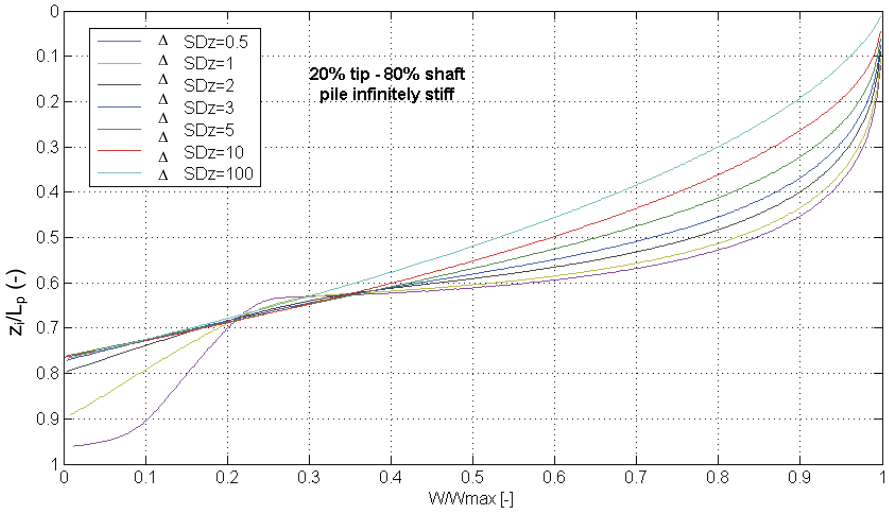
7.2.5 Effect of pile base capacity

For end bearing piles, equation (7.2) needs to be extended to

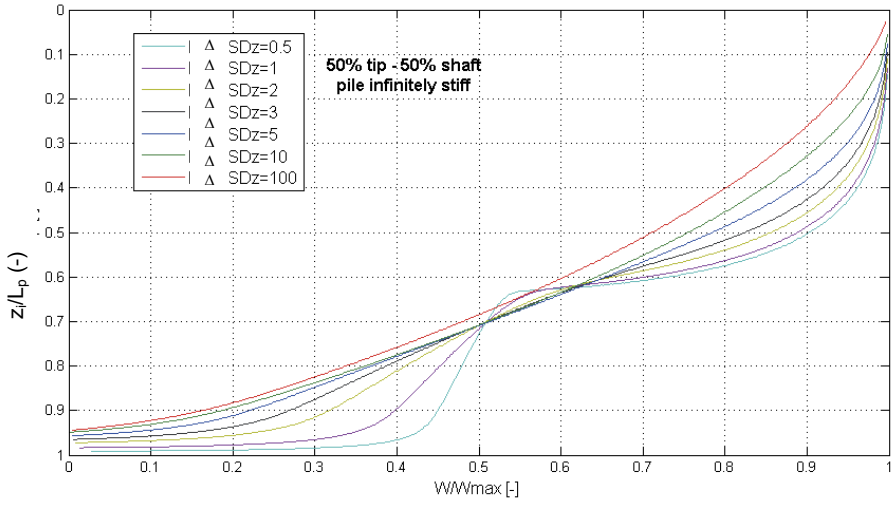
$$W = \int_0^{L_p} \tau \cdot \pi \cdot D dz + A \cdot q_b \tag{7.33}$$

where q_b is the average foundation pressure around the tip in [kN/m^2] with cross section A in [m^2]. A times q_b represents the base capacity Qb in [kN].

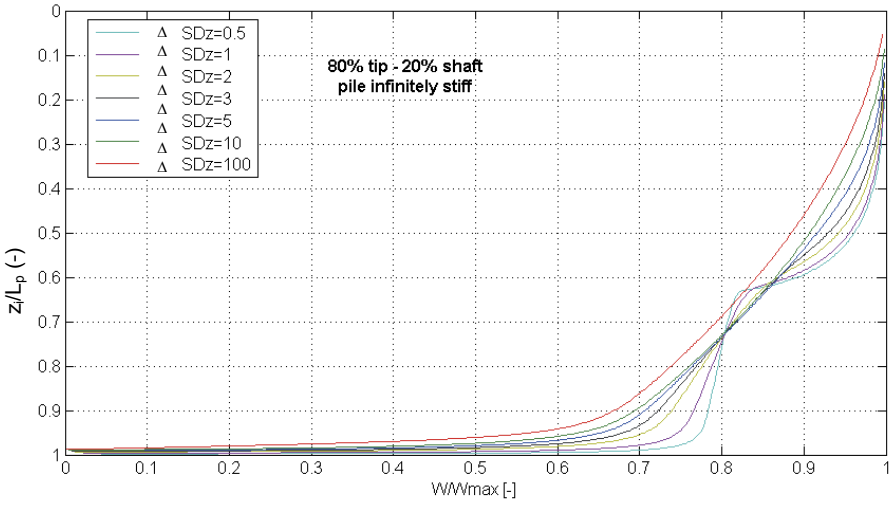
If the pile has base capacity, any pile displacement will also increase the base resistance (until the maximum is reached). The effect this has on the relative pile displacement compared to the soil displacement is shown in Figure 7.10. Two additional dimensionless parameters are involved if the effect of pile base capacity is taken into account. First, this is the relative amount of shaft and base capacity at failure, Qb/Wmax. The graphs are for piles with respectively 20%, 50%, 80% and 99% end bearing. The second dimensionless characteristic is the relative displacement necessary to obtain full base capacity versus full shaft friction. In the examples below, the relative displacement to obtain full base capacity is taken as 10% of the pile diameter. The corresponding dimensionless factor is D/D_z, but this factor has not been varied to limit the number of graphs. This factor D/D_z is also responsible for the rather sudden increase in z_i/L_p for low values of $\Delta S/D_z$ as shown in the graphs. Ultimately, for the theoretical option of a completely end-bearing pile, the interaction depth z_i/L_p is found at the pile toe ($z_i/L_p = 1$), until the pile fails. For piles with a mix of shaft friction and end bearing, the interaction depth increases from 0.5-1.0 towards 0. For piles with at least 50% end bearing and a safety factor of at least 2 ($W/Wmax < 0.5$), the pile follows the soil at a interaction depth of 0.7 or deeper. Piles with larger percentages of shaft capacity or smaller safety factors settle significantly more, ultimately leading to the maximum pile displacement being equal to the maximum soil settlement, which for excavations is found at the surface.


SDz=0.5
SDz=1
SDz=2
SDz=3
SDz=5
SDz=10
SDz=100
20% tip - 80% shaft
pile infinitely stiff
z/Lp (-)
W/Wmax [-]

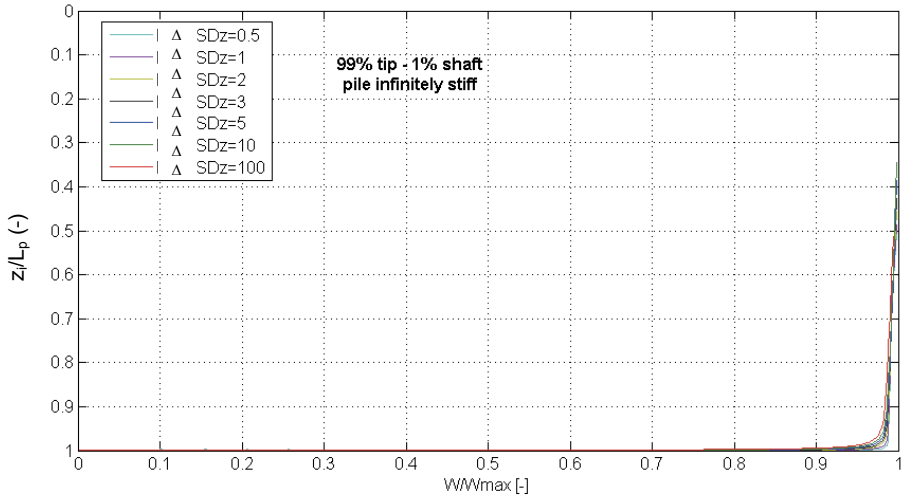
(a)


SDz=0.5
SDz=1
SDz=2
SDz=3
SDz=5
SDz=10
SDz=100
50% tip - 50% shaft
pile infinitely stiff
z/Lp (-)
W/Wmax [-]

(b)



(c)



(d)

Figure 7.10 Results of z_i/L_p versus W/Wmax for piles with 20%, 50%, 80% and 99% end bearing, assuming infinite pile stiffness and $\tau_{max;Lp}/\tau_{max;0}$ =10 and D_{ztip} = 0.05* D

7.2.6 Effect of pile flexibility

In previous sections, the analytical solutions presented have assumed infinite pile stiffness. In reality, piles and certainly old timber piles, are not infinitely stiff.

The effect of the pile stiffness results in a non-constant shaft friction development along the pile. The relative soil displacement (S_z-p) changes as now not only S_z changes with depth but

also p. For each depth the pile displacement has to be corrected for the load in the pile and the stiffness of the pile according to equation (7.34).

$$p_z = p_0 - \frac{\overline{F}_{ax}}{E \cdot A} \cdot z \tag{7.34}$$

with E is modulus of elasticity of the pile in [kN/m^2] , $\overline{F}_{ax}$ is the average axial load in the pile from top to the depth z in [kN], A is the cross section of the pile over the depth in [m^2] and p_0 is pile displacement at the top of the pile in [m].
The axial pile load can be determined from equation (7.35):

$$F_{ax}(z) = W - O \cdot \int_{z}^{0} \tau_z dz \tag{7.35}$$

With $F_{ax} = 0$ for z_{Lp} and $F_{ax} = W$ for z_0.

Figure 7.11 shows a comparison between infinite and realistic pile stiffness for an increasing maximum shaft friction with depth of $\tau_{max;Lp}/\tau_{max;0} = 5$. For timber piles, a realistic pile stiffness E is $1*10^7$ kN/m^2, see Chapter 6. The effect of the pile stiffness is small for timber piles of 10 m long and somewhat more significant for piles of 20 m long. Concrete and steel piles are stiffer, so it is expected that for those piles the effect of pile stiffness is even smaller.

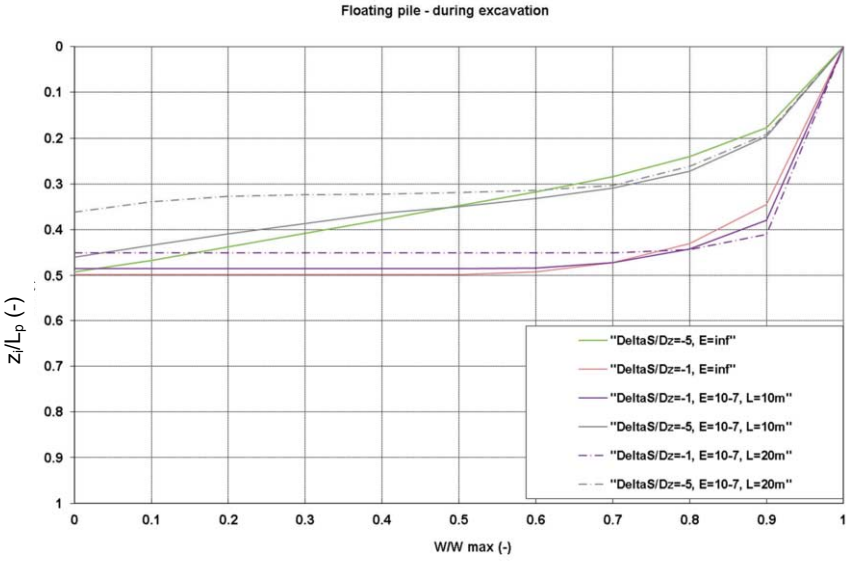


Figure 7.11 Results of z_i/L_p versus W/Wmax with infinite and realistic stiffness for timber piles (10 m long and 20m long, D=0.2m)

7.2.7 Resulting shaft friction with depth

In this section, the previous results are presented in the form of the shaft friction development with depth for better understanding of the mechanisms.

In the simplest case, the pile is considered infinitely stiff, the maximum shaft friction is constant with depth, no base capacity is assumed and the pile diameter is constant with depth. The soil displacement is a linearly decreasing function of the depth along the pile. Figure 7.12 shows the additional negative and positive shaft friction for such a pile for an initial load of 50% of the maximum capacity.

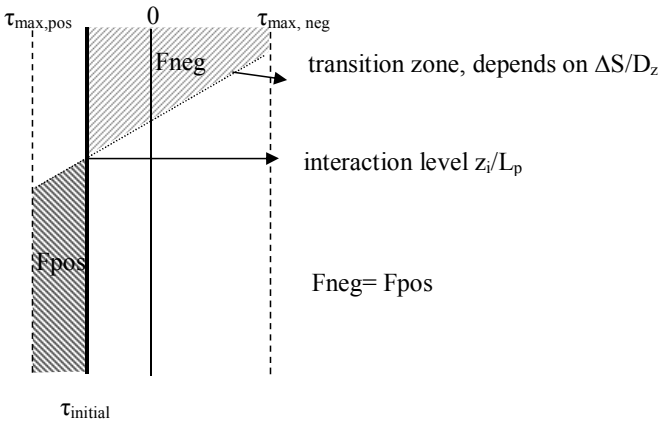


Figure 7.12 Example of development of positive and negative shaft friction due to an excavation.

From the head of the pile to the level which in Figure 7.12 is called "interaction level z_i/L_p", the soil settles more than the pile. The additional positive friction developed at larger depth (in yellow) balances the additional negative shaft friction in the upper blue section. The additional pile displacement compared to the soil displacement depends on the initial load on the pile.

If the pile is not loaded (W=0%) before the soil displacement, the neutral level shifts from the surface (initial) to the centre of the pile (if the shaft friction does not change with depth and positive and negative values are equal). The pile settles the same amount as the soil at the final neutral level, which is the interaction level z_i/L_p. If the pile is loaded to failure (W = 100%), the neutral level starts at the surface and can not move down, because the maximum friction has been reached. The pile settles the same amount as the soil at the initial neutral level, which is equal to the amount at the surface.

If the pile is loaded between 0 and 100%, the remaining shaft capacity is increased at both the positive and negative side, until equilibrium is found at a new neutral level. This level is lower than the original level (which was at the surface). The pile settles an amount in between the soil settlement at the initial and final neutral level. This is again equal to the settlement at the interaction level z_i/L_p.

Figure 7.13 shows the level of the initial and final neutral level for a simplified condition similar the condition in Figure 7.12, as well as the interaction level z_i/L_p. Figure 7.14 shows the corresponding shaft friction with depth for the three phases for the same simplified situation. For more complex loading conditions, the principles are similar.

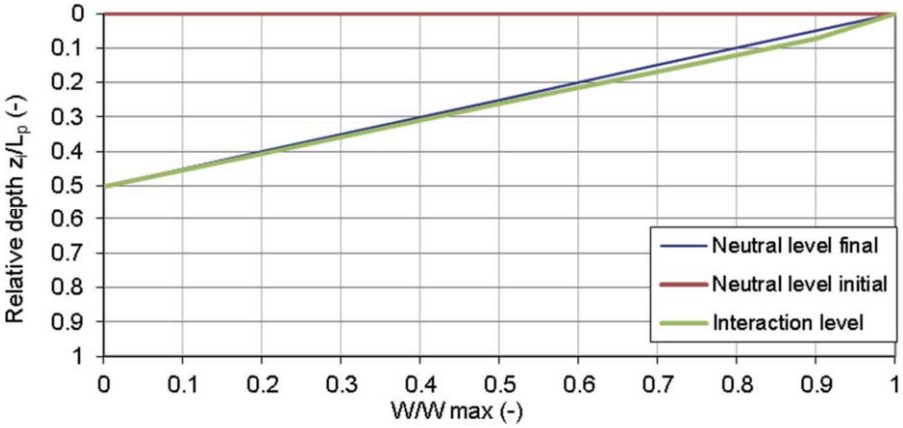
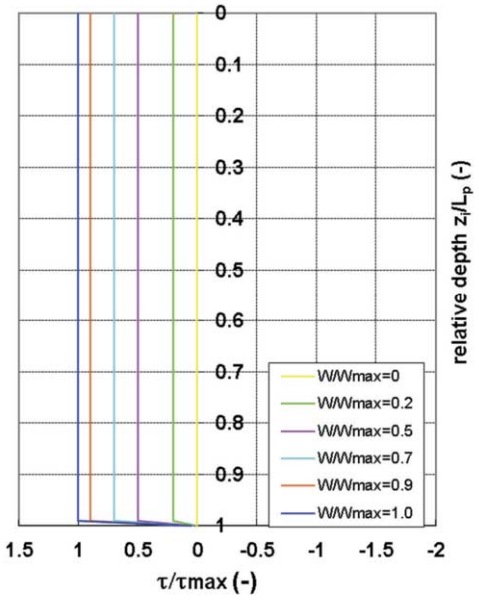
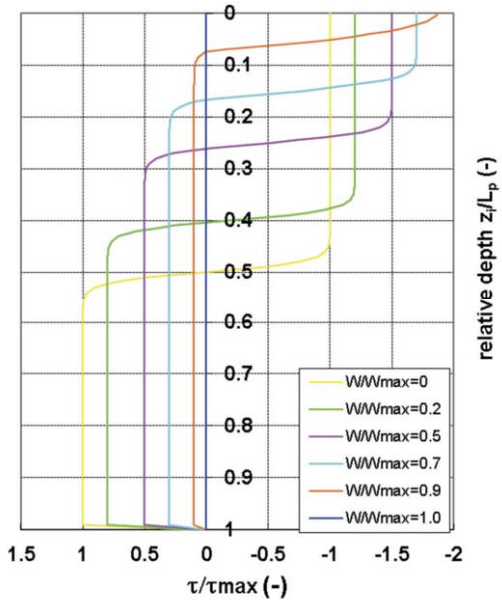


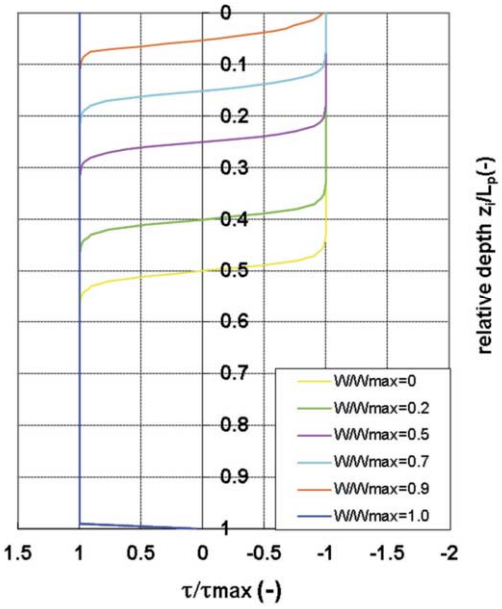
Figure 7.13 Changes of depth of neutral level with initial load increasing from W/Wmax is 0 to 1 for $\Delta S/D_z$= 50.



(a)



(b)



(c)

Figure 7.14 Shaft friction with depth along the pile, initial shaft friction (a), additional friction (b) and final condition (c) for constant shaft friction with depth and $\Delta S/D_z = 50$.

7.2.8 Amsterdam timber pile

For the Amsterdam pile foundation (see Chapter 6), the results of this chapter have been combined into one figure, which shows the pile displacement as a function of the soil displacement. For a large number of parameters a realistic average is assumed, leaving only the load on the pile and the soil displacement as variables. Figure 7.15 can be used to determine the pile displacement of real piles in the Amsterdam situation when soil displacements take place as a result of excavation works. For the piles in this figure, it is assumed that prior to the construction of the deep excavation the negative skin friction (caused by previously placed fill) is already present. This is a realistic assumption, because due to drawdown in the deeper layers and surface loading to raise street levels, the compressible Holocene layers settle under their load. As a result, the interaction lines for soil and pile displacement are equal for all soil displacements.

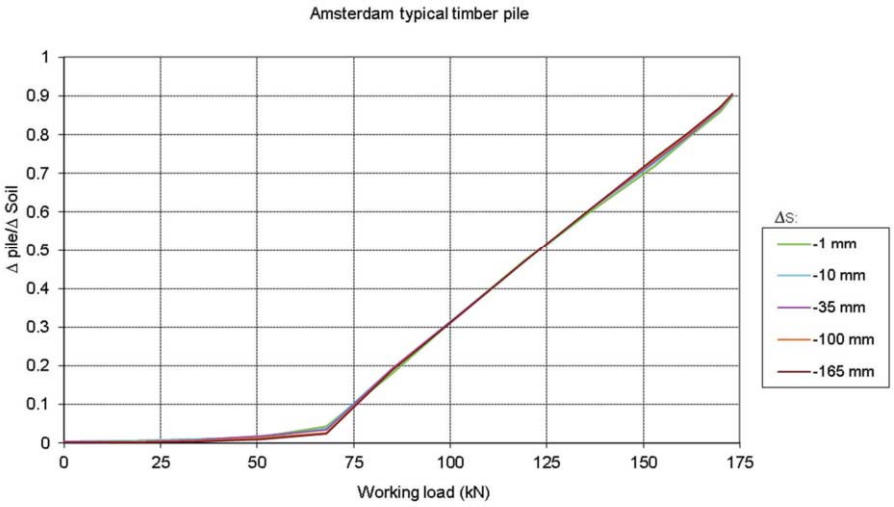


Figure 7.15 Results pile displacement over maximum soil settlement for actual soil profile in Amsterdam, assuming initial negative skin friction present
Pile head 1 m below surface, L = 11 m, L_{soft} = 10.5 m (length of the pile in Holocene, settling soil), Pile diameter 0.17 m average; E = 8E6 kN/m^2
Shaft friction Holocene: 5.3 kN/m, sand layer 35 kN/m, Base resistance 100 kN,
Soil settlement profile linear shape with maximum settlement at the surface
D_z values and all values above according to Chapter 6.

As an example, the pile displacement is determined for a pile load of 100 kN and a soil displacement of 80 mm at the surface and 10 mm at the pile tip level (Δ Soil = 80-10 = 70mm). The resulting Δ Pile/Δ Soil on the vertical axis due to the excavation is 0.31. The overall pile displacement due to the excavation is found by adding the pile tip deformation to the interaction effect:

- Pile displacement due to excavation = 10 mm + 0.31 * 70 mm = 32 mm.

For other pile diameters, it is possible to replace the horizontal axis in Figure 7.15 with W/Wmax, assuming Wmax for the 'standard' pile is 173 kN.

7.2.9 Summary interaction levels

In this section, an overview is given of neutral levels (NL) and interaction levels (z_i/L_p) for different foundation conditions as guidance for damage classification assessments. All graphs in Table 7.1 assume an excavation type settlement profile as shown in Figure 7.16. The figures shows results for piles with 100% end bearing, 50% end bearing and 0% end bearing (100% shaft friction) and for lower respectively higher initial loads. For intermediate loads, the figures need to be interpolated. The pile tip condition is represented by a horizontal bar, which is coloured in grey based on the percentage of the capacity that is mobilized. The gradient of the soil displacement determines the length and shape of the transition zone between positive and negative friction, which for the figures in Table 7.1 is not to scale. It is assumed that both shaft friction and tip resistance need similar relative displacements to fully develop, which is reasonable for small pile diameters such as in Amsterdam, but may be different for larger diameters and/or piles in sand. As shown in section 7.2.6, the pile flexibility is not of major importance and thus not taken into account.

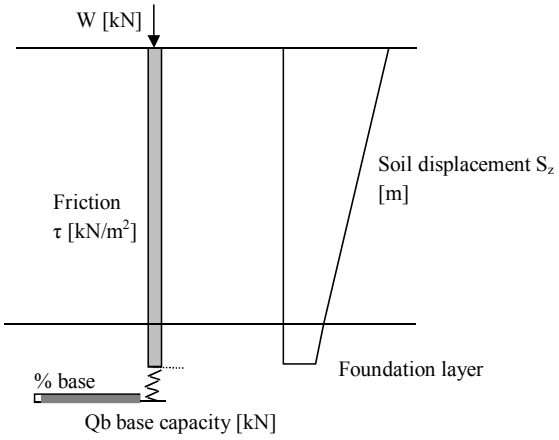
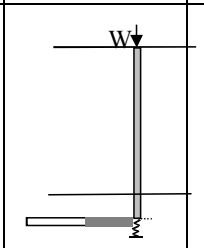
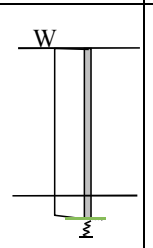
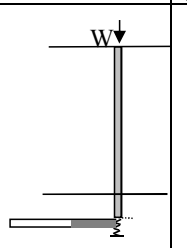
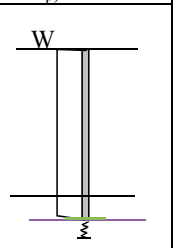
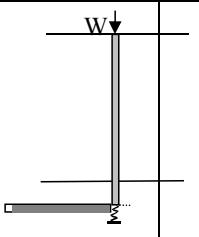
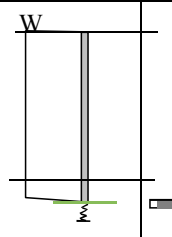
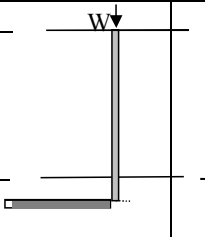
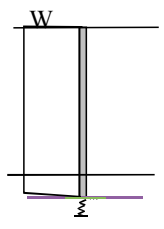
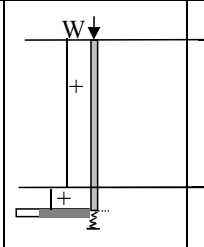
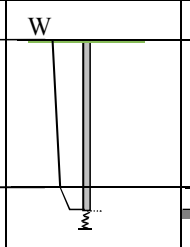
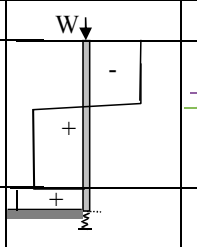
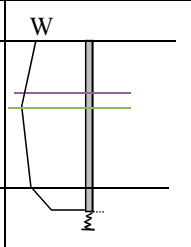
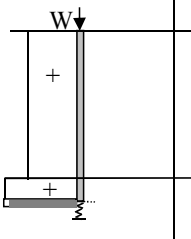
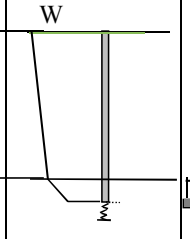
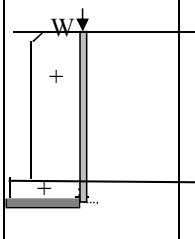
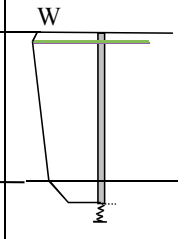
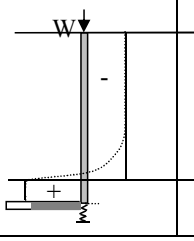
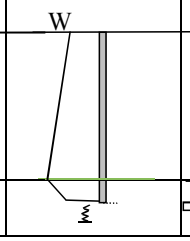
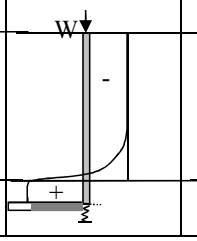
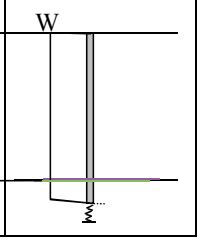
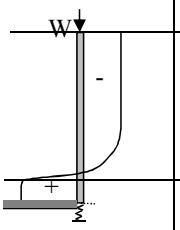
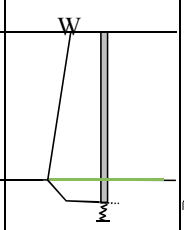
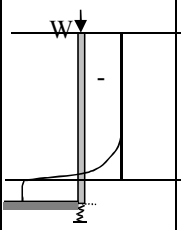
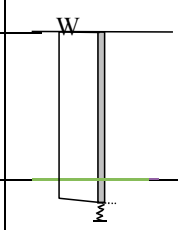
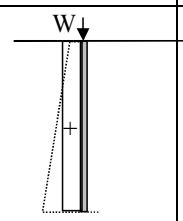
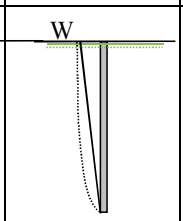
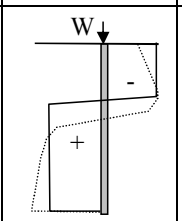
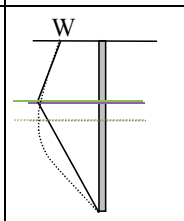
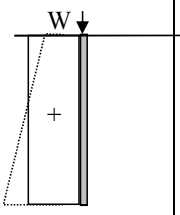
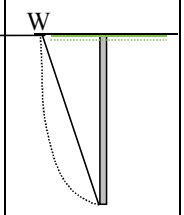
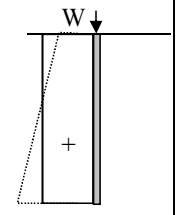
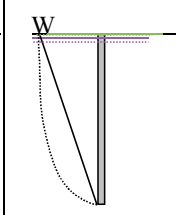


Figure 7.16 Excavation type settlement profile

For piles with 50% end bearing and 50% shaft friction, two conditions are shown in Table 7.1; one condition when no initial soil displacement has taken place and another where negative skin friction has already developed before the excavation takes place. For piles with fully developed negative skin friction before the excavation (for example due to pumping or raising of the surface level) the external pile load is limited by the NSF developed. For these cases, the external pile load W is not compared to Wmax, the pile capacity at full positive friction, but to Weffmax, the maximum load on the pile given a full development of negative friction, according to:
Weffmax =Wtip + Wpos shaft – W neg shaft.

Table 7.1 Neutral levels (NL), interaction levels (z_i/L_p) and axial load in the pile for different foundation conditions

Situation	Friction along pile Initial condition	Axial load in pile initial condition NL ——	Friction along pile final condition	Axial load in pile final condition (z_i/L_p) —— NL ——
A) 100% end bearing pile W<< Wmax				
B) 100% end bearing pile W ≈ Wmax NB For 99% end bearing z_i/L_p moves to surface for W≈Wmax				
C) 50% End bearing - 50% Friction W<< Wmax No soil displacement before excavation				
D) 50% End bearing - 50% Friction W ≈ Wmax No soil displacement before excavation				
E) 50% End bearing - 50% Friction W<< Weffmax NSF developed before excavation				

Situation	Friction along pile Initial condition	Axial load in pile initial condition NL	Friction along pile final condition	Axial load in pile final condition (z_i/L_p) NL
F) End bearing 50% - Friction 50% W ≈ Weffmax NSF developed before excavation If W ≈ Wmax see D)				
G) Friction pile W<< Wmax — Uniform shaft friction ..... Shaft friction increasing with depth				
H) Friction pile W ≈ Wmax — Uniform shaft friction ..... Shaft friction increasing with depth				

7.3 Effects on piles not related to construction

Beside the effect of construction related activities, other causes of displacement of the soil will influence the piled buildings. In many countries with soft soil conditions, some form of displacements and stress changes may occur, for example due to ground water lowering in deep aquifers. The presence of soft soil layers combined with earlier city developments such as raising of the ground level causes subsidence due to consolidation and creep. Old cities in the western part of the Netherlands in general experience ground surface displacements of about 10 to 20 mm/year. More recently developed areas in Jakarta currently experience ground surface displacements of about 50-70 mm per year and similarly in Bangkok of 10-30 mm/year (Hirose et al. 2001; Aobpaet et al. 2010).

Outside the influence of the construction, the natural subsidence causes deformations of the buildings. This will lead to negative skin friction development along the pile shafts and may

also cause displacements under the pile tip. If the soil is homogenous, this effect will not cause differential displacements in the soil. If a fill layer is used to raise and maintain street level over the years, this layer is usually thicker in the streets than under the houses, leading to larger negative skin friction and horizontal displacements at the position of the facades. When the soil is not homogenous and/or the pile capacity is not constant, serious differential deformation of the piles and thus the buildings are possible.

Subsidence of piled buildings can be determined by:

- Subsidence under pile tip level (usually homogenous under a specific building), similar to S2 for piles in the influence zone of excavations
- Additional negative skin friction due to surface displacements, similar to S3 for piles in the influence zone of excavations.

7.4 Summary

The buildings in the influence zone of the excavation experience several phenomena, which combined result in the building deformation:

1. Reduction of pile capacity due to lower stress levels
2. Deformation of the pile tip due to soil displacements below the base of the pile
3. Development of negative (or positive) skin friction due to relative movements of the soil and the pile shaft
4. Redistribution of pile load over the piles under the building slab, the building wall or a foundation cap or beam, depending on the building stiffness
5. Horizontal deformations of the piles (causing bending of the pile).

The deformation of the pile head is determined by the summation of the first four effects described above. Since especially timber piles are rather flexible in horizontal loading, they tend to follow the soil displacements. This effect is not described in this chapter.

This chapter provides more detailed insight into the development of positive and negative shaft friction along a pile due to the initial load on the pile and subsequent excavation or tunnelling soil displacements (point 3 in the list above). To determine the pile displacement, an analytical model has been described relating the pile displacement resulting from the construction works to the soil displacement, using an interaction level z_i/L_p. By definition, the pile displacement due to the construction works is equal to the soil displacement at the interaction level.

The interaction level z_i/L_p depends on the following dimensionless factors:
$\frac{W}{W_{max}}, \frac{\Delta S}{D_z}, \frac{\tau_{max;Lp}}{\tau_{max;0}}, \frac{Q_b}{W_{max}}$ and $\frac{D}{D_z}$.

The interaction level is not always equal to the neutral level of the pile, because the neutral level may shift during the construction works. Only if the shaft friction has already been

fully developed (in negative and/or positive direction), the interaction level is equal to the neutral level and remains constant during the works.

The interaction level is significantly different for friction piles and end bearing piles, as is shown in Table 7.1. Since most piles rely both on end bearing and shaft friction, the interaction level depends on all the factors described above. Common generalizations that end bearing piles settle with the soil at the tip level and friction piles with the surface level are valid only for certain extreme cases. In the majority of the cases, the actual pile displacement or interaction level is found in between those values and described by the following equations:

$$\frac{z_i}{L_p} = \frac{p_2 - p_1}{\Delta S} \tag{7.36}$$

with p_1 is the pile displacement due to the initial load and p_2 due to the load in combination with the soil displacement. This p_2 can be found from:

$$W = \int_0^{L_p} \tau \cdot \pi \cdot D dz + A \cdot q_b \tag{7.37}$$

Equation (7.37) includes the shaft friction, which may depend on the depth along the pile:

$$\tau = \tanh\left(\frac{S_z - p_2}{Dz}\right) \cdot \tau_{\max} \tag{7.38}$$

Depending on the relative pile-soil displacement, the shaft friction is found along this tangent hyperbolic line for loading or from the associated unloading curve, see section 7.2.3.

For piles with a mix of shaft friction and end bearing, the interaction level moves upward from between 50%-100% of the pile length towards the pile head level. For piles with at least 50% end bearing and a safety factor of at least 2 (W/Wmax <0.5), the pile follows the soil at 70% of the pile length or deeper. Piles with smaller percentages of end bearing or smaller safety factors settle significantly more, ultimately leading to the maximum pile displacement being equal to the maximum soil displacement, which for excavations is usually found at the surface.

Figure 7.7 may be used to find the interaction level for friction piles and Figure 7.9 for several percentages of end bearing. Figure 7.15 may be used for typical Amsterdam timber piles.

CHAPTER 8 SOIL- PILE INTERACTION BASED ON MEASUREMENTS IN AMSTERDAM

8.1 Introduction

Construction activities influenced the buildings along the deep excavations for the North South Line at Rokin Station, Vijzelgracht Station and Ceintuurbaan Station. Each of the construction activities had a certain impact on the buildings. The construction activities have been subdivided into predrilling and removal of obstacles; raising of the street level and installation effects of the retaining wall; and wall deflection due to excavation of the station. Most of the buildings are founded in the First sand layer at about 12 to 13 m below surface level. Foundations consist of the original timber piles unless foundation renewal took place. Only certain buildings have foundations that are more recent, founded in the second sand layer.

For each of the stations, the soil – pile interaction was analysed for a number of specific buildings. Buildings were selected based on the availability and the quality of the monitoring data and the historical data about the structure. The second part of this chapter gives an overview of the interaction factors for all buildings with measurements available, related to the characteristics of the buildings.

8.2 Ceintuurbaan

In cross section 13044ES (Govert Flinckstraat) buildings 120, 122, 124 and 126 have been analysed. The foundation type (see Chapter 4) is type1b and foundation class II. The location of the buildings and monitoring points as well as the deep excavation is shown in Figure 8.1 and the corresponding displacements in Figure 8.2. A selection of monitoring points on the facades is shown in the picture in Figure 8.3.

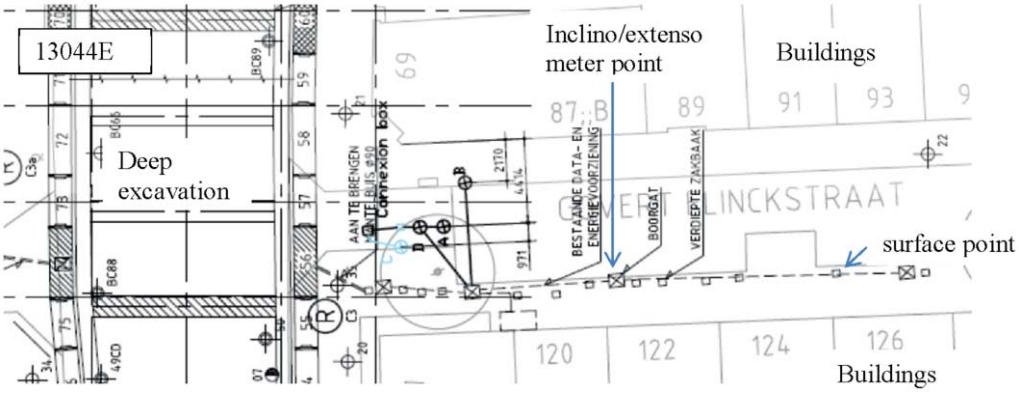


Figure 8.1 Top view of deep excavation and buildings in Govert Flinckstraat (Ceintuurbaan)

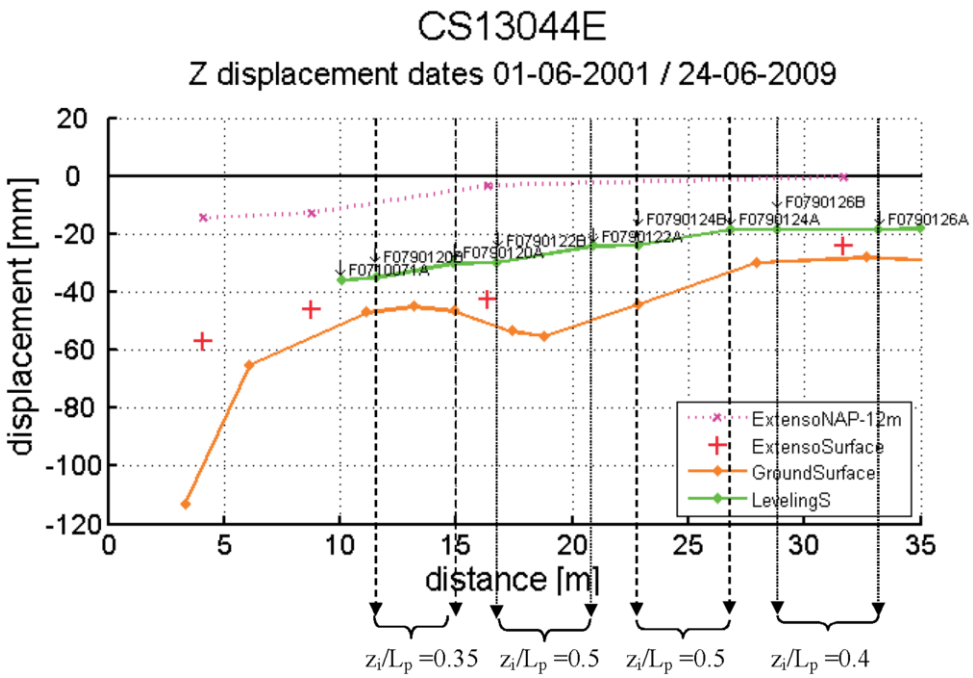


Figure 8.2 Ground and building displacements for Govert Flinckstraat (Ceintuurbaan), showing interaction levels (z_i/L_p) derived from measurements



Figure 8.3 Façade with monitoring points Govert Flinckstraat 124 (Ceintuurbaan)

Based on the soil and building displacements, the average interaction level z_i/L_p is determined in Table 8.1 based on the measurements. The resulting z_i/L_p (see Chapter 7) for these buildings is 0.3 to 0.5, with z is the depth along the pile where the pile and soil settlement during the construction works are equal and L is the length of the pile. When $z_i/L_p = 0$ the pile settlement is equal to the surface settlement. For z_i/L_p values between 0 and 1 a linear soil settlement profile between the surface settlement and the settlement at the first sand layer (foundation level, depth L) is assumed. The z_i/L_p value is also determined for each of the construction stages separately, as is shown in Figure 8.4. The interaction level z_i/L_p seems to vary somewhat between the different construction stages, but the overall average is similar to the initial period 2001-2003 in which no construction activities took place. It is thus concluded that, although with sometimes significant variations, the initial interaction level z_i/L_p is a good reference for the overall interaction level to be expected. This also follows from Chapter 7 if the shaft friction has already been fully developed before construction takes place. The interaction level z_i/L_p is determined using the manual ground surface point and the interpolated results of the extensometer on the first sand layer at NAP -12m. This corresponds to a neutral level after construction of NAP -4.3 m to NAP -6.5m (pile head at NAP -1m).

Table 8.1 Building and ground displacements in the period 2001-07-24 – 2009-06-24 for Govert Flinckstraat 120-126 (Ceintuurbaan) and corresponding interaction level z_i/L_p

name	building settlement [mm]	surface settlement [mm]	extensometer first sand layer [mm]	interaction level z_i/L_p [-]
'F0790120B'	-35.18	-46.7	-9.4	0.31
'F0790120A'	-30.16	-46.5	-5.2	0.40
'F0790122B'	-29.87	-51.7	-3.3	0.45
'F0790122A'	-24.26	-49.6	-2.4	0.54
'F0790124B'	-23.95	-44.4	-2.1	0.48
'F0790124A'	-18.53	-33.2	-1.3	0.46
'F0790126B'	-18.42	-29.7	-0.9	0.39
'F0790126A'	-18.40	-28.3	0*	0.35

*extrapolated value

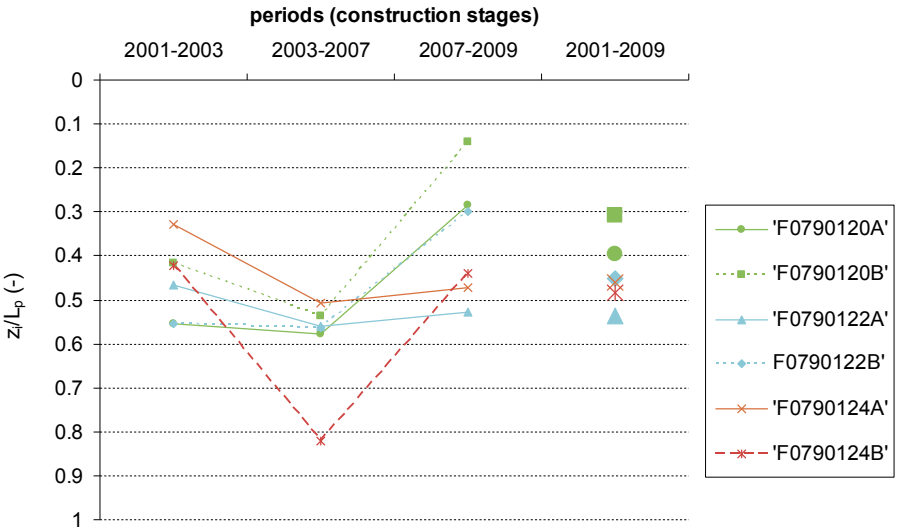


Figure 8.4 Depth z_i/L_p at which the ground and building settlement are similar for each of the construction stages for Govert Flinckstraat 120-124 (Ceintuurbaan)

With the generally available information and some typical values for Amsterdam conditions, an estimate is made for the interaction level zi/Lp based on the pile load and pile capacity. At Govert Flinckstraat 124 a typical Amsterdam timber pile foundation is present as described in Chapter 6 and the pile load and capacity can be estimated. For the 5.9m wide building with two piles beneath each wall section and 1.1 m between the piles along the wall, the average working load is 200 kN/m' wall[1] and thus 200/2*1.1 = 110 kN/pile. The pile capacity is estimated to be about 170 kN/pile based on the characteristics of the Dapperbuurt piles (see Chapter 6).

[1] Working load is determined for a building with 4 floors and 12 m height and includes live load and roof load. Building width 6m, building wall masonry thickness 0.22 m.

W/Wmax thus becomes 65%, leading with Figure 8.5 to $z_i/L_p = 0.55$, which is slightly higher than the measured values in Table 8.1 for Govert Flinckstraat 124. If the pile load is 120-125 kN, W/Wmax=70-75% and z_i/L_p fits the value taken from the measurements best.

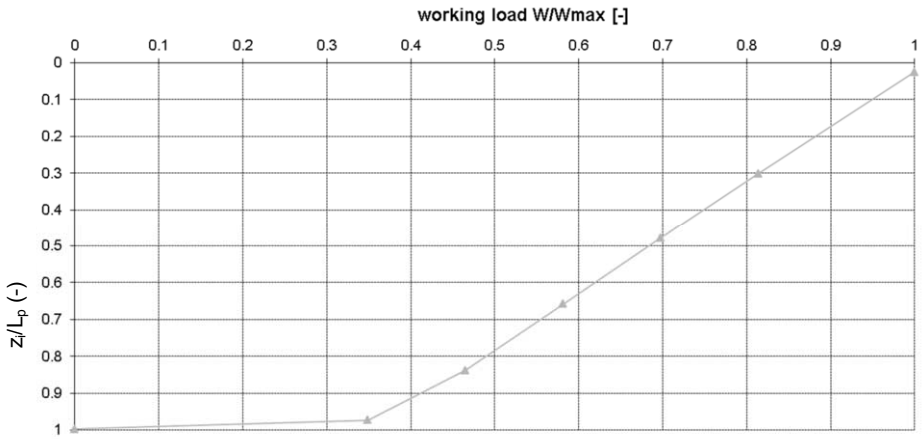


Figure 8.5 Typical z_i/L_p values for pile at Ceintuurbaan with initial negative and positive skin friction fully developed due to subsidence based on DPileGroup calculation.

In cross section 13044E (see Figure 8.1), the buildings Ferdinand Bolstraat 95 and 1st van der Heijdenstraat 90-92 have been analysed. The foundation type for Ferdinand Bolstraat 95 is type 1e, the foundation is renewed in 1971. The pile tips are designed to have a diameter of 0.125m at a depth of NAP -12.25 m, the head of the pile is found at NAP -0.8m. The building has a basement and 6 storeys and the design capacity of the piles was 100-120 kN in 1971. The buildings 1st van der Heijdenstraat 90 and 92 have foundations type 1b, which means the original foundation is still present. The corresponding displacements are shown in Figure 8.6.

Based on the soil and building displacements, the average interaction level z_i/L_p is calculated in Table 8.2 for these buildings. The z_i/L_p value is also determined for the different stages of construction, as is shown in Figure 8.7. This figure shows that the data is not always reliable over shorter periods. The overall values over longer periods show a consistent trend for relatively constant values over time. Between 2007 and 2009, the settlement of the extensometers (both at surface level and at first sand layer) show larger settlements than the manual ground surface and building levelling points, see Figure 8.8. It is thus hard to find good z_i/L_p values for this stage. Consistent monitoring results are obtained for 1st van der Heijdenstraat 92, as is shown in a detailed timeline of the various monitoring systems in Figure 8.9.

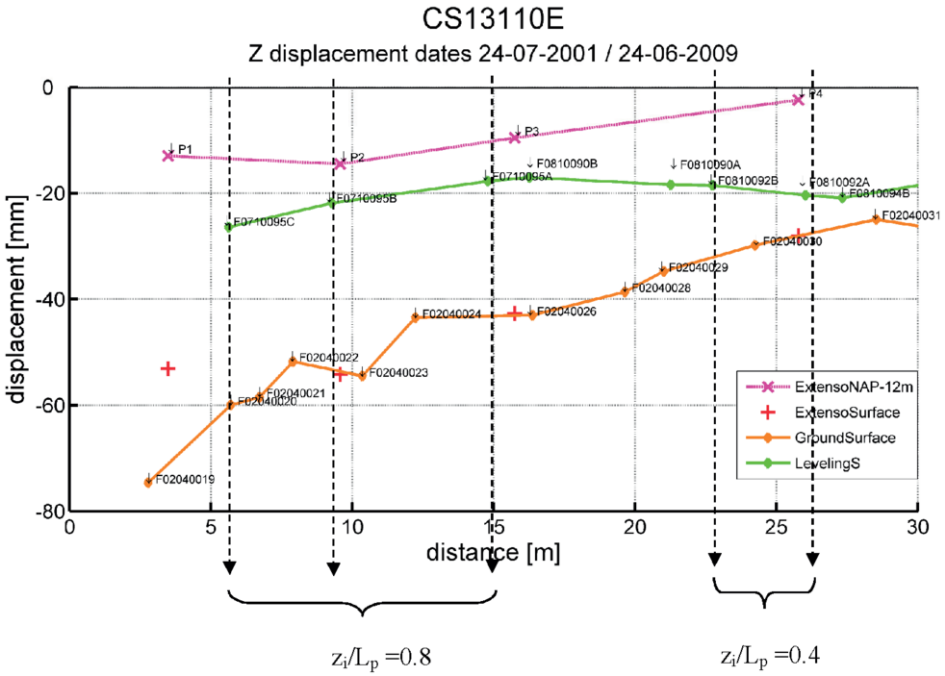


Figure 8.6 Ground and building displacements for Ferdinand Bolstraat 95 and 1e Jan van der Heijdenstraat 90-92 (Ceintuurbaan) in the period 2001-2009 with distance from the deep excavation, with interaction level z_i/L_p derived from measurements

Table 8.2 Building and ground displacements in the period 2001-07-24 – 2009-06-24 for Ferdinand Bolstraat 95 and 1e Jan van der Heijdenstraat 90-92 (Ceintuurbaan) and corresponding interaction level zi/Lp

name	building settlement [mm]	surface settlement [mm]	extensometer first sand layer [mm]	interaction level z_i/L_p [-]
'F0710095C'	-26.4	-60.3	-13.5	0.72
'F0710095B'	-21.9	-53.3	-14.4	0.81
'F0710095A'	-17.7	-43.2	-10.3	0.78
'F0810090B'	-17.0	-43.0	-9.2	0.77
'F0810090A'	-18.4	-34.3	-5.6	0.56
'F0810092B'	-18.5	-32.1	-4.6	0.49
'F0810092A'	-20.4	-27.8	-2.4*	0.29

*extrapolated value

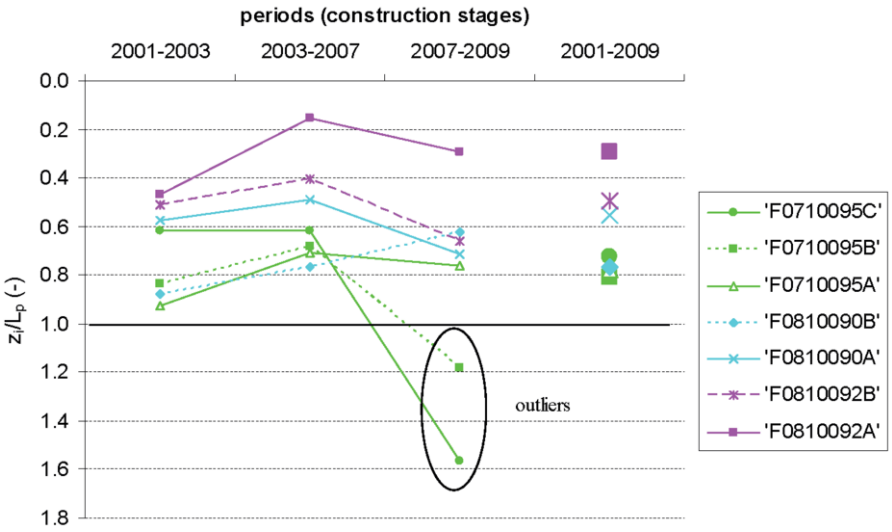


Figure 8.7 Depth z_i/L_p at which the ground and building settlement are similar for each of the construction stages Ferdinand Bolstraat 95 and 1e Jan van der Heijdenstraat 90-92 (Ceintuurbaan)

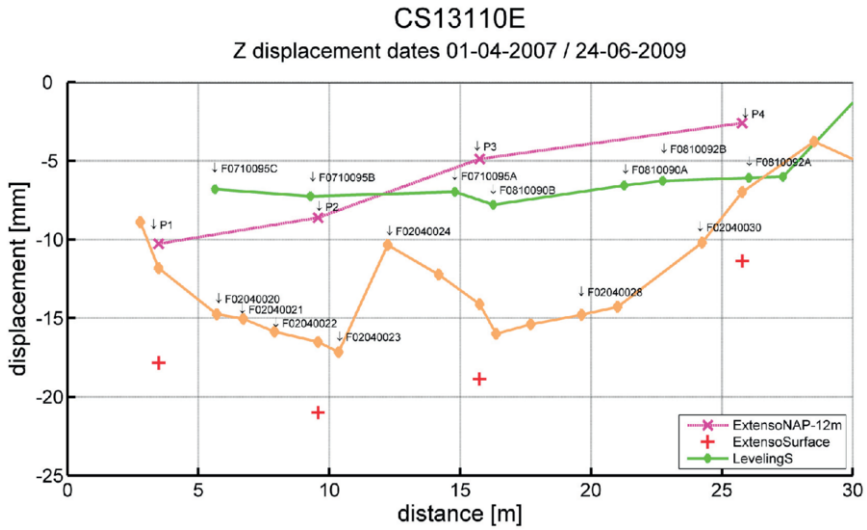


Figure 8.8 Ground and building displacements for Ferdinand Bolstraat 95 and 1e Jan van der Heijdenstraat 90-92 (Ceintuurbaan) during excavation 2007-2009 with distance from the deep excavation.

If for the original foundation of the Jan van der Heijdenstraat 92 the pile load is 140 kN, the interaction level z_i/L_p fits the value taken from the measurements, which is equivalent to W/Wmax=83%. This can be considered as a rather high working load, so possibly some other effect caused such a high interaction level. The result could as well have been affected

by the measurement accuracy, since the settlement at the top of the extensometers (red crosses in Figure 8.8) is larger, leading to a lower interaction level that is more realistic.

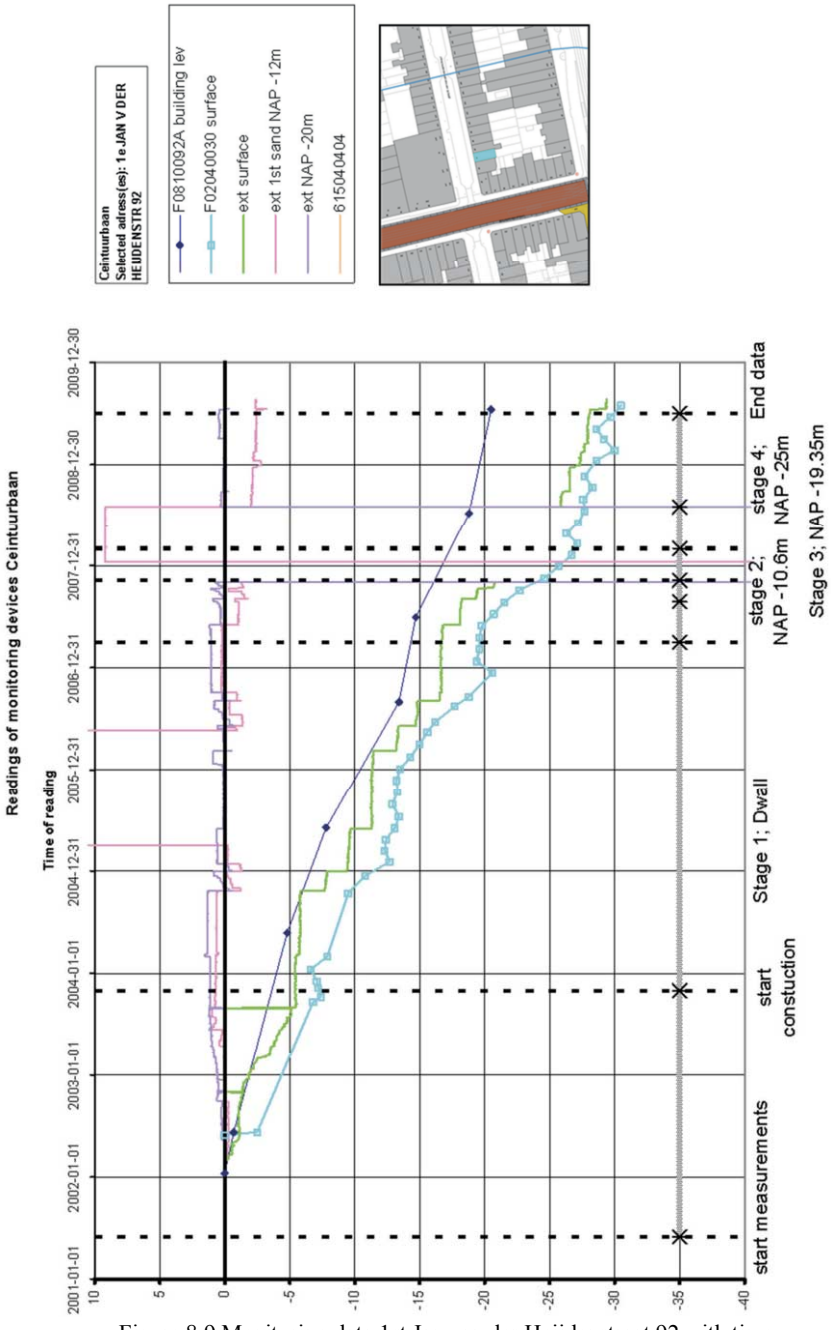


Figure 8.9 Monitoring data 1st Jan van der Heijdenstraat 92 with time

In cross section 13110WN Ferdinand Bolstraat 118 is analysed. The foundation type (see Chapter 4) is type 1e, this means the foundation is renewed. The location of the buildings and monitoring data as well as the deep excavation is shown in Figure 8.10 and Figure 8.11 and the corresponding displacements in Figure 8.13. A selection of monitoring points on the facades is shown in the pictures in Figure 8.12. Ferdinand Bolstraat 118 is constructed in 1893, has four regular storeys, a top floor and no basement. The top of the original foundation is found at NAP - 1 m and the designed pile load is 65 kN (façade 1st Jan vd Heijdenstraat, perpendicular to the station) to 80 kN (walls shared with neighbouring buildings).



Figure 8.10 Aerial view of Ferdinand Bolstraat 118 (Ceintuurbaan) with dimensions

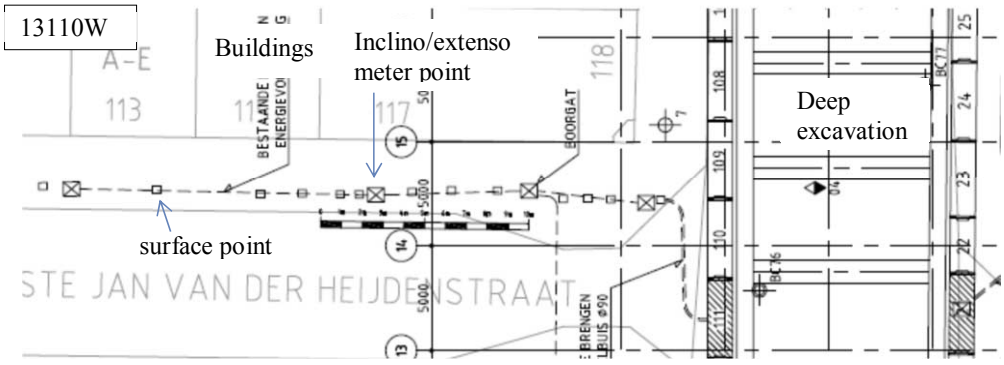


Figure 8.11 Top view of Deep excavation and buildings Ferdinand Bolstraat 118 (Ceintuurbaan)

The building settlements in the period 2001-07-24 – 2009-06-24 are shown in Figure 8.13 and the combined ground and building settlements with corresponding interaction level z_i/L_p in Table 8.3. The building stiffness causes an almost completely rigid rotation of the building, implying the relative rotation is negligible and the expected damage likewise. The average z_i/L_p value is between 0.8 and 1.0 for this building. The interaction level z_i/L_p is determined using the manual ground surface point and the interpolated results of the extensometer on the first sand layer at NAP -12m. As can be seen from Figure 8.14 and in

more detail in Figure 8.15, the extensometer at the surface and the manual ground surface points differ by about 5mm, which leads to a fairly large uncertainty in the determination of z_i/L_p. In the extreme case that the extensometer underestimates the settlement of the first sand layer by about 5 mm, a value for z_i/L_p very close to 1.0 would be found. This is consistent with what is expected for a new, end bearing foundation.



Figure 8.12 Façade with monitoring points Ferdinand Bolstraat 118 seen parallel (left) and perpendicular (right) to deep excavation (Ceintuurbaan)

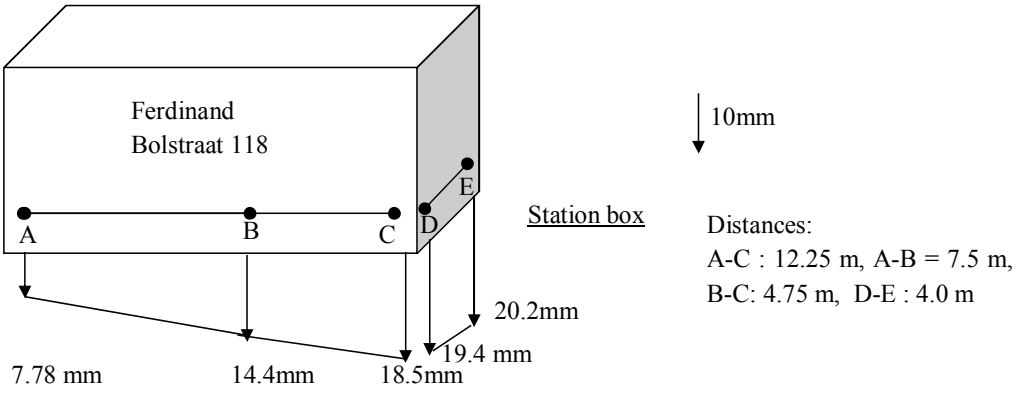


Figure 8.13 Ferdinand Bolstraat 118 building settlements in the period 2001-07-24 – 2009-06-24

Table 8.3 Building and ground displacements in the period 2001-07-24 – 2009-06-24 for Ferdinand Bolstraat 118 (Ceintuurbaan) and corresponding z_i/L_p values

name	**building settlement [mm]**	**surface settlement [mm]**	**extensometer first sand layer [mm]**	z_i/L_p [-]
F0710118A	-7.8	-30.4	-8.1	1.01
F0710118B	-14.4	-40.2	-10.2	0.9
F0710118C	-18.5	-49.8	-13.2	0.9
F0710118D	-19.4	-43.6	-14.9	0.8
F0710118E	-20.2	-43.6	-14.8	0.8

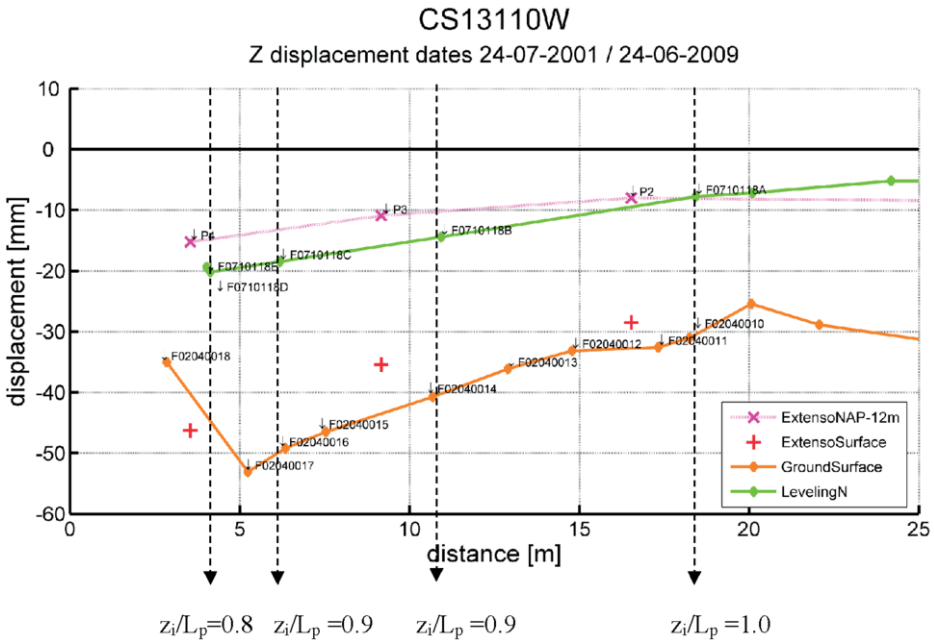


Figure 8.14 Ground and building displacements for Ferdinand Bolstraat 118 (Ceintuurbaan) with distance from the deep excavation, showing interaction levels (z_i/L_p) derived from measurements

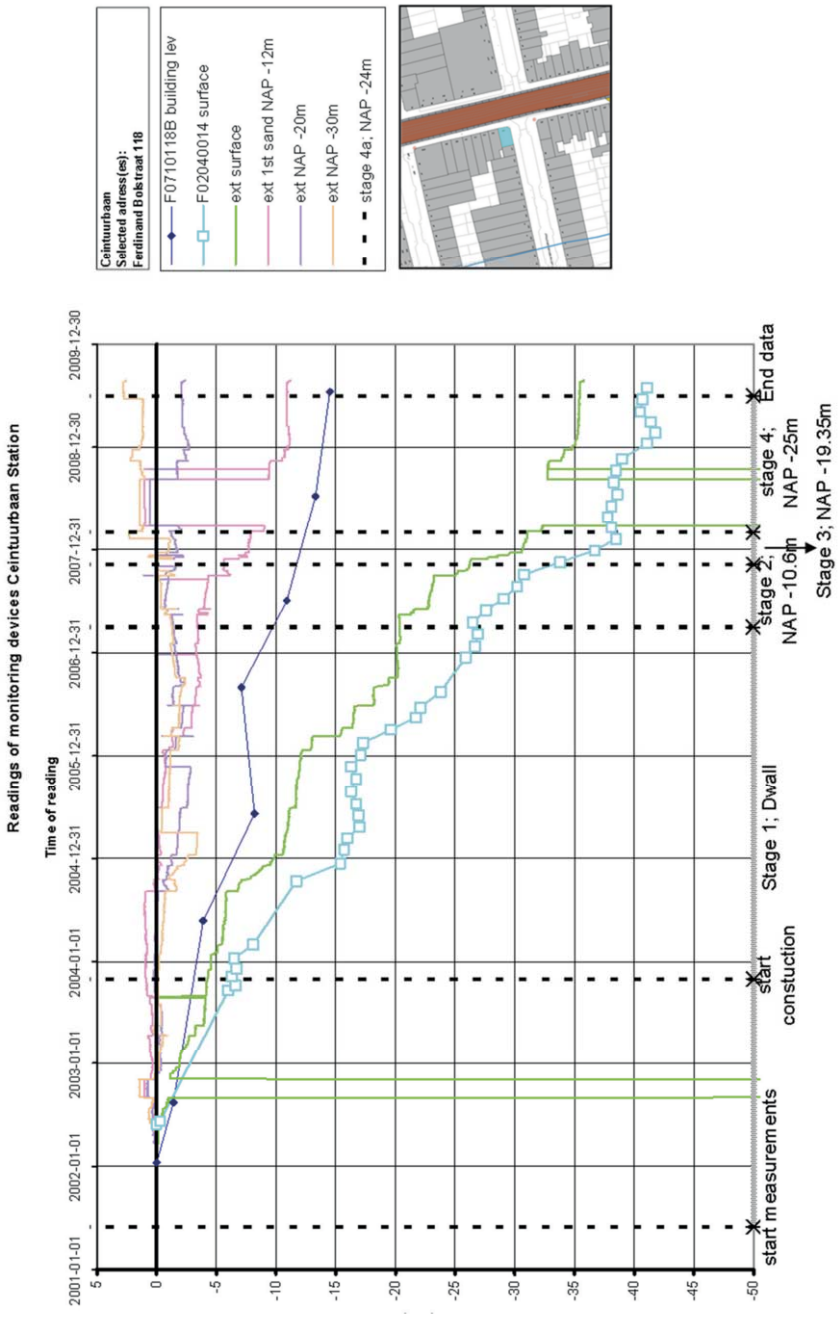


Figure 8.15 Monitoring data Ferdinand Bolstraat 118 with time

8.3 Rokin

At Rokin Station, three different locations are analysed, as shown in the top view of the station in Figure 8.16. For Rokin 93 with its original timber foundation and Rokin 65 with its modern foundation on the East side, and Rokin 84-86 with an old timber foundation on the West side, the soil – pile interaction levels are determined.

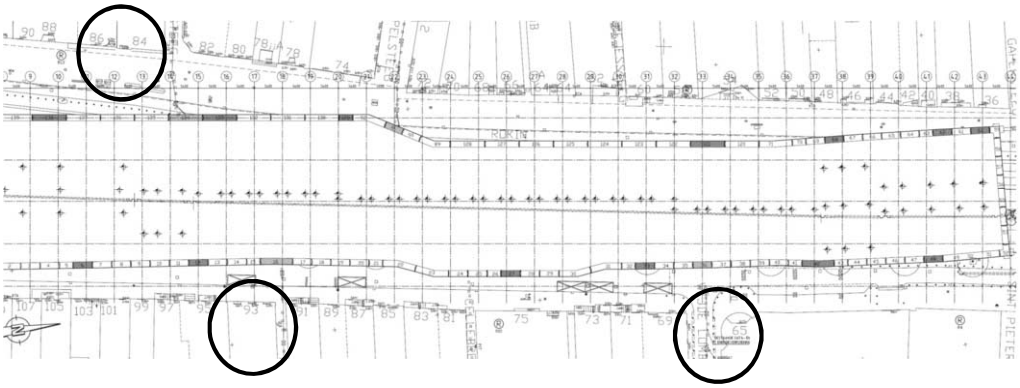


Figure 8.16 Top view of Rokin Station with adjacent buildings

In cross section 11212E Rokin 93 is built in 1896 and still has its original foundation (type 1b). Its foundation class is II. The building has a basement on the Rokin side, a ground floor and 3 storeys above. Monitoring points on the facades are shown in Figure 8.17 and the ground and building displacements in Figure 8.18.

The interaction level z_i/L_p can not be determined for Rokin 93, since the settlement of the extensometer at the first sand layer closest to the excavation shows much larger values than expected. According to Figure 8.18, the building settles less than its foundation layer, which means a 'cantilever' situation seems to be present. Although the building will have some stiffness, a cantilever effect is unlikely. Most likely, there is a 3D effect of the foundation layers' settlement shape. The number of measurements points and their accuracy is not enough to determine the z_i/L_p values for this cross section. What can be determined is that the building settles less than the surface.



Figure 8.17 Façade with monitoring points Rokin 93 (Rokin)

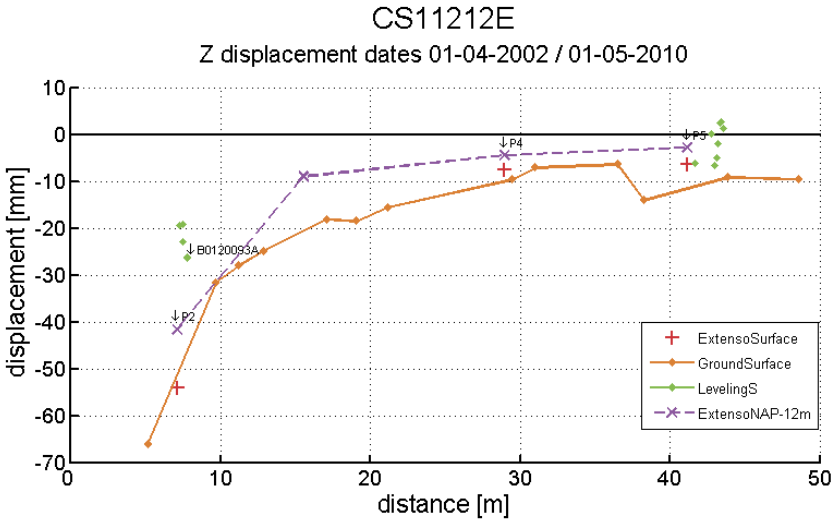


Figure 8.18 Ground and building displacements for Rokin 93 (Rokin) with distance from the deep excavation.

In cross section 11131E, Rokin 65 is a modern building with a concrete pile foundation to the second sand layer (type 2a) at about NAP -20 m depth. The monitoring points are shown in Figure 8.20 with the closest distance to the deep excavation of about 15 m. The subsurface measurements of 11131 can unfortunately not be used, but the settlements of Rokin 65 are so small (within 1-2 mm) over the whole period, that it is safe to state that z_i/L_p is approximately 1.0 for this building. See Figure 8.19 for the settlement of Rokin 65

compared to the surface settlement. This is consistent with a modern end-bearing foundation.

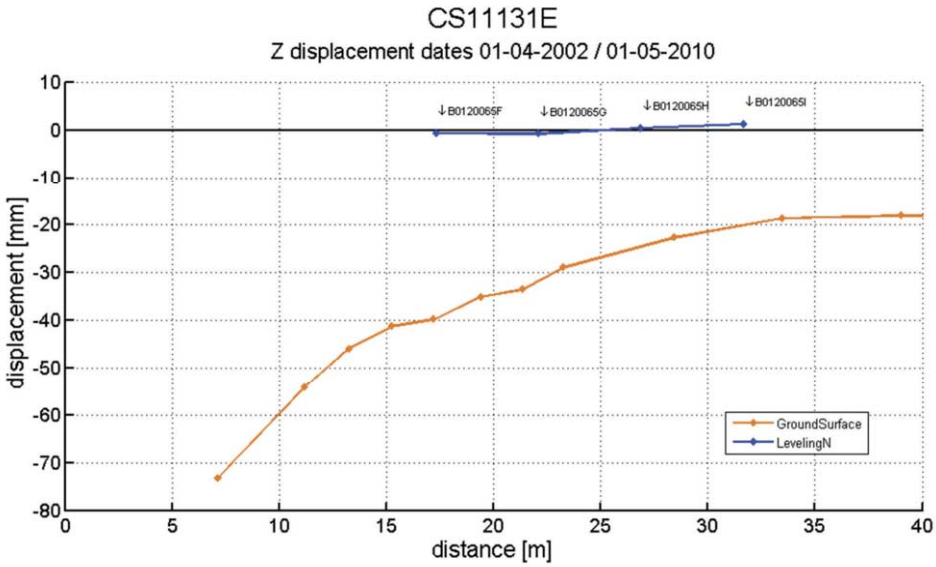


Figure 8.19 Building displacement of Rokin 65 compared to the surface settlement with distance from the deep excavation.



Figure 8.20 Façade with monitoring points Rokin 65 seen from Rokin Station side (Rokin)

In cross section 11233W, the settlement of the buildings Rokin 84 (on the corner), 86 and 88-90 is compared to the ground displacements in this section. Rokin 86's foundation was renewed (type 1e) in 2003 to a depth of NAP -13m, when steel piles with expanded tip, diameter 273/426, were installed to increase the capacity. Rokin 84 and 86 share the foundation of their combined wall. Rokin 88 on the left in Figure 8.21 is built in 1914 and still has its original foundation (type 1b), which was labelled foundation class III during inspection. See Figure 8.22 for location of the monitoring points and Figure 8.23 for the ground and building displacements.



Figure 8.21 Façade with monitoring points Rokin 84 – 86 – 88 – 90 (Rokin)

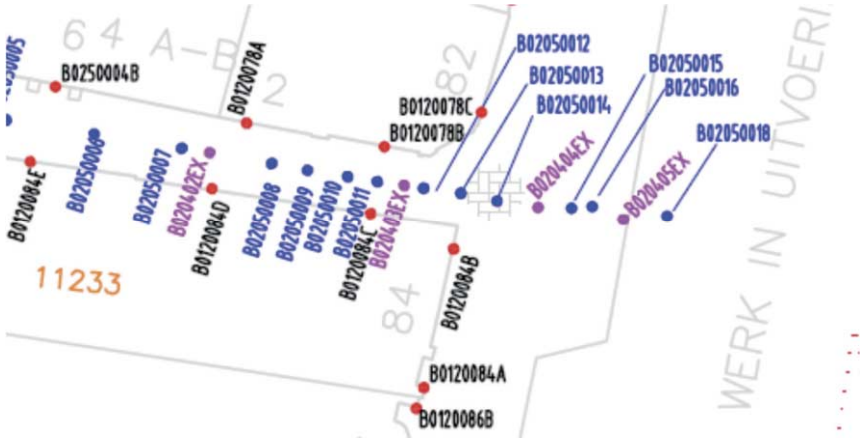


Figure 8.22 Top view of deep excavation (right) and monitoring points in cross section 11233W, Enge Kapelsteeg (Rokin)

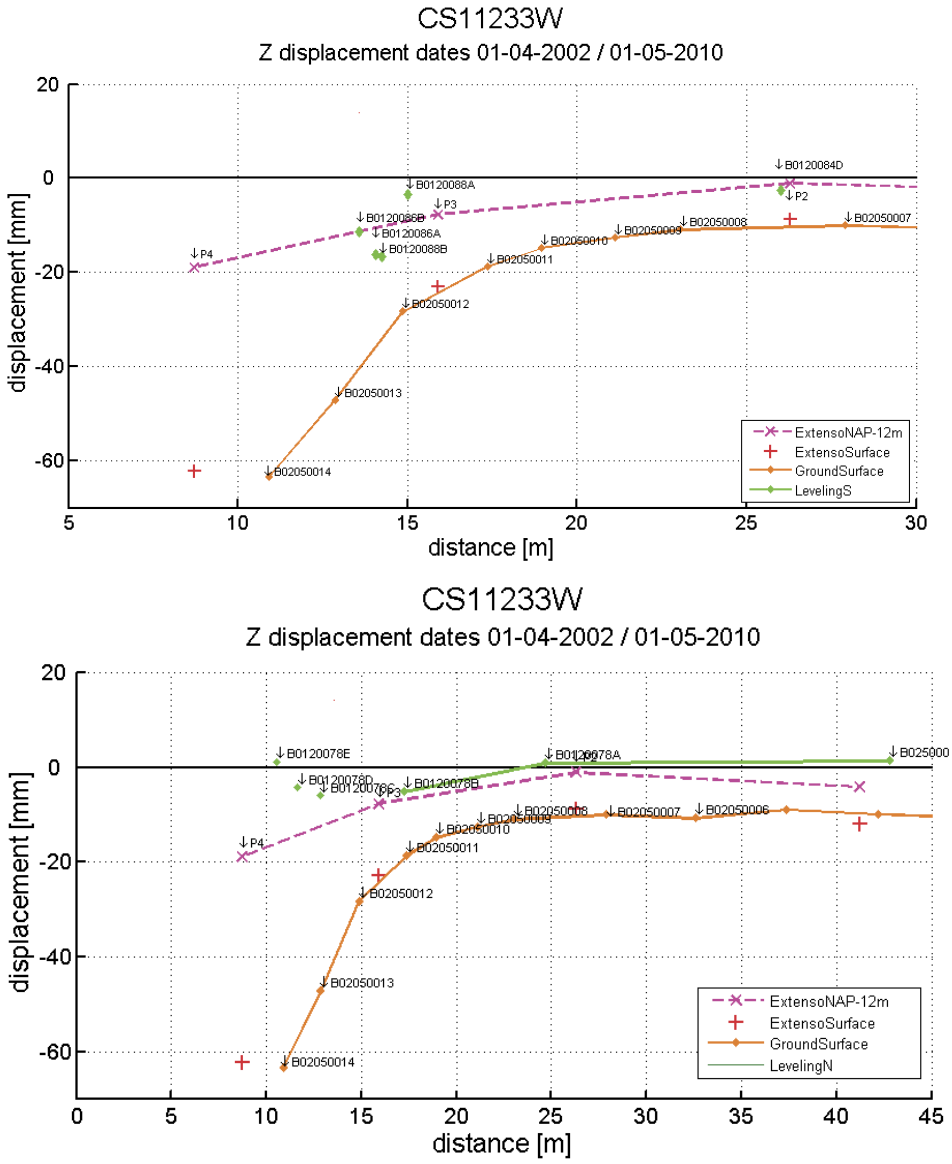


Figure 8.23 Ground and building displacements for Rokin 84-88 (top) and Rokin 82 (bottom) with distance from the deep excavation (Rokin).

Table 8.4 Building and ground displacements in the period 2002-04–01 to 2010-05-01 for Rokin 84-88 (Rokin) and corresponding z_i/L_p values

name	building settlement [mm]	surface settlement in 11233W [mm]	extensometer first sand layer 11233W [mm]	interaction level z_i/L_p [-]
'B0120084D'	-2.6	-10.5	-1.3	0.85
'B0120086B'	-11.5	-40.4	-11.3	0.99
'B0120086A'	-16.2	-36.0	-10.6	0.78
'B0120088B'	-16.6	-34.1	-10.3	0.74
'B0120088A'	-3.5	-27.7*	-9.1*	1.3*

* see explanation below

The average interaction level z_i/L_p in Table 8.4 is between 0.8 and 1.0 for Rokin 84 and 86, who both have a renewed foundation. Also the settlement markers for Rokin 84 that are not shown in this table (A, B, C) result in comparable values for z_i/L_p. The interaction level z_i/L_p is 0.7 for Rokin 88 on the side towards Rokin 86 and larger than 1 for the other side. Rokin 88 is the last building influenced directly by the deep excavation for Rokin Station, half-way this building the shallow excavation for the station's entrance starts. The surface and extensometer measurements in the Enge Kapelsteeg can not be used to determine the interaction level z_i/L_p at this distance away from the side street.

Rokin 82 (monitoring numbers joint with Rokin 78) is located on the north side of cross section 11233W. The building is constructed in 1909 and has an original timber foundation (type 1b) with Foundation Class II with 3 additional steel piles installed in 1977. In Figure 8.23 it looks like the building settles less than foundation layer. Measurement points D and E are located at larger distance from the side street, but points A, B and C are expected to settle at least the same amount as the foundation layer. A small part of this difference can be attributed to the fact that the selected dates for the graph could not be an exact match for the levelling points (measured until 2009-07) and the extensometer (measured until 2010-05), but only 0.5 mm extensometer settlement occurred between 2009-07 and 2010-05. Since the building is supposed to have only 3 new piles and mainly its original foundation, it is rather surprising that it settles such a small amount, even if due to measurement uncertainties the settlement would be the same as the first sand layer (z_i/L_p is close to 1). No further information of the foundation is available to make any more detailed assessment.

Due to problems with the subsurface measurements at cross section 11192W, no useful comparison with building displacements could be made.

8.4 Vijzelgracht

Most of the buildings along the Vijzelgracht are founded on the first sand layer at about 12 to 13 m below surface level. Foundations are either the original timber foundations or steel piles in case foundation renewal took place. Only certain buildings have more recent foundations in the second sand layer (for Vijzelgracht station those are Vijzelgracht 2,

48-58, 51-59, Lijnbaansgracht 310, Weteringschans 2 and 159/161, Nieuwe Vijzelstraat 2 and Nieuwe Weteringstraat 5).

The quality of the measurements is particularly difficult at Vijzelgracht station. The extensometers in 12197E give reasonable results if some periods are filtered out. In cross section 12270E boreholes 01 and 02 are not available after 2005. Cross sections 12197W and 12270W are both influenced by leakage incidents, see Chapters 4 and 10. All surface and manual levelling data are available and reliable.

In the best available cross section, 12197E, the building at Noorderstraat 7 was reconstructed in 1930, has a half-basement, ground floor and 3 storeys, see Figure 8.24. Its foundation is categorized as type 1c and Foundation Class II. Noorderstraat 7 is structurally combined with Vijzelgracht 17 around the corner. Vijzelgracht 19 at the corner itself is also shown in Figure 8.25.



Figure 8.24 Façade with monitoring points Noorderstraat 7 and Vijzelgracht 19 (Vijzelgracht)

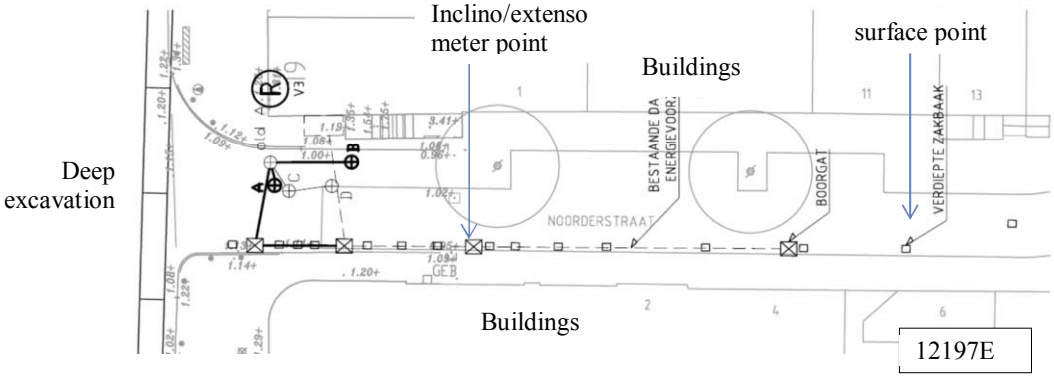


Figure 8.25 Top view of deep excavation (left) and buildings in Noorderstraat (Vijzelgracht)

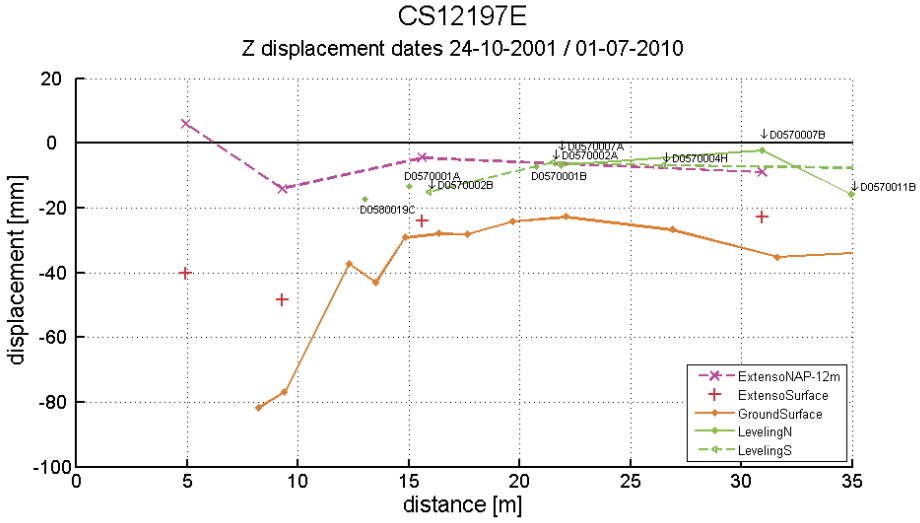


Figure 8.26 Ground and building displacements for Noorderstraat (Vijzelgracht) with distance from the deep excavation.

The building and ground displacements are shown in Figure 8.26. For Vijzelgracht 19 this leads to an interaction level z_i/L_p of 0.7. For Noorderstraat 1, z_i/L_p is 0.7 – 1.0, for Noorderstraat 7 z_i/L_p is around 1.0 and for Noorderstraat 2 (opposite to Vijzelgracht 19) z_i/L_p is between 0.6 and 1.0. The results for the interaction factor z_i/L_p are fairly high, which indicates a good quality of the foundation. The accuracy at larger distances from the wall is low due to limited number of measurement points on first sand layer. The best estimate for z_i/L_p for the buildings in this cross section is most likely about 0.6 to 0.7, based on the three monitoring points within 20 m from the excavation.

The working load W per pile for Noorderstraat 7 is 70-100 kN based on design calculations from 1930 found in the Amsterdam Archive. For an average Amsterdam pile the maximum capacity is about 170 kN, leading to W/Wmax is 40-60% and an initial z_i/L_p due to negative skin friction by subsidence of 0.65-1.0. Based on a modern calculation the working load W is estimated as 85 kN/pile, leading to similar results. The measured and calculated interaction level z_i/L_p are sufficiently close.

In cross section 12270W, the subsurface measurements are not available. It is however interesting to analyse the behaviour or Vijzelgracht 48, which is founded in the second sand layer. The modern building is constructed in 1979 and its foundation consists of concrete piles to NAP -17 m – NAP -20 m, categorized as type 2a. The building has a basement. The location of the monitoring points along cross section 12270W is shown in Figure 8.27 for the building and Figure 8.28 for the surface measurements. Figure 8.29 shows the corresponding displacements. The period considered for this graph is end just before the first incident at the Vijzelgracht (June 2008). The maximum building settlement is 4.3 mm for 48J. The extensometer results are not reliable, so can not be used to compare and find the overall interaction level. The 4.3 mm settlement is caused by diaphragm wall construction and installation of the deep jet grout strut, which both have an influence on the ground displacements at depth and reach at least 15 m away from the works.

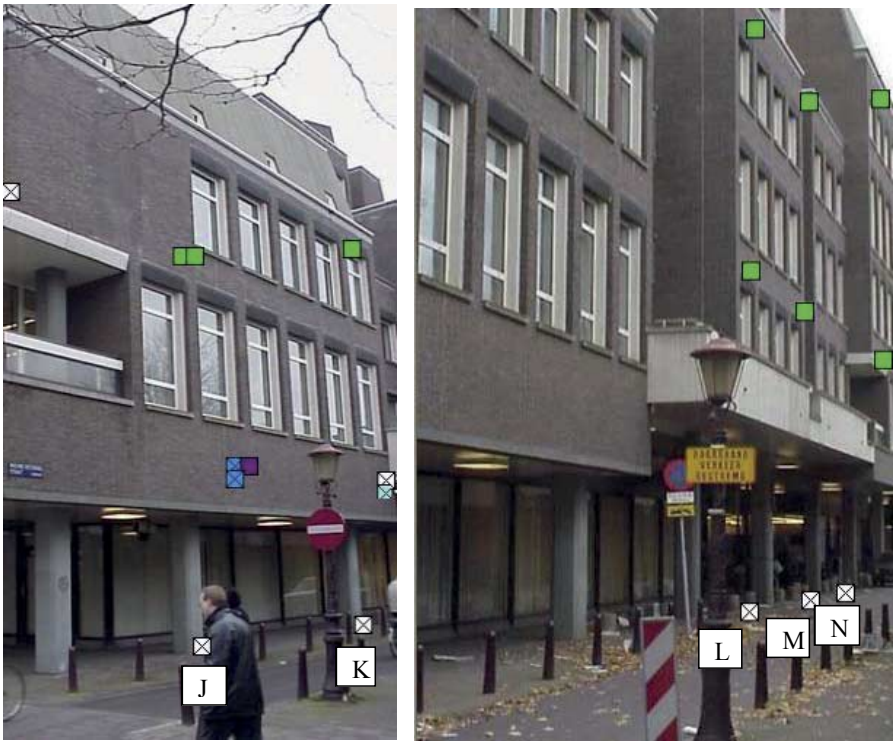


Figure 8.27 Façade with monitoring points Vijzelgracht 48 seen from Vijzelgracht

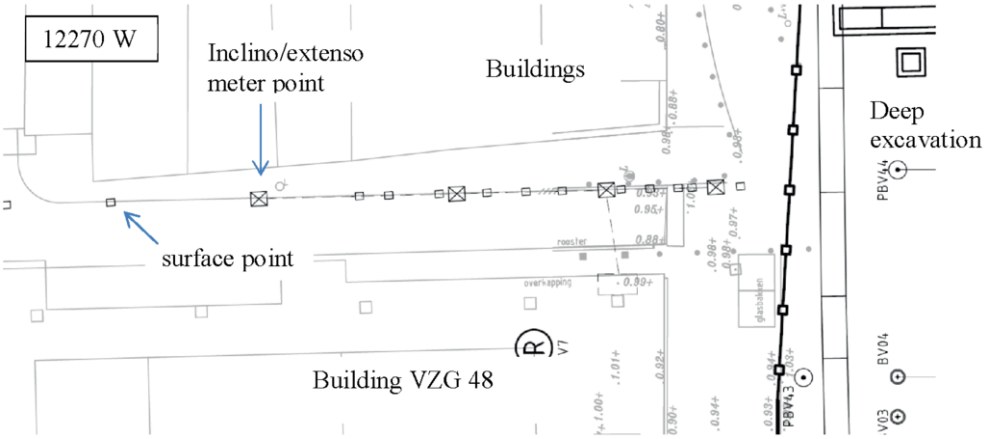


Figure 8.28 Top view of deep excavation and building Vijzelgracht 48 at bottom (Vijzelgracht)

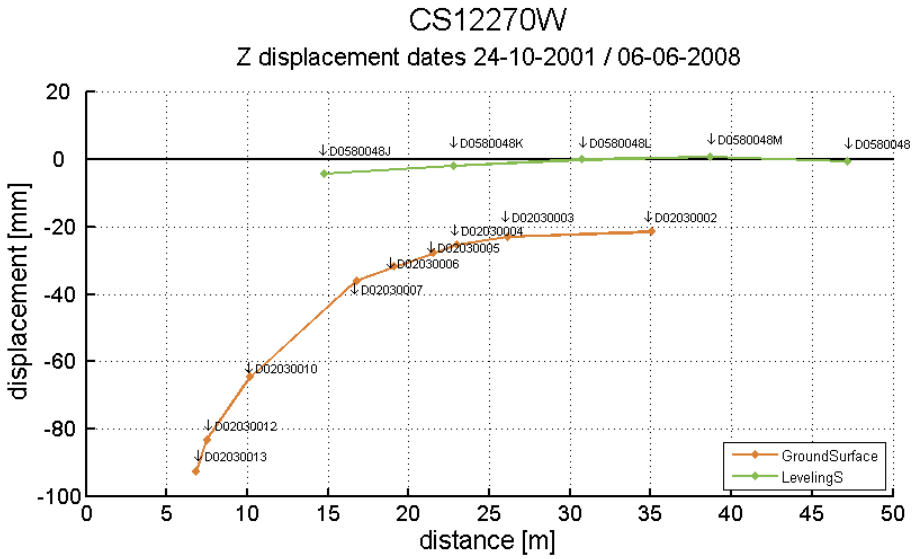


Figure 8.29 Ground and building displacements for Vijzelgracht 48 (Vijzelgracht) with distance from the deep excavation.

8.5 Influence of building characteristics on soil- pile interaction

In sections 8.2, 8.3 and 8.4 for a selection of buildings the interaction between soil and pile has been determined in detail based on an estimate of the foundation capacity and working load of the piles. In most cases in practice, no detailed information is present about the foundation but it would be practical to estimate the amount of interaction based on generally known building characteristics, such as the year of construction, the number of storeys or the presence of a basement. For a large number of buildings along the three stations the

interaction level has been determined based on the monitoring data, without comparing it to a prediction based on foundation details. For these buildings, the interaction level is compared to known building characteristics.

For a selection of building characteristics, an analysis is made to correlate them with the measured interaction level. In Chapter 7 it was determined that the interaction level depends strongly on the following dimensionless factors:

- working load compared to the maximum pile capacity (W/Wmax),
- the ratio of the settlement difference between surface level and foundation level and the relative displacement necessary to fully develop the shaft friction ($\Delta S/D_z$)
- the increase in maximum shaft friction with depth $\tau_{max;0}/\ \tau_{max;Lp}$.

The ground displacement ΔS differs throughout the construction stages. The soil characteristics D_z and τ are similar for all three stations, so can not be used to find correlations.

The pile load and pile capacity can not be determined directly, so indirect characteristics are needed to give an indication for each of the influencing factors. A factor that may determine the working load W is the number of storeys of the buildings. Characteristics that influence the pile capacity Wmax include the year of construction and the foundation class, assuming later buildings have better foundations. For each of these indirect characteristics the correlation with the interaction factor z_i/L_p has been determined in Figure 8.30, Figure 8.31 and Figure 8.32 respectively. It should be noted that the interaction factor for some buildings is smaller than 0 or larger than 1, which is theoretically impossible unless load redistribution or pile failure due to structural problems or stress relief occurs. In addition, uncertainty or deviations in the measurements could cause such otherwise unlikely numbers. In the sensitivity analysis, these values have been included as they indicate a certain trend of values close to 1 or close to 0.

There is some evidence that the Foundation Class can give an indication for the interaction between building and soil. Foundation Class I (good foundations, see Chapter 4) has no values of z_i/L_p smaller than about 0.5 and Foundation Class II not smaller than 0.3. In all foundation classes however, z_i/L_p values up to 1.0 can be found. A foundation in Foundation Class I is less likely to have a neutral level higher than halfway down the pile. There are no buildings in the lowest Foundation Class IV, since they all had their foundation renewed before the excavation started.

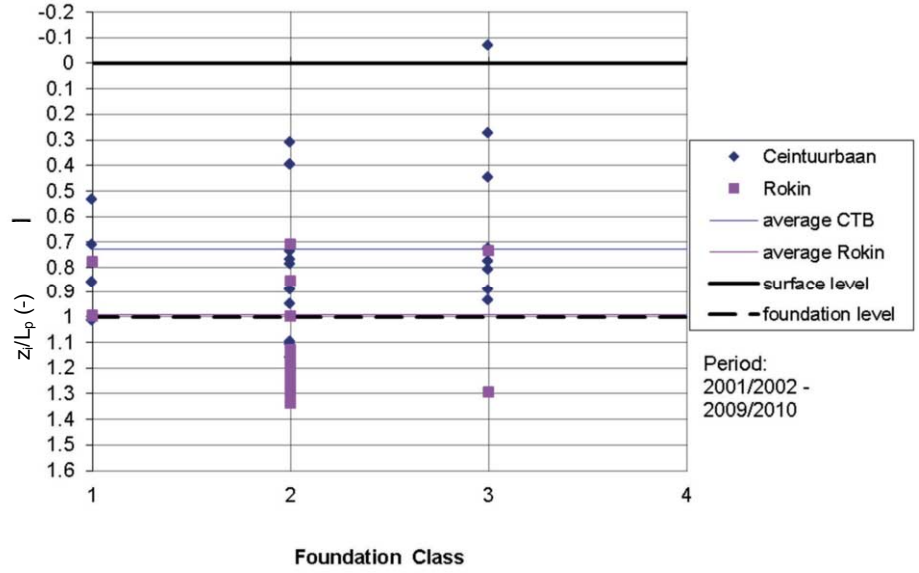


Figure 8.30 Interaction level versus Foundation Class (1: good quality , 2: reasonable, 3: moderate, 4: unacceptable)

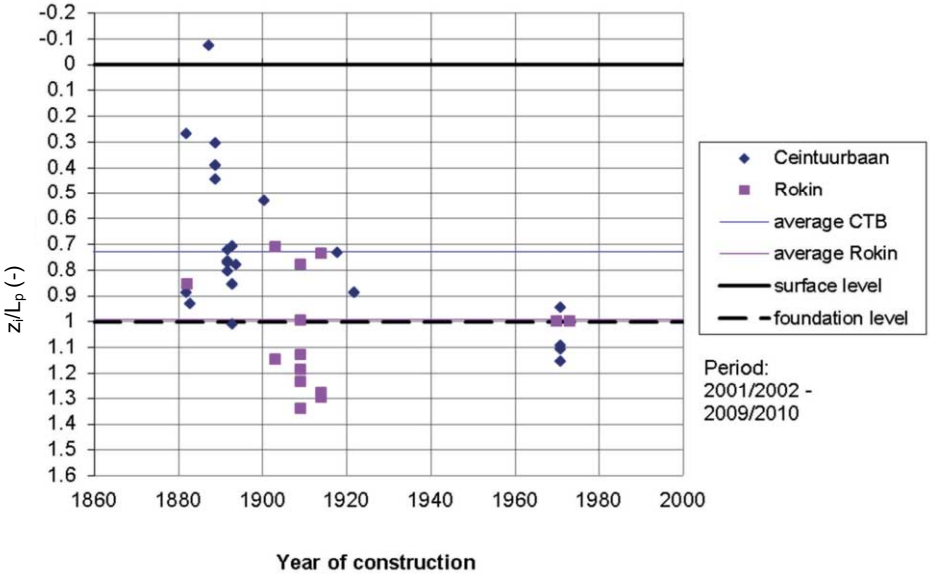


Figure 8.31 Interaction level versus the year of construction

The interaction level versus the year of construction also shows some indication that higher interaction levels (lower z_i/L_p values) are more likely found in the older buildings. After 1900, no z_i/L_p values smaller than 0.5 are found. Due to the specific periods in which the buildings have been constructed along the stations, no buildings between 1920 and 1960

could be evaluated. Only a limited number of modern buildings from the 1970's could be investigated, which usually have an interaction level close to 1.0.

The number of floors could be seen as an indicator for the load on the pile (W). Figure 8.32 however does not show a clear relationship. Most buildings have 5 or 6 floors, so little discrimination could be made. It could also be the case that buildings with more floors are built with more piles.

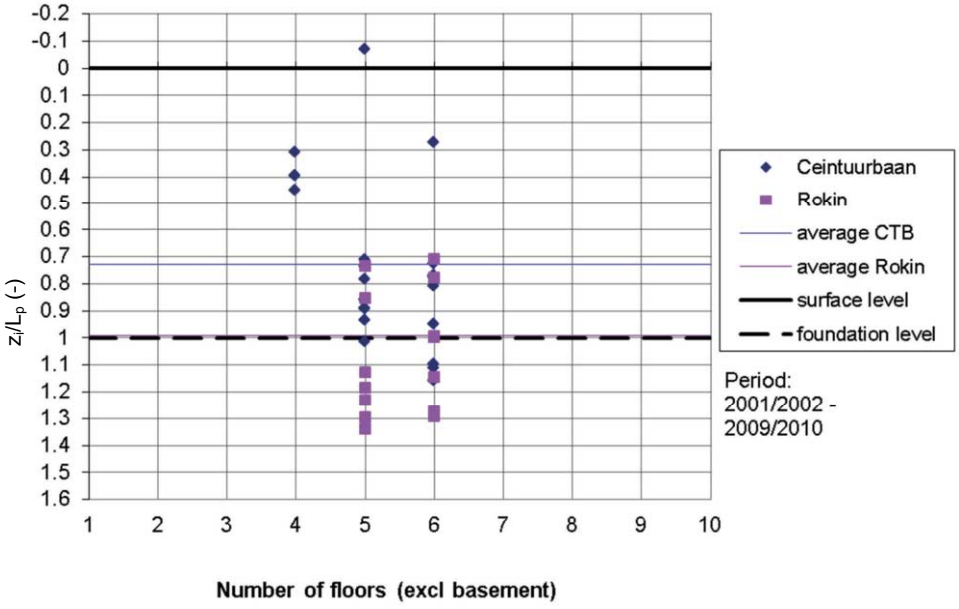


Figure 8.32 Interaction level versus number of floors

Another possibly relevant characteristic is the presence of a basement or half-basement. In case a basement is present, the foundation floor is found below the surface. In addition, the net weight of the building may be less due to presence of uplift force from the ground water. Even without considering the pile foundation, the building is expected to settle not more than the soil at basement level, which is less than at surface level. The interaction level z_i/L_p will most likely not come close to 0. Figure 8.33 indicates that the presence of a basement indeed increases the interaction level z_i/L_p towards 1. Half basements show this effect to a lesser extent.

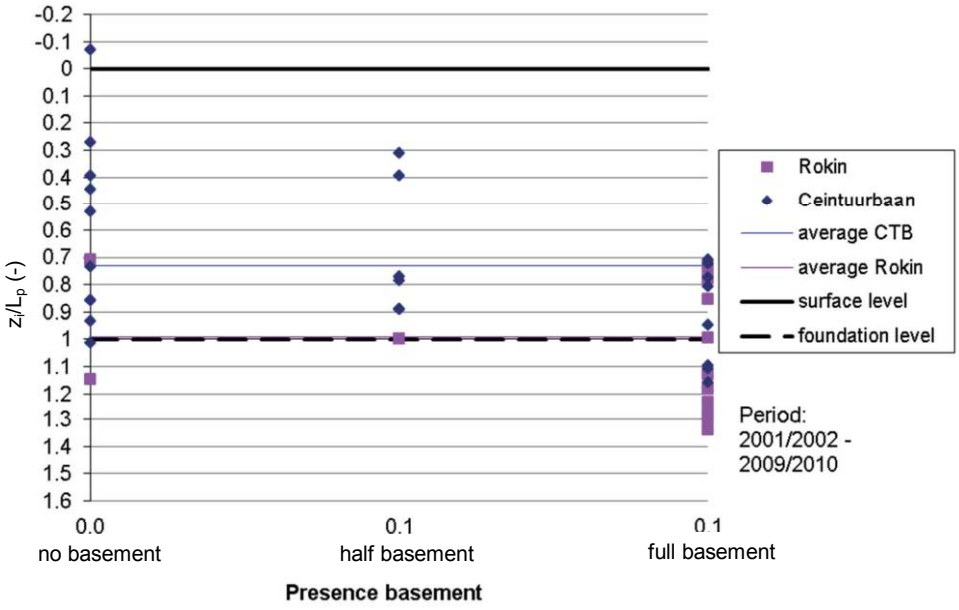


Figure 8.33 Interaction level versus presence of basement

It can be concluded that the most likely buildings to have an interaction level between 0 and 0.5 (high interaction level) are built before 1900, have Foundation Class III and do not have a basement. For all other buildings, any interaction level z_i/L_p between 0.5 and 1.0 is a likely outcome depending mainly on the working load versus pile capacity (W/Wmax).

The effect of the soil settlement profile has been determined by plotting the interaction level z_i/L_p versus ΔS, the difference between the ground displacement at the surface and at the depth of the foundation (NAP -12m) in Figure 8.34.

The lines of W/Wmax in Figure 8.34 have been determined by the numerical solution of DPileGroup for the typical Amsterdam pile (see Chapter 7). This pile has been subjected to ground displacements before the excavation works due to a general subsidence in the area causing negative skin friction. Assuming such a friction has developed prior to the excavation makes z_i/L_p independent of ΔS. The main factor of influence in that particular situation is W/Wmax, since this factor determines the initial neutral level due to the subsidence as well as the interaction level z_i/L_p during excavation works. The measured values in Figure 8.34 show that most of the piles must have had a working load of between 40% and 80% of the maximum capacity, independent of ΔS. If for the typical pile this maximum is 170 kN, the average pile load is between 70kN and 140 kN, which complies well with 100 kN being the generally expected pile load.

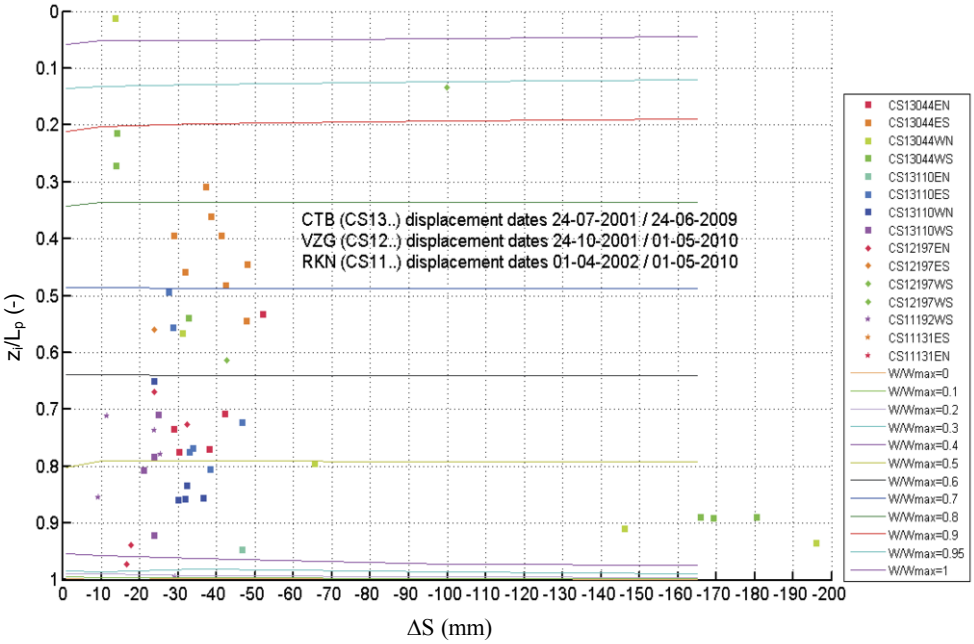


Figure 8.34 Interaction level versus ground settlement difference ΔS (ground settlement at surface level minus ground settlement at pile tip level) and numerically determined lines of equal W/Wmax values

For new construction projects, based on an assumed working load (W/Wmax), the interaction level z_i/L_p can be estimated based on Figure 8.34.

8.6 Horizontal interaction of soil and piled buildings

The construction of deep excavations not only causes deformations in a vertical direction, but also in a horizontal direction. The previous sections of this chapter mainly focussed on the vertical displacements. Horizontal displacements of the buildings however, can be just as important in the development of building damage. In this section, the horizontal interaction between soil and building is studied based on the monitoring results of the Amsterdam deep stations.

Part of this displacement is caused by the rigid rotation of the building, leading to larger displacements at the top of the building compared to the lower parts near the foundation. The horizontal displacement of the building towards the excavation at foundation level is one of the main factors that determine the horizontal strain in the building, which is an important parameter in the damage assessment.

The horizontal strain in a building is the difference between the horizontal displacement at each end of the building divided by its length. In most damage assessment procedures, it is often assumed that the soil displacement at the foundation level of the building is fully

transferred to the building. Thus the horizontal soil strain is taken as representative for the building strain. El-Shafie (2008) already showed that for buildings with shallow foundations, this interaction depends mainly on the roughness of the soil-foundation interface. A larger part of the soil displacements was transferred to buildings with shallow individual footings and/or rough interfaces. In this section this effect is studied for piled buildings and more specific the typical Amsterdam timber pile foundation.

To determine the relative displacement of the building to the soil in horizontal direction, one needs both the horizontal soil displacement and the horizontal building displacement. Unfortunately, for the Amsterdam cases only the vertical soil displacements can be determined from the monitoring data with enough reliability. If a relationship between the horizontal and vertical soil displacement is assumed, the vertical soil displacement could be used instead of the horizontal displacement. Figure 8.36 the building displacement in the X direction (towards the excavation, "Xbuilding") is shown versus the vertical displacement of the soil surface at the same location ("Zsoil"). The building displacement in the X direction is determined using the prism at the top of the building, the prism at mid-height and the height of the building, according to Figure 8.35. Street level is taken equal to the reference level NAP. Due to the flexible nature of the timber piles, it is assumed that the horizontal displacements at the surface are driving the horizontal building strains and not the displacements at depth. This is supported by the fact that no relationship is found between the horizontal building displacement and the vertical building displacement. For the integrity of the piles itself, the difference between the horizontal soil displacements at the top and bottom of the pile are important, but this topic is not investigated here.

Based on the values in Figure 8.36, it can be concluded that a large variation occurs in horizontal building displacements as a result of the construction of the deep excavation. Horizontal building displacements at street level are usually smaller than 10 mm and about 20% of the vertical surface displacement at the same location. For Rokin Station in the period 2002-2010 the horizontal surface displacement compared to the vertical should be about a factor 0.6 based on a Plaxis calculation (including mainly excavation effects). This means the horizontal building displacement at street level is about 0.2 /0.6= 1/3 of the horizontal soil displacement. It seems that the building's interface for piled foundations are not as smooth as in case of the shallow foundations as shown by El-Shafie (2009). The piles force the building to follow the soil displacement to this extent, which causes horizontal strains in the building. For piled buildings in Amsterdam, it is recommended to assume that at least one third of the soil displacements are transferred to the building.

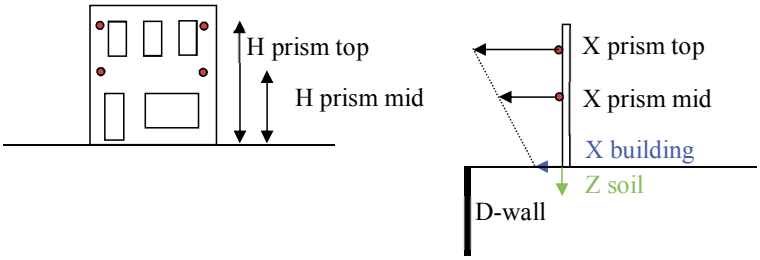


Figure 8.35 Horizontal displacement of building at street level (left: front view, right: side view)

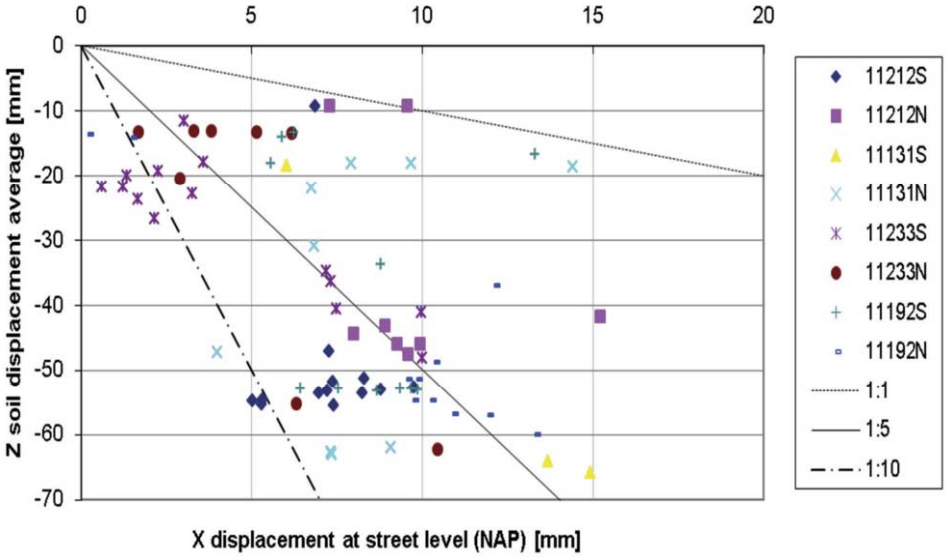


Figure 8.36 Displacements of the building in horizontal (X) direction and soil in vertical (Z) direction for Rokin station (2002-2010) with trend line (1:5), upper- and lower bound values.

Figure 8.37 shows that the Xbuilding/Zsoil values for Rokin and Ceintuurbaan Station combined can be represented by a lognormal distribution (best fit) with a median of 0.19. This means that 50% of the cases the horizontal building displacement is smaller than one fifth of the vertical soil displacement at the same location. Based on the lognormal distribution (with standard deviation 0.66), in more than 93% of the cases the horizontal building displacement does not exceed half of the vertical soil displacement.

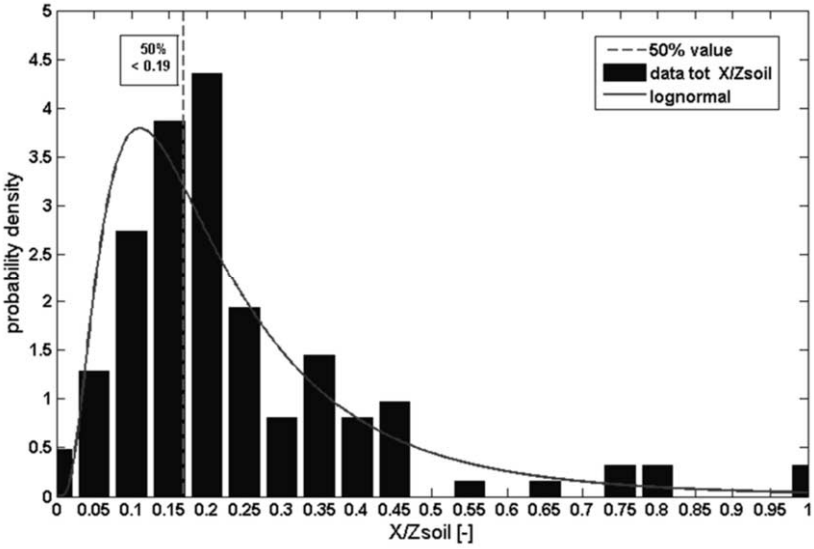


Figure 8.37 Histogram plots and best-fit lognormal distribution for probability of X/Zsoil values for Rokin Station and Ceintuurbaan Station combined

8.7 Summary and conclusions of soil- pile interaction based on measurements in Amsterdam

Construction activities influenced the buildings along the deep excavations for the North South Line. The soil – pile interaction is analysed for a number of specific buildings, which were selected based on the availability and the quality of the monitoring data and the historical data about the structure. The building settlement of the piled buildings is larger than the ground settlement at tip level (Extensometer at NAP-12m), but smaller than the surface settlements. This indicates a neutral level above the foundation layer (positive shaft friction). For each building the interaction factor z_i/L_p has been determined, where z is the depth along the pile where the pile and soil settlement during the construction works are equal and L is the length of the pile. When $z_i/L_p = 0$ the pile settlement is equal to the surface settlement.

Based on the soil and building displacements, the average z_i/L_p factor is 0.3 – 0.8 for most original timber pile foundations and 0.8-1.0 for most renewed foundations in the first sand layer. Some modern buildings in the second sand layer settle very little and indicate the interaction factor z_i/L_p to be close to 1.
The factor z_i/L_p varies sometimes significantly between the different construction stages, which is mainly attributed to measurement accuracies. The initial settlement ratio z_i/L_p proved to be a good reference for the overall settlement ratio to be expected during all construction works.

Buildings for which the pile load and capacity can be estimated, show a good correlation with the calculated interaction factor z_i/L_p. In most cases in practice however, no detailed information is present about the foundation and the interaction factor has to be assessed using generally known building characteristics. Some evidence is found that the Foundation Class and the year of construction can give an indication for the interaction between building and soil as indirect representatives of Wmax. Buildings with a basement are less sensitive (z_i/L_p is higher) than for buildings without basements, but no evidence could be found for such a relationship with the number of floors of a building. Other factors could not be studied due to a lack of variety between the buildings or did not show any significant relevance.

It is concluded that the most likely buildings in Amsterdam to have an interaction factor between 0 and 0.5 (high neutral level) are built before 1900, have Foundation Class III and do not have a basement. For all other buildings, any factor of z_i/L_p between 0.5 and 1.0 is a likely outcome depending mainly on the working load versus pile capacity (W/Wmax). The effect of the shape of the soil settlement with depth is not known for the Amsterdam cases, because the shaft friction was already fully mobilized before the excavation works started (due to subsidence).

A large variation occurs in horizontal building displacements as a result of the construction of the deep excavation. Horizontal building displacements at street level are usually smaller than 10 mm or 50% of the vertical surface displacement at the same location. For piled buildings in Amsterdam, it is recommended to assume that at least one third of the horizontal soil displacements are transferred to the building.

CHAPTER 9 BUILDING DISPLACEMENTS

9.1 Introduction

This chapter intends to provide characteristics to determine the possible damage to the building resulting from the displacements transferred from the soil and the piles to the structure. This is the last step of the building damage assessment procedure. For this step it is important to know which part of the soil displacements will be transferred to the building. This transfer is the main focus of this chapter.

The category of damage the building experiences depends on the differential vertical displacements resulting in a deflection ratio or relative rotation of the building, as described in section 9.2 and the horizontal strain transferred to it as described in section 9.3. Validating current building damage assessment procedures based on these characteristics is beyond the scope of this study. Chapter 10 compares predicted and actual damage related to the incidents that occurred at Vijzelgracht Station.

9.2 Vertical deformations of piled buildings

9.2.1 Construction stages

Figure 9.1, Figure 9.2 and Figure 9.3 show the measured vertical displacements along the streets perpendicular to the stations based on the available prisms. The prisms are usually located at first floor level. Results of prisms at the top of the buildings or manual levelling points at the ground floor level can be seen in section 9.2.2. The results of the prism measurements can be used to determine the contribution of the different construction stages, in the figures shown as reference dates which can be compared to the stages described in Chapter 4. In general, the pink line represents the base monitoring results (no construction works), the orange lines represents the building settlement after the preliminary activities and the subsequent colours indicate the different excavation stages. Rokin and Vijzelgracht station's purple lines correspond with an excavation level of NAP-12 m to NAP -15 m. At Ceintuurbaan Station, the purple line (24-06-2009) relates to the excavation of NAP -25.6m. Building measurements in a particular cross section (or façade) are shown with lines, while measurement points out of these planes are shown as separate points.

From these figures, it follows that the largest influence of the construction on the buildings is due to the preliminary activities (diaphragm wall construction and subsidence over 4 years

between 2003-2007). During excavation of the station, the additional building deformations are usually less than 10 mm. In all stages, deflection ratios are small (in the order of 0.03%). The different facades along a cross section show that in most cases the buildings behave as if they where all part of the same structural units with shared walls, even when this technically is not the case. In some locations, a settlement difference is noticed between two adjacent buildings, as for example at 23 m at 13110WS, 34 m in 13044WS, 23 m in 13044ES and 41 m and 51 m in 13110ES. Specifically the buildings at the north façade of 13044E show a larger settlement prior to construction (2001-2003) due to foundation renewal taking place in that period.

For Vijzelgracht and Rokin Station, the building deformations (excluding the leakage locations described in Chapter 10) are less than at Ceintuurbaan because of the shallower excavation at the time the last measurement for this study was taken. Most of the effects seen at Ceintuurbaan are seen here as well. Due to the nature of the buildings and the narrow cross section streets, the prisms have been located at larger distances apart, making it more difficult to determine the deflection ratio of the buildings, which is however small in most cases. The buildings in cross section 12270WS and 11131EN/S are founded on the second sand layer and show the smallest deformation.

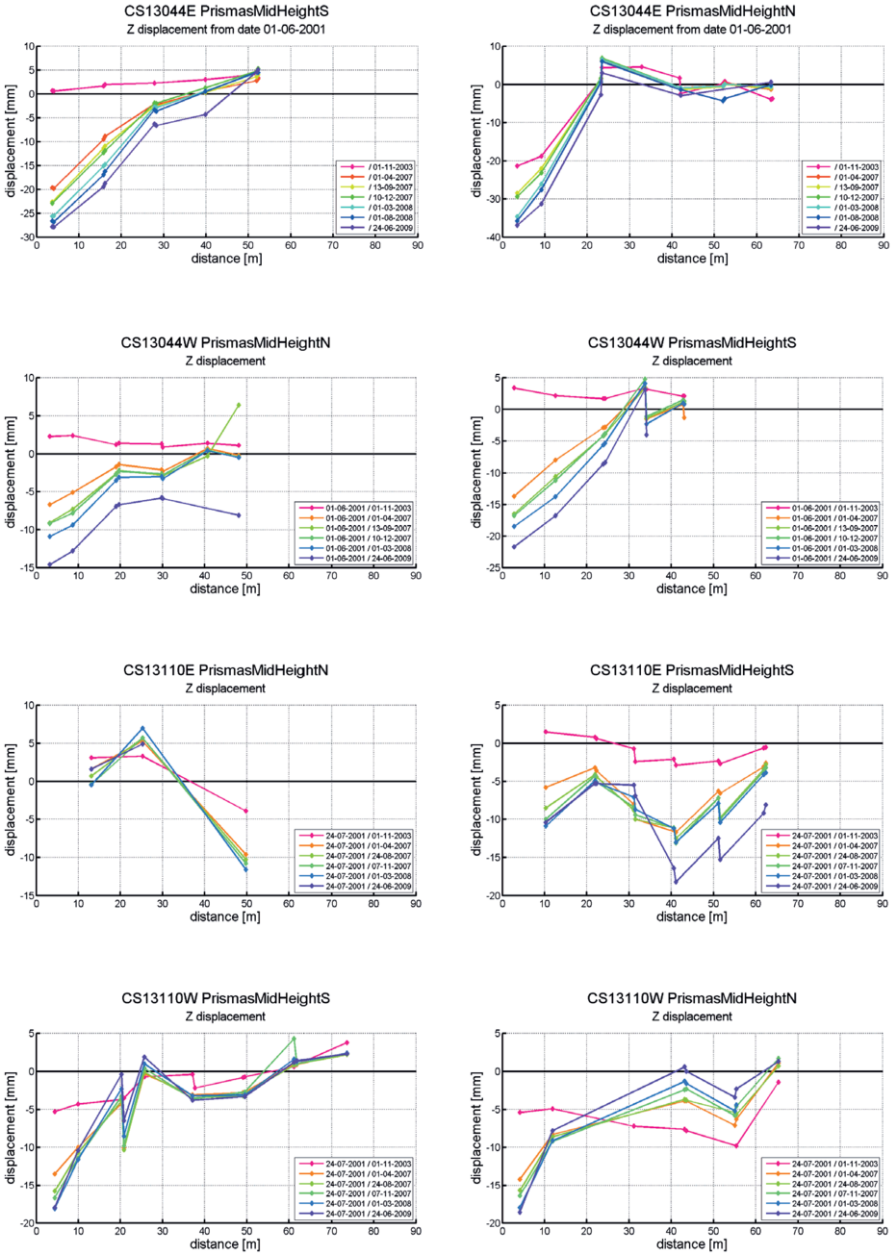
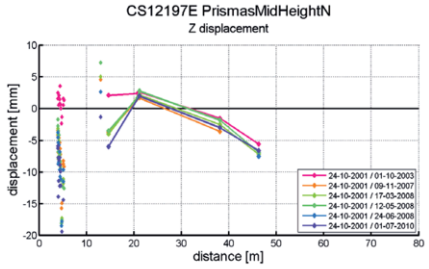
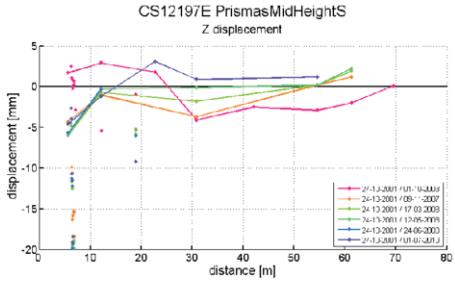
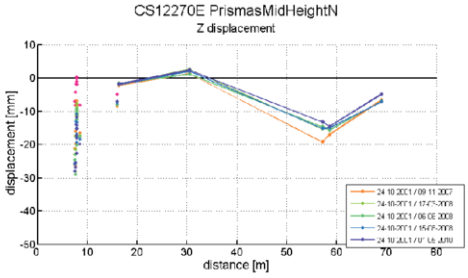
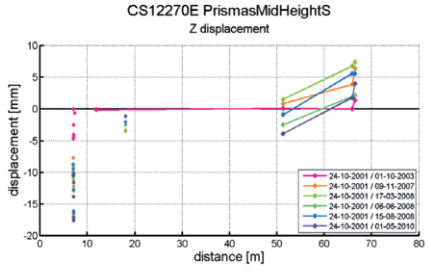


Figure 9.1 Building deformations with time Ceintuurbaan Station









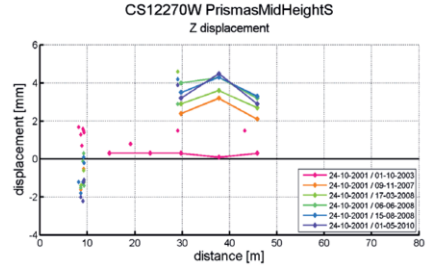


Figure 9.2 Building deformations with time Vijzelgracht Station
(incident locations 12197WN, 12197WS and 12270WN Not shown)

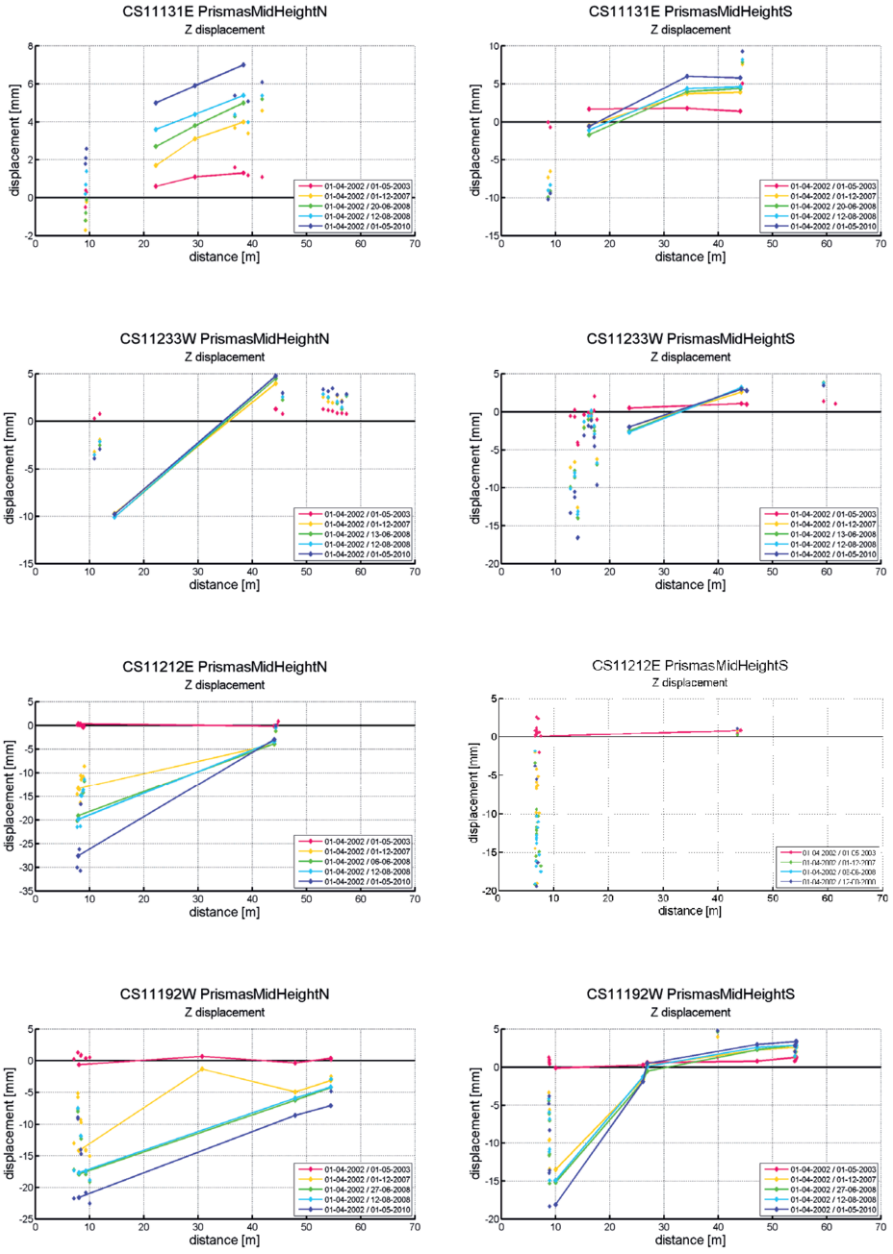


Figure 9.3 Building deformations with time Rokin Station

For each station, the average contribution of the preliminary activities to the building deformation has been determined for all measurements points that show downward movement over the whole construction period, as shown in Table 9.1. Points with

discontinuous measurements or with heave have been disregarded. The percentage shown is the percentage of the building deformation caused by preliminary activities compared to the overall building deformation. The deformation in the period 2003-2007 has been compared with the period 2003-2009 or 2003-2010. Results are shown for the building deformation (for the precise levelling as well as the automatic prism measurements) in Table 9.1.

Table 9.1 Percentage of building deformation caused by preliminary activities

	precise levelling	**automatic prisms**
Ceintuurbaan	65%	55%
Vijzelgracht	81%*	64%
Rokin	68%	60%

* small number of points (<10)

Between 55 and 65% of the building deformation was caused during the preliminary activities. The percentages for all three stations are somewhat higher than the actual values had been if the deformation at the end of construction (after 2012) had been taken into account, instead of the values by 2009 and 2010. Additional building settlements between 2009-2012 have however been very small.

9.2.2 Prism versus manual levelling

The buildings within the influence zone of the North South Line in Amsterdam have been equipped with both automatic prisms measured by total stations as well as manual levelling bolts. Figure 9.4, Figure 9.5 and Figure 9.6 show the measured vertical displacements by both systems for each station. Prism displacements as described in Chapter 4 refer to reference points on buildings outside the excavation's zone of influence, but founded in the first sand layer. This creates a sort of 'floating' reference level as these buildings on the first sand layer themselves settle as a result of subsidence. The manual levelling points are referenced against the stable Third Sand layer at approximately 50 m deep. For all cross sections, the vertical prism displacements are smaller than the manual levelling data. The difference between the two sets is the background settlement due to general subsidence in the area.

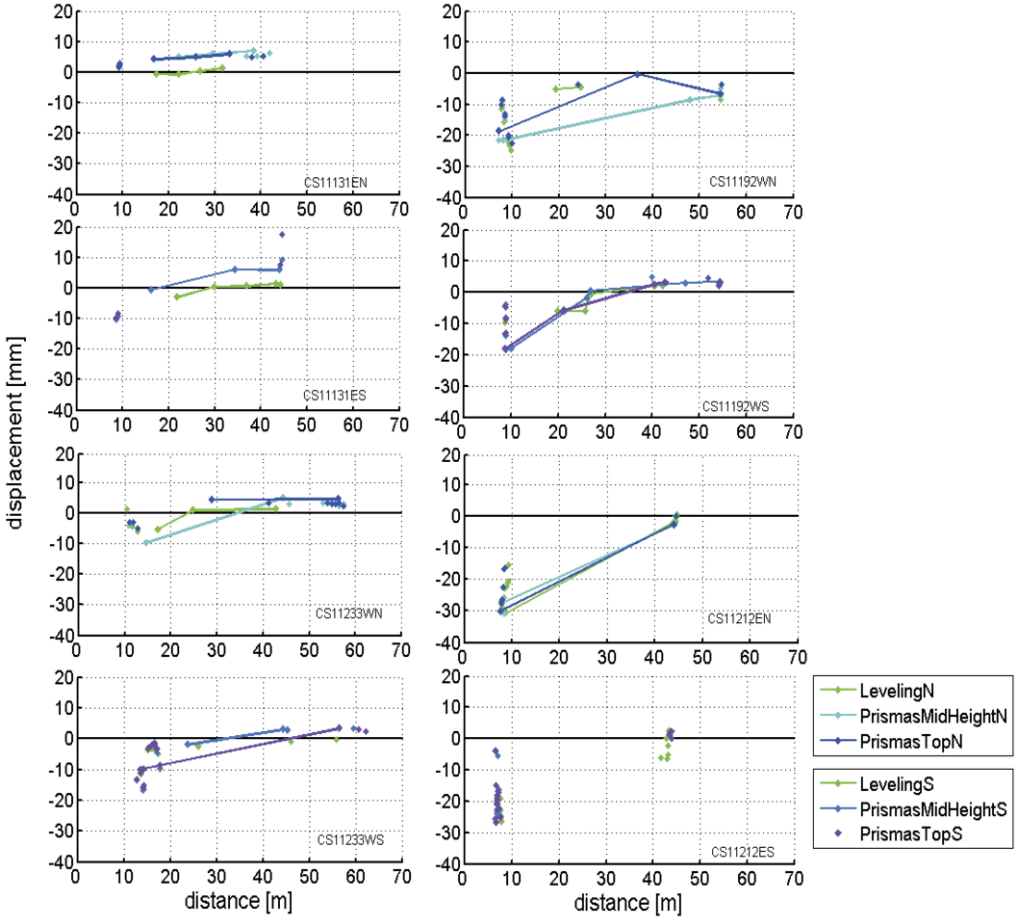


Figure 9.4 Vertical displacements from prism measurements and manual levelling for Rokin Station from 2002 - 2010

At Rokin Station, most manual levelling points show similar data as the automatic prisms. Only at cross section 11131, which buildings are found in the 2nd sand layer, the prism measurements show heave, while the manual levelling shows a slight settlement. The difference is about 5 mm over 8 years, which should be equivalent to the background settlement of the 1st sand layer compared to the 3rd sand layer over that period.

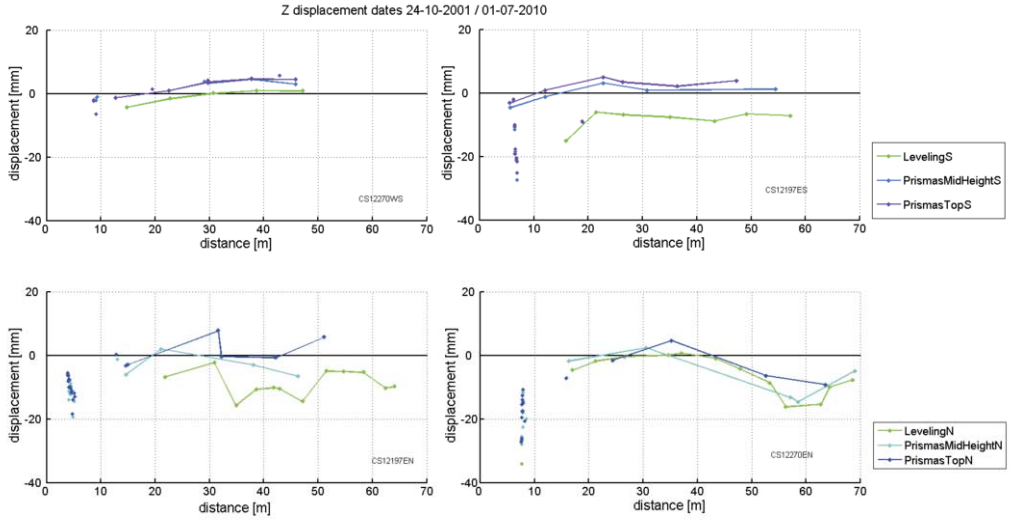


Figure 9.5 Vertical displacements from prism measurements and manual levelling for Vijzelgracht Station from 2001-2010

At Vijzelgracht Station, in cross section 12270EN the levelling points show similar data as the automatic prisms. At the other cross sections, the levelling points settled about 3 mm (12270WS) to 7 or 8 mm (12197ES and 12197EN) more over 8.5 years compared to the prisms. The difference in foundation of the reference points is most likely the cause of the large spread in these results.

At Ceintuurbaan Station, the largest differences are noticed between the manual levelling points and the automatic prisms. The difference is fairly constant about 10 mm over 8 years for the different cross sections. This means the 1st sand layer settles a little over 1 mm per year compared to the 3rd sand layer for the reference locations outside the influence zone of the deep excavation. Ceintuurbaan is the most recently developed area of the three stations, which explains the increasing difference from the oldest part (Rokin) to the relatively newer parts (Ceintuurbaan).

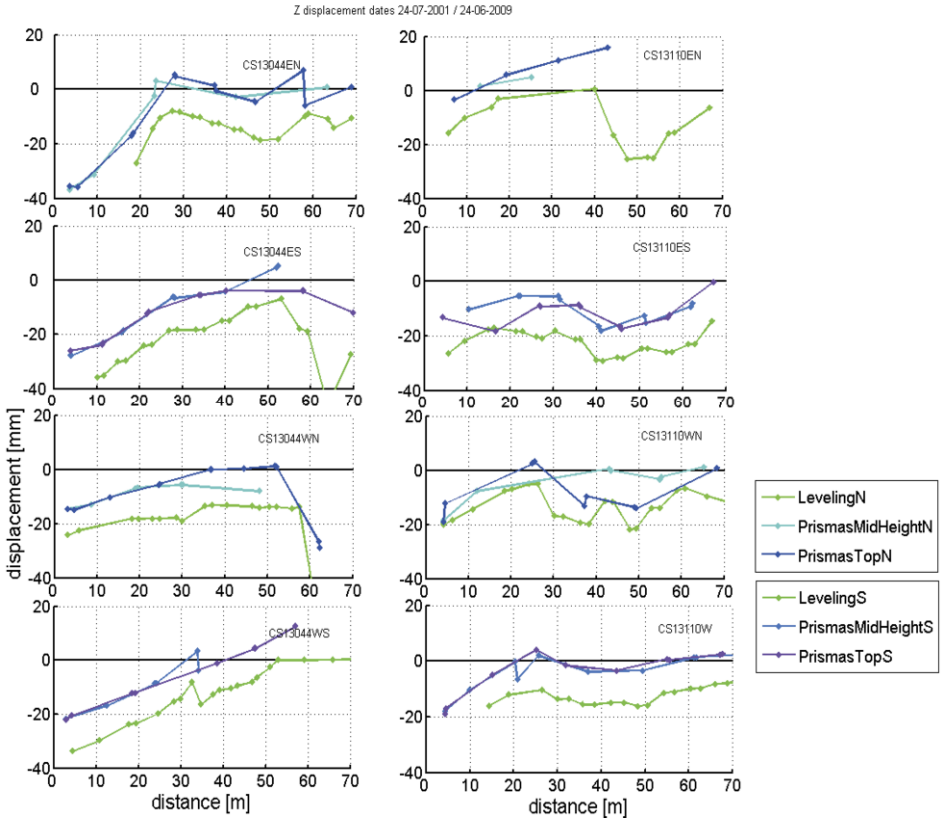


Figure 9.6 Vertical displacements from prism measurements and manual levelling for Ceintuurbaan Station from 2001-2009

The difference between the manual and automatic measurements does not affect the building damage characteristics, because it is mainly a general difference over the whole cross section or façade.

9.2.3 Effect of building stiffness

In this section, the building deflection is compared to the deflection of the soil to study the influence of the stiffness of the building. The buildings concerned all have piled foundations and Chapter 8 already showed that they settle a similar amount as the soil at a level which is between the surface and the foundation level. Soil displacements at the Amsterdam deep excavations are measured at surface level and pile tip level only. Figure 9.9 shows the deformation of the buildings compared to the displacement of the soil, as they were also used in Chapter 8 for one example cross section. The soil deflections are determined for both depths for comparison with the building deflection in Table 9.2 for this and all cross sections as presented in Annex E.

Goh and Mair (2011) presented interaction factors based on FE analyses for deep excavations for different relative stiffness's of buildings with shallow foundations. Goh and Mair used the modification factor as defined by Potts and Addenbrooke (1996):

$$M_{hog}^{DR} = \frac{\Delta/L \text{ hog, building}}{\Delta/L \text{ hog, greenfield}}$$

With M_{hog}^{DR} is the modification factor and Δ/L is the building deflection or the green field (surface) deflection. For the Amsterdam deep excavations, the deformations are mainly in hogging, so only the hogging part of the interaction factors is compared to the measurement results, see Figure 9.7.

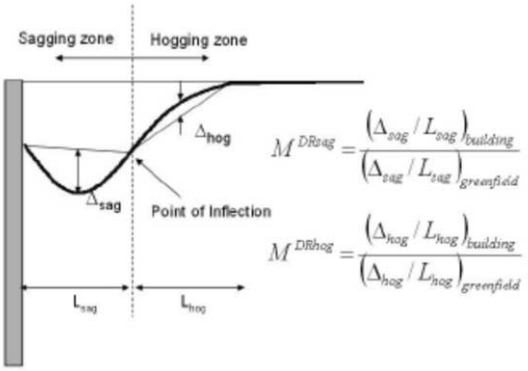


Figure 9.7 Hogging and sagging zones for deep excavation

The modification factors for hogging and sagging depend on the length of the building in relation to the green field settlement trough, the stiffness of the building, the depth of the excavation and the stiffness of the soil, according to Goh en Mair (2011), who combined them into (for hogging):

$$\rho_{hog} = \frac{EI}{E_s L_{hog}^{\ 3}}$$

where EI (in kNm^2/m) is the bending stiffness of the building, Es (in kN/m^2) is the weighted average of the soil stiffness above the excavation level, and L_{hog} (in m) is the hogging length of the building in the greenfield condition. The results give a best estimate and upper bound design line for the modification factor based on the relative bending stiffness as shown in Figure 9.8 for the hogging part of the deformation.

Figure 9.9 shows for cross section 13044E at Ceintuurbaan Station how the soil and building deflection is determined for the specific structural units (houses). Similar plots for other cross sections are given in Annex E, while the numerical results are collected in Table 9.2. The results of Table 9.2 show that the building deflection averages to 0.01%, while the deflection of the foundation layer is 0.02% and the surface deflection even 0.08%. On

average 45% reduction of the deflection is found compared to the foundation level. The variation in these factors can to a certain degree be explained by the different relative stiffness of the buildings compared to the soil, as is shown in Figure 9.10.

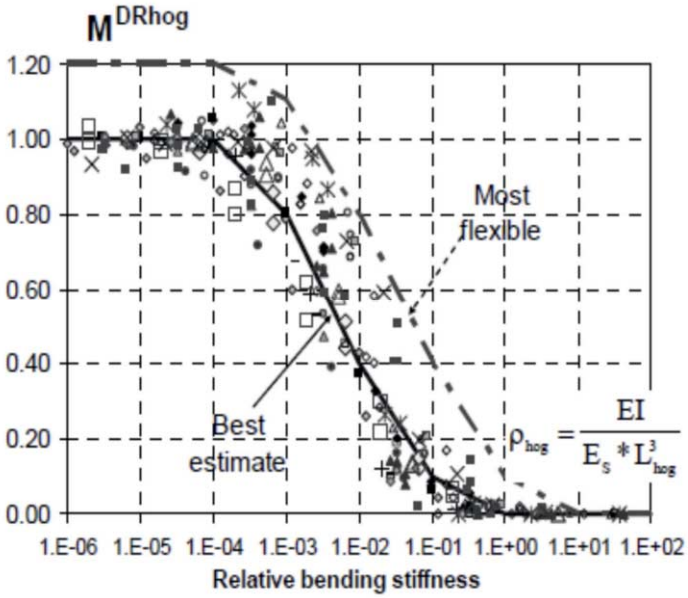


Figure 9.8 Modification factor for bending in hogging based on FE-analysis by Goh and Mair (2011)

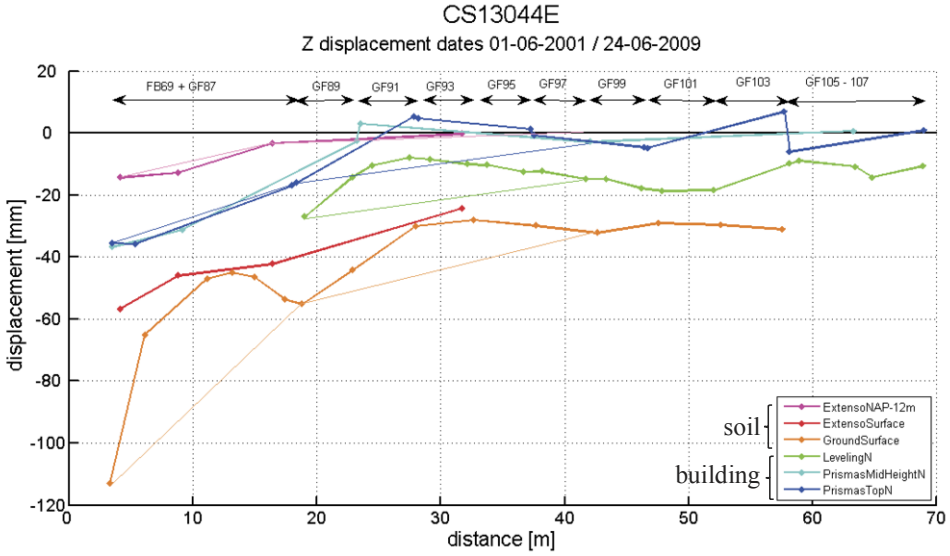


Figure 9.9 Building and soil deformations 2001-2009 Ceintuurbaan Station 13044E (other cross sections in Annex E)

Table 9.2 Building and soil deflection ratio for each station

	building deflection ratio Δ_b/L [%]	surface deflection ratio Δ_s/L [%]	foundation deflection ratio Δ_f/L [%]	M^{DR} surface [-]	M^{DR} foundation [-]
11131ES - RKN69	0.01%	0.04%	x	0.33	
11192WN - RKN72	0.01%	0.05%		0.33	
11192WS - RKN74	0.02%	0.05%	x	0.52	
11233WN - RKN78	0.01%	0.08%	0.03%	0.18	0.53
11233WS - RKN84	0.02%	0.07%	0.03%	0.23	0.61
12197EN - VZG19	x	0.19%	-0.11%		
12197ES - VZG21	0.00%	0.08%	-0.06%	0.00	0.00
12270EN - FS1	0.01%	0.05%	x	0.17	
12270WS – VZG48 2nd sand layer	0.01%	0.17%	x	0.03	
13110EN - FB93	0.01%	0.04%	-0.02%	0.32	-0.72
13110ES - FB95	0.02%	0.04%	-0.02%	0.60	-1.20
13110WN - FB118	0.01%	0.05%	0.02%	0.19	0.49
13110WS - FB120	0.01%	0.05%	0.02%	0.19	0.49
13044EN - FB69	0.01%	0.14%	0.02%	0.10	0.93
13044EN - GF89-97	0.07%	0.06%	0.00%	1.12	>>1
13044ES - FB71	0.01%	0.14%	0.01%	0.10	
13044ES - GF122-126	0.02%	0.04%	0.00%	0.66	
13044WN – FB90	0.01%	0.06%	0.03%	0.11	0.22
13044WN - GF87-85	0.00%	?	0.00%		1.00
13044WS - GF116-112	0.01%	?	0.00%		1.00
13044WS - FB92	0.01%	0.06%	0.03%	0.10	0.19
average	**0.01%**	**0.08%**	**0.02%***	**0.29**	**0.55***

* negative values excluded

The relative stiffness of the buildings is determined based on the following average building characteristics: the masonry facades and walls are 0.22 m thick. The EI of the facades is determined with a correction for window openings of 25%. The EI of the single wall is used for buildings facing the station and a single façade for buildings in the side streets. The contribution of the floors is disregarded, since they are mostly timber floors with relatively low stiffness. The equivalent soil stiffness is a weighted average of E_{50} over the excavation depth, resulting in about 7000 MPa for Rokin and Vijzelgracht and 17000 MPa for the deeper excavation at Ceintuurbaan. The relative building stiffness is found to be between 1E-3 and 1E-2.

A large variation is found in the results of Figure 9.10. The soil at the interaction level settled with a deflected shape somewhere in between that of the surface and foundation level,

leading to an actual modification factor between the values for surface and foundation level respectively. In some of the buildings, clearly some effect of the stiffness of the building is present while other buildings deform rather flexible, as can be seen in the figures in Annex E. Assuming based on the results of Chapter 8 that the interaction level is found about 2/3 down the pile and that the deflection of the soil decreases linearly with depth, the results of Amsterdam are compared with the data on case histories by Goh (2010) and Farrell (2010), taken from Mair (2011) and shown in Figure 9.11.

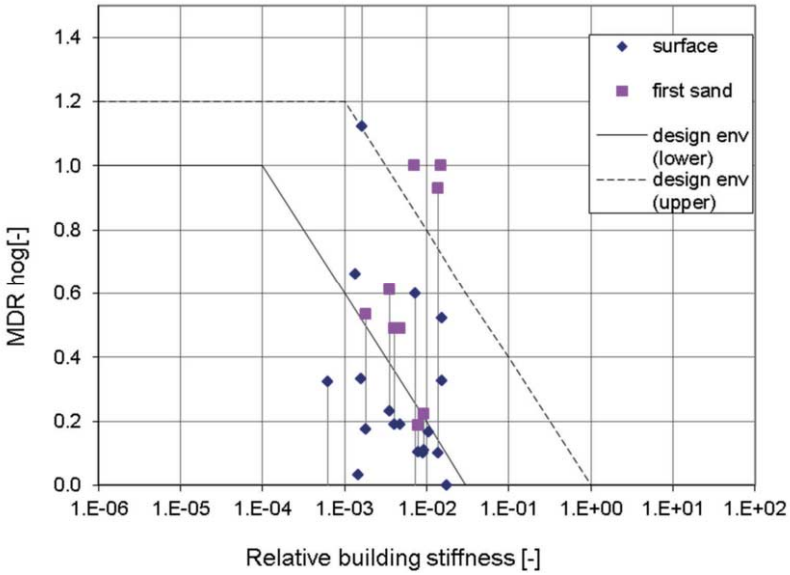


Figure 9.10 Modification factors from Amsterdam deep excavation for surface level and foundation level, compared with the design envelope presented by Mair (2011)

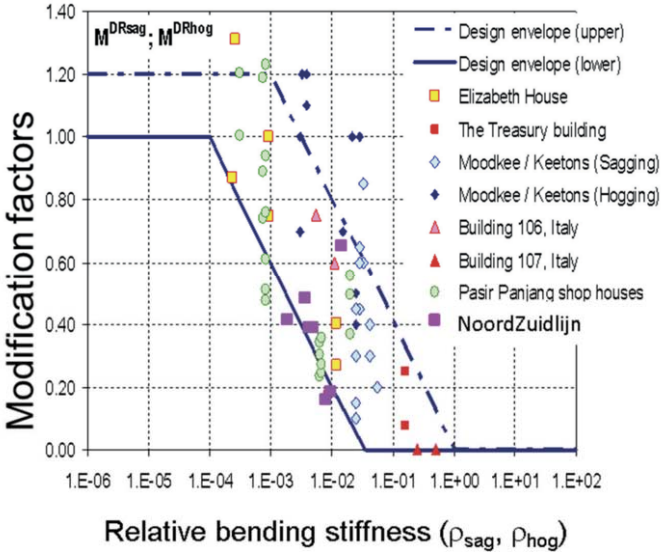


Figure 9.11 Modification factors for interaction level from Amsterdam deep excavation, compared with data presented by Mair (2011)

Given the assumptions and simplifications, it is shown that also for the Amsterdam conditions, the Goh and Mair (2011) method provides a realistic, although rather large range of possible modification factors.

9.3 Horizontal deformations of piled buildings

The horizontal deformation of the buildings are due to tilt in combination with horizontal extension. To determine the damage category, it is important to distinguish between tilt and extension, based on the difference between the prism at MidHeight and at Top level (respectively at about 5-6 m and 12-13 m from street level).

Figure 9.12 shows the ratio of the buildings' horizontal and vertical deformation where the horizontal deformation is determined at the street level. The ratio's median value is 0.8, which means that the horizontal displacement of the building at street level is in the same order as the vertical settlement of the building. This ratio can be used to determine the building's horizontal strain, but is very specific for the Amsterdam situation, since the presence of the foundation determines the amount of vertical deformation and the flexibility of the foundation the amount of horizontal deformation.

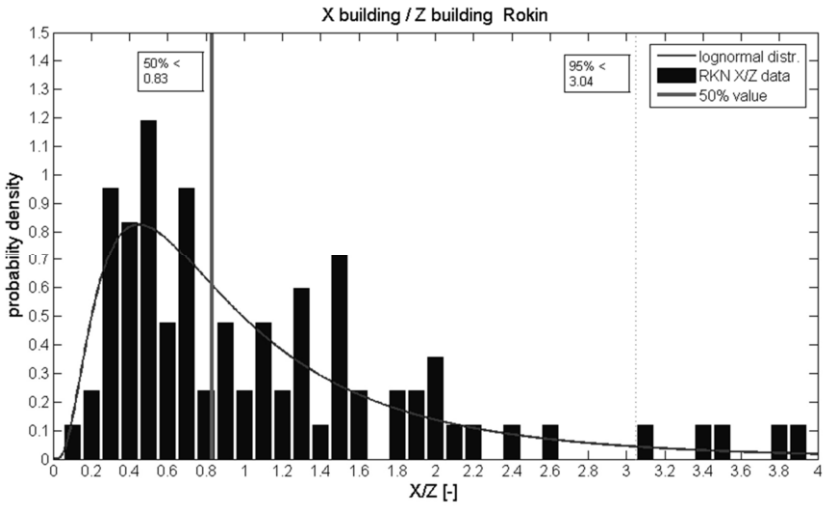


Figure 9.12 Histogram plots for probability of X/Z values for Rokin station with X/Zbuilding

For Ceintuurbaan Station and Rokin Station, Figure 9.13 shows the horizontal displacement of the building at street level versus the distance to the diaphragm wall. It can be clearly noticed that the horizontal deformation at street level (excluding tilt of the building) is rather constant for buildings in the same cross section at different distances from the excavation. This means that negligible amounts of horizontal strain are transferred from the soil to the building.

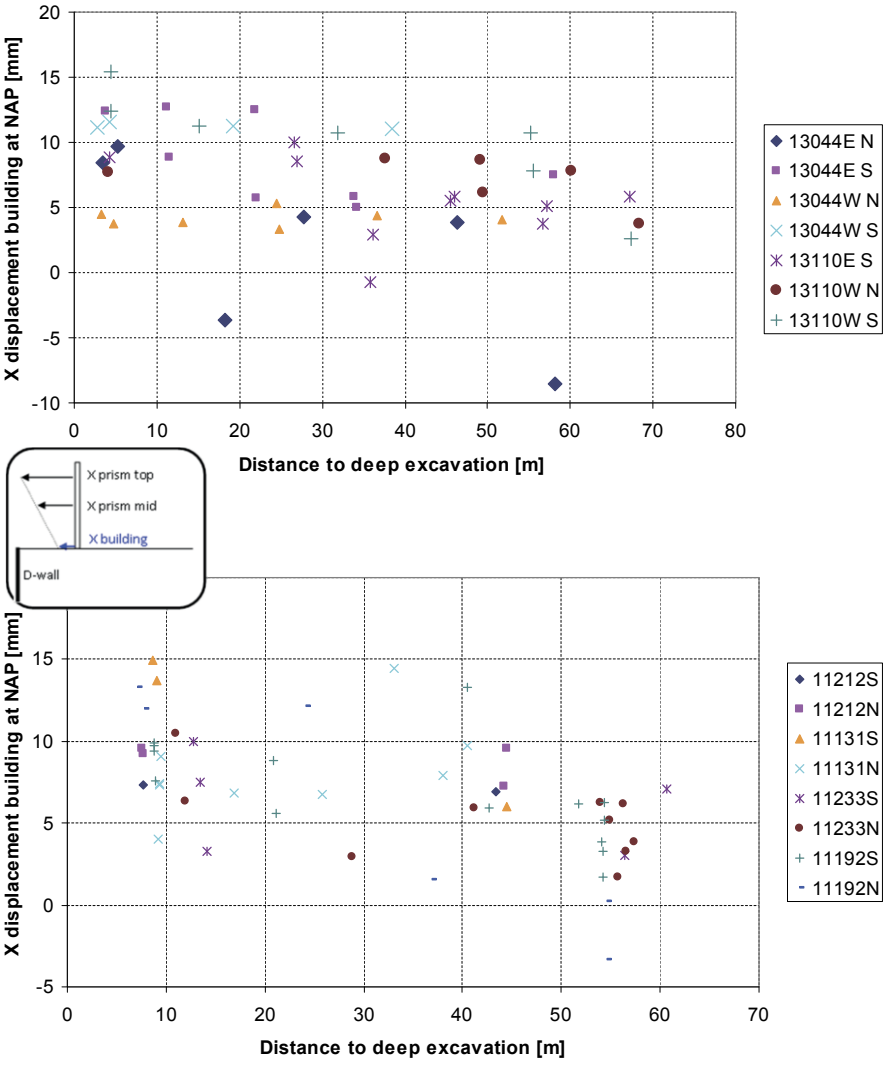


Figure 9.13 Horizontal displacement of buildings at street level during period 2001-2009 at Ceintuurbaan station (top) and Rokin (bottom)

From the same measurements of the prisms, the tilt of the buildings can be determined, see Figure 9.14. The tilt clearly depends on the distance to the excavation, with the largest tilt closest to the excavation as can be expected. At about once the excavation depth or 25-35 m for Ceintuurbaan station the building tilt is smaller than 0.0005 or 1:2000. For Rokin this relationship is less clear. The average tilt of the buildings (based on absolute values of the additional displacements during the period 2001-2009) at Rokin is 1:2200 and for Ceintuurbaan 1:1150. This tilt is in X direction (perpendicular to the excavation). There is

also a sometimes significant tilt and distortion of the buildings directly along the station in parallel direction to the excavation, but this is beyond the scope of this study.

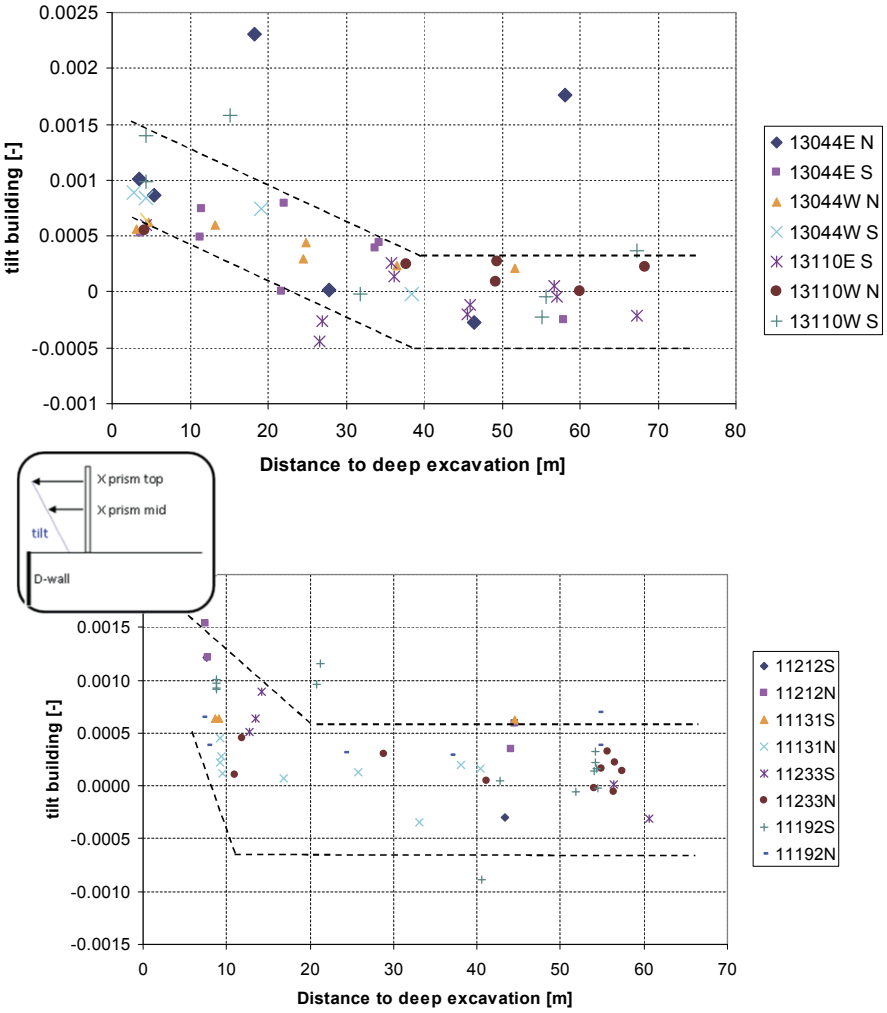


Figure 9.14 Tilt of buildings in direction of excavation during period 2001-2009 at Ceintuurbaan station (top) and Rokin (bottom)

9.4 Summary of building displacements

The largest influence of the construction works (between 55 and 65% of the building deformation) is due to the preliminary activities (diaphragm wall construction, jet grout strut installation and subsidence over 4 years between 2003-2007). During excavation of the station, the additional building deformations are less than 10 mm. In all stages, deflection ratios are small (in the order of 0.03%). The different facades along a cross section show that

in most cases the individual buildings behave like they are part of structural units with shared walls even when this is technically not the case.

At Ceintuurbaan Station, the largest difference is noticed between the vertical building deformations measured by the manual levelling points and the automatic prisms of about 10 mm over 8 years. This means the 1st sand layer settles a little over 1 mm per year compared to the 3rd sand layer for the reference locations outside the influence zone of the deep excavation. Ceintuurbaan is the most recently developed area of the three stations, which explains the smaller difference in the oldest part (Rokin, about 5 mm over 8 years) and at Vijzelgracht (0 - 8 mm over 8 years), which is in between the other stations. The difference between the manual and automatic measurements does not affect the building damage characteristics, because it is mainly a general difference over the whole cross section or façade.

The horizontal deformation of the building at street level is in the same order as the vertical deformation of the building. This factor, which can be used to determine the horizontal strain in the building, is very specific for the Amsterdam situation.

The buildings' tilt towards the excavation, based on absolute values of the additional displacements during the period 2001-2009, at Rokin is 1:2200 and at Ceintuurbaan 1:1150. At about once the excavation depth or 25-35 m for Ceintuurbaan station the building tilt is smaller than 0.0005 or 1:2000. For Rokin this relationship is less clear.

The deflection of the building is compared to the deflection of the soil at surface level and pile tip level. Although a large variation is found in the results, the soil at the neutral level settled with a deflected shape somewhere in between the surface and foundation level. In some of the buildings, clearly some effect of the stiffness of the building is present while other buildings deform rather flexibly. The Goh and Mair (2011) method provides a realistic, although rather large range of possible modification factors for the deflection of buildings next to excavations, deforming in hogging shape.

All results presented in this chapter excluded the incidents of leakage at Vijzelgracht Station that occurred in 2008. Chapter 10 describes the building damage specifically related to these incidents.

CHAPTER 10 BUILDING DAMAGE AT VIJZELGRACHT

10.1 Introduction and events leading to building damage

During the excavation for Vijzelgracht Station, leakage through the wall resulted in large settlements and damage to historic buildings, which threatened the continuation of the project. With the application of robust preventative measures at two of the deep excavations it was possible to continue the project. This chapter reports on the cause of the events, the damage to the buildings and the counter-measures taken. It includes lessons learned for the project and for the foundation industry. The work in this chapter has been published during the PhD study in Korff et al. (2011b). The author performed the analysis in section 10.4 to 10.6 and participated in the analysis described in the other sections.

Vijzelgracht Station is one of the deep stations for the North South metro Line in Amsterdam, for details see Chapter 4. The diaphragm walls consist of panels made by traditional grabs. At Vijzelgracht Station in particular, and to some extent at Rokin Station, numerous joints in the D-wall panels leaked during the excavation down to about NAP –12 m. These leaks varied from damp patches to more significant water flows, but down to that depth, the walls did not leak much. A standard procedure of drilling into the wall and polyurethane injections stopped these leakages.

The first incident of severe inflow of water and soil through panel joint 89/90 occurred on 19th June 2008 in the west wall of Vijzelgracht Station. The excavation was to approximately NAP –12m at that time. The leak was attributed to a steel stop end (CWS type as described by Puller (2003)), which could not be removed at this location, and the failure of the jet grouting performed behind the wall at the location of the joint. This inflow of water and soil (estimated to be 20 m^3/hour) resulted in substantial settlement – up to 140mm – and damage to the adjacent buildings. It was possible to stop the inflow only after substantial backfilling of the excavation and polyurethane injection.

On 17th June, two days before the inflow, a large bentonite inclusion (measuring approximately 0.4x1.0m) was discovered during excavation at NAP -12m just next to a panel joint in the east wall. Immediately after the discovery, water with soil or bentonite started to flow in. Fortunately, the contractor was able to stop the intrusion of water by immediate backfilling in front of the joint.

After these events occurred geophysical leakage detection was carried out in the half-excavated station by a geophysical, multi-sensor survey system (Electric Chemical Respons, ECR®) with application of spatially targeted electrical impulses (Electric Flux Tracking, EFT®). Analysis of these measurements showed that there were many small leakages to be expected along the wall, but none of the joints showed major leakage. The work resumed with trial excavations at the joints.

On 10th September 2008, a second incident of severe leakage of soil and water occurred, resulting in settlement in adjacent buildings of up to 250mm. This leak was caused by a large bentonite inclusion next to panel joint 69/70 in the west wall during a trial excavation from NAP -13 to -17m. The maximum width of the inclusion was approximately 0.2m and the height was at least 2m. When the contractor first noticed the inclusion, it was dry (no leakage). In the next 4 hours the contractor made preparations for containing the bentonite inclusion with steel plates. After holes had been drilled to anchor the third plate in the wall, water suddenly started to flow. Within half an hour, the flow of water and soil was almost impossible to control and it took hours to stop it. After 12 hours the contractor, municipal officials and consultants concluded that the situation was stable. During those 12 hours, almost 700 litres of polyurethane had been injected and approximately 450m^3 of soil had been backfilled.

10.2 Technical analyses cause of the leakage

These serious events originated from two separate causes, the first incident being due to a steel stop end and the second incident due to the presence of a large bentonite inclusion in the D-wall. In both cases the resulting inflow of water and sand could not be stopped quickly enough to prevent serious erosion and loosening of the sand strata outside the excavation.

Unfortunately, the precise cause of the bentonite inclusions could not be identified. A visual inspection indicated that the quality of the D-walls at Vijzelgracht Station was significantly worse than at Rokin and Ceintuurbaan, even though they were installed by the same contractor. The overall quality of the walls at Vijzelgracht was reviewed by an independent team of experts. The quality was rated below what might reasonably have been expected. The presence of three large bentonite inclusions and many smaller ones has led to doubts about the workmanship and quality control.

The bentonite inclusions were most likely caused by a combination of suboptimal circumstances during the installation of the walls, such as delays when removing the steel stop ends and cleaning the bentonite slurry, the inclination of the stop ends and closely spaced, large reinforcement bars relative to the aggregate size of the concrete. Moreover, the bentonite slurry had to be replaced entirely in several panels probably because of an unfavourable interaction with the lean concrete columns, used to stabilise the soft ground in the Holocene layers. In addition, the 5.2m-wide trenches were cleaned from just one pump position and concreted with only one tremie pipe. The bentonite inclusions can also be attributed to the trench being not fully cleaned with fresh bentonite just before concreting

(Figure 10.1a). During concreting, the thick bentonite would probably not have been removed by the concrete, as seen in Figure 10.1b. The result is a bentonite inclusion in the concrete, as shown in Figure 10.1c.

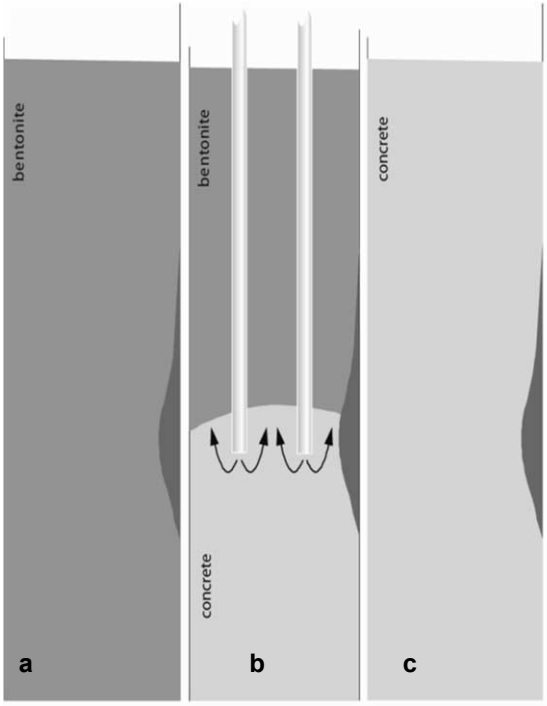


Figure 10.1 Forming of a bentonite inclusion during the concreting of a panel in three subsequent stages.

Although the bentonite inclusions explain the direct cause of the leakage, questions remained as to why the inflow of sand could occur. Up to the first event, measures to control the situation in case of a serious leak included a procedure with Polyurethane (PU)-injection and placing of steel plates. After the first incident and the geophysical leakage detection, excavation resumed in small inspection pits at the joints in order to be able to backfill immediately in case of severe inflow of water and to obtain in such a way a validation of the (ECR®) / (EFT®) measurements. The second incident occurred when the inclusion was found in the inspection pit but as no water flow was observed it was not considered as a serious problem; instead of backfilling the contractor started drilling holes in the adjacent concrete to fix the steel plates. The inclusion may have liquefied due to the drilling, resulting in the inflow of water and sand.

10.3 Effect on the soil around the excavation

Investigations were undertaken, including cone penetration tests (CPTs) to determine the amount of soil disturbance, which reached at least 16m away from the joint where the soil

inflow occurred, see Figure 10.2. Examination of CPTs undertaken immediately after the first incident (see Figure 10.3) indicates that there is clear evidence of the 1st sand layer (between NAP –12 and –14) having been disturbed in the region of the panel joint 89/90. The second sand layer also shows disturbance. Bosch and Broere (2009) confirmed the general shape of the settlement profile by undertaking FEM calculations of the effects of disturbance. They modelled the incident in plane-strain with transient groundwater flow by increasing the permeability of the diaphragm wall. The best results were found reducing the phreatic head in both the first and second sand layer and a volumetric contraction for the loss of soil of about 3 m^3/m wall.

CPTs were also undertaken adjacent to and along the line of the diaphragm wall after the second leakage incident. These show cone resistance, q_c, values of the 1st sand layer to have reduced significantly adjacent to houses 4 to 8 Vijzelgracht. The largest reduction to 6 – 7 MPa was found at the location of the houses 4 and 6 Vijzelgracht. Other CPTs at greater distance from this region show q_c values in excess of 20 MPa. The reduced q_c values of the 1st sand layer are consistent with considerable loosening caused by a significant volume of sand being washed through the leaking panel joint. During the second incident, some disturbance of the second sand layer was also evident from the CPTs.

The settlement was therefore mainly the result of ground loss into the excavation resulting in loosening and strong reduction of the cone-resistance of the first sand layer, which is the bearing stratum of the wooden pile foundations; consolidation effects due to pore pressure reduction were minor.

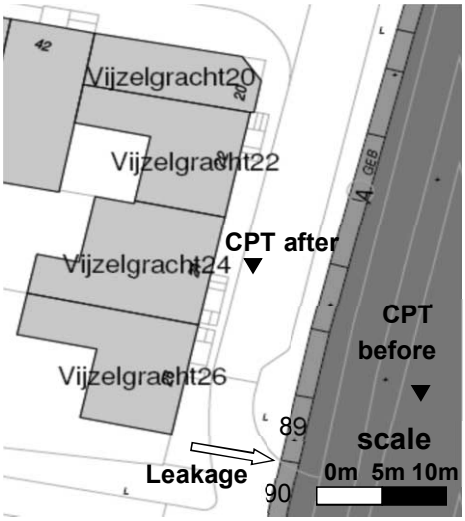


Figure 10.2 Location of CPTs at first incident

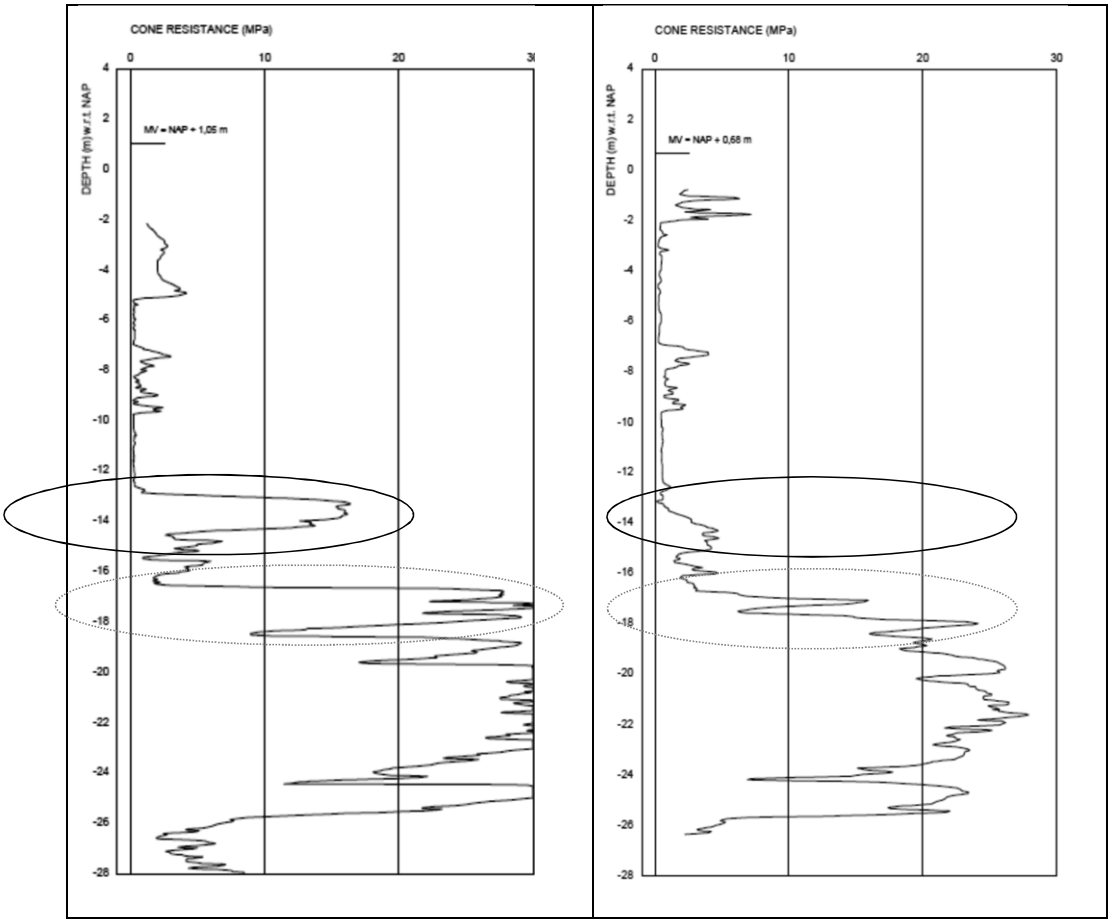


Figure 10.3 CPT before (left) and CPT after (right) first leakage incident showing large reductions in first sand layer (at -14m) and top of second sand layer (at -17m). The CPT before the incident is representative for a larger area as the first and second sand layers very consistently show q_c values of 10-20 MPa and over 20 MPa respectively.

10.4 Damage to the buildings

The houses influenced by both incidents are historic buildings from around 1670. The buildings were part of originally more than 200 houses, specifically built for weavers, wool combers and spinners. Figure 10.4 shows the original drawing with view of the façade and plan of the ground floor.

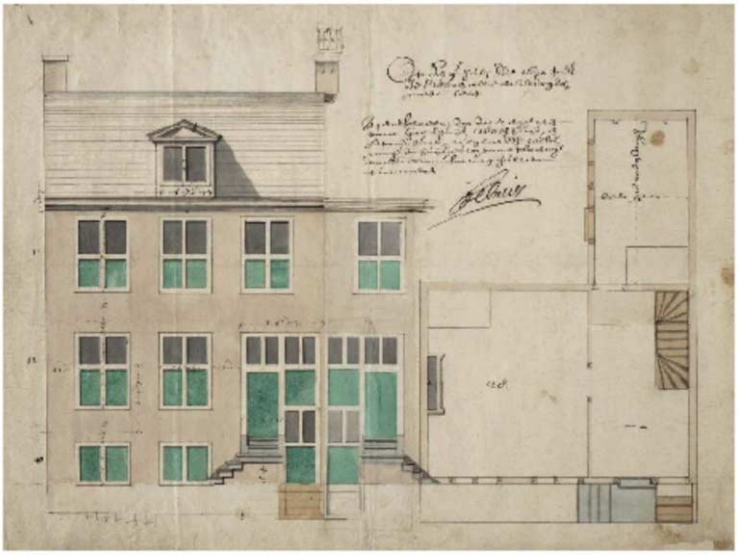


Figure 10.4 Original drawing of Weavers' building (drawing by Philip Vingboons from Archive Amsterdam)

The buildings all have a semi-basement, a raised ground floor, and a first floor with a vaulted roof. The rear of the houses include a kitchen addition. The height of the buildings is about 9 m. A foundation consisting of 52 timber piles per house to the first sand layer at a level of around NAP -13 m. The piles are placed under the brick walls in rows of 2 piles. Due to the use of lime mortar instead of cement at the time of construction, the houses deformed in a rather flexible way due to considerable natural soil deformations. Before construction of the North South Line these buildings were equipped with monitoring instruments, comprising optical prisms for total station surveying at two levels and manual levelling bolts at street level, see Figure 10.5.



Figure 10.5 Weaverbuilding Vijzelgracht 26 with prism locations (picture Dienst NoordZuidlijn)

10.5 Deformations and damage arising from first incident

To stabilise the historic buildings a timber framework was installed on the outside, see Figure 10.6, as well as inside.



Figure 10.6 Damaged buildings Vijzelgracht 20-26 due to first incident June 2008

As shown in Figure 10.7, the block of houses Vijzelgracht 20-26 settled a maximum of 150 mm as a consequence of the first incident in June 2008. The building tilted towards the corner of VZG 26, and towards the excavation and the location of the leakage. A slight sagging was found between VZG 26 and VZG 24 and hogging towards VZG 22. The cracks on the inside and outside of the buildings are shown in Figure 10.8 and Figure 10.9. The cracks reported are mainly new cracks or previous cracks that opened significantly.

Cracks 1 to 4 were found on the outside of number 24 and have a maximum width of 20 mm, 10 mm, 8mm and 8mm respectively. Cracks 5 to 9 were found on the inside and are smaller than 5 mm. Crack 10 indicates a cracked window. Crack 11 is out of plane of the drawing, separating the staircase from the house. Cracks 12 to 14 were found on the outside of number 26 and have maximum widths of 2 mm, 7 mm and 2 mm respectively. The location and direction of the cracks indicate a shear deformation with the largest crack width mainly in VZG 24, consistent with the differential settlements. Cracks at the rear are not shown, but indicate a twist movement of the building together with horizontal extension. There are no deformation measurements available of the rear façade. It is thus not possible to relate the deformations of the rear to the direction of the cracks.

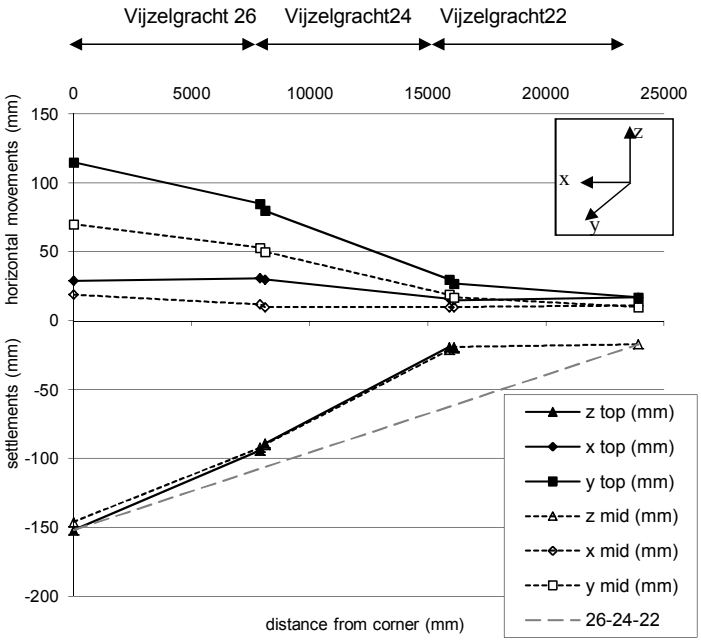


Figure 10.7 Deformations after incident June 2008 (measurements dated July, 31st 2008)

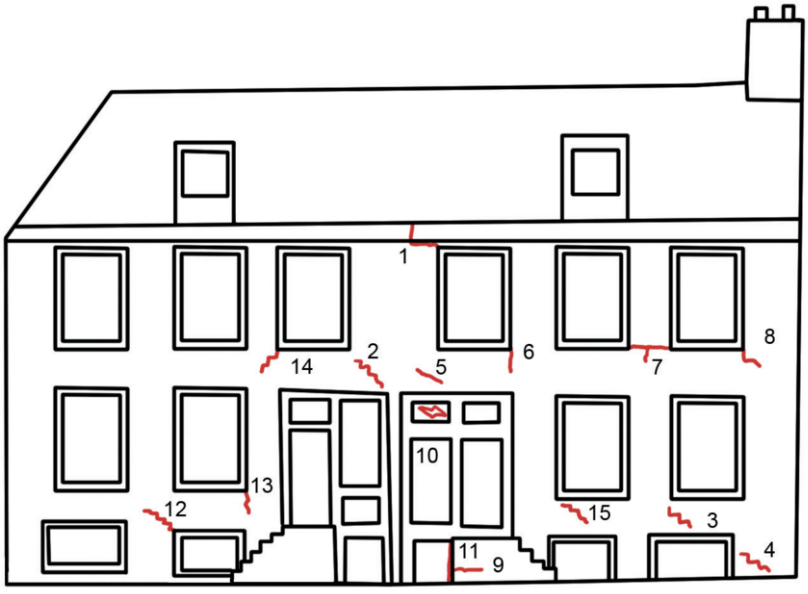


Figure 10.8 Cracks at the front façade (VZG 26 on the left side, VZG 24 on the right)

The actual damage derived from the observations for these buildings (26, 24) would be category 5, very severe (Burland *et al.* 1977). A significant tilt of the buildings was

observed, with severely sloping floors. The stability of the buildings was also in question, so the buildings were temporarily braced by wooden supports. The front façade experienced a maximum tilt of 1:78 perpendicular to the façade and 1:184 parallel to the façade at the corner of Vijzelgracht 26 and between VZG 26 and VZG 24 respectively. Both relative rotation and deflection ratio have been calculated for the front façade. For the relative rotation the calculation method of Son and Cording (2005) has been used. This method calculates the slope of the building and defines the relative rotation as β = slope – tilt. The tilt based on the differential horizontal movements of VZG 26 and 24 averages 0.27% or 1:367 parallel to the façade. Combining relative rotation and horizontal strain results in damage category 'severe to very severe' for Vijzelgracht 26/24. If one disregards the tilt and uses only the slope as the relative rotation (i.e. assuming β = slope), the damage category would also be 'severe to very severe'. The method of Mair et al.(1996) can also be used, combining deflection ratio with the horizontal strain, and this too indicates a damage category of 'severe to very severe'. Table 10.1 includes the results of the various calculations.

Table 10.1 Damage criteria Vijzelgracht 26-24 front facade

Criterion	**Calculation**	**Damage category**
Maximum slope	(89-19)/8m = 0.9% or 1:111	Severe to very severe
Relative rotation β (average tilt)	0.9%-0.27% = 0.62% or 1:160	Severe to very severe
Relative rotation β (max. tilt)	0.9%-0.54% = 0.35% or 1:282	Moderate
Deflection ratio Δ/L	43mm/24m= 0.47%	Severe to very severe
Horizontal strain ε_h average	10mm/24m= 0.04%	Included in damage category

It can be concluded that the damage to the façade is mainly caused by shear deformation and horizontal extension in the plane of the wall. The damage categories inferred from the deformation measurements are consistent with the actual observed damage. Damage to the buildings as a whole is especially severe in terms of serviceability due to the overall rotation of the building perpendicular to the facades. Severe sloping and tilting of floors and walls are clearly noticeable, which is consistent with Charles and Skinner (2004) who concluded that for low-rise buildings a tilt of 1:250 is noticeable and a tilt of 1:100 requires remedial action, even without any deflection. Separation of the rear façade from both the main house and the kitchen addition is caused by horizontal extension. Its effect can not be quantified because measurements have not been taken at the rear of the buildings; they are also not easily described in terms of 'traditional' damage criteria.



Figure 10.9 Details of cracks; left: crack 1, width max. 20 mm, right: crack 4, width max. 8 mm.

10.6 Deformations and damage arising from the second incident

Block Vijzelgracht 4-10 settled a maximum of 240 mm directly after the second leakage incident. The foundations of Vijzelgracht 4-8 have been renewed before the construction activities started. The new steel piles and the old timber piles are both founded in the first sand layer. Figure 10.10 shows the buildings before the leakage damage occurred and Figure 10.11 the same buildings after the leakage. It can be seen that there was already a large shear deformation before the leakage.

Figure 10.12 shows the cracks on the outside of VZG 8 (left), VZG 6 (mid) and VZG 4 (right). Crack 1 is a separation crack of about 60-80mm at the top, due to tilt of VZG 8 away from the neighbouring building on the left side (VZG 10). Cracks 2, 11, 12, 15 and 18 are generally up to 5 mm wide. Cracks 3, 4, 5, 7, 8, 9, 10, 16 and 17 are 5-10 mm wide. Cracks 13 and 14 are 20 mm and 15 mm wide respectively. Figure 10.12, Figure 10.14 and Figure 10.15 focus on new cracks and existing cracks that re-opened.



Figure 10.10 Vijzelgracht 8-6-4 before the incident (2002)



Figure 10.11 Vijzelgracht 8-6-4 after the incident (2008)

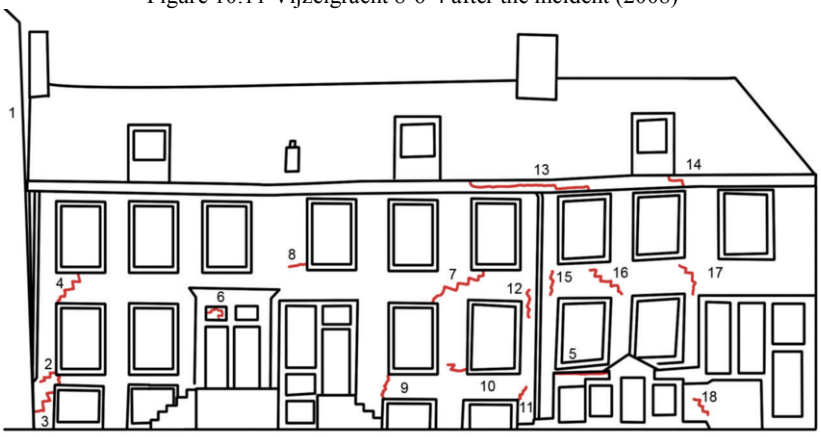


Figure 10.12 Cracks at the front façade VZG 8 -6 – 4

Figure 10.13 shows the observed deformations after the second leakage incident (all deformations being relative to the beginning of the station construction: previous historical deformations are not shown). The cracks in Figure 10.12 and the deformations in Figure 10.13 show that the houses deformed partly in hogging mode (VZG 8-6) and partly in sagging mode (VZG 6-4), with the largest differential settlement found between VZG 4 and 6. The diagonal direction of the cracks indicates a shear deformation. Both the hogging and sagging modes are consistent with the direction of the cracks.

The largest slope in the building was found to be perpendicular to the Vijzelgracht façade, due to tilt of the buildings towards the leakage. Parallel to the Vijzelgracht facade damage indicators can be calculated, splitting the block into a hogging and a sagging part. The hogging part (VZG 10 and 8) consists of two semi-separated buildings, divided by a 'crack' of about 60mm at the top, due to the differential slopes of the buildings of 1:550 and 1:100. Vijzelgracht 10 did not experience much damage itself. For the sagging part of Vijzelgracht 4 and 6, the maximum slope is 1:65 and the deflection ratio is 0.4%. Combining these with the horizontal strain, according to Mair et al.(1996), the maximum calculated strain becomes

0.7% for sagging, resulting in the damage category 'severe to very severe'. Based on the relative rotation β, the same category is found according to Boscardin and Cording (1989). The tilt of 1:125 parallel to the façade is clearly noticeable and required remedial measures based on Charles and Skinner (2004). Table 10.2 includes the results of the calculations for the sagging part of the block.

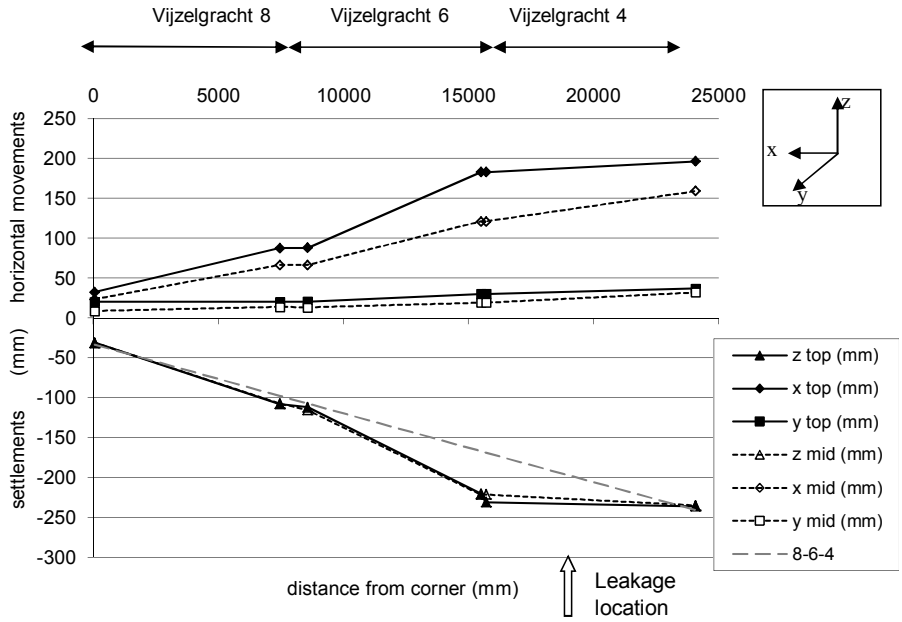


Figure 10.13 Deformations after second incident (measurements dated 29th October 2008)

Table 10.2 Damage criteria Vijzelgracht 4-6 front façade (sagging zone)

Criterion	Calculation	Damage category
Maximum slope ⊥ VZG 4	(235-60)/9 m = 0.019 or 1:51	Severe to very severe
Maximum slope // VZG 6	(220-111)/7 m = 0.016 or 1:65	Severe to very severe
Relative rotation β = slope –tilt	0.016 – 0.008 = 0.008 or 1:125	Severe to very severe
Deflection ratio Δ/L	62 mm/15.5 m = 0.4%	Severe to very severe
Horizontal strain ε_h average VZG 4-6 Mid	18 mm/15.5m = 0.12%	Included in damage category

The damage clearly evident from the observations for these buildings (VZG4-8) is category 5, very severe. This is associated mainly with the sloping of the floors and walls and the separation of the different houses from each other, resulting in severe serviceability problems. The stability of the buildings was also in question, so the buildings were temporarily braced by wooden supports.



Figure 10.14 Details of cracks shown in Figure 10.12; left: crack number 1 between Vijzelgracht 10 – 8, right: crack number 9 (crack width max. 10 mm)

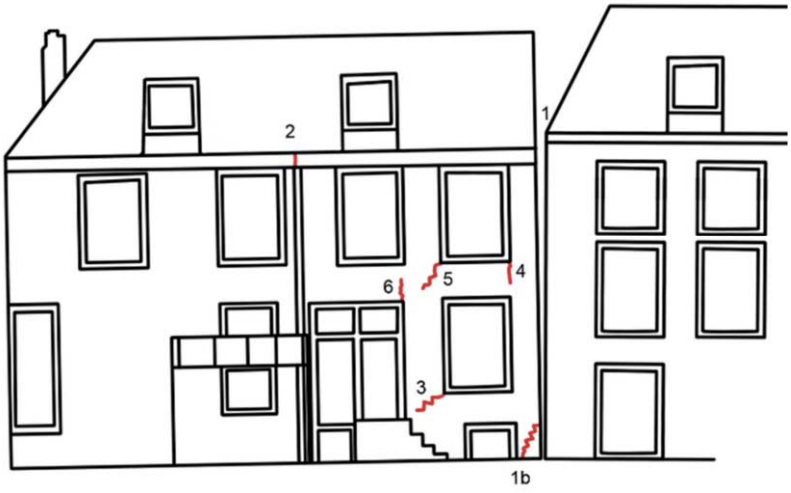


Figure 10.15 Cracks side façade (Vijzelgracht 4 on the left, 1e Weteringdwarsstraat 70 on the right)

Description of the cracks:

1 vertical crack between buildings, maximum width of about 250 mm

2 –6 on the outside.

10.7 Repair of the buildings

10.7.1 Corrective grouting of the buildings affected by the first incident

After bracing the buildings, it was decided to use corrective grouting to increase the bearing capacity of the sand and to lift the buildings. For the final restoration of the buildings a new foundation will be installed. It was implicitly demonstrated that the end bearing capacity of the pile foundations had been restored, when lifting of the buildings proved possible and stability of the building had been assured. Moreover, it showed that it was possible to apply further grouting to compensate for future settlements from on going construction of the station.

Although lifting of the buildings was successful, it appeared that for these conditions (loose sand due to ground loss) the efficiency of the corrective grouting process was very low. On going settlements were found up to at least 5 months after finishing the grouting. The buildings responded to the grouting in a relatively stiff manner, probably due to the temporary stabilizing timber cross beams, which made analysis of the grouting process difficult. Details of the corrective grouting can be found in Bezuijen et al. (2009).

10.7.2 Lifting the buildings affected by the second incident

Since the buildings of the second incident already had foundation renewal prior to the start of construction, it was decided to test the remaining capacity of the piles by static pile load tests, using the building as counter weight. Most of the piles had an ultimate capacity above 400 kN, which was the test level. The original pile load is about 250 to 280 kN. For a group of piles close to the leakage (See
) the ultimate capacities ranged from 300 to 350 kN. A few piles further away had capacities as low as 125 up to 225 kN, which could either be due to an irregular shape of the leakage effect or due to an originally low capacity. Both pile load tests in the annex on the right side of Vijzelgracht 4 were stopped at low test levels to avoid damage to the upper structure. From the load tests it appeared that only a few piles had insufficient bearing capacity. It was decided to lift the whole block by jacking the piles; 5 piles were added in Vijzelgracht 6 to compensate for the loss of bearing capacity of the affected piles. The maximum lift to be obtained was 220 mm at the corner of Vijzelgracht 4, as shown at location C in Figure 10.17. The procedure for lifting the buildings is described in De Nijs and Kaalberg (2010).

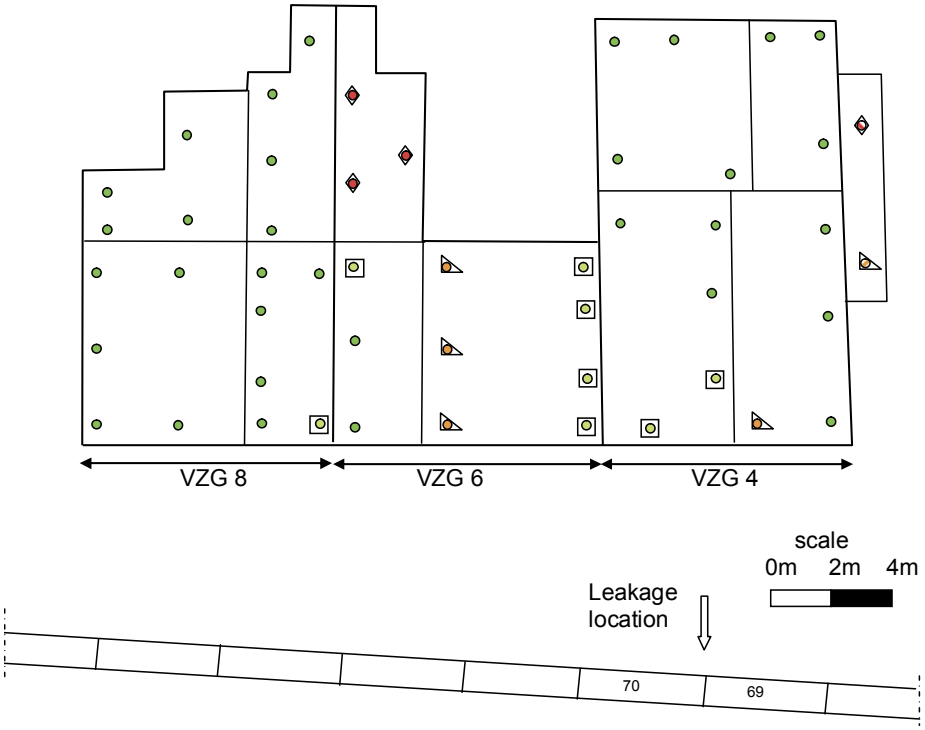


Figure 10.16 Schematic plan of Vijzelgracht 8, 6 and 4 with location of leakage and results of pile load tests (● piles test result = 400kN, ◻ piles test result 350-400 kN; ◺ piles test result 300-350 kN; ◇ piles test result <300 kN)

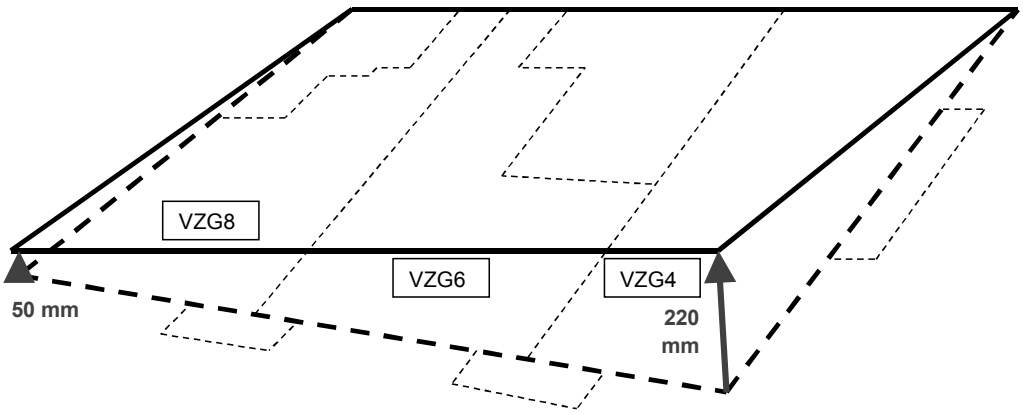


Figure 10.17 Jacking plan with main lift direction from De Nijs and Kaalberg (2010)

10.8 Continuation of the excavation

To continue the excavation after the leakage incidents, it was necessary to reassess the risks related to the leakage. Qualitative relationships could be established – using an analysis of the diaphragm wall panel production data, the construction log books, the electrical measurements and the observations during excavation – prior to further excavation about the quality of the walls and about the locations and severity of possible bad spots in the diaphragm walls. The analysis focused particularly on determining in advance which suspect locations could be so serious that they will fail immediately upon excavation, resulting in a breakthrough of water and sand. However, it was not possible to establish any direct, unambiguous relationship between the construction data, the geophysical ECR®) / EFT® results and the observed quality of the joints. In order to ensure an adequate level of certainty during the subsequent excavations, each joint had to be considered a potential severe leak. As the project organization recognized that a new event, comparable with the two incidents that occurred before, would stop the project permanently because of public and political concern, it was decided that it was necessary to seal all of the diaphragm wall panel joints before further excavation could start.

Because of the impossibility or unacceptability to carry out works from street level, it was decided to seal the joints from inside the excavation by freezing the joints. Adjacent to every joint two freezing pipes were installed close to the diaphragm wall, see Figure 10.18.

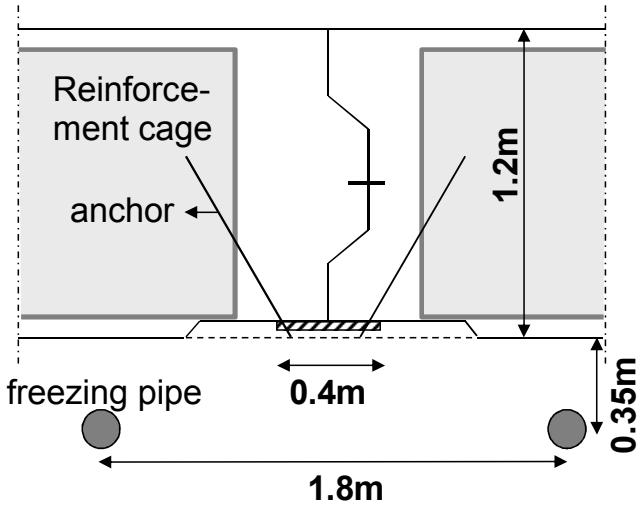


Figure 10.18 Cross section of diaphragm wall with location of freezing pipes and reinforcement cages. Steel plates (400x600x10mm) are anchored in the wall to cover the joint, after (partial) removal of the frozen soil mass and the outer skin of the diaphragm wall.

After creating the frozen body - consisting of frozen soil, D-wall and possible inclusions in the wall -, the staged excavation was continued in layers of about 4 m. During each stage the joints were excavated first and covered with steel plates which were fixed to the diaphragm wall

while the freezing process continued deeper down for the next stage of excavation. This preventative sealing covers all sand layers in the depth of the excavation. Excavation in the Eem-clay was considered to pose no severe leakage risk.

The same procedure was adopted for Rokin Station as this excavation was at the same level at the time of the events and the risk analysis was similar to that for Vijzelgracht Station. At Ceintuurbaan Station, the excavation had already reached the Eem-clay layer, no severe leakages had occurred, and therefore no additional measures were taken.

10.9 Conclusions and lessons learned

The lessons from these events have been learned at different levels. The organisational structure of the project level has been adapted, with other and new personnel and new working methods introduced. Clients, consultants and contractors united in a CUR-committee (CUR is comparable with CIRIA) to improve the D-wall installation and excavation process.

Related to D-wall problems Van Tol *et al*. (2010) reported lessons learned in the Netherlands and in Belgium over the last years, including the Vijzelgracht events. They concluded the following:

- The observed leakages occur at or directly adjacent to the panel joints in the zones outside the reinforcement cages.
- The process of excavation, cleaning the bentonite, placing the reinforcement and concreting should be uninterrupted.
- Two-phase excavation of the panels should be avoided except where the grab is fully guided on the stop end system. A one-phase or three-phase excavation will lead to higher excavation accuracy.
- During excavation, steps must be taken immediately when water flows through the joints, even when small amounts of water are involved. The measures required should be included in the specifications.
- The present leakage detection systems like ECR® and EFT® are not yet able to detect bentonite inclusions. The feasibility of sonic logging and geophysical logging to detect weak spots in the D-walls, before starting excavation, should be researched.

Van Tol *et al*. (2010) argue that diaphragm walls are still the most favourable solution for retaining walls in deep excavations in urban areas. A more detailed monitoring of the execution process in accordance with EN1538, supplemented by the lessons learned, is necessary. When only limited general construction information is available, good quality control is impossible, both for the contractor and the supervisors. If the execution process is monitored in detail, however, the quality of the product can be guaranteed and the risks of severe leaks can be minimised.

Relating to the building damage, the following lessons were learned:

- The damage criteria proposed by several authors, such as Skempton and MacDonald (1956), Burland *et al.*(1977), Boscardin and Cording (1989), Mair *et al*. (1996) and Son and Cording (2005), describe the observed damage to the facades reasonably well, even for the large deformations that occurred.
- Additionally, rigid body tilt can in extreme circumstances cause severe problems of serviceability and stability to buildings as also stated by Charles and Skinner (2004). In the Amsterdam cases, this proved more problematic than the curvature and resulting cracking of the building, possibly due to the flexible nature of the construction. Rigid body tilt usually does not receive much attention for low-rise buildings.

Regarding the repair of the buildings the following can be concluded:

- Pile capacity decreased significantly in the zone of influence of the leakage and even at locations further away.
- Corrective grouting proved successful in lifting the buildings
- For conditions with loosened sand due to ground loss, the efficiency of the corrective grouting process is rather low.

CHAPTER 11 CONCLUSIONS AND RECOMMENDATIONS FOR FUTURE RESEARCH

11.1 Introduction

In underground construction, (deep) excavations are commonly used. The construction works affect buildings and structures directly adjacent to them. To identify which buildings will be influenced and to what extent, an assessment of the building damage usually consists of the following steps: 1) determine green field displacements, 2) impose displacements onto building, 3) assess potential damage, 4) design measures if necessary. Most methods to assess the impact on the buildings are originally developed for tunnelling projects and buildings with shallow foundation and have in this study been validated specifically for piled buildings near deep excavations. Since trends in construction of deep excavations include deeper excavations situated closer to buildings, this research aimed to gain insight into mechanisms of soil-structure interaction for piled buildings adjacent to deep excavations and to find a reliable method to design and monitor deep excavations in urban areas with soft soil conditions. The results presented are valid mostly for 10-30 m deep excavations, constructed by means of diaphragm walls, and top down in soft soil conditions with a high ground water table. The analytical model for the pile-soil interaction of Chapter 7 and section 11.3 may be used in any situation where piles are influenced by vertical soil displacements.

Each of the following sections involves one of the steps in the building damage assessment procedure, with the exception of the last step, the mitigating measures. The conclusions answer the general question from Chapter 1: How can we predict the behaviour of one or more (piled) buildings an adjacent deep excavation will be constructed?

11.2 Ground displacements

The ground displacements for the Amsterdam cases have been compared to several, mostly empirical, relationships to determine the green field surface displacements and displacements at depth. Most methods assume that the shape of the displacements is related to the shape of the deformed wall and the soil type. The effect of the relative flexibility or stiffness of the system (wall and supports) compared to the soil stiffness, the safety against basal heave and the duration of the excavation could not been assessed due to a lack of variables present in the deep excavations studied.

From the Amsterdam cases it is concluded that the surface displacement behind the wall is 0.3 – 1.0% H (for an average system stiffness and sufficient basal stability). Better results are possible (0.2-0.5%H) for diaphragm walls with good supports, if installation effects are controlled sufficiently. Surface displacements behind the wall can be much larger than the wall deflections, as proved in the Amsterdam deep excavations, and may reach over a distance of 0.75H from the wall and become negligible at 2-3 times the excavated depth away from the wall. The shape of the surface settlements resemble the hogging shape as defined by Peck (1969). For the excavation stage only, the shape of the surface settlement consists of a sagging part close to the excavation and a hogging part at larger distance (comparable to a tea spoon) and complies well with results generally found in FEM calculations for deep excavations. The shape of the displacement fits the profile of Hsieh and Ou (1998) best for the excavation stages.

Although the subsurface measurements are located at close distance (2-3m) from the nearest building facades, no clear relationship is found between the amount or the shape of the settlements with the distance to the facades. The measured soil displacements can be considered as similar to 'free field' displacements.

In all three of the Amsterdam cases, the largest effect on the ground surface displacement can be attributed to the preliminary activities, which took in total about 4 of the 6 years presented. The actual excavation stage caused only about 25-35% of the surface displacements, with 55-75% attributed to the preliminary activities.

The main displacements caused by the excavation and its construction works take place within about 2 times the excavated depth at the surface level. At larger excavation depths, the influenced zone is significantly smaller. Most prediction methods overestimate the influence zone at depth compared to the measured values for the deep stations. It must be mentioned that only a limited number of extensometers show trustworthy results, which means that this conclusion is based on a limited number of cross sections. At the sections presented, this effect however is clearly shown.

The diagonal line from Aye et al. (2006) could be used as an estimate for the influence area, since it is a conservative line. Also the curvature of the displacement profiles from this method can be considered conservative. For a better fit, the maximum distance from the wall for significant surface displacements (D_0) could be taken as 2 times the excavated depth (instead of 2.5 times as suggested by Aye et al. (2006), see Figure 11.1).

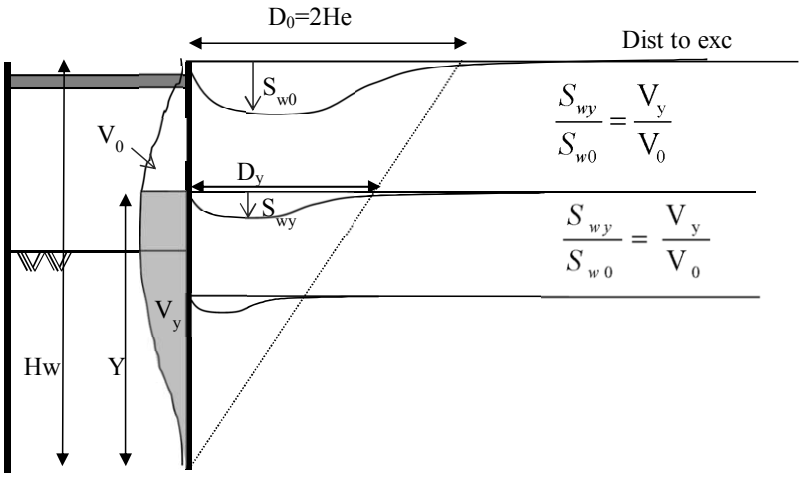


Figure 11.1 Proposed influence area for vertical soil displacements, modified from original Aye et al. (2006).

11.3 Soil – pile interaction

11.3.1 Pile behaviour

Most of the piles under the buildings along the North South Line are about 100 year old timber piles. In clay, the maximum shaft friction develops at about 25 mm and in sand at about 15 mm relative displacement. The maximum base capacity for piles with 130 mm diameter is reached at about 10% of the diameter, as can be found in common design methods. The old piles find in failure 60% of their capacity at the toe, 10% as friction in the sand layer and 30% as friction in the Holocene layers.

The shaft friction of old timber piles is about 40% lower than for new timber piles, based on the tests at the Dapperbuurt in Amsterdam. This may be explained as a side effect of the bacterial decay of timber piles, leading to a 'smearing' layer around the shaft. This layer affects both the positive and negative shaft friction.

11.3.2 Response to deep excavations

The buildings in the influence zone of the excavation experience several phenomena, which combined result in the building settlement:

1. Reduction of pile capacity due to lower stress levels
2. Settlement of the pile tip due to soil deformations below the base of the pile
3. Development of negative (or positive) skin friction due to relative movements of the soil and the pile shaft
4. Redistribution of pile load over the piles under the building slab, the building wall or a foundation cap or beam, depending on the building stiffness
5. Horizontal deformations of the piles (causing bending of the pile).

The settlement of the pile head is determined by the summation of the first four effects described above. Since timber piles are rather flexible in horizontal loading, they tend to follow the soil deformations. This effect is not part of the interaction model.

11.3.3 Interaction level

End bearing piles with sufficient capacity to accommodate full negative skin friction along the pile tend to follow the settlement of the foundation layer of the pile. This settlement is generally much smaller than the surface settlement. This is significantly different for friction piles. The settlement of friction piles is determined mainly by the working load in relation to the failure load. For larger working loads, the pile settlement approaches the surface settlement. For small working loads, the settlement of the pile is smaller than the surface settlement, but larger than the settlement of the foundation layer.

Since most piles both rely on end bearing and shaft friction, the interaction depends on all the factors described above. Common generalizations that end bearing piles settle with the soil at the tip level and friction piles with the surface level are valid only for certain extreme cases. In the majority of the cases, the actual pile settlement is found in between those values.

By definition, the pile settlement due to the construction works is equal to the soil displacement at what is called the 'interaction level' in this study. This relative depth along the pile z_i/L_p depends on the following dimensionless factors:

- the working load on the pile compared to the maximum failure load $\frac{W}{W_{max}}$
- the percentage of end bearing and shaft friction $\frac{Q_b}{W_{max}}$
- the shape of the soil settlements with depth $\frac{\Delta S}{D_z}$
- the distribution of the maximum shaft friction with depth $\frac{\tau_{max;Lp}}{\tau_{max;0}}$

The interaction level is not always equal to the neutral level of the pile, because the neutral level may shift during the construction works. Only if the shaft friction has already been fully developed (in negative and/or positive direction), the interaction level is equal to the neutral level and remains constant during the works.

For piles with a mix of shaft friction and end bearing, the interaction level moves upward from between 50%-100% of the pile length towards the pile head level. For piles with at least 50% end bearing and a safety factor of at least 2 (W/Wmax <0.5), the pile settlement follows the soil at 70% of the pile length or deeper. Piles with smaller percentages of end bearing or smaller safety factors settle significantly more, ultimately leading to the maximum pile settlement being equal to the maximum soil settlement, which for excavations is found at the surface.

11.3.4 Specific for the Amsterdam Cases

The neutral level of the buildings in Amsterdam depends on the relative load on the pile and the soil displacement experienced prior to the construction works. In general, prior to construction, the neutral level for the historic buildings is found about halfway through the depth of the compressible layers.

During construction, the old pile foundations in Amsterdam generally have interaction levels z_i/L_p around 0.5 for the original foundations and 0.8-1.0 for the renewed foundations. Modern pile foundations have interaction levels z_i/L_p close to 1.0. This means the building deformation is close to the free field displacement of the foundation layer. For buildings where the pile load and pile capacity can be estimated, the calculated interaction level z_i/L_p is in good agreement with the measured values. In most cases in practice, however, no detailed information is present about the foundation.

If a basement is present under the building, the settlement of the building is generally smaller than without a basement. The interaction level z_i/L_p for buildings with basement is thus closer to 1.0 than for buildings without basement. This is explained by the fact that the load on the piles is smaller if a basement is present (due to the uplift pressure), that buildings with basement more often have renewed foundations, that the pile length over which negative friction may occur is shorter and that even without piles the buildings would follow the level at which the basement is founded and not the surface level.

The theoretical interaction level z_i/L_p is assumed constant for piles that have experienced significant soil displacements before construction works started and is found at the same depth as the neutral level. The maximum positive and/or negative friction have already developed to the maximum and the neutral level remains at the same position when additional soil displacements occur. The interaction level z_i/L_p determined from measurements varies sometimes significantly between the different construction stages, but the initial z_i/L_p level is a good reference for the overall settlement to be expected during all construction works.

The foundation class used in Amsterdam to determine the state of the foundation related to this decay can to a certain extent be used as an indicator for the relative amount of settlement of the building, but large variations still occur as a result of varying relative pile loads.

It is concluded that the most likely buildings in Amsterdam to have an interaction level between 0 and 0.5 are built before 1900, have Foundation Class III and do not have a basement. For all other buildings, any interaction level z_i/L_p between 0.5 and 1.0 is likely depending mainly on the working load versus pile capacity (W/Wmax). The effect of the soil settlement profile is not present for the Amsterdam cases, because the shaft friction is already mobilized before the excavation works started (due to subsidence).

11.4 Building response

The largest influence of the construction works (between 55 and 65% of the building settlements) is due to the preliminary activities (diaphragm wall construction and subsidence over 4 years between 2003-2007). During excavation of the station, the additional building deformations are less than 10 mm. In all stages, deflection ratios are small (of the order of 0.03%). The different facades along a cross section show that in most cases the individual buildings behave like structural units even when this is technically not the case.

At Ceintuurbaan Station, the largest difference is noticed between the building settlements measured by the manual levelling points and the automatic prisms of about 10 mm over 8 years. This means the 1st sand layer settles a little over 1 mm per year compared to the 3rd sand layer for the reference locations outside the influence zone of the deep excavation. Ceintuurbaan is the most recent area of the three stations, which explains the smaller difference in the oldest part (Rokin, about 5 mm over 8 years) and at Vijzelgracht (0 - 8 mm over 8 years), which is in between the other stations. The observed settlement difference between the manual and automatic measurements does not affect the building damage characteristics, because it is mainly a general difference over the whole cross section or façade.

The horizontal displacement of the building at street level is of the same order as the vertical settlement of the building. This observation, which can be used to determine the horizontal strain in the building, is very specific for the Amsterdam situation.

The buildings tilt towards the excavation, based on absolute values of the additional displacements during the period 2001-2009, at Rokin is 1:2200 and at Ceintuurbaan 1:1150. At about once the excavation depth or 25-35 m for Ceintuurbaan station the building tilt is smaller than 0.0005 or 1:2000. For Rokin this relationship is less clear.

The deflection of the building is compared to the deflected shape of the soil at surface level and pile tip level. Although a large variation is found in the results, the soil at the neutral level settled with a deflected shape somewhere in between the surface and foundation level. In some of the buildings, clearly some effect of the stiffness of the building is present while other buildings deform rather flexible. The Goh and Mair (2011) method provides a realistic, although rather large, range of possible modification factors for the deflection of buildings next to excavations, deforming in hogging shape.

For the incidents that happened at Vijzelgracht some well known damage indicators have been evaluated. The damage criteria proposed by several authors, such as Skempton and MacDonald (1956), Burland et al. (1977), Boscardin and Cording (1989), Mair et al. (1996) and Son and Cording (2005), describe the observed damage to the facades reasonably well, even for the large deformations that occurred. Additionally, rigid body tilt can in extreme circumstances cause severe problems of serviceability and stability to buildings as also stated by Charles and Skinner (2004). In the Amsterdam cases, this proved more problematic

than the curvature and resulting cracking of the building, possibly due to the flexible nature of the construction. Rigid body tilt usually does not receive much attention for low-rise buildings.

11.5 Recommendations for future research

11.5.1 General recommendations

Since the largest part of the soil displacements is caused by the preliminary activities, such as diaphragm wall installation, predrilling, raising of the ground level and installation of the jet grout strut, it is recommended to study the installation effects of in situ ground improvement techniques in more detail. Displacements caused by diaphragm wall installation and excavation of the station have been studied in much more detail than the in situ techniques, but caused a smaller part of the overall displacements.

Especially for piled buildings, the amount and shape of soil displacements at depth are more relevant than the surface displacements, which have been extensively studied by many authors. Validation of FE-methods and the analytical method by Aye et al. (2006) could be undertaken by analysing other deep excavations case histories or experimental modelling. To obtain good quality field data, deep excavations should be equipped with robust systems such as manual back up displacement monitoring. Research should be undertaken to study the performance of subsurface monitoring systems such as inclinometers and extensometers. Currently it is not possible to determine which systems are reliable over a longer period of time. An evaluation of automatic and manual systems could improve monitoring results for future projects.

Related to the foundation piles, the interaction analysis performed in this thesis should be validated with experimental modelling and finite element modelling to further improve the assessment of building response. Experimental modelling could focus on the effect of the working load on the pile and the group effects caused by load redistribution. Numerical modelling could focus on the effect of the relative stiffness of the soil compared to the pile (shaft and tip). Numerical modelling of displacement piles including installation effects is not evident, so at first the potential of the current methods should be determined for this topic. The development of meshless techniques will give the opportunity to realistically model the pile and pile-soil interface.

11.5.2 Recommendations for typical Dutch conditions with timber piles

The behaviour of old timber piles proved in this study to deviate from new timber piles. The origin and impact of this effect should be studied since it is important to understand the response of piled buildings. Old and new timber piles could be tested for the Young's modulus in the axial direction of the pile and the friction coefficient between shaft and different soil types as a function of possible degradation of the shaft.

In Amsterdam, the effect of the subsidence on all of the buildings founded on the first sand layer may be significant. The monitoring for the North South Line project helped tremendously to improve the insight into this effect. To determine long term impact of this effect, it is recommended to continue monitoring (at least some of) the manual levelling points. The results should be analysed after 5 or 10 years to decide how to deal with this effect in the future.

The monitoring results collected from the Amsterdam deep excavations may be used for many more validations and analyses related to the response of buildings to the construction of deep excavations. It is recommended that, for example, the actual building deformations and resulting damage should be compared to the theoretical building damage indicators.

References

ABNZL (2000) *Grondonderzoek Noord/Zuidlijn, parameterset definitief ontwerp*. Ref. 01270L/R991835.D1. 31-03-2000 Adviesbureau Noord/Zuidlijn (in Dutch)

ABNZL (2004) *parameterset5.xls*, Draft DO2 date 21-4-2004 Adviesbureau Noord/Zuidlijn (in Dutch)

ABNZL (2008) *Station Rokin Monitoringssommen. PLAXIS berekeningen*, 16-9-2008 6E5145/R020/902394/Rott. Adviesbureau Noord/Zuidlijn (in Dutch)

Alonso, E. E., Josa, A. and Ledesma, A. (1984) Negative skin friction on piles: a simplified analysis and prediction procedure. *Géotechnique* 34, No. 3. 341-357

American Petroleum Institute API (1993) *Recommended Practice for Planning, Designing and Constructing Fixed Offshore Platforms - Working Stress Design*. API RP 2A-WSD, 20th Edition, Washington, 1 July 1993, pp 59-61

Aobpaet, A., Caro Cuenca, M., Hooper, A., Trisirisatayawong, I. (2010) Land subsidence evaluation using INSAR time series analysis in Bangkok metropolitan area. *Proceedings Fringe 2009 Workshop*, Frascati, Italy, ESA SP-677.

Aye, Z.Z., Karki, D. and Schulz, C. (2006) Ground Movement Prediction and Building Damage Risk-Assessment for the Deep Excavations and Tunneling Works in Bangkok Subsoil. *International Symposium on Underground Excavation and Tunnelling* 2-4 February 2006, Bangkok, Thailand

Berezantzev, C.V., Khristoforov, V. and Golubkov, V. (1961) Load bearing capacity and deformation of piled foundations, *proc. 5th. int. conf. on soil mechanics and found. eng. Paris*, vol 2. pp 11-15

Bezuijen, A and Van der Schrier, J. (1994) The Influence of a bored tunnel on pile foundations, *Proceedings of Centrifuge 94*: pp 681-686.

Bezuijen, A., Kaalberg, F.J., Kleinlugtenbelt, R. and Roggeveld, R.P. (2009) Corrective grouting in sand to restore pile foundations, Vijzelgracht, Amsterdam. *Int. Conference of Soil Mechanics and Geotechnical Engineering*, Alexandria, Egypt. pp 2449-2452.

Biarez, J and Hicher, P-Y. (1994) *Elementary Mechanics of Soil Behaviour, Saturated remoulded soils*, Balkema

Bijnagte J.L. and Luger, H.J. (2000) *3D modelling of single piles and pile groups. Manual D-Pilegroup version 5.1.* Deltares, Delft, The Netherlands

Bjerrum, L. (1963) Allowable settlement of structures. *Proceedings of the European Conference on Soil Mechanics and Foundation Engineering*

Bjerrum, L., Johannessen, I. J. and Eide, O. (1969) Reduction of skin friction on steel piles to rock. *Proceedings of 7th International Conference of Mechanics and Foundation Engineering*, Vol.2, Mexico, pp. 27-34.

BMA Amsterdam (2008) Weaver buildings. www.bma.amsterdam.nl

BMA Amsterdam (2009) Rokin picture http://www.nieuwbouw.amsterdam.nl/contents/pages/108930/rokin.jpg

Bolton, M.D. (1986) The strength and dilatancy of sands. *Géotechnique,* 36 (1): pp 65-78

Bolton, M.D., Lam, S.Y. and Osman, A.S. (2008) Supporting excavations in clay – from analysis to decision-making. In C.W.W. Ng, H.W. Huang & G.B. Liu (eds), *Proc. 6th intern. symp. on Geotechnical Aspects of Underground Construction in Soft Ground, Shanghai, 10-12 April 2008*: pp 15–28. London: Taylor & Francis Group.

Bonshor, R. B. and Bonshor, L.L. (1996) *Cracking in buildings*, BRE Publication, Construction Research Communications Ltd. Watford, Herts, UK.

Boone, S. J., Westland, J. and Nusink, R. (1999) Comparative evaluation of building responses to an adjacent braced excavation. *Canadian Geotechnical Journal* 36(2): pp 210-223.

Boone, S.J. (2001) Assessing construction and settlement-induced building damage: a return to fundamental principles. *Proc. Underground Construction*, *Institution of Mining and Metalurgy, London*: pp 559–570.

Boscardin, M.D. and Cording, J.C. (1989) Building response to excavation-induced settlement. *ASCE Journal of Geotechnical Engineering*, 115(1): pp 1–21.

Bosch, J.W. and Broere, W. (2009) Small incidents, big consequences. Leakage of a building pit causes major settlement of adjacent historic houses. Amsterdam North-South metro line project. *ITA 2009*, Budapest, Hungary. Paper O-10-06.

Boutelje, J.B. and Bravery, A.F. (1968) Observations on the bacterial attack of piles supporting a Stockholm building. *Journal of the Institute of Wood Science*, No. 20, pp 47-57. Butterworths.

Bowles, J. E. (1988) *Foundation Analysis and Design*, McGraw-Hill Inc.

Bozozuk, M. (1972) Downdrag measurements on a 160-ft floating pipe pile in marine clay. *Canadian Geotechnical Journal* 9(4): pp 127–136

Broms, B.B. and Badholms, C. (1976) High capacity precast concrete piles at Thames Refinery Project. *Ground Engineering* Volume 9, Issue 5, July 1976, pp 19-23

Brassinga, H.E. and Tol, A.F. van (1991) Deformation of a high-rise building adjacent to a strutted diaphragm wall, *10th European Conference of Soil Mechanics and Foundation Engineering* Florence, Balkema, pp 787-790.

BRE (1995) Assessment of damage in low-rise buildings. *BRE Digest Concise reviews of building technology*, BRE.

Briaud, J. L., Jeong, S. and Bush, R. (1991) Group Effect in the Case of Downdrag. *ASCE GSP* 27: pp 505-518.

Burland, J.B. and Wroth, C.P. (1974) Settlement of buildings and associated damage: Session V review paper. *Conference on Settlement of Structures, Cambridge, April 1974*: pp 611–654, London: Pentch Press.

Burland, J,B., Broms, B.B. and De Mello, V.F.B. (1977) Behaviour of foundations and structures: state-of-the art report. *Proc. of the 9th International Conference on Soil Mechanics and Foundation Engineering, Tokyo,* 2: pp 495–546.

Burland, J.B. (1995) Assessment of risk of damage to buildings due to tunnelling and excavations. *Invited special lecture to IS-Tokyo 95: 1st Int. Conf. on Earthquake Geotechnical Engineering*, Tokyo.

Burland, J. B., Mair, R. J. and Standing, J.R. (2004). Ground performance and building response due to tunnelling. Conference on advances in geotechnical engineering - the Skempton conference. Thomas Telford London, ICE: pp 291-344

Carter, M. and Bentley, S.P. (1991) *Correlations of soil properties*, Pentech Press, London.

Caspe, M. S. (1966) Surface settlement adjacent to braced open cuts. *Journal of Soil Mechanics and Foundations division*, ASCE 92(SM4): pp 51-59.

Chao, H.C., Hwang, R.N. and Chin, C. T. (2010) Influence of Tip Movements on Inclinometer Readings and Performance of Diaphragm Walls in Deep Excavations. *Earth Retention Conference (ER2010)*. pp 326-333

Charles, J.A. and Skinner, H.D. (2004) Settlement and tilt of low-rise buildings. *Geotechnical Engineering*, vol 157, issue GE2, Institution of Civil Engineers: pp 65-75

Chen, L.T., Poulos, H.G. and Loganathan, N. (1999) Pile responses caused by Tunneling. *Journal of Geotechnical en Geoenvironmental Engineering*: pp 207-215

Clemente, F.M. Jr. (1981) Downdrag on bitumen coated piles in a warm climate. *Proceedings of the 10th international conference on soil mechanics and foundation engineering*, Stockholm, pp 673–676

Clough, G.W. and O'Rourke, T.D. (1990) Construction induced movements of in-situ walls. *ASCE Geotechnical special publication No.25 – Design and Performance of Earth Retaining structures*: pp 439–470.

COB (2009) *Eindrapport Bouwputten Tunnel Pannerdensch Kanaal, F501*. (in Dutch)

COB (2011a) *Soils, Buildings and foundations in Amsterdam, Background information for Dataset NoordZuidlijn*. Deltares & Witteveen+Bos for COB committee F531, 1203958-003-GEO-0001-jvm, draft 14 June 2011

COB (2011b) *Data set Rokin Station*. Deltares & Witteveen+Bos for COB committee F531, 1203958-003-GEO-0004-, draft version 02, Juli 2011

COB (2011c) *Data set Vijzelgracht Station* NoordZuidlijn. Deltares & Witteveen+Bos for COB committee F531, 1203958-003-GEO-0003-sr, draft August 2011

COB (2011d) *Data set Ceintuurbaan Station.* Deltares & Witteveen+Bos for COB committee F531, 1203958-003-GEO-0002-, draft June 2011

Cooke, D.K. (2006) Robotic Total Stations and Remote Data Capture: Challenges in Construction. *Geotechnical Instrumentation News*, December 2006.

Combarieu, O. (1974) Adhesion Effect and a Method of Evaluating Negative Friction (In French). *Lab Cent Ponts Chaussees Bull Liaison Lab Ponts Chaussees* 71, pp 93-107

Cording, E. J., Long, J. H., Son, M., and Laefer, D. F. (2001) Modeling and analysis of excavation-induced building distortion and damage using a strain-based damage criterion. *London Conference on Responses of Buildings to Excavation-Induced Ground Movements*, Imperial College, London.

Cording, E. J., Long, J. L., Son, M., Laefer D. and Ghahreman B. (2010) Assessment of excavation-induced building damage. Earth Retention Conference (ER2010). pp 101-120

CUR (1995) *Tunneling close to foundation piles* (in Dutch) Gouda, Stichting CUR.

Davies, R.V. and Henkel, D. (1982) Geotechnical problems associated with the construction of Chater Station, Hong Kong. *The Arup Journal* 17(1): pp 4-10.

De Beer, E. (1966) Berekening van de negatieve wrijving op palen. *Tijdschrift der openbare werken van Belgie*, No. 6, 1966, p. 29. (in Dutch).

De Nicola, A. and Randolph, M.F. (1993) Tensile and compressive shaft capacity of piles in sand, *Journal of Geotechnical Engineering*, ASCE, 119:12, pp 1952-1973

De Nijs, R.E.P. and Buykx, S.M. (2009) Instrumentation and Monitoring at Deep Excavation in Historic City of Amsterdam - Design and Performance Analysis of Monitoring System at Ceintuurbaan Station, *ITA-AITES*, Hungary 2009

De Nijs, R.E.P. and Kaalberg, F.J. (2010) Recovery of pile bearing capacity (In Dutch: Herstel paaldraagvermogen). *Cement 2010/8*. pp 48-53.

De Ruiter, J. and Beringen, F. L. (1979) Pile foundations for large North Sea structures. *Marine Geotechnology 3*, No. 3, pp 267-314.

Delfgaauw, S., Buykx, S.M. and Bosch, J.W. (2009) Jet Grout Strut for Deep Station Boxes of the North/South Metro Line Amsterdam – Design and Back Analysis. *Proceedings ITA world conference*, Budapest Hungary

Dimmock, P.S and Mair, R.J. (2008) Effect of building stiffness on tunnelling-induced ground movement. *Tunnelling and Underground Space Technology*, 23(4): pp 438–450.

DIN (1986) *Cast-in-situ concrete diaphragm walls; design and construction*. DIN4126 Deutsches Institut Fur Normung

Elshafie, M. Z. E. B. (2008) *Effect of building stiffness on excavation induced displacements*. Ph.D. thesis, University of Cambridge, UK.

Farrell, R.P. (2010) *Tunnelling in sands and the response of buildings*. Ph.D thesis, Cambridge University, UK.

Fellenius, B. H. (1972) Down-drag on piles in clay due to negative skin friction. *Canadian Geotechnical Journal*, 9 (4), pp 323–337. http://dx.doi.org/10.1139/t72-037

Fernie, R., Shaw, S. M, Dickson, R. A, St John, H. D, Kovacedic, N, Bourne-Webb, P. and Potts, D. M. (2001) Movement and deep basement provisions at Knightsbridge Crown Court, Harrods, London. *Int. Conf. Response of Buildings to Excavation Induced Ground Movements*. CIRIA

Finno, R. J., Calvello, M. and Bryson, S.L. (2002) *Analysis and Performance of the Excavation for the Chicago-State Subway Renovation Project and its Effects on Adjacent Structures,* Department of Civil and Environmental Engineering, Northwestern University Evanston, IL 60208: 347.

Fleming, K., Weltman, A., Randolph, M. and Elson, K. (2009) *Piling Engineering* – third edition. Taylor & Francis, Oxon, UK.

Frankenmolen, S.F. (2006) *Analyse Noord/Zuidlijn monitoringsdata* (Analysis of Noord/Zuidlijn monitoringdata, in Dutch), MSc thesis, Delft University of Technology.

Franzius, J. N., Potts, D. M., Addenbrooke, T.I. and Burland, J.B. (2004) The influence of building weight on tunnelling-induced ground and building deformation. *Soils and Foundations* 44(1): pp 25-38.

Franzius, J. N. and Potts, D. M. (2006) The influence of the soil-structure interface on tunnel induced building deformation. *Numerical Methods in Geotechnical Engineering*: pp 291-297.

Franzius, J. N., Potts, D. M. and Burland, J. B. (2006) The response of surface structures to tunnel construction. *Proc. Institution of the Civil Engineers, Geotechnical Engineering*, 159(1): pp 3–17

Fukuya, T., Todoroki, T. and Kasuga, M. (1982) Reduction of negative skin friction with steel tube NF pile, Proceedings 7th Southeast Asian Geotechnical Conference, Hong Kong, pp 333–347

Gaba, A.R., Simpson, B., Powrie, B. and Beadman, D.R. (2003) *Embedded retaining walls guidance for economic design.* CIRIA C580, London: CIRIA.

Goh, K.H. (2010) *Response of ground and buildings to deep excavations and tunnelling*. Ph.D thesis, Cambridge University, UK.

Goh, K.H. and Mair, R.J. (2011) The response of buildings to movements induced by deep excavations. *Geotechnical Aspects of Underground Construction in Soft Ground - Proceedings of the 7th International Symposium on Geotechnical Aspects of Underground Construction in Soft Ground*, Rome. pp 903-910.

Goldberg, D.T., Jaworski, W.E., and Gordon, M.D. (1976) Lateral support systems and underpinning. *Reports FHWA-RD-75-128 to 131,* Washington D.C: Federal Highway Administration.

Grant, R., Christian, J. T. and Vanmarcke, E. H. (1974) Differential Settlement of Buildings. ASCE, *Journal of Geotechnical Engineering Division* 100(GT 9): pp 973-991.

Hirose, K., Maruyama, Y., Murdohardono, D., Effendi, A. and Abidin, H.Z. (2001) Land subsidence detection using JERS-1 SAR Interferometry. *2nd Asian conference on remote sensing.* Centre for remote imaging, sensing and processing (CRISP), NUS, Singapore.

Hoekstra, J. and Bokhoven, W. (1974) *Systematisch funderingsonderzoek van de Dapperbuurt ("Systematic foundation research in the Dapperbuurt area"),* Laboratorium voor Grondmechnica, Delft, reference CO-21606/503 (In Dutch)

Hogenes, C.A.G. (1998) *Meetboutennet Amsterdam (NAP-hoogtemerken)*. Omegam, 7 augustus 1998

Hsieh, P. G. and Ou, C. Y. (1998). Shape of ground surface settlement profiles caused by excavation. *Canadian Geotechnical Journal*, 35: pp 1004–1017.

Hull, T.S., Lee, C.Y. and Poulos, H.G. (1991) *Mechanics of pile reinforcement for unstable slopes.* Research Report - University of Sydney, School of Civil and Mining Engineering
Issue 636, April 1991, p36

Indraratna, B., Balasubramaniam, A.S., Phamvan, P. and Wong, Y.K. (1992) Development of negative skin friction on driven piles in soft Bangkok clay. *Canadian Geotechnical Journal* 29(3): pp 393–404

Jacobsz, S. W. (2002). *The effects of tunnelling on piled foundations*. Geotechnical Department. Cambridge, University of Cambridge. Doctor of Philosophy.

Jacobsz, S. W., Bowers, K.H., Moss, N.A. and Zanardo, G. (2005) The effects of tunnelling on piled structures on the CTRL. *Geotechnical Aspects of Underground Construction in Soft Ground, Amsterdam*, Taylor&Francis Group, London.

Kaalberg, F.J., Teunissen, E.A.H., van Tol, A.F. and Bosch, J.W. (2005) Dutch research on the impact of shield tunnelling on pile foundations. *Geotechnical Aspects of Underground Construction in soft ground* Taylor & Francis Group, London: pp. 123-131

Klaassen, R. (ed) (2005) *Preserving cultural heritage by preventing bacterial decay of wood in foundation piles and archaeological sites.* Final report EVK4-CT-2001-00043, Wageningen

Konstantakos, D. C. (2008) Online database of deep excavation performance and prediction. *6th international conference on case histories and geotechnical engineering*. Arlington, paper 5.16, pp 1-12

Korff, M., De Nijs, R. and Kimenai, J. (2011a) Ground and building movements during predrilling activities. *FMGM conference Berlin 2011*

Korff, M., Mair, R.J., van Tol, A.F. and Kaalberg, F.J. (2011b) Building damage and repair due to leakage in a deep excavation. *Proceedings of the Institution of Civil Engineers: Forensic Engineering* 164 (4) , pp. 165-177

Lam, S.Y. (2010) *Ground movements due to excavation in clay: physical and analytical models.* Ph.D thesis, Cambridge University, UK.

Lam, S.Y. and Bolton, M.D. (2011) Energy Conservation as a Principle Underlying Mobilizable Strength Design for Deep Excavations. *Journal of Geotechnical and Geoenvironmental Engineering*, Vol. 137, No. 11, November 1, 2011. ASCE

Lange, G. de, Dankelman, J.E., de Gans, W., Keestra, S.D. and Zwaan, H. (1999) *Geologische toetsing en beschrijving Noord/Zuidlijn*, (in Dutch: Geological review and description for NorthSouth Line) Report number 005.40162.01.01, 31-05-1999, TNO.

Lee, S. J., Song, T.W., Lee, Y.S., Song, Y.H. and Kim, I.K. (2007). A case study of building damage risk assessment due to the multi-propped deep excavation in deep soft soil. *4th Int. Conf. Soft Soil Eng. Vancouver*, London, Taylor Francis.

Lehane, B. M., Schneider J.A. and Xu X. (2007) The UWA-05 method for prediction of axial capacity of driven piles in sand. *Proc. Contemporary Issues in Deep Foundations (GSP 158)(Part of Geo-Denver 2007: New Peaks in Geotechnics).* ASCE.

Leonards, G. A. (1975) Discussion on Differential Settlement of Buildings. *ASCE, Journal of Geotechnical Engineering Division*(GT 7): pp 700-702.

Leung, C. F., Liao, B. K., Chow, Y. K., Shen, R. F. and Kog, Y. C. (2004) Behavior of pile subject to negative skin friction and axial load. *Soils and Foundations*, Vol. 44, No. 6, pp 17-26.

Leung, E. H. and Ng, C.W. (2007) Wall and ground movements associated with deep excavations supported by cast in situ wall in mixed ground conditions. *Journal of Geotechnical and Geoenvironmental Engineering* 133(2): pp 129-143.

Loganathan, N., Poulos, H.G. and Stewart, D.P. (2000) Centrifuge model testing of tunnelling-induced ground and pile deformations. *Géotechnique* 50 (3), pp 283-294

Long, M.M. (2001) Database for retaining wall and ground movements due to deep excavations. *ASCE Journal of Geotechnical and Geoenvironmental Engineering* 127(3): pp 203–224.

Lunne, T., Robertson, P.L. and Powell, J.J.M. (1997) *Cone Penetration Testing in Geotechnical Practice*, Blackie Academic&Professional, London.

Mair, R.J, Taylor, R.N. and Burland, J.B (1996) Prediction of ground movements and assessment of risk of building damage due to bored tunnelling. In R.J. Mair and R.N. Taylor (eds.), *Proc. intern. symp. on Geotechnical Aspects of Underground Construction in Soft Ground, London, 15-17 April 1996*: pp 713–718. Rotterdam: Balkema.

Mair, R.J. and Taylor, R.N. (2001) Settlement predictions for Neptune, Murdoch, and Clegg Houses and adjacent masonry walls. In J.B. Burland, J.R. Standing, and F.M. Jardine (eds), *Building Response to tunnelling – Case studies from construction of the Jubilee Line Extension, London. Vol. 1: Projects and Methods*: pp 217–228, London: Thomas Telford.

Mair, R.J. (2003) Research on tunnelling-induced ground movements and their effects on buildings – lessons from the Jubilee Line Extension. In F.M. Jardine (ed.), *Response of buildings to excavation induced ground movements, Proc. intern. conf., London, 17-18 July 2001*: pp 3–26. London: CIRIA.

Mair, R.J. (2011) Tunnelling and deep excavations - Ground movements and their effects. *Proceedings of the XV European Conference in Soil Mechanics and Geotechnical Engineering(ECSMGE-Athens).*
Meigh, A.C. (1987) *Cone Penetration Testing - Methods and Interpretation*, CIRIA

Mestat, P., Bourgeois, E. and Riou, Y. (2004) MOMIS: A database devoted to comparing numerical model results with in situ measurement: Applications to sheet piling. *Bulletin de Laboratoires des Ponts et Chaussées*. 252-253: pp 49-76

Meyerhof, G.G. (1953) Some recent foundation research and its application to design. *The Structural Engineer* 31: pp 151-167

Mierlo, W.C. van and Koppejan, A.W. (1952) Lengte en draagvermogen van heipalen; vaststelling hiervan en enige daarbij verkregen ervaringen. *Bouw* 3 (In Dutch)

Moorman, Ch. and Moorman, H.R. (2002) A study of wall and ground movements due to deep excavations in soft soil based on worldwide experiences. *Proc. 3rd intern. symp. on Geotechnical Aspects of Underground Construction in Soft Ground, Toulouse, 23-25 October 2002*: Lyon: Spécifique. pp 477–482

Mroueh, H. and Shahrour, I. (2002) Three dimensional finite element analysis of the interaction between tunnelling and pile foundations. *International journal for numerical and analytical geomechanics*, vol 26, pp 217-230
Müller-Breslau, H. (1906) *Erddruck auf Stutzmauern*, Stuttgart: Alfred Kroner-Verlag (in German)

NEN (2011) *Geotechnical design of structures - Part 1: General rules*, NEN 9997-1:2011 NL (Dutch version of Eurocode 7, including National Annex and Additional National Standard NEN9097)

Netzel, H. (2009). *Building response due to ground movements.* Ph.D. thesis, Delft University of Technology, the Netherlands.

Ong, D.E.L. (2004) *Pile behaviour subject to excavation-induced soil movement in clay.* PhD thesis NUS, Singapore

O'Rourke, T.D. (1993) Base stability and ground movement prediction for excavations in soft clay. *Retaining Structures*, Thomas Telford, London, pp 131-139.

Osman, A.S. and Bolton, M.D. (2007) Back analysis of three case histories of braced excavations in Boston Blue Clay using MSD method. *4th Int. Conf. Soft Soil Eng. Vancouver*, London, Taylor Francis, pp 755-764.

Oversteegen, M.J. (1998) *Basisrapport Casco-funderingsonderzoeken. Panden in de 19e –eeuwse gordel*. Stedelijke Woningdienst Amsterdam. Bureau P/A. 19-05-98

Peck, R.B. (1969) Deep excavations and tunneling in soft ground. *Proc. 7th International Conference on Soil Mechanics and Foundation Engineering,* Sociedad Mexicana de Mecanica de Suelos, A.C.*Mexico City*: pp 225–290.

Polshin, D.E. and Tokar, R.A. (1957) Maximum allowable non-uniform settlement of structures. *Proc. 4th International Conference on Soil Mechanics and Foundation Engineering, London, 12-24 August 1957,* 1: pp 402–405. Butterworth's scientific

Potts, D. M. and Addenbrooke, T. I. (1996) The influence of an existing structure on the ground movements due to tunnelling. *Geotechnical Aspects of Underground Construction in Soft Ground*, London.

Potts, D.M. and Addenbrooke, T.I. (1997) A structures influence on tunnelling-induced ground movements. *Proc. Institution of the Civil Engineers, Geotechnical Engineering* 125(2): pp 109–125.

Poulos, H. G. and Chen, L. F. (1997) Pile response due to excavation induced soil movement. *J. Geotech. Geoenviron. Eng.*, 123(2), pp 94–99.

Pound, C. (1999) *Second Opinion review of Eem Clay geotechnical properties*, report 40664/F&G/REP/104

Puller, M. (2003) *Deep excavations: a practical manual.* 2nd edition. Thomas Telford, London.

Rankin, W.J. (1988) Ground movements resulting from urban tunnelling: prediction and effects. *Engineering geology of underground movements*. Engineering Geology Special Publication No. 5. Geological Society. pp 79-92

Sagaseta, C., 1987. Analysis of undrained soil deformation due to ground loss. *Géotechnique* 37 (3), pp 301–320

Salet, Th. A. M. and Van 't Verlaat, J. (2004) Zorg om de omgeving primair bij uitvoering. *Land + Water* 8, August 2004 (In Dutch)

Salet, Th.A.M., De Kort, P.J.C.M. and Crawley, J.D. (2006) Amsterdam North South Line Metro -Construction of deep diaphragm walls for three underground stations. *Proc. Tenth International Conference on Piling and Deep Foundation*, Linderberg, Bottiau & van Tol (Eds), Amsterdam. DFI, Emap. pp 868-881

Samuel, A.L. (1994) The Effect of Live Load on Downdrag Forces. *ASCE Geotechnical Special Publication*, Vol. 2, Issue 40, pp 949-961

Sarlemijn, B.M.M., Bijkerk, J., Gerritsen, J., van Tol, A.F. and Racke, H.K. (1993) The Rotterdam Railway tunnel – design, construction, organisation, *Options for Tunnelling 1993*, ed. H. Burger, pp 203-230

Selemetas, D. (2004) On the assessment of pile settlement due to tunnelling: some lessons learned from a full-scale trial, *Proc. 16the European Young Geotechnical Engineers' Conference*, Vienna, Austria, pp 333-342

Shen, R.F. (2008) *Negative skin friction on single piles and pile groups*, PhD thesis NUS, Singapore

Shong, L.S. (2002) Pile Design with Negative Skin Friction. *Tripartite Meeting and Technical Courses - Geotechnical Engineering*, Johore.

Simpson, B.N.D., Banfi, M., Grose, B. and Davies, R. (2008) Collapse of the Nicoll Highway Excavation, Singapore. *4th International Conference on Forensic Engineering*. London, UK, ICE.

SISGEO (2009) www.sisgeo.com/pdf/schede/S400_EN.pdf

Skempton, A.W. and MacDonald, D.H. (1956) Allowable settlements of buildings. *Proc. Institution of the Civil Engineers* 5(3): part III, volume 5(No. 50): pp 727–768.

Slopeindicator (2009) www.slopeindicator.com/pdf/course%20material/data%20reduction.pdf

Son, M. and Cording, E.J. (2003) Tunneling, building response and damage estimation. *Tunnelling Underground Space Technology*(21): 6.

Son, M. and Cording, E.J. (2005) Estimation of building damage due to excavation-induced ground movements. *ASCE Journal of Geotechnical and Geoenvironmental Engineering* 131(2): pp 162-177

Staveren, M. van (2006) *Uncertainty and Groud Conditions: A Risk Management Approach*. Elsevier Ltd.

Stoel A.E.C. van der (2001) *Grouting for Pile Foundation Improvement*, PhD thesis Delft University of Technology, Delft, The Netherlands

Stoel, A.E.C. van der (2003) *Parameters jet grouting stempels diepe bouwkuipen stations*, 5.2-7.2-ES017818, 2003-05-23 (In Dutch)

Ter Linde, M.J.W. (1999) *Zakkingen van belendingen ten gevolge van het vervaardigen van diepwanden* (Building settlements due to diaphragm wall installation, in Dutch), MSc Thesis Delft University of Technology.

TNO (1995) *Onderzoek naar te verwachten zettingschade bij de aanleg van de Noord/Zuidlijn in Amsterdam, Diana studies, fase 1*.

Tol, A.F. van and Brassinga, H.E. (1991) Ontoelaatbare zakking monument Witte Huis vergt maatregelen, *Civiele Techniek*, 2 (in Dutch)

Tol, A.F. van and Brassinga, H.E (1992) Evaluatie gedrag grondkeringen bouwput Blaak. *Civiele Techniek*, 4 (in Dutch)

Tol, A.F. van and Brassinga, H.E (1993) Evaluatie gedrag grondkeringen bouwput Binnenrotte. *Civiele Techniek*, 1 (in Dutch)

Tol, A.F. van (1994) *Hoe betrouwbaar is de paalfundering?*, Lecture at installation as professor at Delft University of Technology

Tol, A. F. van (2007). Schadegevallen bij bouwputten (Damage caused by Deep Excavations) (in Dutch). *Cement* 6 (Year 59): pp 6-13.

Tol, A.F. van, Veenbergen, V. and Maertens, J. (2010) Diaphragm Walls, A reliable solution for Deep Excavations in Urban Areas? *DFI / EFFC, Proc. of the 11th International Conference* (electronic version, day 3 session 4), DFI, London.

Tomlinson, M. and Woodward, J. (2008) *Pile Design and Construction Practice.* Fifth edition, Taylor&Francis, Oxon

Toolan, F. E., Lings, M. L. and Mirza, U.A. (1990) An appraisal of API RP2A recommendations for determining skin friction of piles in sand. *Proc. 22nd Offshore Technol. Conf. Houston*, OTC 6422, vol. 4, pp 33-42

Top010 (2009) http://www.top010.nl/html/het_witte_huis.htm, date 2009-11-11

Vardanega, P.J., Williamson, M.G. and Bolton, M.D. (2012) Bored pile design in stiff clay II: mechanisms and uncertainty. *Geotechnical Engineering, Proceedings of ICE*, Vol 165. Issue GE4. pp 233-246

Weele, A.F. Van and Riethoff, H.J.W. (1982) Fundering en constructie G81 (lecture notes foundation engineering, in Dutch), Delft University of Technology

Wikipedia (2009) http://nl.wikipedia.org/wiki/Witte_Huis_(Rotterdam), date 2009-11-11

Xu, K.J. and Poulos, H.G. (2001) 3-D elastic analysis of vertical piles subjected to "passive" loadings. *Computers and Geotechnics* 28. pp 349-375

Zantkuijl, H. J. (1993) *Bouwen in Amsterdam - Het woonhuis in de stad* (Building in Amsterdam). Amsterdam, Architectura & Natura.

Zeevaert, L. (1959) Reduction of point bearing capacity because of negative friction. *Proc. First Pan American Conference on Soil Mechanics and Foundation Engineering*, Vol. 3, pp 1145-1152

Zeevaert, L. (1983) *Foundation Engineering for difficult subsoil conditions*. Van Nostrand Reinhold Company, Chapter 8, pp 335-423

Zhang, L. M. and Ng, A. M. Y. (2005) Probabilistic limiting tolerable displacements for serviceability limit state design of foundations. *Géotechnique* 55(2): pp 151-161

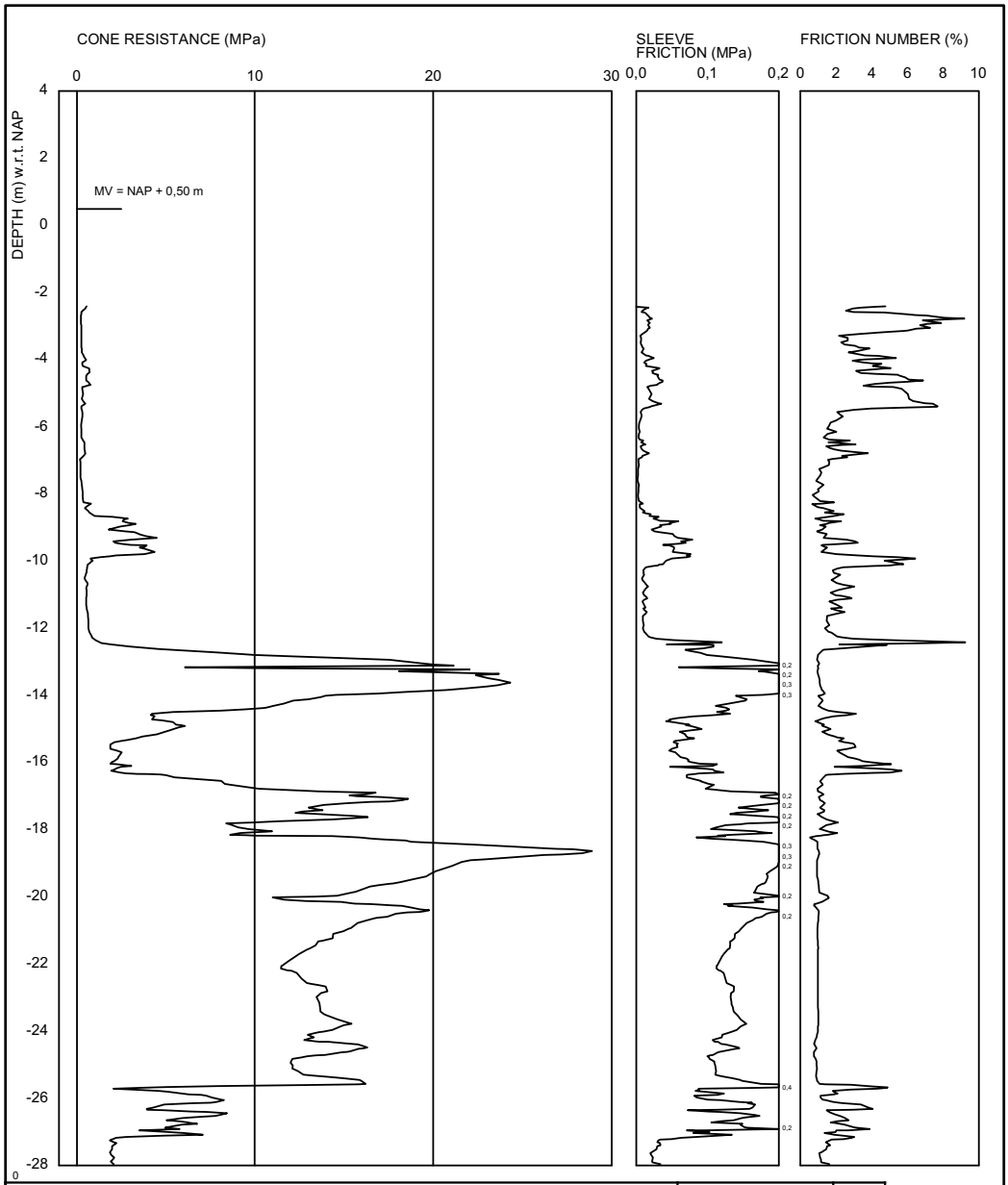
Zhang, L. M. and Ng, A. M. Y. (2007) Limiting tolerable settlement ad angular distortion for building foundations. *GSP 170 Probabilistic Applications in Geotechnical Engineering*, GeoDenver.

Zhang, R., Zheng, J., Pu, H. and Zhang, L. (2010) Analysis of excavation-induced responses of loaded pile foundations considering unloading effect. *Tunnelling and Underground Space Technology* 26. Elsevier Ltd. pp 320–335 doi:10.1016/j.tust.2010.11.003

This page intentionally left blank

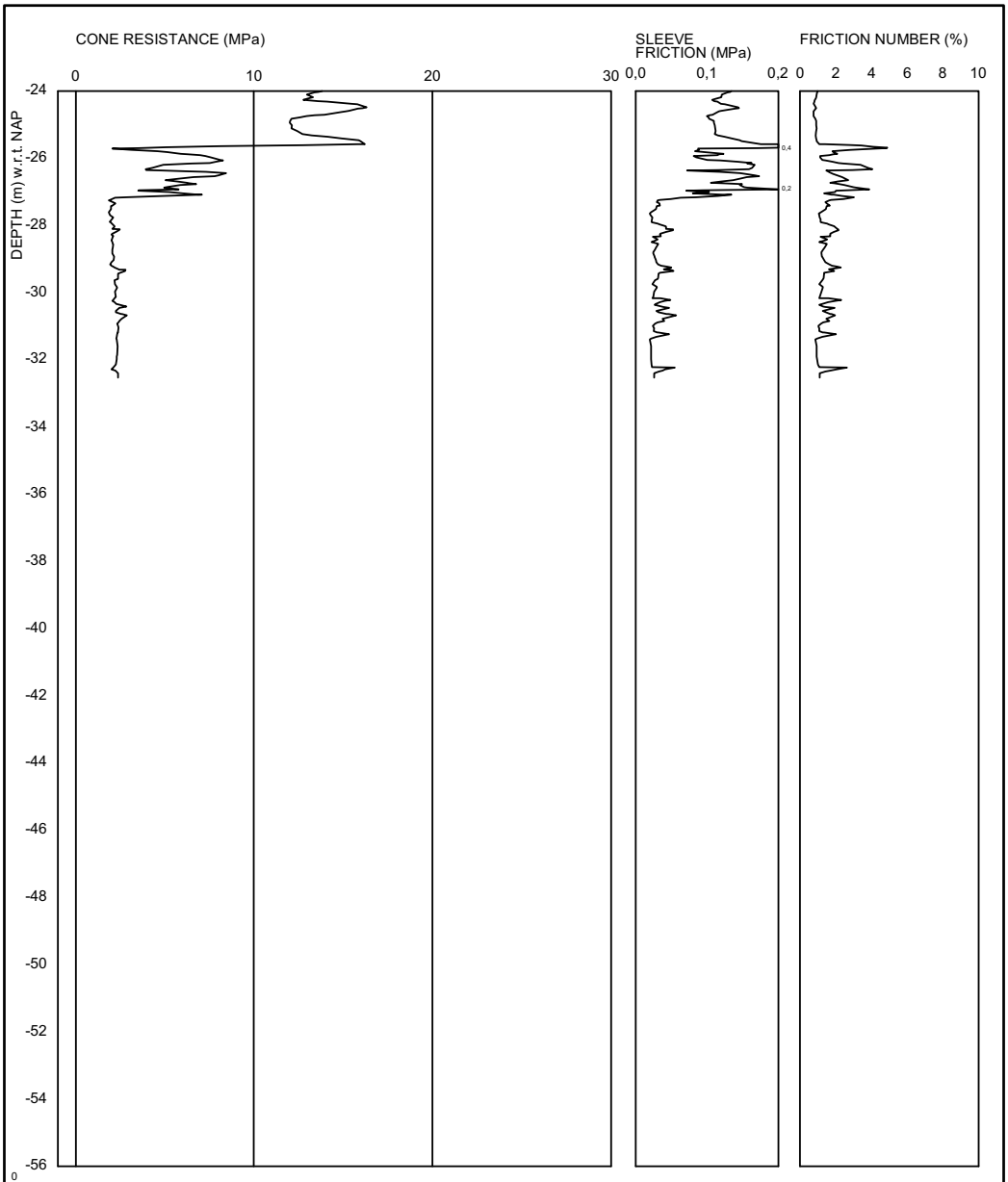
ANNEX A TYPICAL CPT PER STATION

This page intentionally left blank



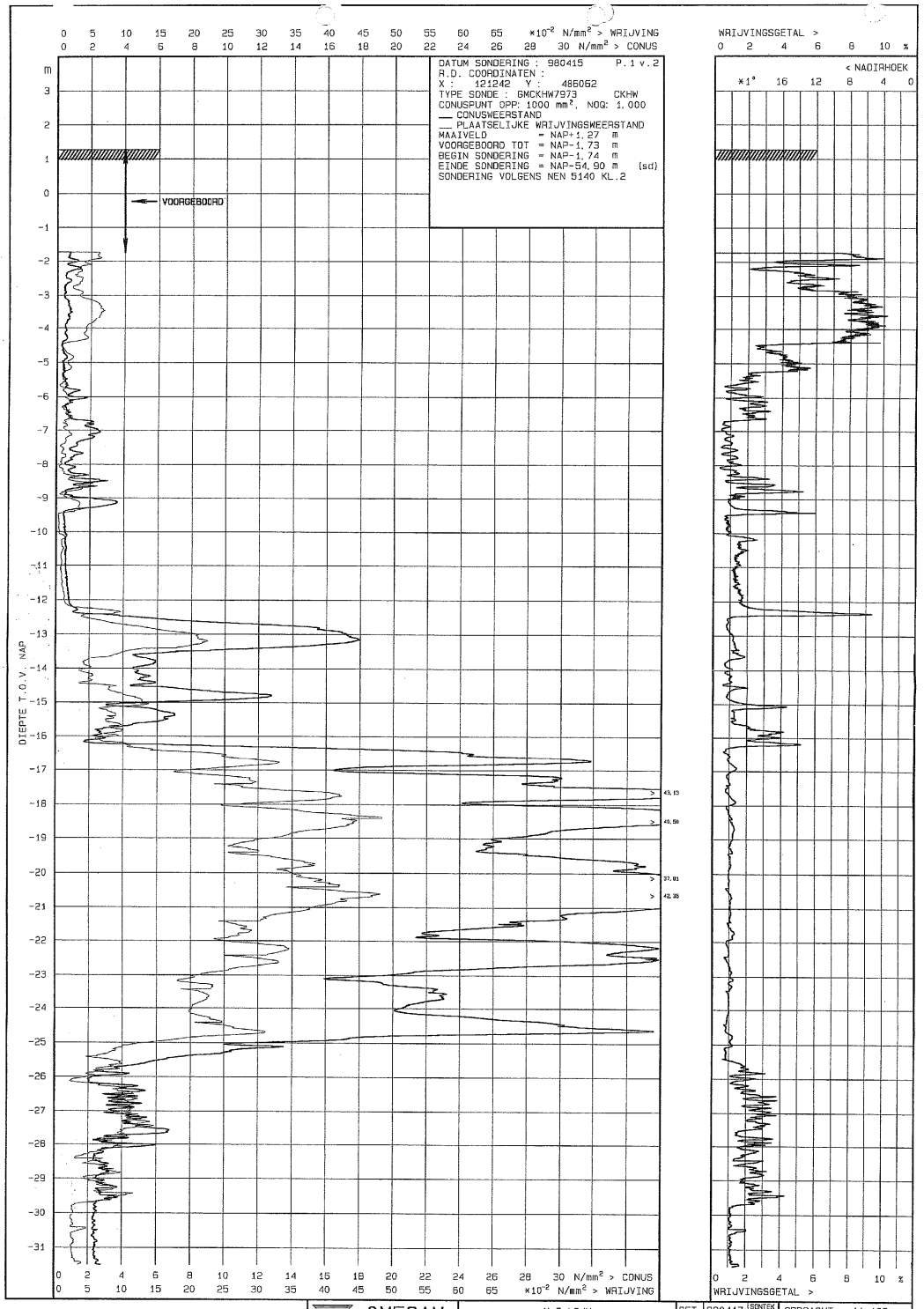
Deltares
Stieltjesweg 2
2628 CK Delft
Phone +31(0)88-3357200
Fax +31(0)15-2610821

	date 2011-07-12	drw. -
- -	CO--/-	ctr.
CPT 3223S (OMEGAM) (GEDIGITALISEERD) [Sheet 1 / 2]	ANNEX -	form. A4



Deltares
Stieltjesweg 2
2628 CK Delft
Phone +31(0)88-3357200
Fax +31(0)15-2610821

	date 2011-07-12	drw. -
- -	CO--/-	ctr.
CPT 3223S (OMEGAM) (GEDIGITALISEERD) [Sheet 2 / 2]	ANNEX -	form. A4



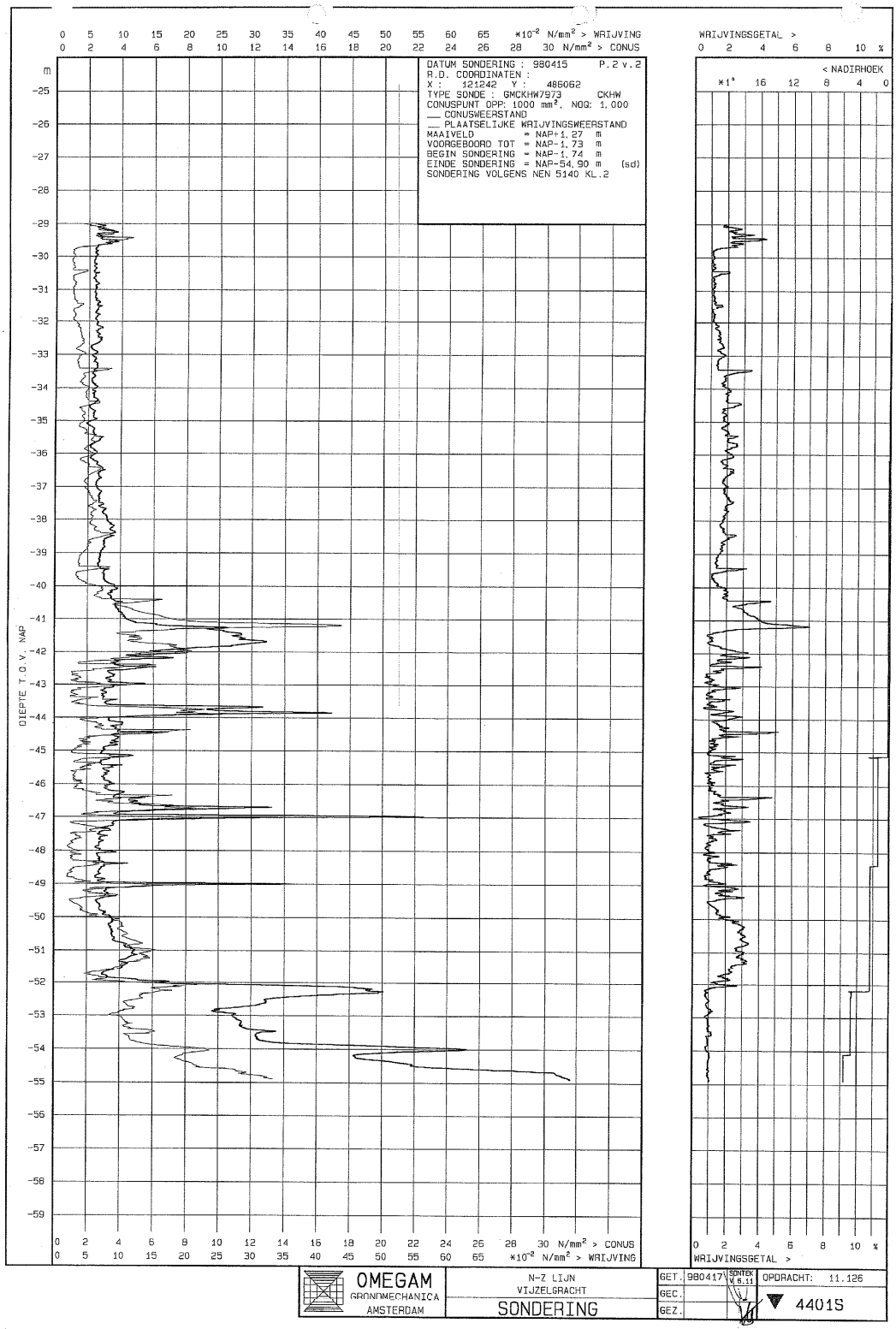
OMEGAM
GRONDMECHANICA
AMSTERDAM

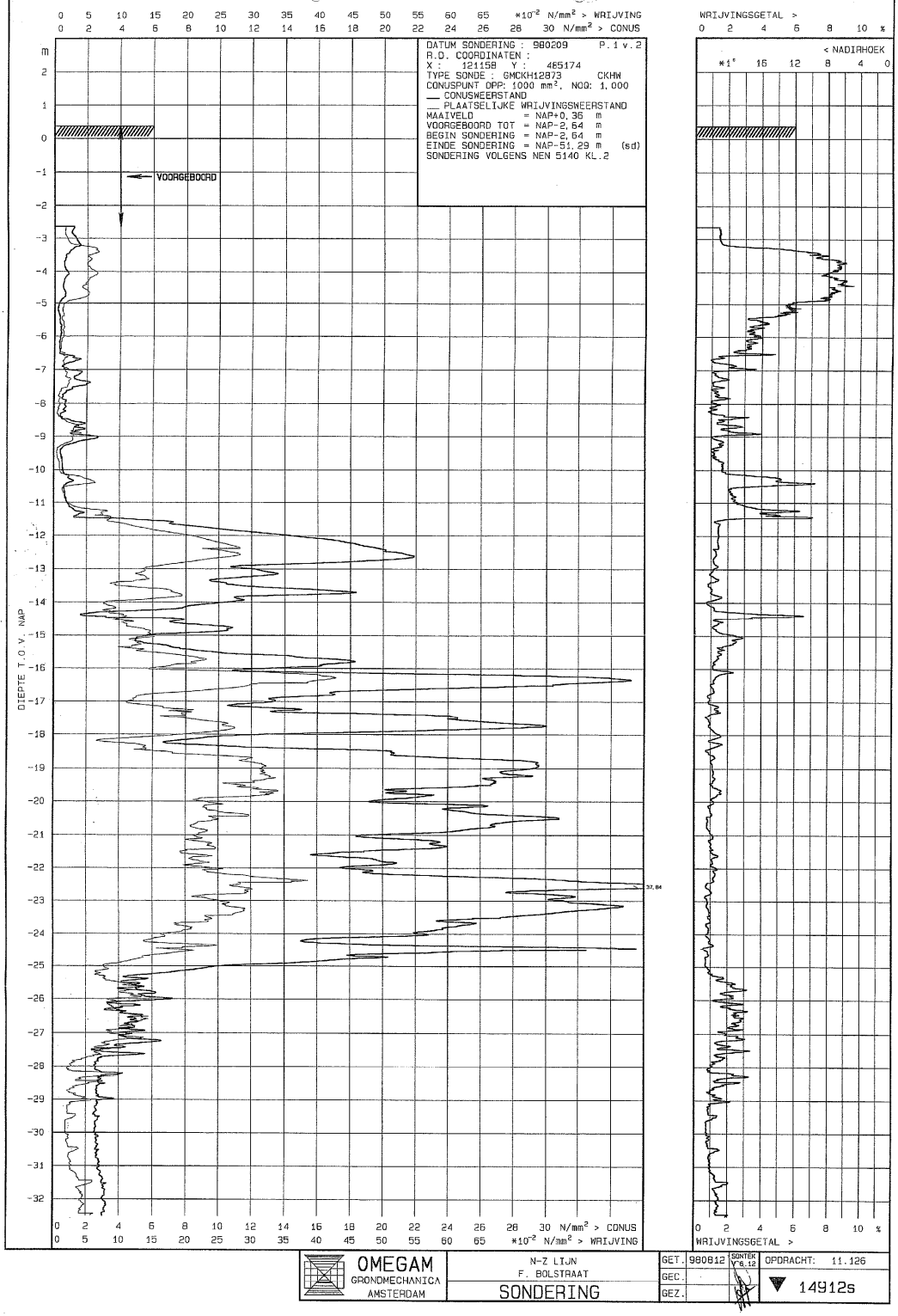
N-Z LIJN
VIJZELGRACHT

SONDERING

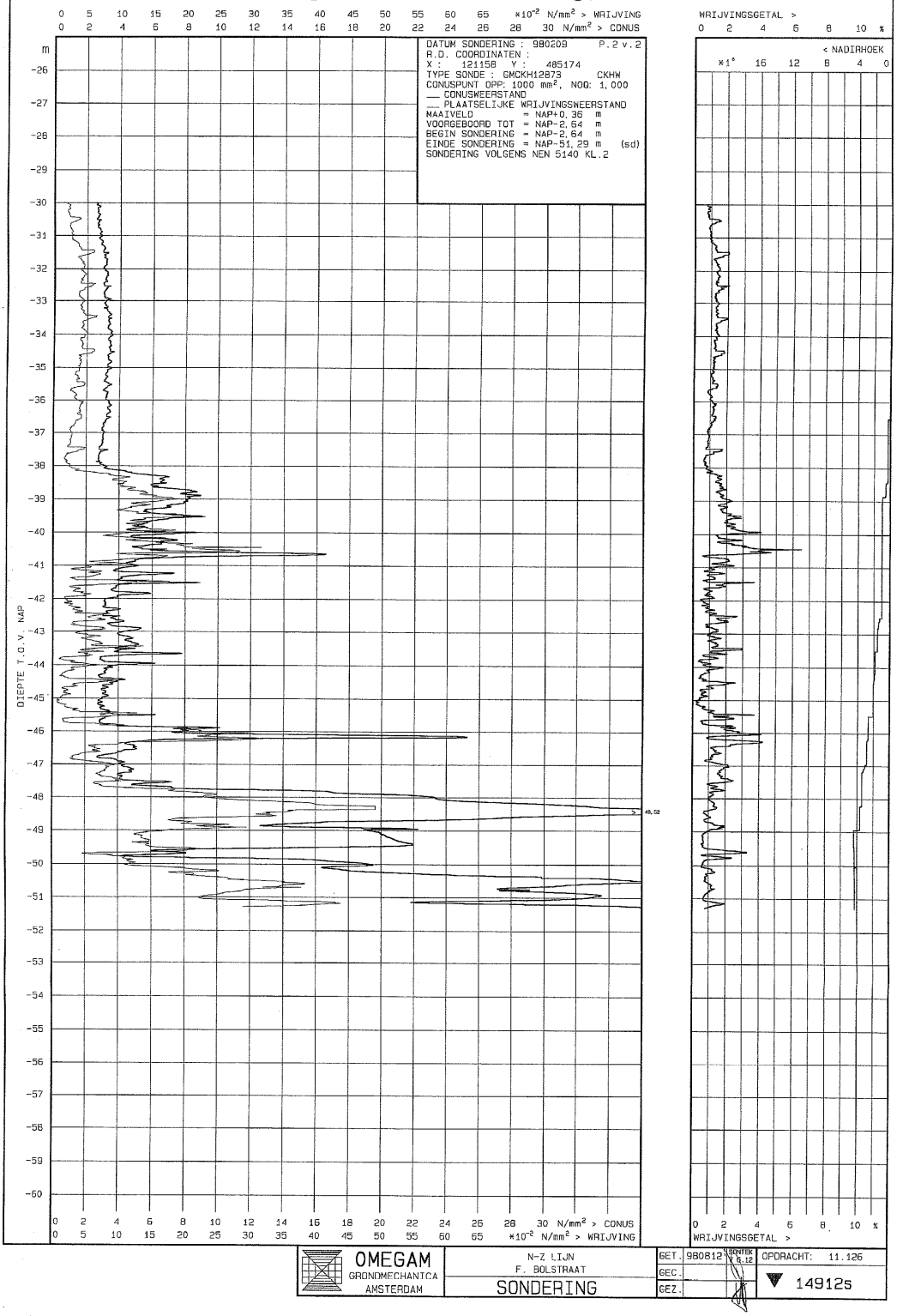
GET. 980417 SONTEK V6.11 OPDRACHT: 11.126
GEC.
GEZ.

4401S


0 5 10 15 20 25 30 35 40 45 50 55 60 65 *10-2 N/mm2 > WRIJVING
0 2 4 6 8 10 12 14 16 18 20 22 24 26 28 30 N/mm2 > CONUS
m
DIEPTE T.O.V. NAP
-25 -26 -27 -28 -29 -30 -31 -32 -33 -34 -35 -36 -37 -38 -39 -40 -41 -42 -43 -44 -45 -46 -47 -48 -49 -50 -51 -52 -53 -54 -55 -56 -57 -58 -59
DATUM SONDERING : 980415 P.2 v.2
R.D. COORDINATEN :
X : 121242 Y : 486062
TYPE SONDE : GMCKHW7973 CKHW
CONUSPUNT OPP: 1000 mm2, NOG: 1.000
___ CONUSWEERSTAND
___ PLAATSELIJKE WRIJVINGSWEERSTAND
MAAIVELD = NAP+1.27 m
VOORGEBOORD TOT = NAP-1.73 m
BEGIN SONDERING = NAP-1.74 m
EINDE SONDERING = NAP-54.90 m (sd)
SONDERING VOLGENS NEN 5140 KL.2
0 2 4 6 8 10 12 14 16 18 20 22 24 26 28 30 N/mm2 > CONUS
0 5 10 15 20 25 30 35 40 45 50 55 60 65 *10-2 N/mm2 > WRIJVING
WRIJVINGSGETAL >
0 2 4 6 8 10 %
< NADIRHOEK
*1° 16 12 8 4 0
0 2 4 6 8 10 %
WRIJVINGSGETAL >
OMEGAM
GRONDMECHANICA
AMSTERDAM
N-Z LIJN
VIJZELGRACHT
SONDERING
GET. 980417
GEC.
GEZ.
SONTEK V 6.11
OPDRACHT: 11.126
4401S



OMEGAM GRONDMECHANICA AMSTERDAM	N-Z LIJN F. BOLSTRAAT SONDERING	GET. 980812 SONTEK V°6.12 GEC. GEZ.	OPDRACHT: 11.126 14912s



OMEGAM
GRONDMECHANICA
AMSTERDAM

N-Z LIJN
F. BOLSTRAAT

SONDERING

GET. 980812 (SONTEK X 6.12)
GEC.
GEZ.

OPDRACHT: 11.126

14912s

ANNEX B SOIL PARAMETERS

This page intentionally left blank

Table B.1 Soil parameters based on ABNZL (2004), average values, Classification and Atterberg Limits

Layer number	Soil Layer	$\gamma_{;dry}$ [kN/m^3]	$\gamma_{;sat}$ [kN/m^3]	wL [%-]	wP [%-]	Ip [%]	D_{50} [μm]
01A	Fill man made	15.0	18.4				
08	Peat	2.5	10.5	213	113	100	
09	Old Seaclay	11.0	16.5	51	28	23	
10	Waddeposit, with sand	13.3	17.9				59
11	Hydrobiaclay	9	15.2	98	47	51	17
12	Peat	4.2	11.7				
13	First sandlayer	16.8	19.8				123
14	Allerød	14.4	18.5				65
17	Second sand layer	15.9	19.0				200
19	Eemclay	13.1	17.9	42	23	19	29
20	Harting layer	8.3	14.5	103	60	43	
21	Intermediate sand layer	16.0	19.4				136
22	Glacial Drente clay	15.9	19.7	28	18	10	180
23	Glacial Warven clay	14.0	18.5	59	24	35	
24	Third sand layer	17	19.6				457

Table B.2 Soil parameters based on ABNZL (2004), average values,

Strength and Stiffness

Layer number	Soil Layer	c' [kPa]	φ' [°]	c_u [kPa]	E'_{50} [kPa]	K_0 [-]	OCR [-]
01A	Fill man made		25				
08	Peat	5	19	20	500	0.65	
09	Old Seaclay	7	26	30	4000	0.5	
10	Waddeposit, with sand	2	27		4300	0.4	
11	Hydrobiaclay	8	27	30	7500	0.59	
12	Peat	6	21	20	1200	0.65	
13	First sandlayer		33		31000	0.4	
14	Allerød	3	28		13600	0.4	
17	Second sand layer		33		31000	0.4	
19	Eemclay	15	29	150	23000	0.68	2.0
20	Harting layer	10	28	100	14950	0.57	1.5
21	Intermediate sand layer		30		30000	0.4	
22	Glacial Drenthe clay	15	29	180	40000	0.54	1.5
23	Glacial Warven clay	5	26	180	25000	0.54	1.5
24	Third sand layer		33		75000	0.4	

φ' based on 0.5% strain (sand) or 1.0% strain (clay)

E'_{50} is for average in-situ horizontal effective stress

ANNEX C GROUND DISPLACEMENTS

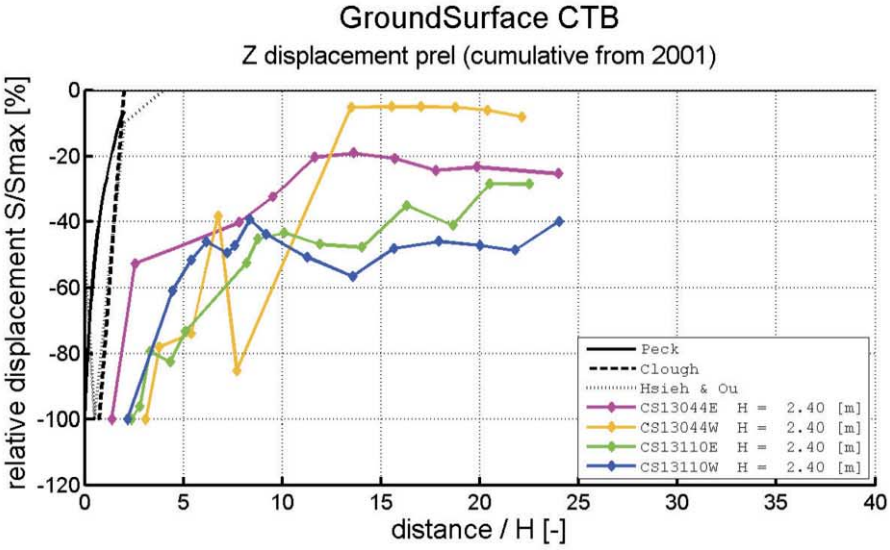
Period 1 – period 7: all values are total values with reference date for all periods 2001.

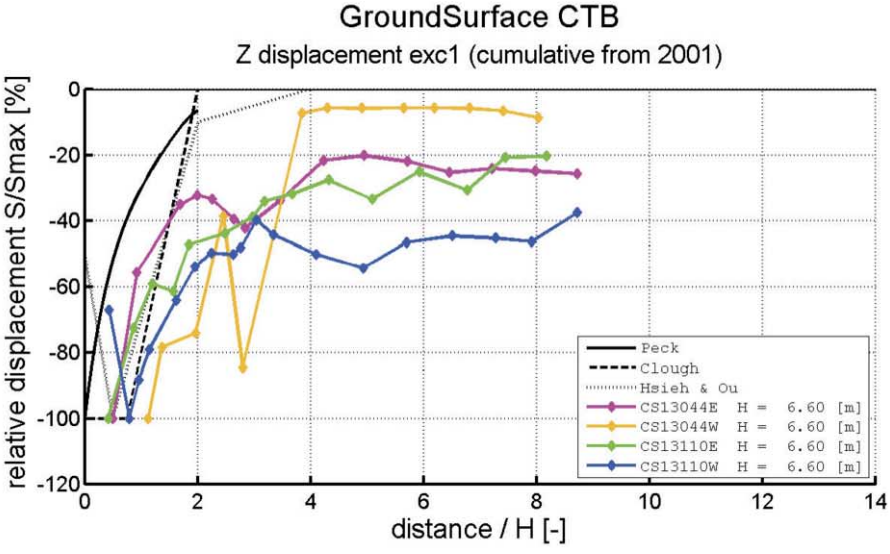
CTB = Ceintuurbaan Station

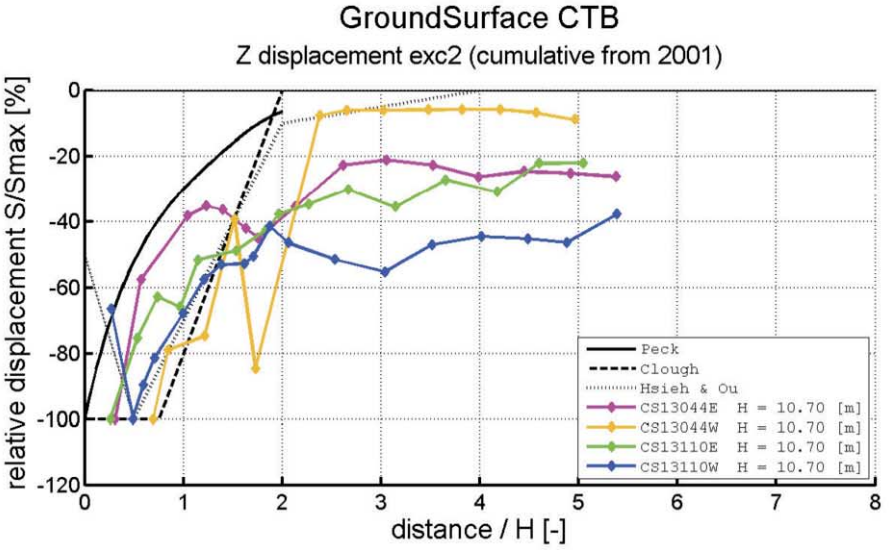
VZG = Vijzelgracht Station

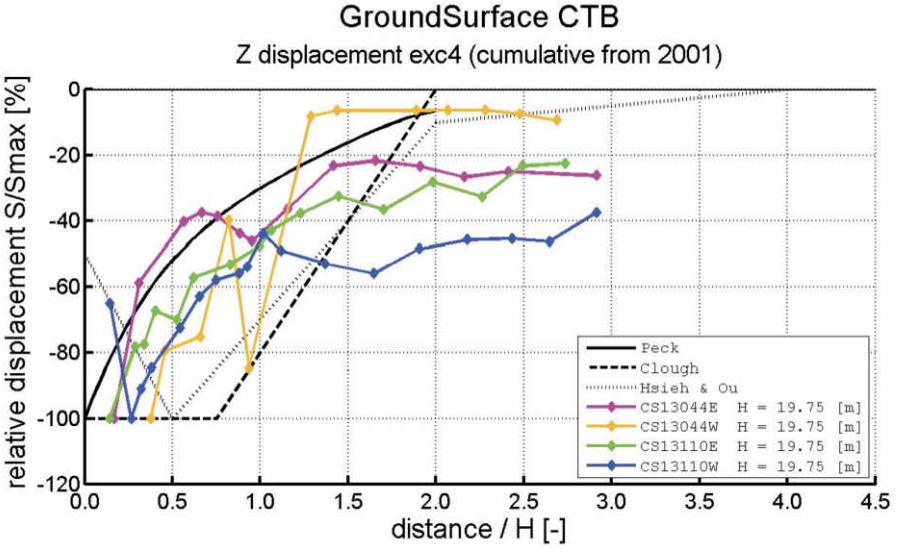
RKN = Rokin Station

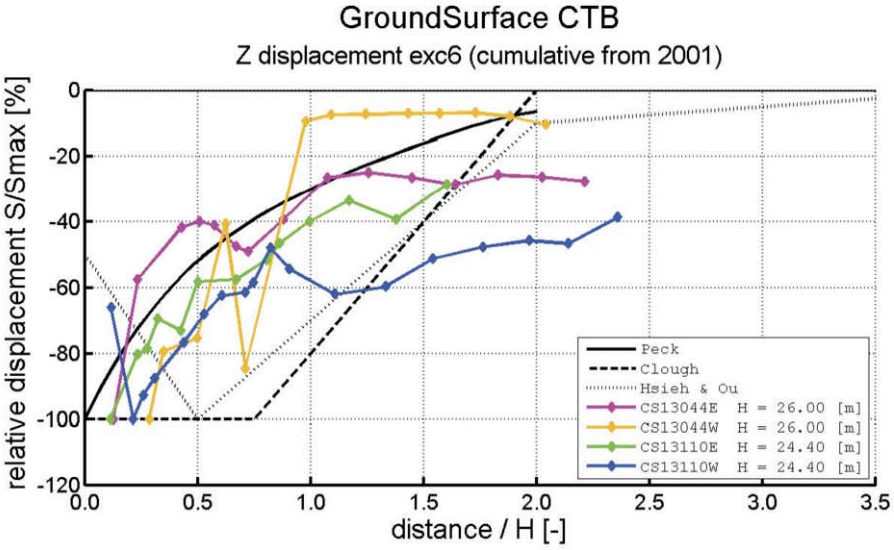
This page intentionally left blank

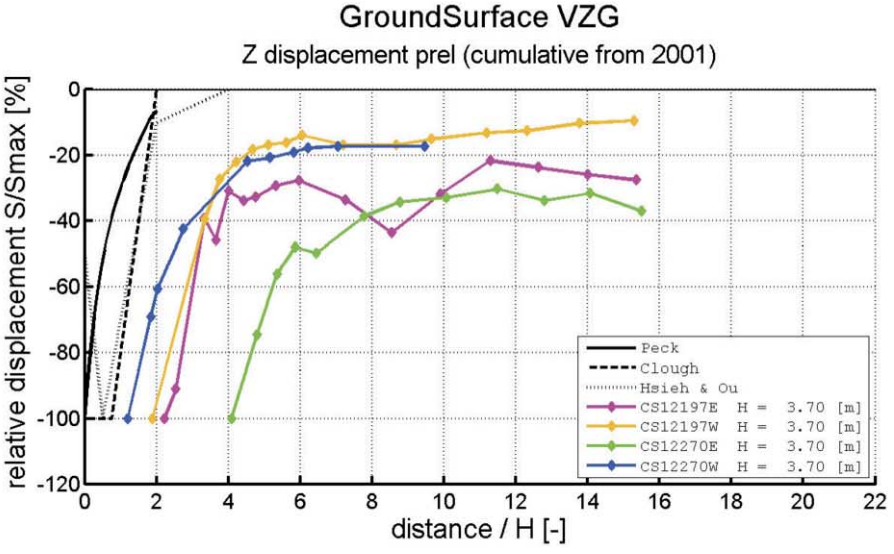

GroundSurface CTB
Z displacement prel (cumulative from 2001)
relative displacement S/Smax [%]
distance / H [-]
Peck
Clough
Hsieh & Ou
CS13044E H = 2.40 [m]
CS13044W H = 2.40 [m]
CS13110E H = 2.40 [m]
CS13110W H = 2.40 [m]

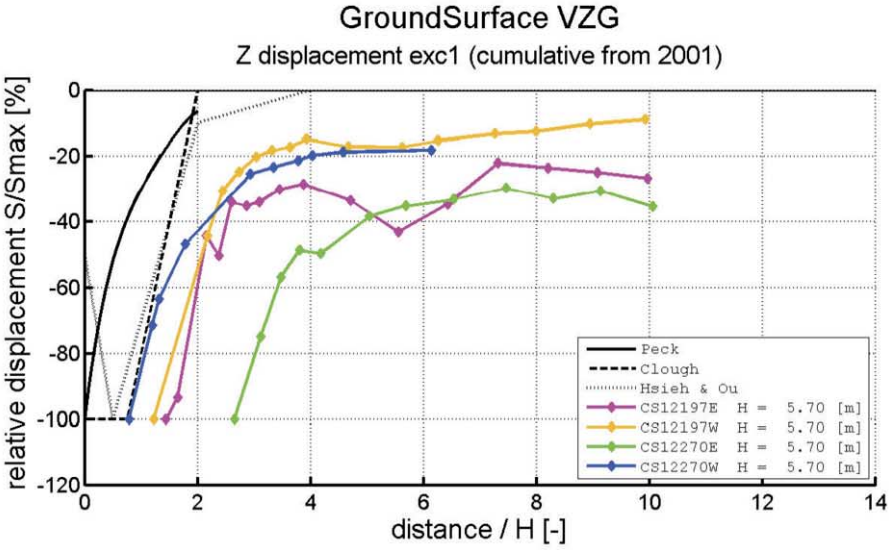

GroundSurface CTB
Z displacement exc1 (cumulative from 2001)
relative displacement S/Smax [%]
distance / H [-]
Peck
Clough
Hsieh & Ou
CS13044E H = 6.60 [m]
CS13044W H = 6.60 [m]
CS13110E H = 6.60 [m]
CS13110W H = 6.60 [m]

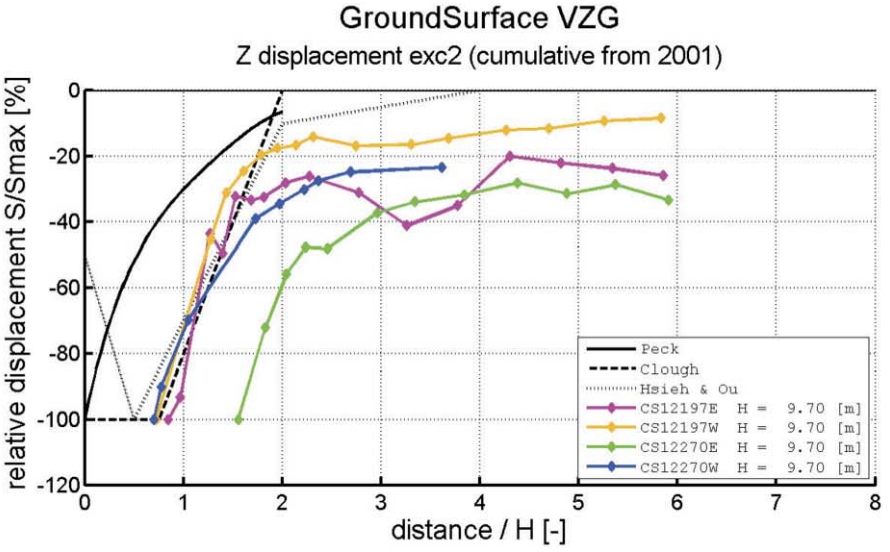

GroundSurface CTB
Z displacement exc2 (cumulative from 2001)
relative displacement S/Smax [%]
distance / H [-]
Peck
Clough
Hsieh & Ou
CS13044E H = 10.70 [m]
CS13044W H = 10.70 [m]
CS13110E H = 10.70 [m]
CS13110W H = 10.70 [m]

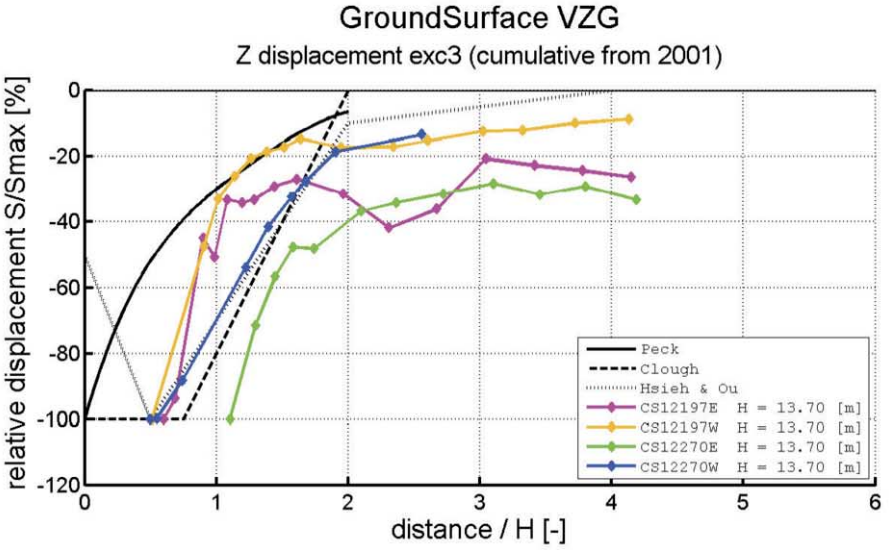

GroundSurface CTB
Z displacement exc4 (cumulative from 2001)
relative displacement S/Smax [%]
distance / H [-]
Peck
Clough
Hsieh & Ou
CS13044E H = 19.75 [m]
CS13044W H = 19.75 [m]
CS13110E H = 19.75 [m]
CS13110W H = 19.75 [m]

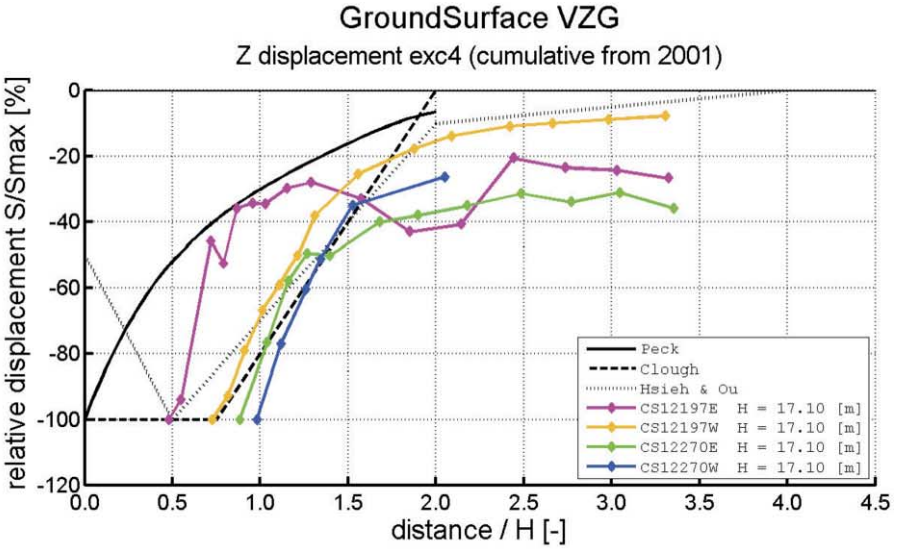

GroundSurface CTB
Z displacement exc6 (cumulative from 2001)
relative displacement S/Smax [%]
distance / H [-]
Peck
Clough
Hsieh & Ou
CS13044E H = 26.00 [m]
CS13044W H = 26.00 [m]
CS13110E H = 24.40 [m]
CS13110W H = 24.40 [m]

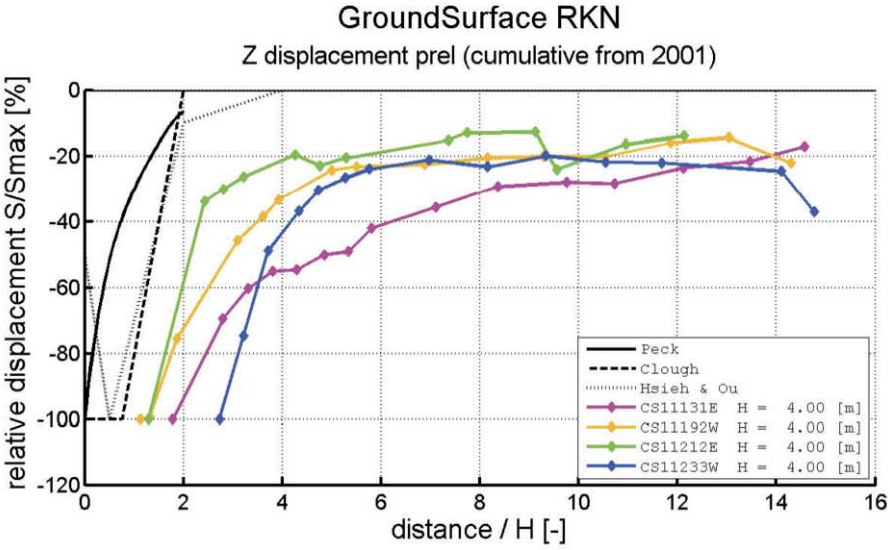

GroundSurface VZG
Z displacement prel (cumulative from 2001)
relative displacement S/Smax [%]
distance / H [-]
Peck
Clough
Hsieh & Ou
CS12197E H = 3.70 [m]
CS12197W H = 3.70 [m]
CS12270E H = 3.70 [m]
CS12270W H = 3.70 [m]

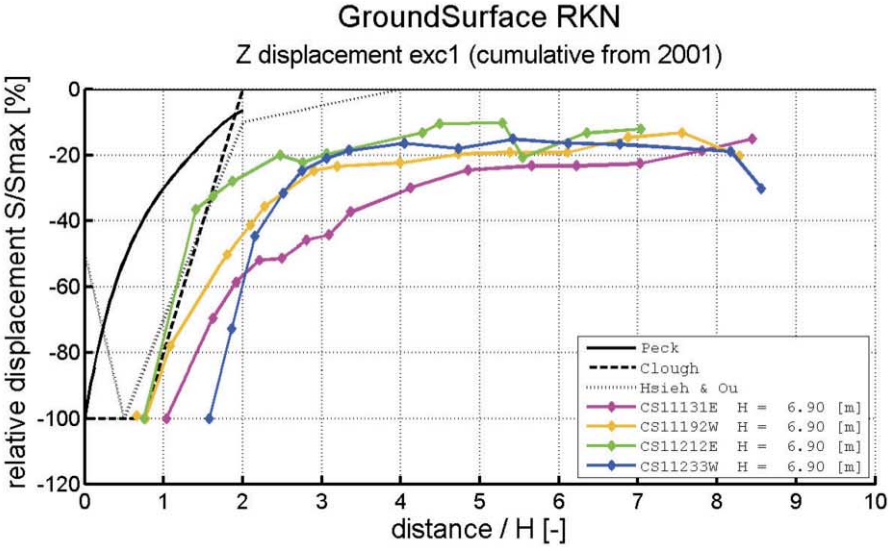

GroundSurface VZG
Z displacement exc1 (cumulative from 2001)
relative displacement S/Smax [%]
distance / H [-]
Peck
Clough
Hsieh & Ou
CS12197E H = 5.70 [m]
CS12197W H = 5.70 [m]
CS12270E H = 5.70 [m]
CS12270W H = 5.70 [m]

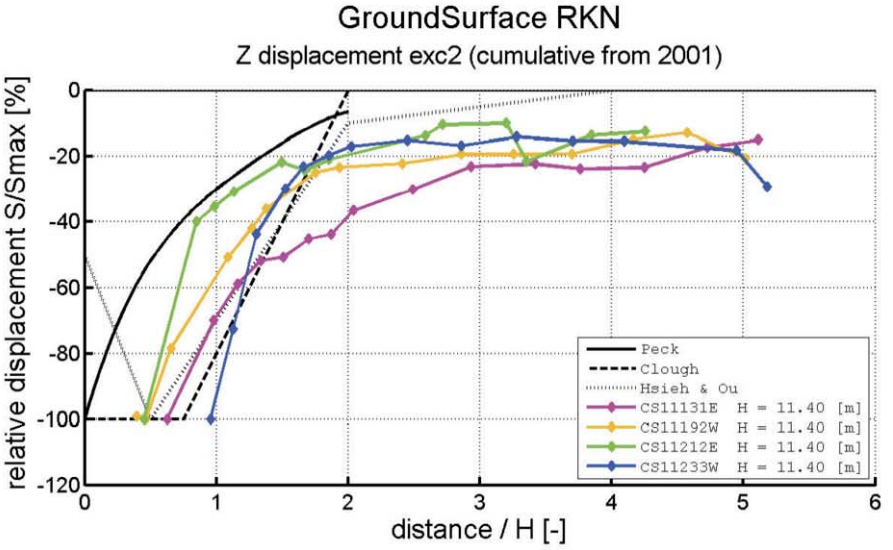

GroundSurface VZG
Z displacement exc2 (cumulative from 2001)
relative displacement S/Smax [%]
distance / H [-]
Peck
Clough
Hsieh & Ou
CS12197E H = 9.70 [m]
CS12197W H = 9.70 [m]
CS12270E H = 9.70 [m]
CS12270W H = 9.70 [m]

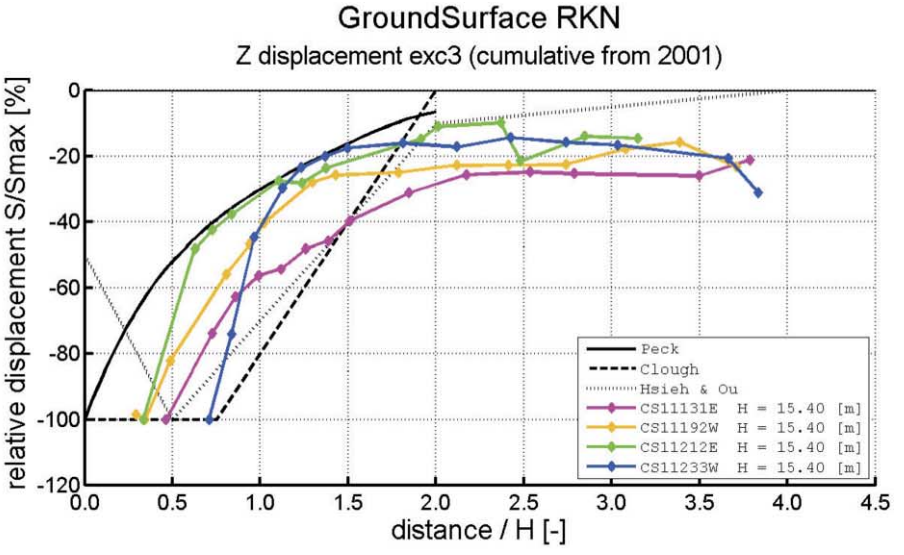

GroundSurface VZG
Z displacement exc3 (cumulative from 2001)
relative displacement S/Smax [%]
distance / H [-]
Peck
Clough
Hsieh & Ou
CS12197E H = 13.70 [m]
CS12197W H = 13.70 [m]
CS12270E H = 13.70 [m]
CS12270W H = 13.70 [m]


GroundSurface VZG
Z displacement exc4 (cumulative from 2001)
relative displacement S/Smax [%]
distance / H [-]
Peck
Clough
Hsieh & Ou
CS12197E H = 17.10 [m]
CS12197W H = 17.10 [m]
CS12270E H = 17.10 [m]
CS12270W H = 17.10 [m]


GroundSurface RKN
Z displacement prel (cumulative from 2001)
relative displacement S/Smax [%]
distance / H [-]
Peck
Clough
Hsieh & Ou
CS11131E H = 4.00 [m]
CS11192W H = 4.00 [m]
CS11212E H = 4.00 [m]
CS11233W H = 4.00 [m]


GroundSurface RKN
Z displacement exc1 (cumulative from 2001)
relative displacement S/Smax [%]
distance / H [-]
Peck
Clough
Hsieh & Ou
CS11131E H = 6.90 [m]
CS11192W H = 6.90 [m]
CS11212E H = 6.90 [m]
CS11233W H = 6.90 [m]


GroundSurface RKN
Z displacement exc2 (cumulative from 2001)
relative displacement S/Smax [%]
distance / H [-]
Peck
Clough
Hsieh & Ou
CS11131E H = 11.40 [m]
CS11192W H = 11.40 [m]
CS11212E H = 11.40 [m]
CS11233W H = 11.40 [m]


GroundSurface RKN
Z displacement exc3 (cumulative from 2001)
relative displacement S/Smax [%]
distance / H [-]
Peck
Clough
Hsieh & Ou
CS11131E H = 15.40 [m]
CS11192W H = 15.40 [m]
CS11212E H = 15.40 [m]
CS11233W H = 15.40 [m]

This page intentionally left blank

ANNEX D DAPPERBUURT TEST

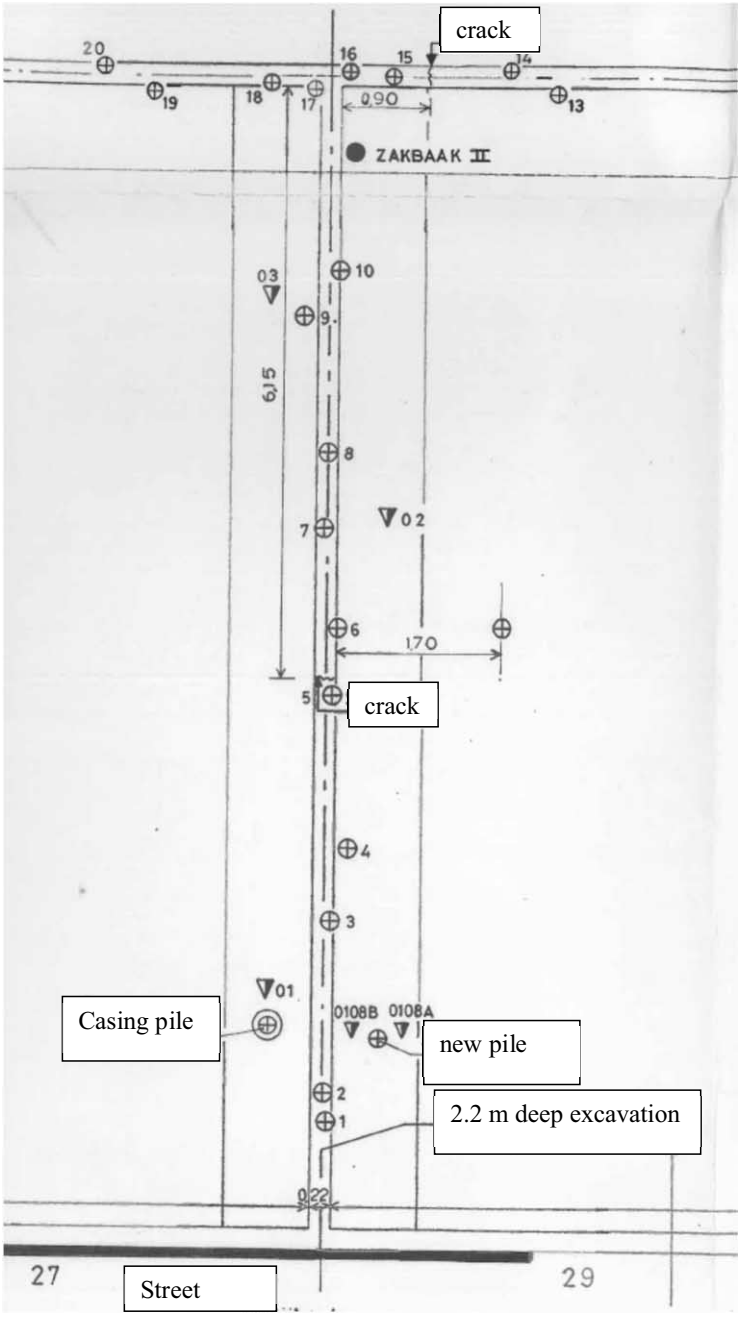


Figure D.1 Pile and CPT locations Dapperbuurt top view

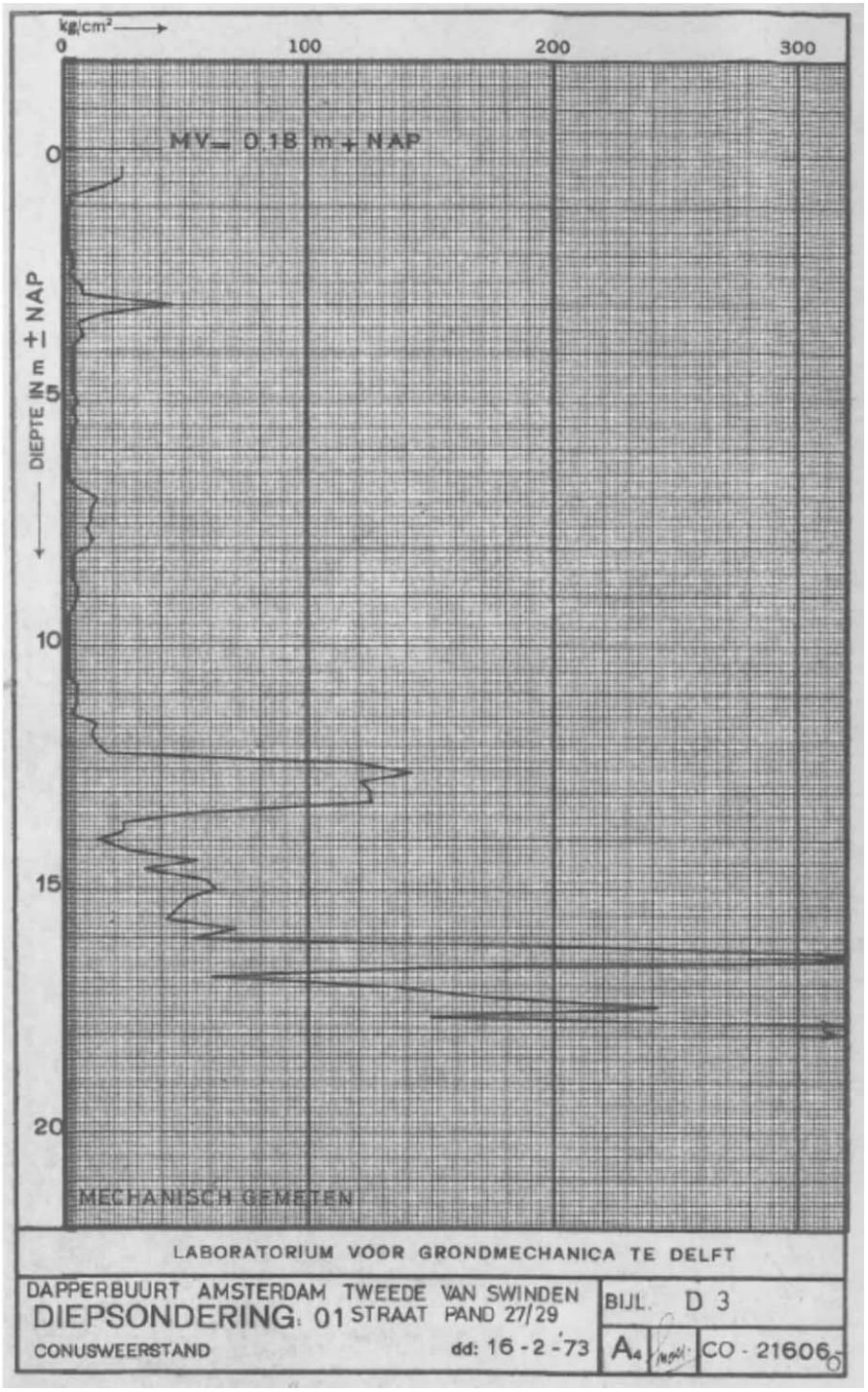
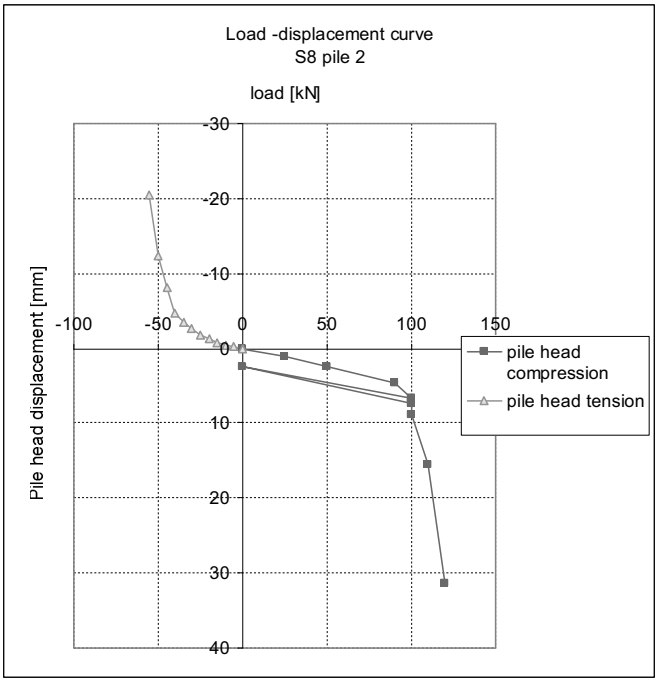
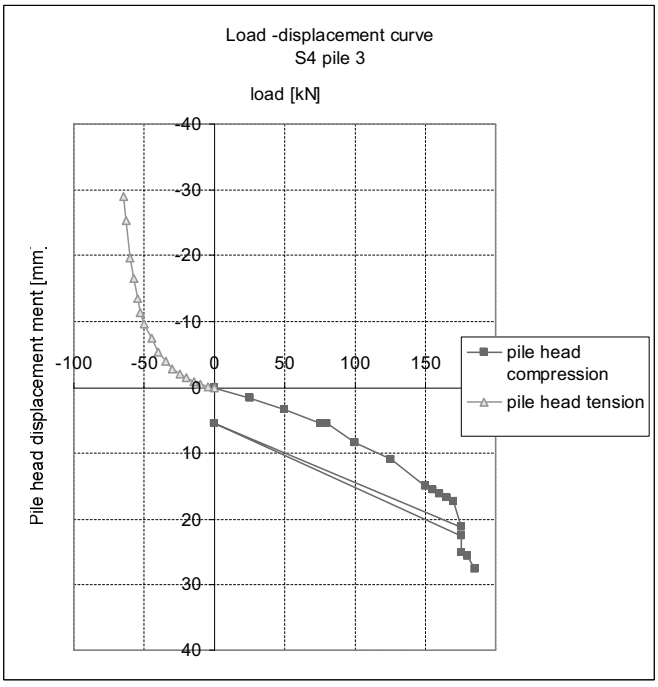
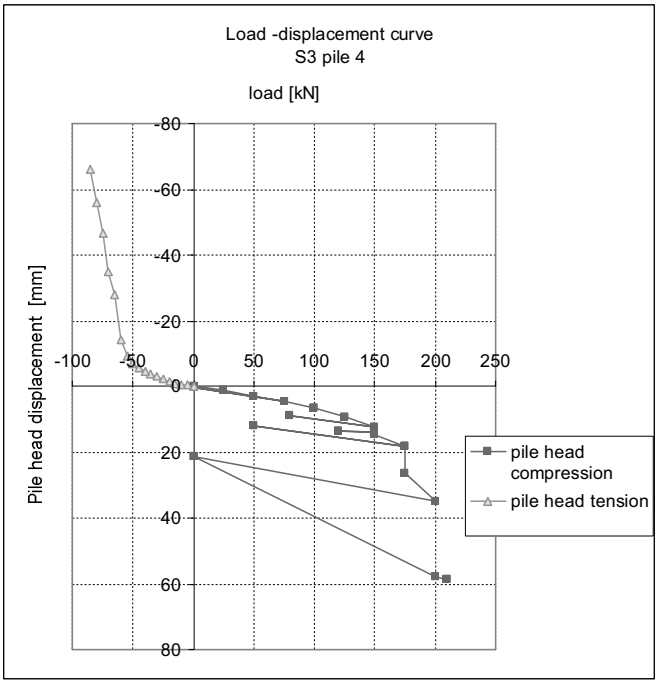
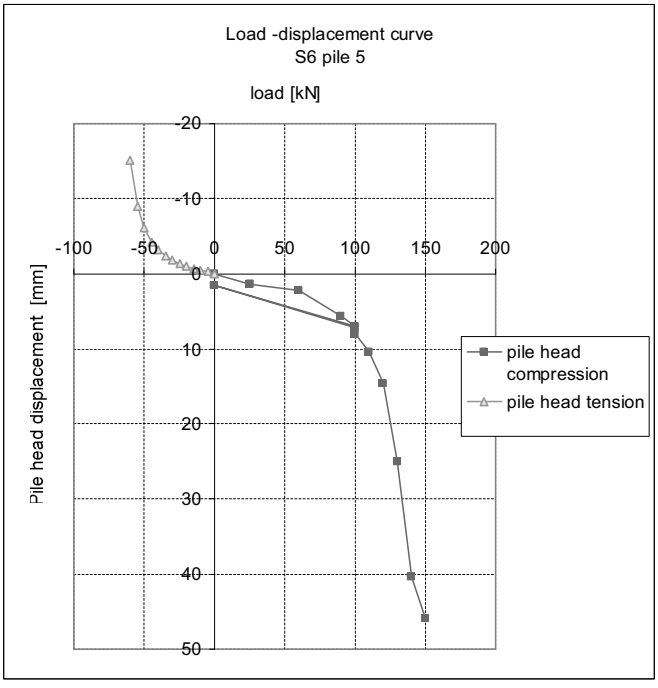


Figure D.2 CPT 01 at Dapperbuurt


Load -displacement curve
S8 pile 2
load [kN]
Pile head displacement [mm]
-30
-20
-10
-100
-50
0
50
100
150
0
10
20
30
40
pile head compression
pile head tension


Load -displacement curve
S4 pile 3
load [kN]
Pile head displacement ment [mm]
-40
-30
-20
-10
-100
-50
0
50
100
150
0
10
20
30
40
pile head compression
pile head tension


Load -displacement curve
S3 pile 4
load [kN]
Pile head displacement [mm]
-80
-60
-40
-20
0
20
40
60
80
-100
-50
0
50
100
150
200
250
pile head compression
pile head tension


Load -displacement curve
S6 pile 5
load [kN]
Pile head displacement [mm]
-20
-10
0
10
20
30
40
50
-100
-50
0
50
100
150
200
pile head compression
pile head tension

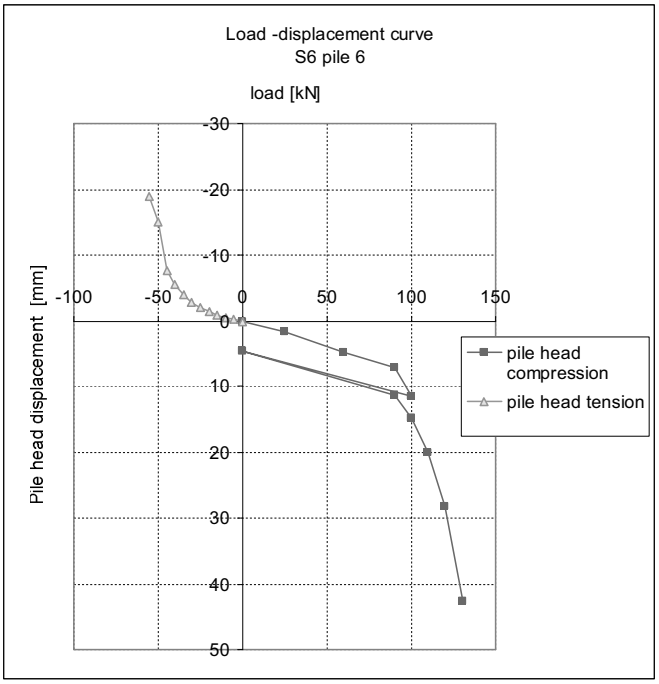
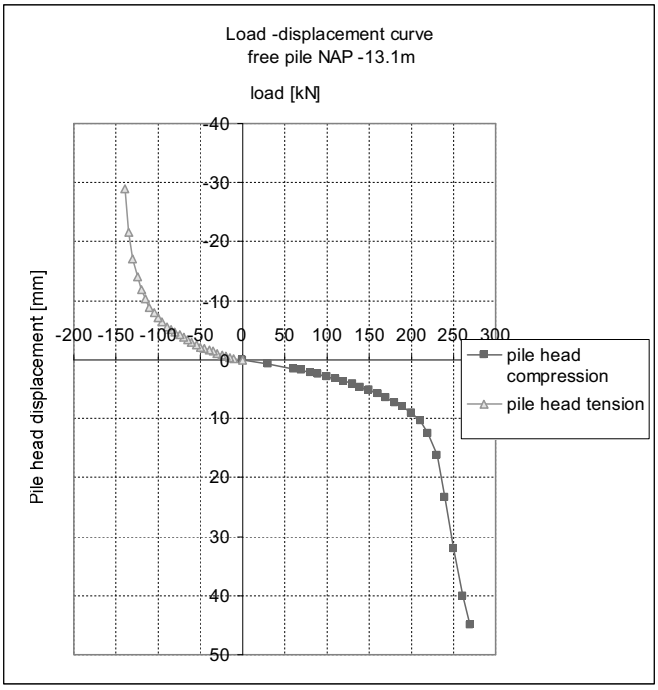
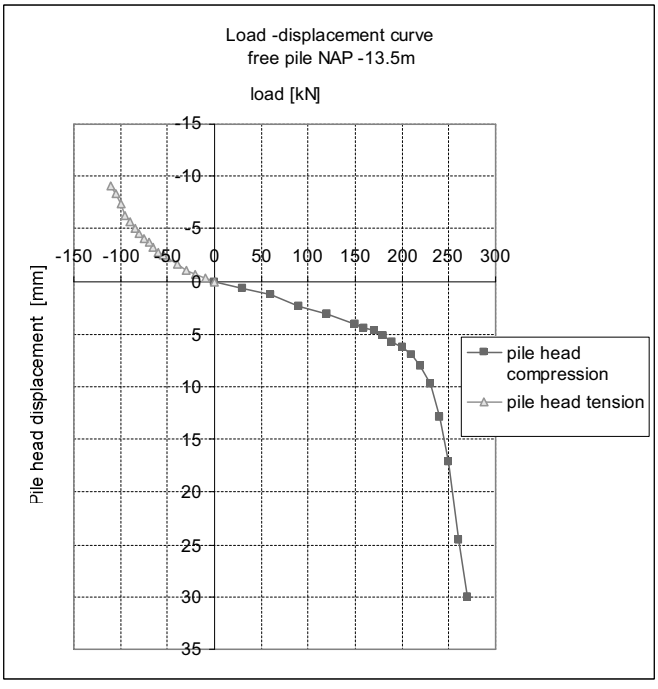
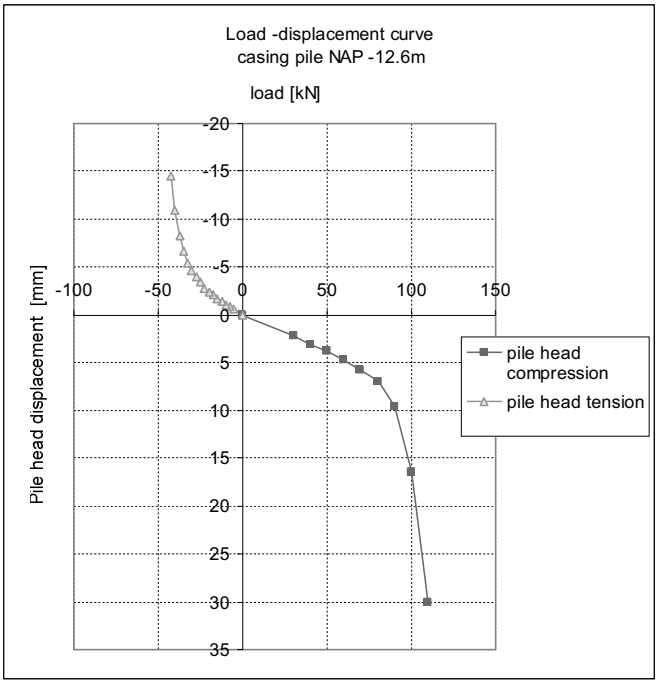


Figure D.3 Pile load test results old piles 2, 3, 4, 5 and 6


Load -displacement curve
free pile NAP -13.1m
load [kN]
Pile head displacement [mm]
-40
-30
-20
-10
-200 -150 -100 -50 0 50 100 150 200 250 300
0
10
20
30
40
50
pile head compression
pile head tension


Load -displacement curve
free pile NAP -13.5m
load [kN]
Pile head displacement [mm]
-15
-10
-5
-150 -100 -50 0 50 100 150 200 250 300
0
5
10
15
20
25
30
35
pile head compression
pile head tension



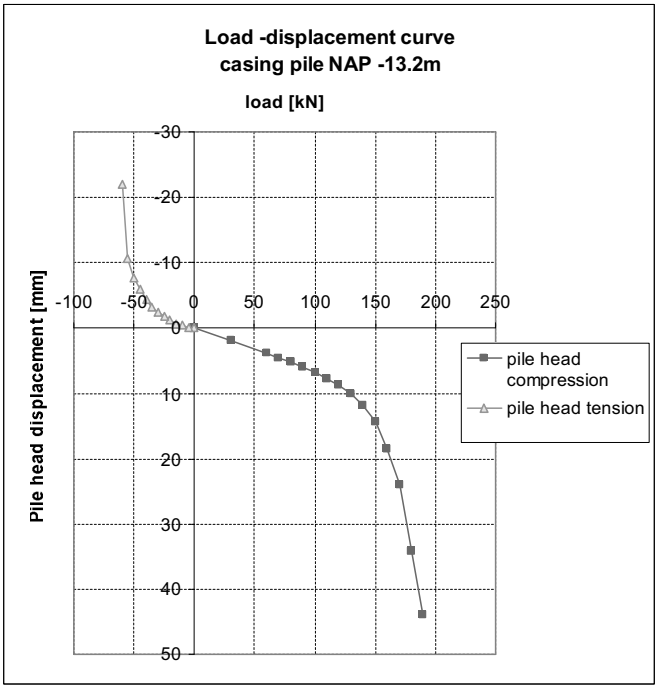


Figure D.4 Pile load test results on new piles



Figure D.5 Pile test set up



(a)



(b)

Figure D.6 piles after removal from soil



Figure D.7Broken pile 5

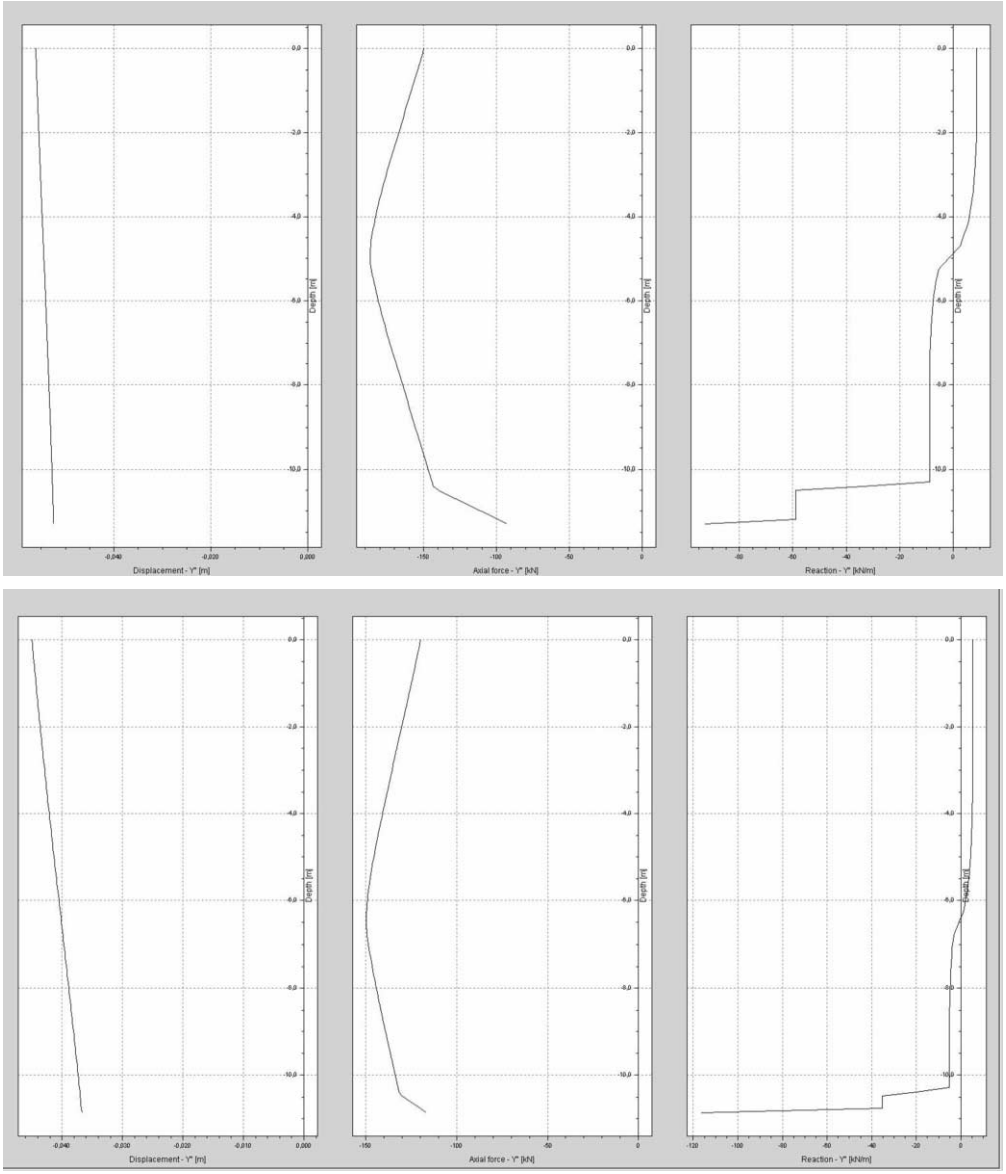


Figure D.8 Result of DPileGroup for neutral level new pile 150 kN (top) and old pile 120 kN (bottom)

ANNEX E BUILDING AND SOIL DEFORMATIONS

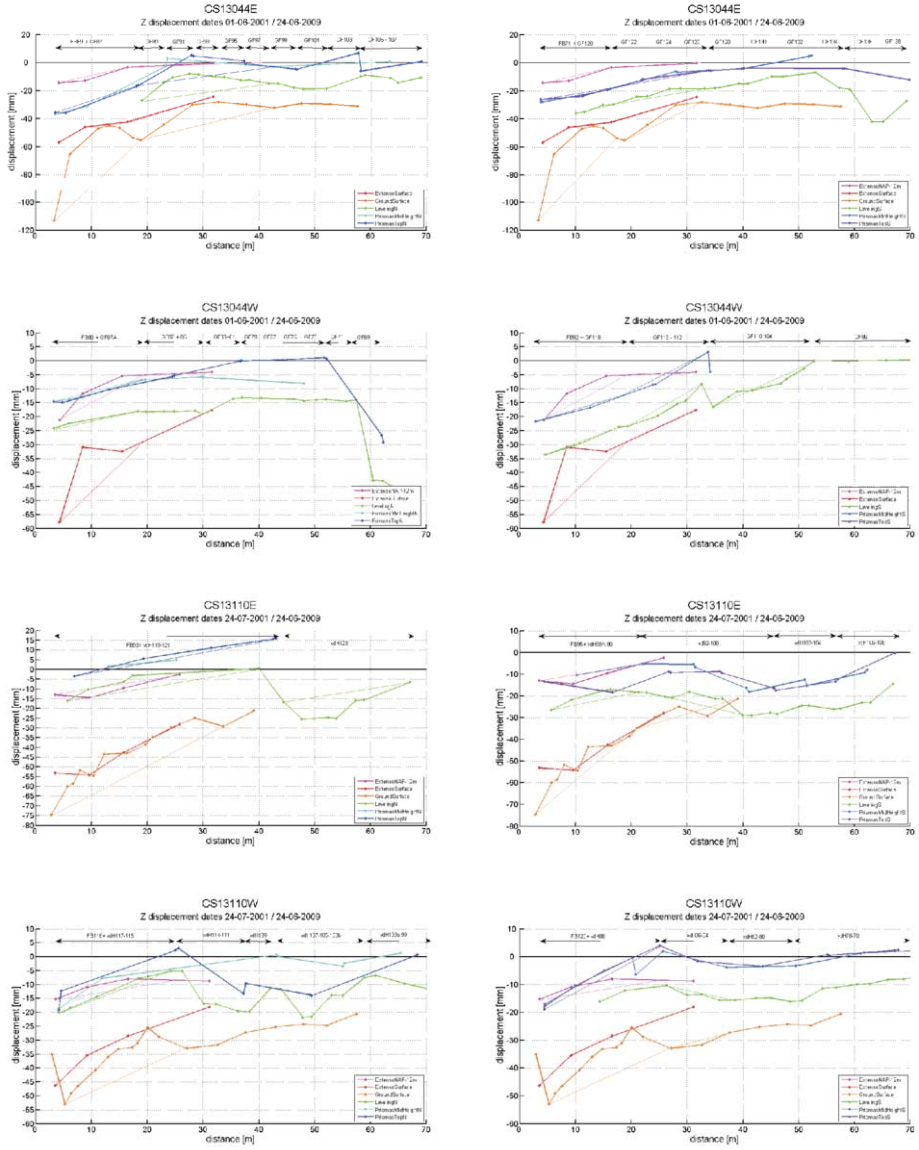
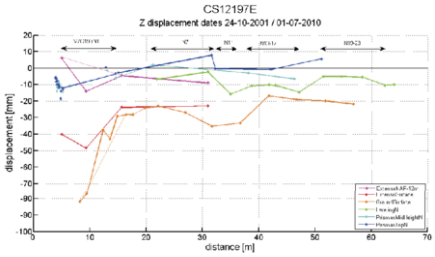
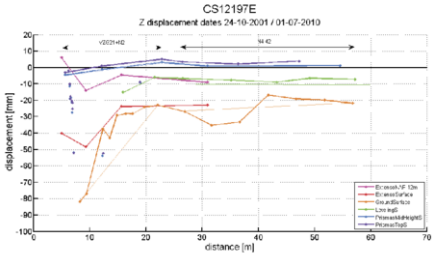
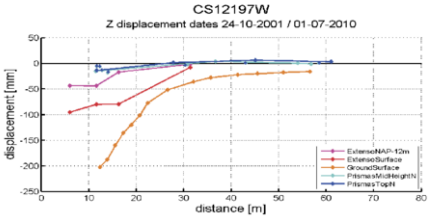


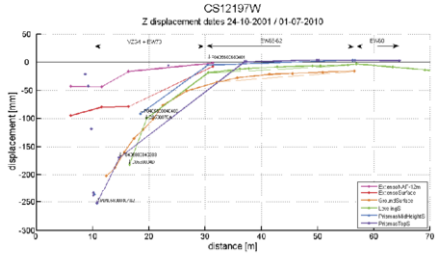
Figure E.1 Building and soil deformations 2001-2009 Ceintuurbaan Station



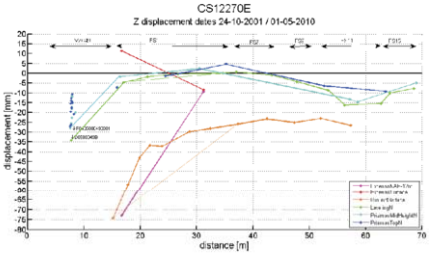




Foundation in 2nd sand layer, incident location



Incident location



12270ES not enough prisms

12270WN not enough prisms

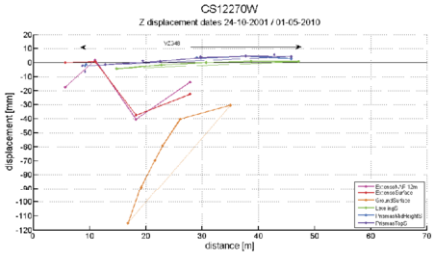
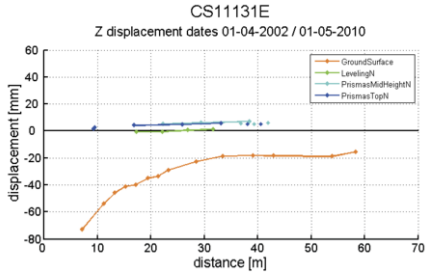
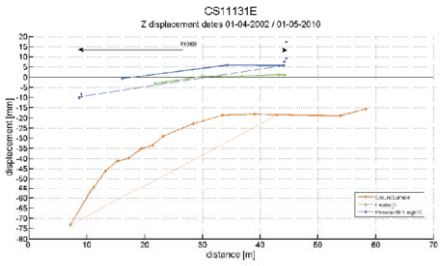
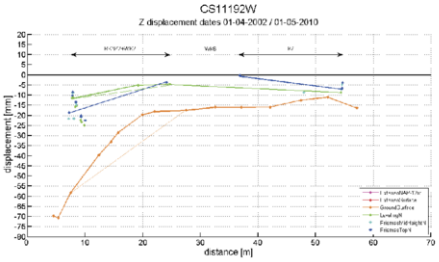


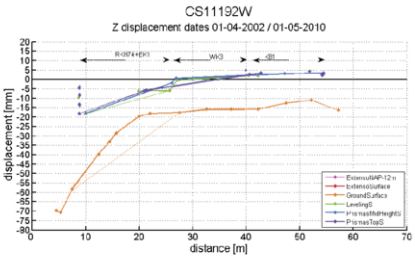
Figure E.2 Building and soil deformations 2001-2010 Vijzelgracht Station

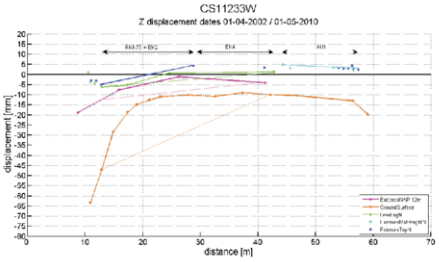




Foundation in 2nd sand layer







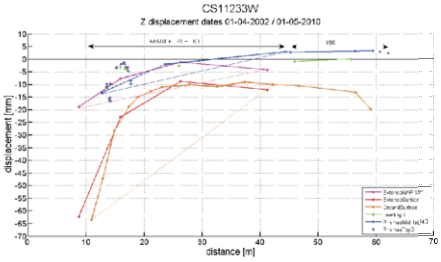


Figure E.3 Building and soil deformations 2002-2010 Rokin Station
11212EN and 11212ES excluded due to lack of prisms

This page intentionally left blank

Biography



Mandy Korff graduated in 1999 as MSc in Civil Engineering from Delft University of Technology. In 2000 she joined GeoDelft as a consultant and researcher in the field of foundations and underground construction. She gained experience in geotechnical risk management. Since Deltares was formed in 2008 she works as a strategic advisor, mainly for underground construction and was at the same time engaged in a part-time PhD study supervised by prof. Robert Mair, at the University of Cambridge. At present, Ms. Korff works as expert in the field of risk management, forensic geo-engineering, the application of the observational method and building response related to underground construction. She currently contributes to projects such as the Amsterdam subway (North South line), the Delft railway tunnel and projects in Singapore. Since 2013 Ms. Korff is member of the Deltares Scientific Council. She will receive her PhD degree from the University of Cambridge on July 20, 2013.

Ms. Korff is active in the network of geotechnical engineering; in The Netherlands as chair of the Geotechnical department of the Royal Institute of Engineers and internationally as member of TC204 and TC207 on Underground construction and Soil Structure interaction in the International Society of Soil Mechanics and Geotechnical Engineering (ISSMGE). In 2011 Ms. Korff chaired the 21st European Conference for Young Geotechnical Engineers in Rotterdam, The Netherlands.

Linkedin: nl.linkedin.com/in/mandykorff
Publications on Google Scholar:
http://scholar.google.nl/citations?user=E9jgXdwAAAAJ&hl=nl

This page intentionally left blank

Deltares Select Series
Volume 13
ISBN 978-1-61499-273-8 (print)
ISBN 978-1-61499-274-5 (online)
DOI 10.3233/978-1-61499-274-5-i

Deltares is an independent Dutch research institute for water, subsurface and infrastructure issues. Its mission is to develop and apply top-level expertise to these issues for people, planet and prosperity. Worldwide, around 900 staff are working to find innovative solutions that make living in the world's deltas, coastal areas and river basins safe, clean and sustainable. Since 2009 Deltares has been publishing the Deltares Select Series. Alongside peer reviewed proceedings of symposia organized by Deltares, this series publishes dissertations, edited volumes and monographs by Deltares employees. The editor-in-chief of the series is dr. Jaap Kwadijk, Chief Scientist of Deltares. For more information, see www.deltares.nl.

Previously published in this series:

Volume 12. C. den Heijer, The Role of Bathymetry, Wave Obliquity and Coastal Curvature in Dune Erosion Prediction
Volume 11. C. Harteveld, Making Sense of Virtual Risks – A Quasi-Experimental Investigation into Game-Based Training
Volume 10. G. Hoffmans, The Influence of Turbulence on Soil Erosion
Volume 9. A.H. te Linde, Rhine at Risk? Impact of Climate Change on Low-probability Floods in the Rhine Basin and the Effectiveness of Flood Management Measures
Volume 8. I. Pothof, Co-current Air-Water Flow in Downward Sloping Pipes
Volume 7. M. Van, E. den Haan & J. van Deen, A Feeling for Soil and Water - A tribute to prof. Frans Barends
Volume 6. C. Schipper, Assessment of Effects of Chemical Contaminants in Dredged Material on Marine Ecosystems and Human Health
Volume 5. M. Marchand, Modelling Coastal Vulnerability – Design and Evaluation of a Vulnerability Model for Tropical Storms and Floods
Volume 4. S.A.M. Karstens, Bridging boundaries. Making Choices in Multi-actor Policy Analysis on Water Management.
Volume 3. J.S.M. van Thiel de Vries, Dune Erosion During Storm Surges
Volume 2. P.M.S Monteiro & M. Marchand (Eds.), Catchment2Coast, a Systems Approach to Coupled River-Coastal Ecosystem Science and Management
Volume 1. F.J. Los, Eco-Hydrodynamic Modelling of Primary Production in Coastal Waters and Lakes Using BLOOM

This page intentionally left blank